BOOK of ABSTRACTS

LOSS PREVENTION 2025

18th EFCE International Symposium on Loss Prevention and Safety Promotion in the Process Industries

Venue
Bologna, Italy
Bologna Fiere Congress Centre
Piazza Costituzione, 4/a,

Date
From June 8 to June 11, 2025

Organized by

AIDIC SERVIZI SRL
Via Giuseppe Colombo 81A, 20133 Milano
Website: www.aidic.it
Email: aidic_accounting@aidic.it
Phone: +39 02 70608276

Symposium Contacts
Email: lp2025@aidic.it
Phone: +39-02-70608276
Website: https://www.aidic.it/lp2025

Sponsor

CONTENT

PREFACE

ABSTRACT Index

AUTHOR Index

ABSTRACTS

PREFACE

Welcome to the 18th EFCE International Symposium on Loss Prevention and Safety Promotion in the Process Industries!

After 12 years, this most prestigious conference in the world in the field of risk and safety related to the chemical and process industries has returned to Italy, in Bologna, the site of the oldest European university. Since its first edition in 1974 in Delft, occupational and process safety professionals, researchers, scientists, academics and practitioners have been meeting on a triennial basis at the EFCE Loss Prevention Symposia somewhere in Europe. This prestigious symposium comes back to Italy where the 14th edition held in Florence faced emerging challenges in those days related to process safety and transfer to practice, e.g., closing the loop from operational experience back to design and development of the newly introduced resilience engineering approach.

Over the years, the Loss Prevention Symposia series has been successful in stimulating and sharing both theoretical and practical knowledge among the Loss Prevention community.

Considerable progress has been achieved in the field of safety in the chemical and process industries worldwide. Actually, even more industries are involved and have been profiting from advances in safety knowledge. Industries operating in the energy, pharmaceutical, food, transportation, manufacturing sectors and in the related services also use chemicals and/or hazardous materials on a daily basis and are exploiting the safety knowledge matured withing years of academic and industrial research, development and practice.

These are challenging times due to the need to contrast climate change with new decarbonized technologies and with adaptation strategies, as well as to raise the safety and security of production and storage sites. New opportunities and new vulnerabilities proceed hand in hand with the advancement of IT technologies and data analytics. Smart and interconnected systems unlock the potential of new production processes, but need to contrast the risk of complex cascading events. Exchanging information, disseminating data and stimulating the development of new methods to reduce the risk of incidents/accidents in the process industries, is indeed a must and a need. To promote dissemination of results and to foster new ideas, the sixth "EFCE Excellence Award for Process Safety" for outstanding PhD research work will be presented at this conference.

Transfer to practice is as important as the development of know-how, and many challenges still need to be addressed in order to make further progress in safety, and process safety in particular. To name a few: developing worldwide databases of near-misses and accidents able to provide an effective support to data analytics and lesson learning, addressing climate-related risks bridging climate models to Natech scenario modelling and prevention, developing user-friendly and effective models for cascading events in security and cyber-security scenarios, further developing resilience engineering, harmonized education of process safety, economic theories and models into safety and security decision making, develop specific approaches to unfold the potential of artificial intelligence applied to process safety.

Let us therefore take the opportunity of this 18th Loss Prevention Symposium, to learn from each other and exchange best practices, to transfer experience by presenting new scientific results and concepts, learn from case studies, and to preserve existing know-how for the benefit of the process industries, of the workers and of the society at large.

Bruno Fabiano, *Chairman EFCE WP Loss Prevention*
Ales Bernatik, *Secretary EFCE WP Loss Prevention*
Valerio Cozzani, *Chairman, Organizing Committee*

ABSTRACTS INDEX

AUTHOR INDEX

The Questions of Recurring Incidents; Why and How to Stop Them?

Ian R. Clarke

Senior Risk Engineer, Swiss Re Corporate Solutions, London, UK

ian_clarke@swissre.com

1. Introduction

In the insurance industry we spend a lot of money paying claims for incidents, that on paper, look remarkably similar to what has gone before. We, being the risk engineering component of this insurance community, visit clients regularly and conduct risk engineering surveys. During these we talk about process safety leadership, operational discipline, operations and integrity management systems and a host of other systems and processes which we try to examine and critically assess for efficacy. There is little doubt that there are numerous moving parts to this discussion, but I want to focus on just one.

The topic for this presentation is competency validation, or, more accurately, how to try and ensure the operator at the sharp end of the process does what you want him to do, every time. Whether it is during standard operations, which is relatively simple, through to an emergency situation, which is more difficult. There are undeniably a host of organisational factors that influence operator or technician behaviour in an emergency situation, such as the safety culture, leadership directives both communicated but also implied by actions rather than policies, and the organisational structure that determines whether said operator or technician is afforded both the time, resource and degree of empowerment necessary to make the correct decision. We are not going to touch on these issues.

Instead, through a series of ultimately preventable events, we will examine how to try and improve the chances of the right outcome being achieved. Putting aside the organisational factors, which we know play a significant, indeed the most significant, role, how do we improve the knowledge, training and ultimately the decision making of the person at that sharp end? More importantly, how do we validate that we have done it and retained a level we are happy with year on year? All too often we go to sites where the success of the operator training programme is measured by the number of training sessions the client has run, not whether we have actually improved the likelihood of the operators and technicians going home safely. All too often we measure quantity, but not quality.

2. Methods

This is not going to be a description of a competency validation programme, as I am not an expert in that field. After over thirty years in insurance, most of it in the downstream oil and gas arena such as refineries, petrochemical plants, gas plants, ammonia and ammonia based fertiliser plants and tank farms, the only thing I consider myself an expert in is process safety and risk assessment.

However, in recent years we have begun to tackle the question of loss analysis and learning from losses. As many would know, this is a difficult topic to cover in the public arena as not all losses are investigated in that domain, and many losses we see in the insurance industry we investigate on the basis of loss adjuster reports which cannot be shared in the wider environment. This point is amply demonstrated by several instances in this paper where I have used losses from our own internal claims database to illustrate a point, while protecting the anonymity of the client.

However, we do have loss information in the public domain. Some are studies of large losses (Marsh, 2024), some are numerical analysis of large losses (Lloyds Market Association (LMA), 2015), and of course we have the excellent loss reports issued in the public domain by various regulators, the most well known probably being the US Chemical Safety Board (CSB), some of whose reports I will use to illustrate points in this paper.

If you spend any time at all studying losses in our industry one of the first things that becomes apparent is that there is very rarely anything new to learn, especially these days. Losses typically follow one of many well known paths, with contributing factors that are all too familiar to all of us. This begs the question – Why? Why does it happen? Why do the same causes and contributing factors appear again and again, despite our best intentions? Despite what some of my colleagues in the insurance market might think, nobody, well almost nobody, goes to work on a given day with the intention of causing a major catastrophe which may kill themselves or their fellow workers and cause irreparable damage to their workplace and possibly the public and environment. So, why?

Unfortunately there is no single answer to the question of why the same losses occur, but it certainly can be argued that most of these losses are in no way different to what has come before. Like the causes and contributing factors, the answers are very rarely new either. Now the first point to make, which is a very valid one, is that virtually all these losses have organisational and/or design components which are the main reasons for why they occurred. I will present later statistics that show the vast majority of incidents that would fit under an operational heading, rather than asset integrity based failures, occur during transient conditions, such as start ups, shut downs or emergency situations. There are a wide range of things that influence operator behaviour in an emergency such as the safety culture of the facility and the leadership directives which are both communicated formally through policies and those implied by actions. Their behaviour is also influenced by the organisational structure and how emergency situations are managed, plus by the availability of the time, resource and level of empowerment to come to the correct decision. There is plenty of theory and, I'm sure, numerous papers on process safety leadership and culture at this very conference.

The various process safety management system elements that we have become used to seeing are designed to identify the hazards and build a framework of systems and procedures that control them. However, frequently these systems can be used to justify existing levels of controls, avoiding capital spend on technological hardware based solutions which may improve the management of the hazard. As an example, one of the things we look for in Process Hazard Analysis and Hazard and Operability studies (PHA/HAZOPs) is whether credit is taken for human interventions. Anything that is a single operator error away from disaster, you are pushing your luck and potentially putting people in harm's way. Again, I am sure there will be a host of presentations at this conference around improving these systems and procedures.

What I want to concentrate on is improving our very last, or what should be our very last, line of defence, the operator. I accept that the organisational, hardware and software (in this context, management systems) deficiencies on the facilities we operate are the main causes of loss, and I urge everyone to learn lessons from the following losses, including how to make this last line of defence as resilient as possible. Because while most of the losses I am going to use as examples have a myriad of organisational, hardware and software causes, it doesn't alter the fact that if the operators had behaved differently, they may not have happened.

3. Incidents

3.1 Potential Commonality Problems

The first type of incident I want to highlight is the honest mistake made by operators where design provides us with a significant opportunity to make such a mistake. The loss in question occurred on an ethylene cracker unit when an operator opened the wrong manual blind valve on the furnace charge deck, leading to a flash fire. These blind valves were installed to allow the ethane feed lines to be blinded and isolated without the need for opening flanges. The plant in question had 16 cracking furnaces and the valves were located on a series of common charge decks each serving two of these furnaces. The ensuing fire damaged steelwork supports, electrical and control systems, instrumentation and piping throughout the unit, and all furnaces suffered some damage to tubes and refractory due to the thermal shock.

The operators were preparing to shut down one furnace for decoking and start up the adjacent one. During the activity a flash fire occurred. The control room operators immediately activated the water drench systems but the two operators on the charge deck suffered serious burns before being evacuated. The plant was safely shut down and depressurised, with fire fighting efforts beginning almost immediately, preventing fire spread to other areas of the plant. As the manual blind valve on the operating furnace was open following the incident, and there was no reason for it to be so, it was concluded that the fire was caused by a release from this valve.

This loss shares some similarities with the Formosa polyvinyl chloride (PVC) plant explosion which occurred in Illinois some ten years earlier, although the damage was in this instance much more severe. The similarities in the layout between the groups of four reactors within the reactor building, which housed all 24 reactors, led to an operator inadvertently opening the lower drain line on an operating reactor (D310) instead of the one that was being cleaned (D306), despite him having to defeat an interlock to do so. The figure (Figure 1a) on the next page, from the CSB report, shows a diagram of the arrangement. A large cloud of vinyl chloride monomer (VCM) was released into the building and subsequently ignited. Four operators were killed and another died two weeks later. The resultant fire and smoke required roads to be closed and 150 people evacuated. The plant was destroyed and was never rebuilt.

There were a large number of extenuating circumstances as follows:
- The operators were on two levels with no means of communication, so the upper level operator, who controlled the batch system instrumentation, could not speak directly to the operator on the lower level

- The previous owner installed an overpressure safeguard, allowing reactors to vent into adjacent empty reactors to relieve pressure. However, there were interlocks installed on the lines to prevent the valves from being opened if the system was live. Under the previous ownership circumventing this interlock could only be done at the supervisor level, the entire layer of which were removed by Formosa to reduce costs
- As can be seen from the diagram (Figure 1a), the layout was the same for each group of reactors, so a mistake was more likely even given all reactors and consoles were labelled
- There had been a number of previous near misses, and the previous operator had recommended upgrading the interlock system in a PHA some years prior. However, the plant was sold and Formosa had not revalidated the PHA prior to the incident. The PHA, in any event, did not cover transient operations such as cleaning and returning to service

In order to try and prevent incidents of this type, we encourage the following safeguards:
- A brief, pre-task meeting, similar to the "toolbox talk" or job safety analysis (JSA) discussion that would occur prior to a maintenance activity
- Ideally, implement Safety Critical Task Analysis (SCTA). Using the instance of the blind valve above, any hydrocarbon system which requires potentially opening it to atmosphere should be covered by this activity. The subsequent analysis will identify a need for increased training, signage and the like
- Transient operations should be covered by checklist type procedures with every step initialled and, ideally for the most hazardous activities, verified by a second operator
- Note signage is not always a cast iron guarantee (as the Formosa loss showed)
- Increased training refers to effective training, rather than leaving operators to refamiliarize themselves with procedures once every few years. For training to be effective, it requires field validation and testing, and then drills/exercises. Most plants drill only for emergency situations. The best plants will carry out drills not only on emergency situations but also transient operations like switching, reactor changes for cleaning, etc. They will also carry out drills leading up to start ups, covering the different conditions and hazards occurring during these operations, and similarly shut downs. Attendance should be documented and understanding should be confirmed by testing
- Effective training is not sitting the shift in a room, reading through the procedure and getting everyone to sign a piece of paper confirming their attendance

3.2 Hazard Awareness

The second type of incident to discuss are those exacerbated by a lack of hazard awareness. This one is more difficult to address as there is corporate hazard awareness and individual hazard awareness. It goes without saying that individuals can suffer from a lack of hazard awareness, and that this should be addressed by training, upskilling, etc. However, if the organisation itself suffers from a lack of hazard awareness, then that is a different thing entirely. Also note here I am referring to a genuine lack of awareness, rather than conscious decisions to put profits before safety.

An explosion at an ONGC gas plant in India in 2019, which occurred during torrential monsoon rain, showed a lack of hazard awareness throughout the organisation. The ensuing explosion caused massive damage to the plant, as well as four fatalities. The enquiry report (PNGRB, 2020) identified a number of contributing events, including those below:

- The event occurred during the monsoon, and indeed the amount of rainfall was a major contributing factor. Drains were not capable of handling the worst case events and the level of oil water separators across the site were not systematically measured
- The site had a history of spills from pigging activities, including a large fire in 2004, as there were a large number of incoming and outgoing pipelines at the facility. The leak in question occurred in the aftermath of pigging operations

However, the lack of hazard awareness is evident from the fact that a number of personnel had difficulty breathing due to hydrocarbon vapours in the air. Despite this, personnel, some of them fire brigade members, made an effort to start vehicles in order to move around the plant and search for what was clearly a large hydrocarbon leak. The vehicles did not start as the atmosphere was too rich. Eventually the leak, most likely from pigging activities, flowed around the site on the increasingly large volume of water, and found an ignition source.

In another event, in 2009, a large explosion occurred at a CAPECO tank farm in Puerto Rico (Figure 1b). The CSB report (CSB, 2015), outlines the sequence of events, where the offloading of gasoline from a vessel overflowed a storage tank and then ignited, causing a massive explosion and subsequent secondary explosions, damaging 17 of the 48 tanks. There was significant offsite damage to property and the environment, and the fire burned for some 60 hours. Fortunately there were no fatalities. The contributing factors included:

- Malfunctioning level measurement equipment
- Inadequate tank filling procedures and design quirks in the system which meant more than one tank had to be filled at a time, increasing the difficulty in manual fill time calculations
- There were no independent high-high alarm systems or overspill prevention
- Emergency response shortcomings

The lack of hazard awareness is evident in the lack of an appropriate level of caution. When handling an incoming package which is larger than the vessel into which it is being deposited the potential for loss is always high. This is by no means an unusual situation and one wonders how many near misses occurred on this site, which should have acted as warnings. The parallels to Buncefield, which I have not mentioned as the event and investigation is much more well known here in Europe, are obvious.
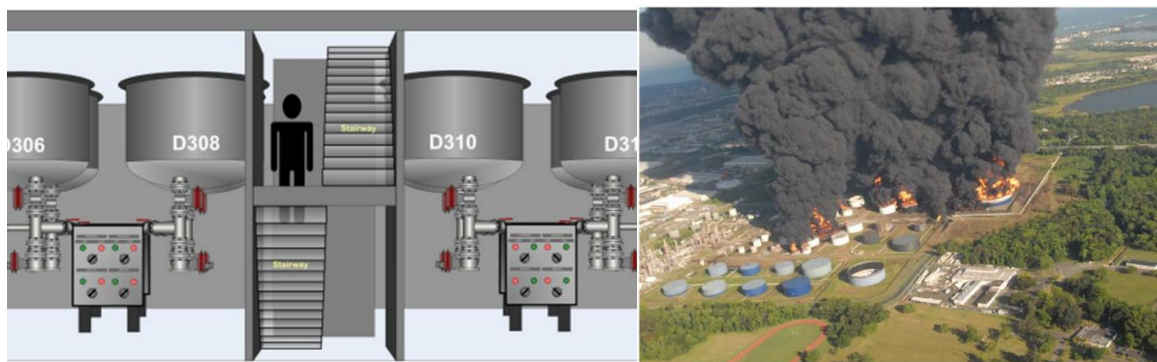
Figure 1a: Reactor layout at Formosa PVC plant (from CSB)

Figure 1b: Fire at CAPECO (from CSB)

The recommendations from the CSB report focused on regulatory shortcomings that allowed many of the contributing factors listed on the previous page to be present. However, both these incidents, neither of which occurred that long ago, show a distinct lack of organisational and personal hazard awareness. This is common in situations where the Process Safety Management (PSM) and Health, Safety and Environment (HSE) functions on a site act as the policeman rather than as a support act to the line management functions. The line management functions are where responsibility for PSM/HSE resides. Within the insurance industry we are typically looking for:

- PSM implemented with element champions at operations or maintenance level
- HSE/PSM function is a facilitator, not the driver
- Auditing is an accepted part of the process
- Leading and lagging Key Performance Indicators (KPIs) are employed to inform management of problem areas and the efficacy of action plans to fix these problems
- One of the elements of the PSM programme focuses on effective operator training, including PSM, to improve hazard awareness and understanding of the safe operating limits within the facility

There are a number of other, less recent, losses with hazard awareness at their heart, including a major oil spill in Michigan in 2010 and a fire at a refinery in California in 1999. Included in the references are the technical reports by the National Transportation Safety Board (NTSB, 2012) and the CSB (CSB, 2001) respectively for these two events, and I'm sure delegates can think of many more.

3.3 Transient Operations

The third type of incident has already been touched on as part of the commentary on the Formosa PVC plant loss. Here I want to briefly digress to refer to the LMA publication referred to earlier. An Analysis of Common Causes of Major Losses in the Onshore Oil, Gas and Petrochemical Industries was published by the Lloyds Market Association in September 2016 and was also presented as a paper at the 2017 Hazards conference. The document contains a detailed review of loss causation in these industries.

Recently there has been work undertaken to update the document to include more recent losses. While this work is not complete at this time, the overall statistical conclusions in terms of loss causation remain largely unchanged.

I recommend the document for a breakdown of the losses into various categories, including across industry types (refining, petrochemicals, other) and, of particular relevance in this topic, across operational status differences. In particular, it is interesting to note that 63% of operational losses (e.g those not related to asset integrity issues) occur during what we call transient operations (Figure 2). These include start-up, shut-down but also emergency situations caused by power or other utility failures and also non-standard operations such as equipment switching. A further 28% occur during maintenance operations.
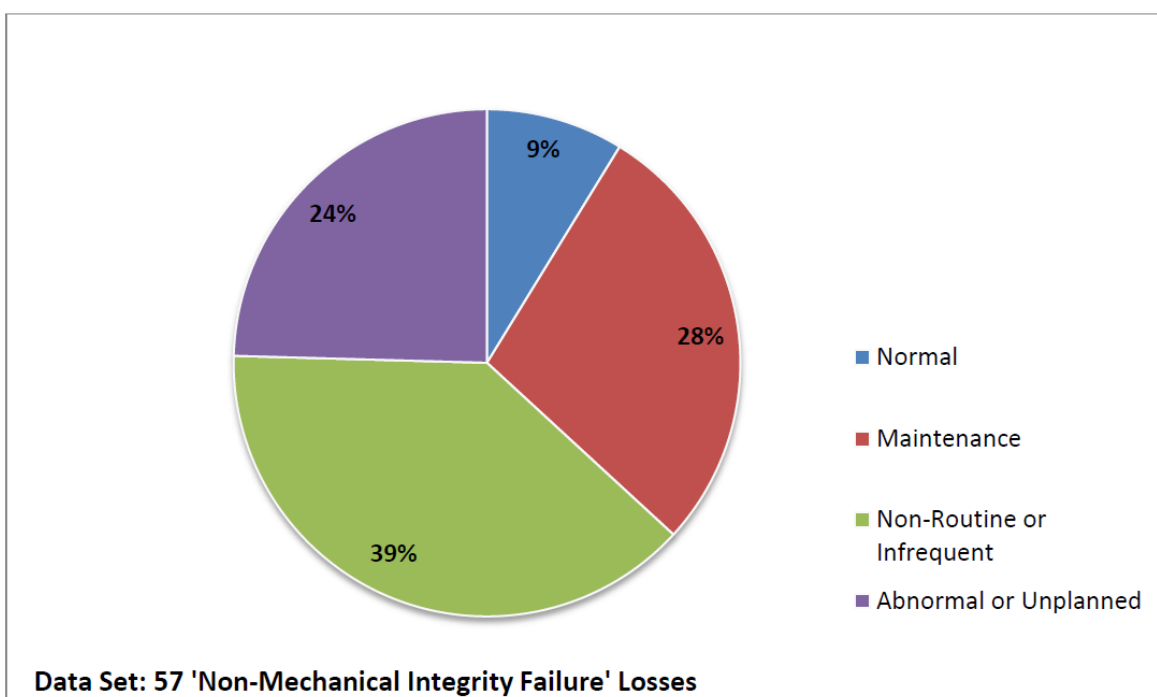
Figure 2: Breakdown of Operational Losses (from LMA)

Many incidents occur during transient operations, and indeed most of the losses above could be used equally well to demonstrate this point. I have turned to some other less known events to further elaborate on the issues raised by transient operations, as it is obvious from the above diagram the part it plays in major losses.

Damage occurred to an oil and gas production platform in offshore Malaysia in 2020. A ship impacted the platform in heavy weather, causing damage to three bridges and the three platforms linked by them, including piping and instrumentation. The ship was anchored only 30m from the platform instead of the 90m required in a heavy swell, which was defined as greater than 2.5m. The sea state at the time was 3.8m. Subsequent damage was less than US$100m, although given previous incidents that have occurred with ship collisions to platforms, notoriously the Mumbai High incident in 2005, this could probably be considered a near miss.

Observations that occur to the author include pending natural hazard events should prompt a review of all relevant procedures and operators should be trained in how to respond to deviations from normal activities, e.g. during abnormal, non-routine or unplanned events.

In 2018 there was a large fire at a petrochemical plant in Saudi Arabia. The fire was caused by overpressure and rupture of a lower pressure (LP) rated blowdown vessel downstream of the high pressure blowdown vessel on the polypropylene (PP) plant. A manual isolation valve in the PP plant blowdown system should be closed at a specific point in the procedure when solids are being drained from the LP vessel, but then reopened afterwards. This did not happen and the system was overpressurised and caused a fire. It became clear during interviews operators were not clear on the procedure and they did not use the checklist except during start-ups and shut-downs. Observations that occur to the author include better use of SCTA would have identified the potential for overpressure and led to a more robust management system around a manual process, and operators should be trained in, and drilled on, the hazards associated with transient operations such as clearing blockages on polymer plants.

There are a number of other, less recent, losses with transient operations at their heart, including a massive vapour cloud explosion (VCE) at a petrochemical plant in Texas and the rather more well known explosion at a gas plant in Australia in 1998. Included in the references are the excellent book by Australian author Andrew Hopkins (Hopkins, 2000) on the latter loss. In fact, for all you need to know about process safety leadership and organisational failures, I would recommend all of the books by the same author.

4. Conclusions

I would like to begin the conclusion by reiterating my first point. The losses I have used as examples all had management failures of one kind or another as their chief cause. These failures are the major cause of these losses, not operator error, which is possibly the most useless phrase ever invented in the field of incident and loss investigation. Attributing a loss to operator error has most likely never helped prevent a similar accident, except for the operators and workers concerned, who now have personal experience as their guide. It would be good if we didn't have to learn lessons this way, though.

Many of these losses occurred during a transient or unusual operation. It is my experience that organisations, even when analysing their processes with tools such as HAZOP, do not adequately address these transient operations. Similarly, the take up of tools such as SCTA, referred to earlier, in industry is poor. However, the focus of this paper is what can we do to improve the response of operators and other workers at the sharp end of incidents. Unfortunately, many organisations use risk analysis tools such as PHA and HAZOP as an excuse to shift the critical actions onto these personnel, rather than relying on design or other engineering (e.g. more costly) solutions.

Also unfortunately, the training of operators and use of drills and simulations frequently does not cover and/or practice the proper response in these transient or emergency states. In the days of higher reliability and greater run lengths between turnarounds, some operators may not experience power interruptions, start-ups or shut-downs for many years. It seems obvious that then expecting operators to behave in a certain way, often in stressful and/or complicated situations, is ambitious at best.

References

Hopkins A., 2000, Lessons from Longford: The Esso Gas Plant Explosion, CCH Australia

Jarvis R. and Goddard A., 2016, An Analysis of Common Causes of Major Losses in the Onshore Oil, Gas and Petrochemical Industries, Lloyds Market Association

Marsh, 2024, 100 Largest Losses in the Hydrocarbon Industry, Marsh

National Transportation Safety Board, 2012, Enbridge Incorporated: Hazardous Liquid Pipeline Rupture and Release, NTSB

Petroleum and Natural Gas Regulatory Board, 2019, Major Fire at ONGC's Gas Processing Plant at Uran, PNGRB

US CSB, 2015, Final Investigation Report: Caribbean Petroleum Tank Terminal Explosion and Multiple Tank Fires, Caribbean Petroleum Corporation, US CSB

US CSB, 2007, Investigation Report: Vinyl Chloride Monomer Explosion, Formosa Plastics Corp., US CSB

US CSB, 2001, Investigation Report: Refinery Fire Incident, Tosco Avon Refinery, US CSB

The Resilience of Fully Automated Plants

Florin Omota

Fluor, Taurusavenue 155, 2132LS Hoofddorp, The Netherlands

Florin.Omota@Fluor.com

1. Introduction

Within the context of energy transition and the 4th Industrial Revolution, companies in chemical and energy sectors are adopting new automation and digital technologies to enhance the health and resilience of downstream operations. The ultimate vision of Industry 4.0 is to create fully autonomous plants that operate without errors and in an optimal, cost-effective manner. These plants integrate best-of-breed digital technologies, including advances in Industrial Internet of Things, Big Data, and Artificial Intelligence.

Autonomous plants operate continuously without human intervention. This leads to higher production rates and reduced downtime due to shift changes or breaks. Robots and automated systems can handle dangerous tasks, such as handling chemicals or working in extreme conditions without exposing the operator to hazardous scenarios. Labor costs decrease significantly when fewer human operators are needed, or when they manage remotely all plant operations.

2. Methods

Resilience engineering focuses on understanding how complex adaptive systems cope effectively with unanticipated events, preventing production loss and plant unavailability. On one side, the mechanical equipment, and Basic Process Control System (BPCS) should have high availability to ensure that the plant operates efficiently and meets the production targets. On the other hand, the Safety Instrumented System (SIS) should have high reliability in preventing hazards and production loss. Spurious trips are safe, however, having a negative impact on plant availability.

Both availability and reliability of BPCS and SIS can be modelled and consequently improved by Fault Tree Analysis (FTA) and probabilistic calculations. SIS reliability modeling is well known and already implemented as per international safety standard for process industry IEC 61511:2016 (e.g. exSILentia software provided by EXIDA). In this work, the reliability and availability of both SIS and BPCS were modelled based on benefit-cost analysis. This methodology provides an evidence-based evaluation, helping organizations become more logical and data-driven.

3. Results and discussion

Two case studies will be explained in detail. The first case considers selection of the most effective configuration of instrumentation for a highly available control loop. BPCS control loop failure is one of the most frequent causes identified in risk analysis. The consequences of BPCS failures are not related directly to safety in autonomous plants, but mainly causing equipment damage and production loss. Therefore, a benefit vs. cost analysis was used to optimize the instrumentation configuration. The cost of plant unreliability can be calculated based on hazardous scenarios identified in the Hazard and Operability Studies (HAZOP). The configurations of redundant instrumentation considered in this study were as follows:

transmitters with 1oo1, 1oo2 and 2oo3, and final elements mainly control valves based on 1oo1, 1oo2 and 2oo4 voting. Based on the severity of consequences, there is an optimal combination of instrumentation that minimizes financial loss and increases plant resilience. The Mean Time to Fail Spurious (MTTFS) as well as benefits of redundant instrumentation are illustrated for a fully automated green Hydrogen plant with a capacity of 40 MW. In case of less than one day production loss, there are no benefits of implementing redundant instrumentation for this case.

Table 1: Redundant instrumentation benefits when avoiding one week production loss

Transmitters	MTTFS	Benefit, €/y	Valves	MTTFS	Benefit, €/y
1oo1	30	0	1oo1	15	0
2oo2	150	+5585	1oo2	75	+10520
2oo3	94	+8866	2oo4 [1]	43	+17560

[1] Configuration with two control valves and two on-off valves, same risk of failure in both directions, either valves open or valves closed

The second example explains the design concept of a control loop fully sharing the instrumentation with a high reliability safety function achieving SIL 3. Increasing the availability of BPCS makes the process safer and reduces the demand of SIS.

The next figure illustrates the configuration of a highly reliable BPCS control based on redundant instrumentation as well as SIL 3 safety function in SIS. The level control consists of a master/slave configuration LC/FC in two parallel lines. The safety function consists of a level trip implemented as 2oo4 voting, or 2oo3 with an extra spare instrument for maintenance.
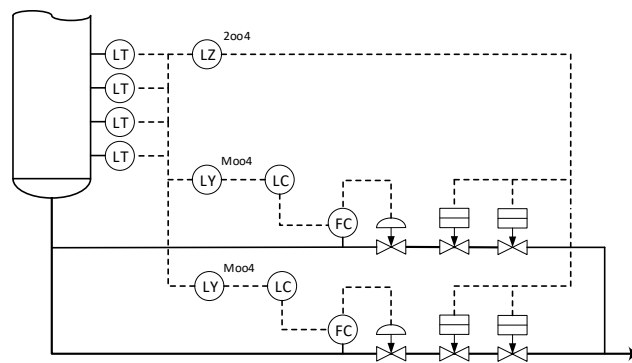
Figure 1. High availability of level control and very reliable level trip.

The reliability calculations for BPCS and SIS were calculated based on FTA and the approach proposed by Omota (2024). The presence of two control valves installed in parallel configuration ensures high availability of the flow control in BPCS. Failure of any flow or level transmitter is also tolerable. From a safety perspective it should be noted slightly lower reliability with four on-off valves instead of a simpler 1oo2 configuration. Overall, the MTBF for BPCS system is about 100 years while the risk reduction factor (RRF) of SIS function is higher than 1000.

The scheme shown in Fig. 1 has also high flexibility allowing full valve stroke testing at any time, as well as full testing of any other instrument, either online or offline.

4. Conclusions

Random failures or other upsets occurring in fully automated plants can be effectively managed by a proper design by installing adequate spare equipment and instrumentation. The methodology proposed demonstrates how FTA and probabilistic calculations are cost effective solutions in the design of fully automated plants, increasing both availability of BPCS and reliability of SIS.

Overall, this approach not only boosts the resilience and safety of automated plants but also provides a practical framework for implementing robust design strategies.

References

Chakrabarti, G., Don, D., Smith, M., Vora, P., 2021. The autonomous plant: Entering a new digital era. Mckinsey & Company, 1-11.

Ham, D.-H., 2020. Safety-II and Resilience Engineering in a Nutshell: An Introductory Guide to Their Concepts and Methods. Saf. Health Work, 12(1), 10-19.

IEC 61511:2016. Functional safety - Safety instrumented systems for the process industry sector.

Kabir, S., 2017. An overview of fault tree analysis and its application in model based dependability analysis. Expert Systems with Applications. 77, 114-135.

Nascimento, L., de Oliveira, A.L., Villela, R., Wei, R., Hawkins, R., Kelly, T. (2024). From Fault Tree Analysis to Runtime Model-Based Assurance Cases. In: Barolli, L. (eds) Advanced Information Networking and Applications. AINA 2024. Lecture Notes on Data Engineering and Communications Technologies, vol 200. Springer, Cham. https://doi.org/10.1007/978-3-031-57853-3_38.

Omota, F., 2024. Basic Process Control System (BPCS) Reliability in Risk Analysis. AIChE NL/B. https://www.aiche.nl.

Determination of Long-Term Stabilities of Weak Autocatalytically Decomposing Substances

David Zink*[1], Sebastian Kimpel[2], Julian Sartorius[1], Christina Kuchta[1], Christian Bernstein[2]

1 consilab, Industriepark Höchst G830, 65926 Frankfurt am Main
2 consilab, Chempark Leverkusen, Q18L, 51369 Leverkusen
*David.Zink@consilab.de

1. Introduction

The safety-related assessment of the thermal stability for decomposing substances in context of process safety is typically based on DSC measurements or adiabatic calorimetry described for example in the German guideline TRAS 410. In case of autocatalytically decomposing substances, the assessment is quite challenging. Technical regulations give no specific support and the assessment is typically based on a worst-case consideration (e.g. H.3 SADT test).

For strong autocatalytic reactions the assessment of the safe storage of a substance based on isothermal induction times is possible, if no relevant heat production rate is present during the induction time. That is for example the case for stabilized acrylates, which show a quasi-autocatalytic reaction behavior. During the period in which stabilization is still present, the heat production rate is nearly zero. If the stabilizer is consumed the polymerization and therefore the heat production rate increases rapidly.

But what is a possible strategy to assess the storage of a weak autocatalytically decomposing substance? Weak autocatalytic decomposition means that a significant heat production rate is already present for a fresh, thermally non-aged substance and the heat production rate increases with increasing thermal history, the autocatalytic reaction path of the decomposition. Typically, a worst-case consideration is not target oriented, because it is too conservative for safety-related application. On the other hand, an assessment based on methods for non-autocatalytically decomposing substances underestimates the criticality of the decomposition reaction.

Nitro aromatic compounds are typical representatives for weak autocatalytic decomposition. Hereby, depending on the melting point of the substance a storage at higher temperatures is necessary and makes a safety-related assessment more relevant.

2. Methods

DSC-measurements

The thermal stability of a compound is determined by Differential Scanning Calorimetry (DSC). Here some milligrams of material are weighed into a glass or gold-plated stainless-steel crucible. The glass crucible is then sealed using an oxyhydrogen flame, the steel crucible is closed using a crucible press. These crucibles are then placed in the equipment DSC-1 Star DSC of Mettler-Toledo to record the DSC thermal-trace of the compound. The sample is measured in comparison to a reference crucible. In case of the glass crucible the reference crucible is filled with aluminium oxide. The gold-plated steel reference crucible remains empty. Both, the sample and the reference, are heated with a heating rate of 3 K/min.

The preparation of the sample is carried out under air. Hence there will be residual oxygen within the crucible after sealing. During the test, this residual oxygen may react with the substance and thus cause heat generation of approximately -20 J/g. Because of the low heat generation and the small amount of oxygen present, this effect can be neglected.

The DSC-equipment is regularly calibrated according to established standards. Therefore, the heat generation of a chemical reaction can be determined reliably. According to DIN EN ISO 11357-1 energy values of endothermic signals are indicated by a positive sign, exothermic signals by a negative sign.

Pressure/ Heat Accumulation Test

The determination of the adiabatic reaction behaviour is performed in the adiabatic heat-storage test and is carried out according to UN-Transport Guideline, UN-Test H.2. in the experimental setup according to Grewer and Klais and VDI-Guideline 2263 Page 1, respectively.

The test setup consists of a pressure vessel with a volume of approx. 0.75 L. In this autoclave a Dewar-vessel with a capacity of approximately 0.2 L is placed. The Dewar-vessel is thermally isolated from its surroundings by a double walled vacuum jacket with a reflective coating. The autoclave is closed, placed in an oven and heated up. After a reaction starts the temperature of the oven is regulated to track the sample temperature. Therefore, above the start temperature reactions or decompositions can be investigated under quasi-adiabatic conditions. The sample temperature is measured with a thermocouple, which is placed in the centre of the sample and surrounded by a glass cover; hence the sample is only in contact with glass. Additionally, the pressure in the headspace is measured and recorded.

The time resolved course of the temperature and the pressure during the experiment are recorded.

The experiments are typically carried out under nitrogen atmosphere.

3. Results and discussion

First, a dynamic DSC of the nitro-aromatic-compound was measured. Figure 1 shows the thermogram. From this thermogram an autocatalytic decomposition behavior is not obvious. The isothermal DSC at 250 °C (see Figure 2) clearly shows a weak autocatalytic reaction behavior. At the beginning of the measurement (0 to 100 min), a significant heat flow of approx. -5 W/kg is already detected, which, however, increases to a maximum heat flow of -90 W/kg after approx. 1700 min under isothermal conditions. This behavior, an increase of the heat flow with the measuring time, clearly proves the autocatalytic decomposition properties. The evaluation of thermal stability, for example on the basis of the safe handling temperature T_{exo} in the sense of TRAS 410, can no longer be regarded as sufficiently reliable. If an autocatalytic decomposition mechanism is detected, an initial worst-case assessment based on isothermal calorimetry is recommended. This evaluation option is also used in the SADT-UN test H.3. As an example, a total of five isothermal DSC measurements of the nitro-aromatic compound were measured at temperatures between 250 °C and 290 °C (see Figure 3 a)). The peak maxima detected at the corresponding temperatures are plotted according to 0 th. order Arrhenius kinetics and linearly adjusted. For safety-related conservative reasons, it is advisable to calculate a confidence interval (95 % in this example), whereby the straight line with the higher temperature-dependent heat production rates should serve as the basis for further calculations (see Figure 3 b) red straight line). Unlike in conventional screening DSC measurements, small sample weights should be preferred when carrying out isothermal calorimetric measurements. Exothermic

decomposition can lead to heat build-up inside the crucible, if the used sample amount is too much, causing the temperature of the test object to exceed the reference/oven temperature. As this effect increases with increasing temperature within a series of measurements and the heat production rate is therefore overestimated at higher temperatures, the activation energy of the derived kinetics increases incorrectly. This leads to lower heat production rates and therefore less critical results when extrapolating towards lower temperatures. In the isothermal DSC measurements shown, the sample weight used was approx. 5 mg.
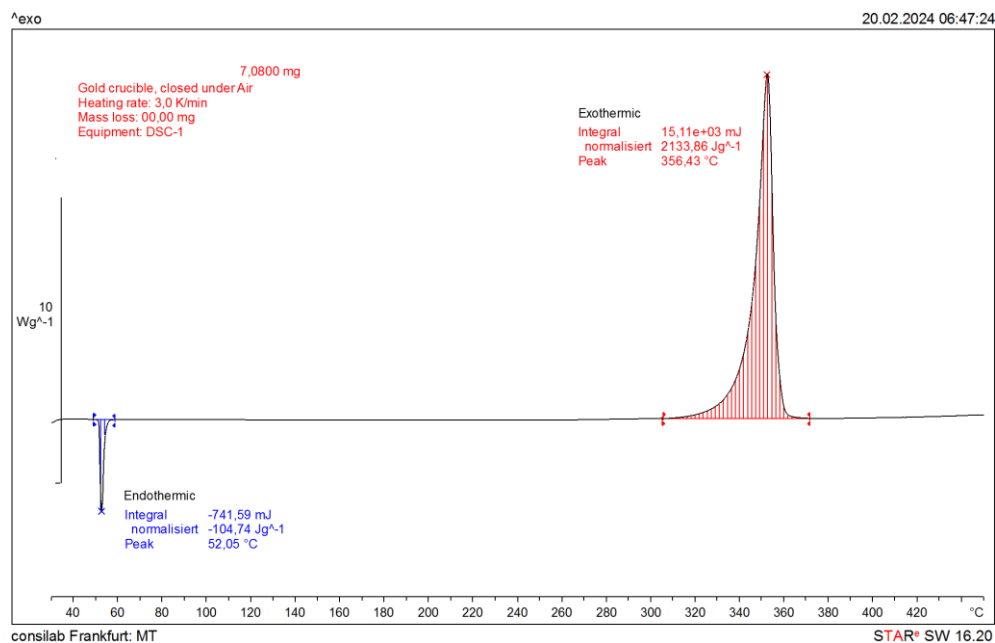
Figure 1. Dynamic DSC of nitro-aromatic compound in closed crucible (3 K/min)
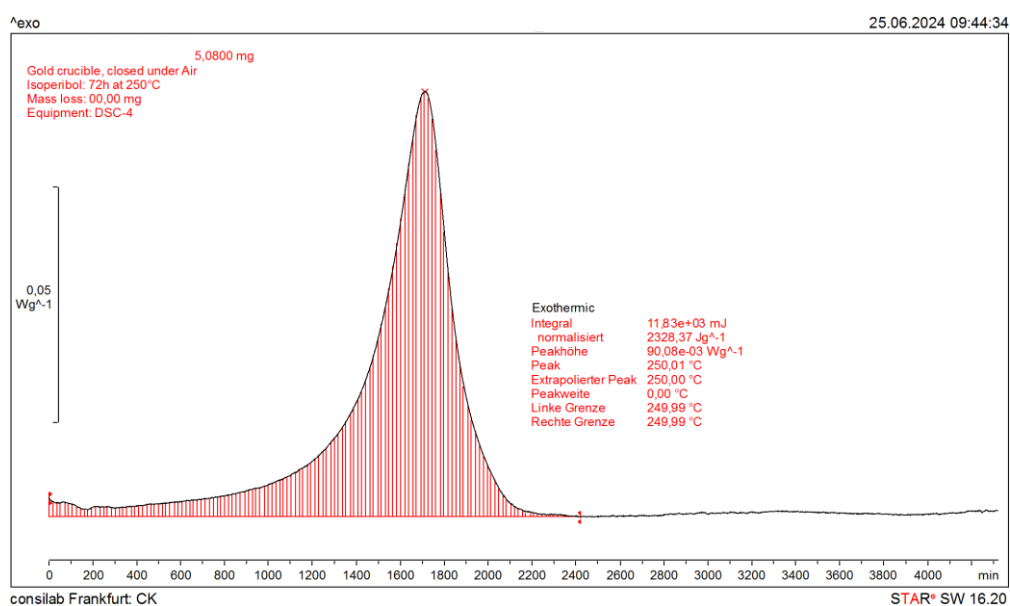
Figure 2. Isothermal DSC of a nitro-aromatic compound in closed crucible at 250 °C
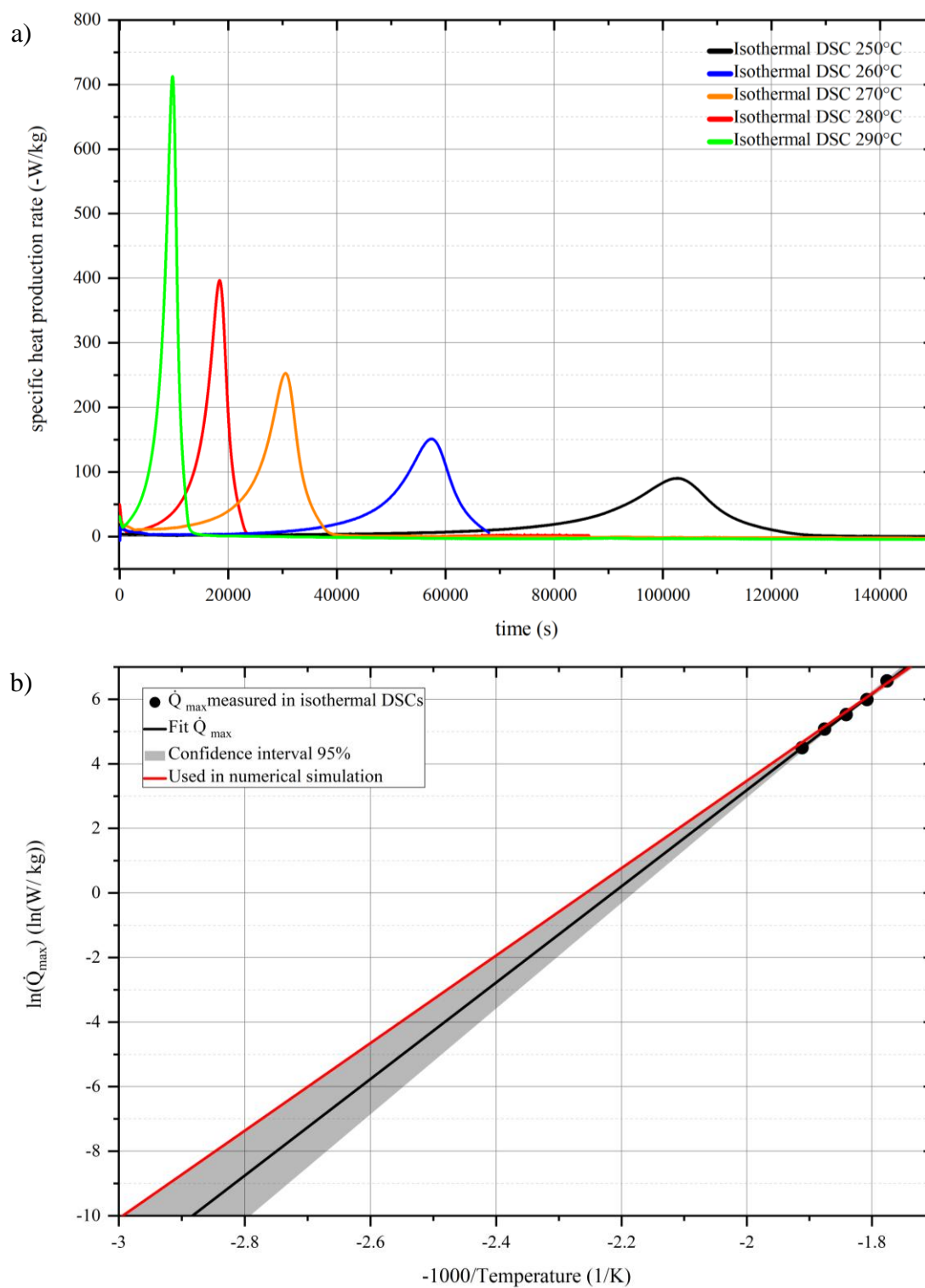
Figure 3.a) Isothermal DSCs of a nitro-aromatic compound in closed crucible at different temperatures – time-dependent specific heat production rate, b) Arrhenius-plot with fit of the maximum heat production rates

Based on the derived worst-case kinetics (Figure 3 b, red line), adiabatic induction times or SADTs can be determined by means of a simple numerical simulation, taking into account a heat dissipation term. This is shown in Figure 4 for the temperatures 130 °C, 140 °C and 160 °C, where the temperature curve over time was calculated under adiabatic conditions and taking into account a heat dissipation term of 30 mW/(kg·K). The numerical simulation can be programmed using Microsoft Excel VBA, for example.
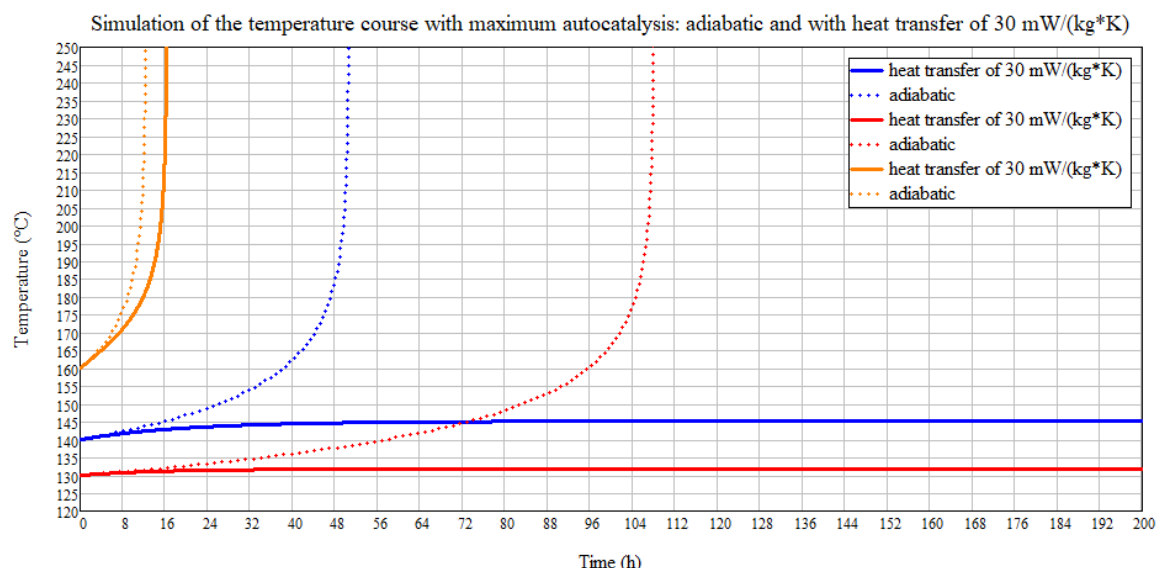
Figure 4. Numerical simulation of the time-dependent temperature course based on the maximum autocatalysis kinetic (worst-case consideration) under adiabatic conditions and under consideration of a heat transfer of 30 W/(kg·K)

The advantage of this worst-case consideration of autocatalytic decomposition is the time-independence of the calculated safety-related parameters. A maximum temperature for the heating medium can be derived taking into account a representative heat dissipation term, particularly for smaller appliances or pipes. A main result of this worst-case consideration is that, for example, a critically self-accelerating decomposition reaction (heat explosion) can be excluded within a pipe network by limiting the teamperature of the heating medium to 140 °C, regardless of the residence time. This consideration is particularly helpful for pipe networks, as a representative temperature monitoring inside pipes is difficult to implement. Due to its conservatism, this worst-case consideration as a basis for the safety assessment is not expedient for all process conditions. If, for example, maximum heating temperatures of 130 °C are required in larger tanks, the worst-case consideration would result in an adiabatic induction time of approx. 48 hours. As a result of which the storage of the nitro aromatic compound at 130 °C would be classified as too critical and unsafe by a safety-related assessment.

At this point, it makes sense to derive more detailed decomposition kinetics that take the time dependency of the autocatalytic decomposition into account. Therefore, the nitro aromatic compound is investigated by an adiabatic heat-pressure-accumulation test. The temperature-pressure curve over time is shown in Figure 5. The detected temperatures and pressures illustrate the criticality of the runaway reaction of a nitro-aromatic-compound.
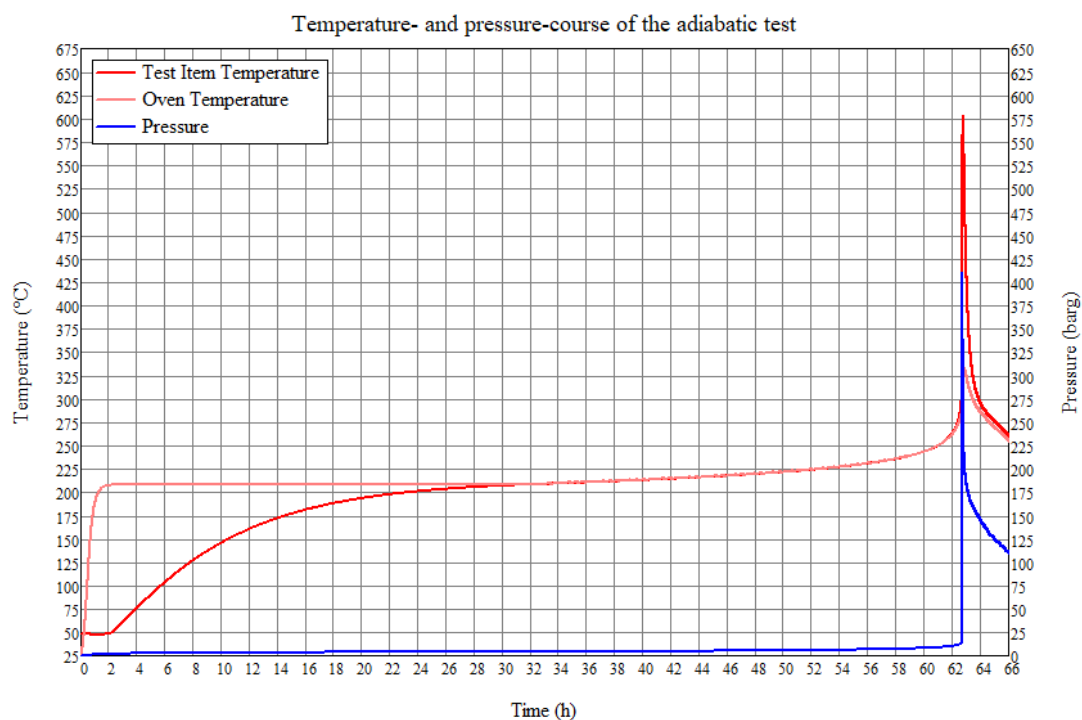
Figure 5. Temperature and pressure course measured in the adiabatic heat storage test of an aromatic nitro compound

The Arrhenius plot of the adiabatic temperature curve is shown in Figure 6. The decomposition kinetics at low conversion are determined by fitting a 0 th. order kinetics in a small temperature range (in this example 210 °C to 230 °C) at the beginning of the decomposition. The temperature-dependent heat production rate obtained in this manner characterizes the decomposition at a conversion of 0 % (see fit Figure 6). Compared to the DSC with a sensitivity of approx. 10 W/kg, the adiabatic heat storage test with a sensitivity of 0.03 W/kg is more reliable to get correct results for low heat production rates (see Figure 7).
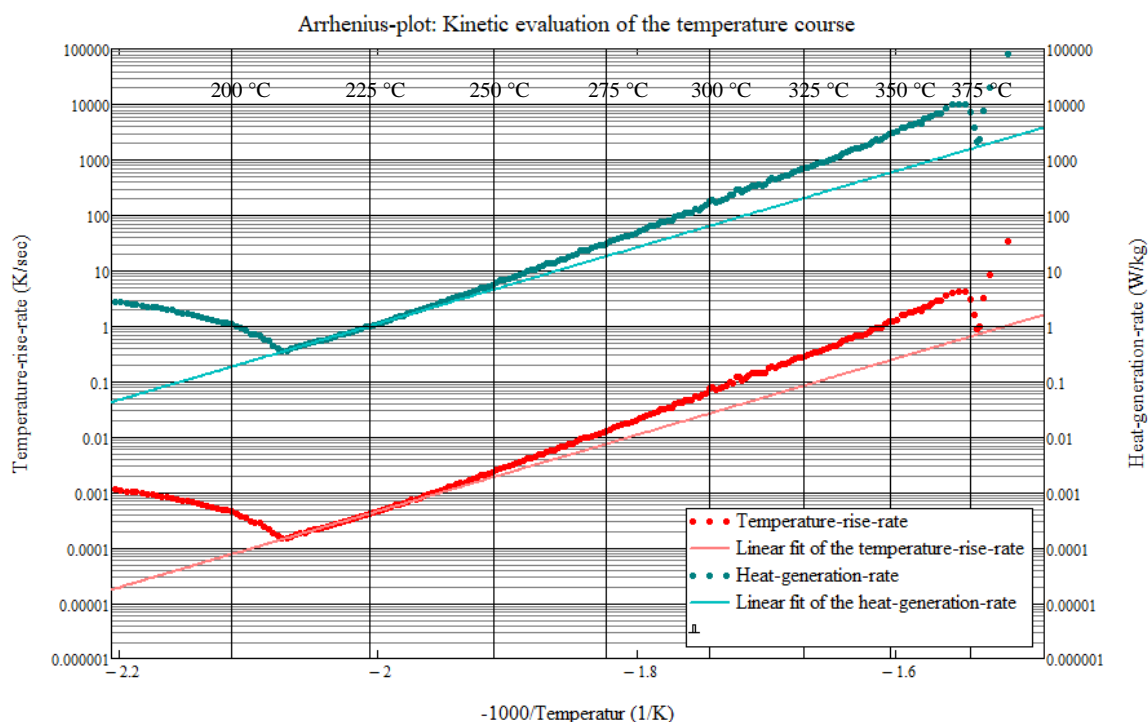
Figure 6. Kinetic evaluation at low conversion of the temperature in the Arrhenius-plot based on the adiabatic heat storage measurement. The kinetic fit is used as the baseline for 0 % conversion in the numerical simulation.

Figure 7 explains how the conversion dependence of autocatalysis can be described in a simple way. Here, the heat production rates recorded in the isothermal DSCs are plotted against the decomposition energy released up to the respective point in time. The maximum heat production rates (maximum autocatalysis) are achieved for the investigated nitro-aromatic-compound at a decomposition energy of approx. -1500 J/g. In order to be able to describe the conversion dependency of the autocatalytic decomposition reaction, the function $\dot{Q}(T,C)$ must be determined (C corresponds to conversion). The plane $\dot{Q}(T,C)$ is spanned by a simple linear interpolation of the derived kinetics for 0 % conversion (adiabatic-heat-pressure-accumulation test) and the worst-case kinetics (100 % conversion corresponds to -1500 J/g) (see Figure 8, projection $\dot{Q}(T,C)$ into the $\dot{Q}(T)$ plane). From a conservative safety point of view, it is assumed in the simulation that the maximum heat production rate is already reached at a released energy of -1000 J/g. As can be seen from Figure 7, the specific temperature- and conversion-dependent heat production rate used for the simulation is higher than the values determined in the DSCs. The following five parameters are therefore necessary in the description of the heat production rate $\dot{Q}(T, C)$: the description of the Arrhenius kinetics for 0 % conversion based on the adiabatic pressurized heat accumulation test with the pre-exponential factor $\dot{Q}_{0,0\%conversion}$ and the activation energy $E_{A,0\%conversion}$，the description of the Arrhenius kinetics for 100 % conversion (maximum autocatalysis) based on the isothermal DSCs with the pre-exponential factors $\dot{Q}_{0,100\%conversion}$ and the activation energy $E_{A,100\%conversion}$，as well as the value $Q_{max.\ autocatalysis}$ (here -1000 J/g) which describes the conversion dependency. The smaller $Q_{max.\ autocatalysis}$ is selected (see experimental data from the isothermal DSCs Figure 7), the more conservative the model is in terms of safety.

If wide extrapolations to low temperatures are necessary, additional isothermal microcalorimetric measurements, e.g. with TAM or C80, can be used as base point for a better model fit.
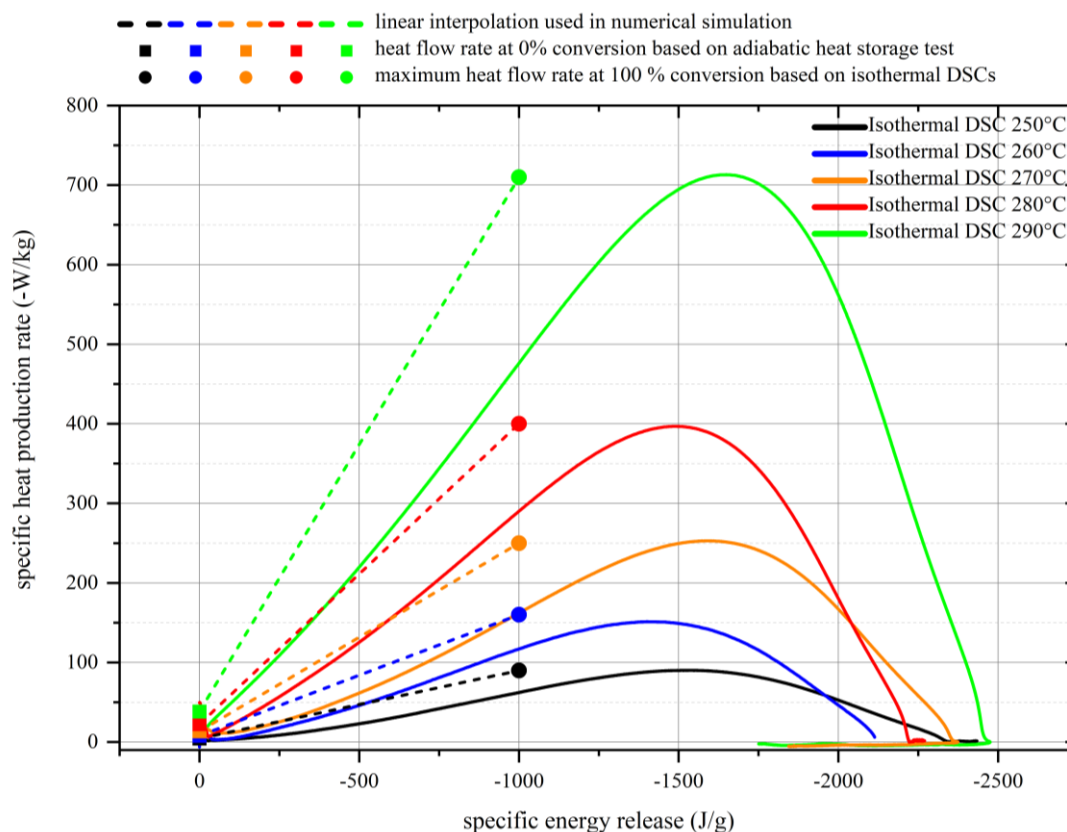
Figure 7. Derivation of the temperature- and conversion-dependent heat production rate based on isothermal DSCs and an adiabatic heat storage test

Based on this empirical kinetic model, the heat balance can be calculated numerically. The calculated adiabatic time-dependent temperature curve starting from 130 °C of the thermally unaged nitro aromatic compound is shown in Figure 8.
Without taking autocatalysis into account an adiabatic induction time of approx. 7500 hours (blue temperature curve Figure 9) is obtained. The adiabatic induction time based on the worst-case model results in an adiabatic induction time of 48 hours (orange temperature curve). Taking the dependency of the autocatalysis into account results in an adiabatic induction time of approx. 4300 hours.
The safety assessment of the storage of the nitro aromatic compound at 130 °C can be carried out on the basis of this adiabatic induction time of 4300 hours, e.g. taking into account the maximum residence time in the storage tank. If thermal aging takes place in upstream process steps at elevated temperatures, the adiabatic induction time for subsequent storage is reduced. These possible pre-aging processes or failure scenarios should be evaluated in a failure analysis. Based on the model presented, the effect of pre-aging on the adiabatic induction time can be taken into account without further experimental investigations.
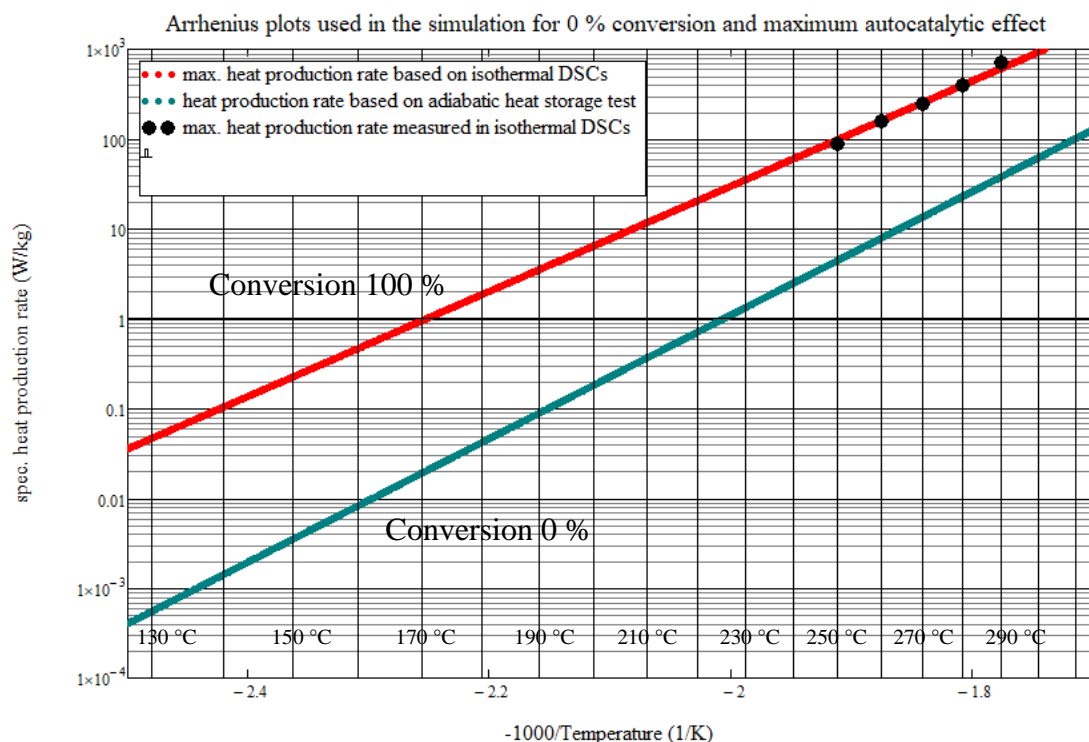
Figure 8. Arrhenius plots used in the simulation for 0 % conversion based on adiabatic testing and maximum autocatalytic effect based on isothermal DSCs. The conversion dependency of the heat production rate is described by a simple linear extrapolation at specific temperature between these Arrhenius plots (see explanation Figure 4)
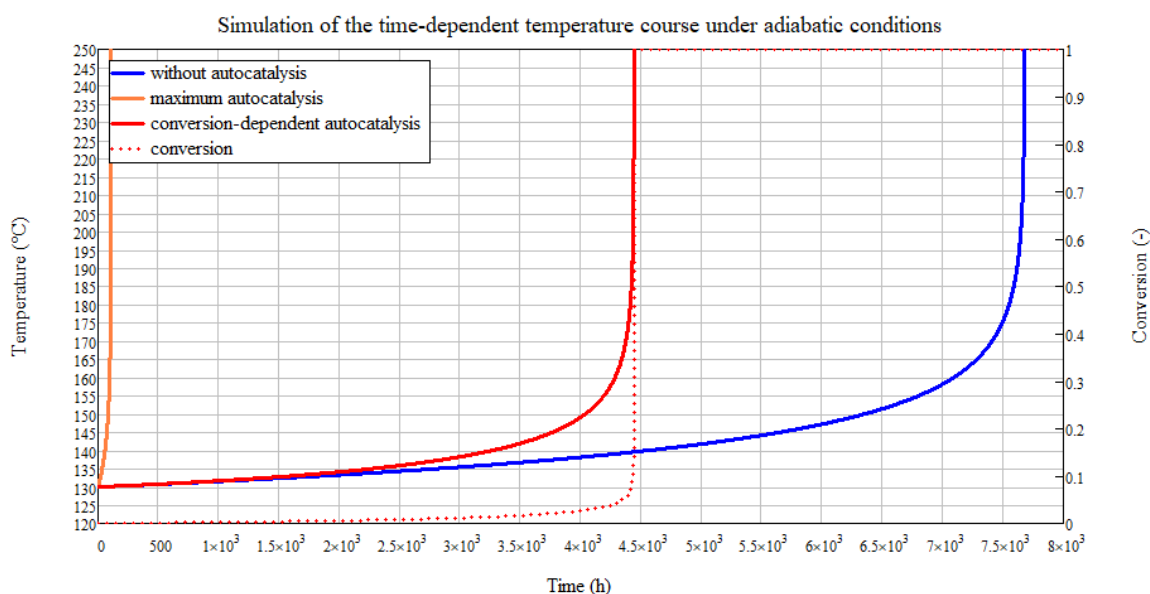
Figure 9. Numerical simulation under adiabatic conditions of the time-dependent temperature course with the detailed conversion dependent kinetics in comparison to the worst-case kinetics and the non-autocatalytic kinetics based on the adiabatic heat storage test

21

4. Conclusions and outlook

The presented empirical model approach for the description of weak autocatalytic decompositions enables a comprehensive safety assessment with a comparatively low experimental effort. This is made possible by the combination of isothermal DSC measurements and adiabatic calorimetry. The simple linear adjustment of the conversion dependency of the autocatalysis avoids the complex adjustment of a kinetic model. Simple numerical simulation can be used to calculate adiabatic induction times or induction times taking heat dissipation into account, on the basis of which the safety assessment of the process step can be carried out.

This was demonstrated using the example of a nitro-aromatic compound. Once the specific heat production rate $\dot{Q}(T,C)$ has been determined, the influence of increased ageing due to, for example, increased residence times caused by errors in operational processes, on the adiabatic induction times can be calculated using an adapted simulation.

Overall, it should be noted that autocatalytic systems react sensitively to impurities and varying compositions. The derived empirical kinetic model is only applicable to the specific sample composition investigated. This must be taken into account when planning experiments with regard to different sample compositions. In order to be able to identify critical samples, the use of isothermal DSC measurements is recommended, especially for autocatalytically decomposing compounds.

References

UN-Transportbook:
UN Recommendations on the Transport of Dangerous Goods: Manual of Tests and Criteria, Rev. 8 (2023) and UN-Model Regulations, Rev. 23 (2023)

VDI Guideline 2263, Part 1: "Dust fires and dust explosions; hazards, assessment, safety measures; safety related parameters of bulk goods." (2022)

TRAS 410: „Erkennen und Beherrschen exothermer chemischer Reaktionen"

F. Stoessel: Thermal Safety of Chemical Processes" by Francis Stoessel, Wiley-VCH (2020)

S. Kimpel, C. Hernandez, J. Horn, 2016: An Alternative Way to Determine the Self-Accelerating Decomposition Temperature by Using the Adiabatic Heat- Pressure Accumulation Test, Chemical Engineering Transactions. 48, 139-144

Th. Grewer, O. Klais: Exotherme Zersetzung — Untersuchung der charakteristischen Stoffeigenschaften, VDI-Verlag (1988)

Comparison of Silanes in UN O.2 Test for Liquid Oxidizer

Kroesche Christoph

Evonik Operations GmbH, 63457 Hanau, Germany

christoph.kroesche@evonik.com

1. Introduction

Decachlorotetrasilane, octachlortrisilane and hexachlorodisilane show false-positive results in the UN Test O.2. The cause of this unexpected result had been explained in former investigations (Kroesche, 2018; Kroesche, Budde, Malow, 2021). To clarify whether it is possible to obtain false-positive test results in this statutory and legally required test also with other silanes, representatives of different silanes were compared with each other. They showed the expected results in the UN Test O.2 (UN TDG, 2015), leading to the classification as "non-oxidizing". Based on investigations, it can be presumed that it is primarily the chlorosilanes with at least one polychlorinated Si-Si unit that cause false-positive results in the UN Test O.2 (Kroesche, 2024).

It is now being investigated whether the increase in pressure in the chlorinated silanes can be caused by released chlorine. In addition, it is examined in this investigation whether the classification results change if the resulting molar amount is taken into account for the evaluation instead of the used weight (=2.5g).

2. Methods

The UN Test O.2 describes in detail a method to test liquids for oxidizing properties (UN-TDG, 2015).

Basic principle: A substance will be assessed by comparing the relative oxidation strength with known oxidizing agents. Reference oxidizing agents are perchloric acid, aqueous sodium chlorate solution, and aqueous nitric acid, which are mixed with dried cellulose as the reference substance to be oxidized.

The equipment used and the preparatory measures taken for our investigations are described in detail in Kroesche, Budde, Malow, 2021 (including pictures).

Interestingly, chloropropyltrichlorosilane (Cl_3Si-$CH_2CH_2CH_2$-Cl) reacts faster with cellulose than does hexachlorodisiloxane Cl_3Si-O-$SiCl_3$, although intuitively, hexachlorodisiloxane was assumed to be the more reactive partner due to the higher Cl content. This indicates that other factors than electronegativity considerations may play a role here. However, it is also possible that this is a 'quantity effect': Since, according to the specification, 2.5 g of the substance to be examined is always used, 12 mmol chloropropyltrichlorosilane (MM 212) or 9 mmol hexachlorodisiloxane (MM 285) react with the cellulose.

Increasing the amount of cellulose from 2.5 g to 5 g without a test substance roughly halves the pressure increase time (since twice the amount of combustion gases should be formed). This shows that the reference substance itself also contributes to the pressure increase. However, it can also be seen that, compared to cellulose, hexamethyldisilane and hexamethylsiloxane have a 'phlegmatisation' effect on the reaction.

As expected, of the substances examined, hexamethyldisiloxane has the lowest rate of pressure increase.

3. Results and discussion
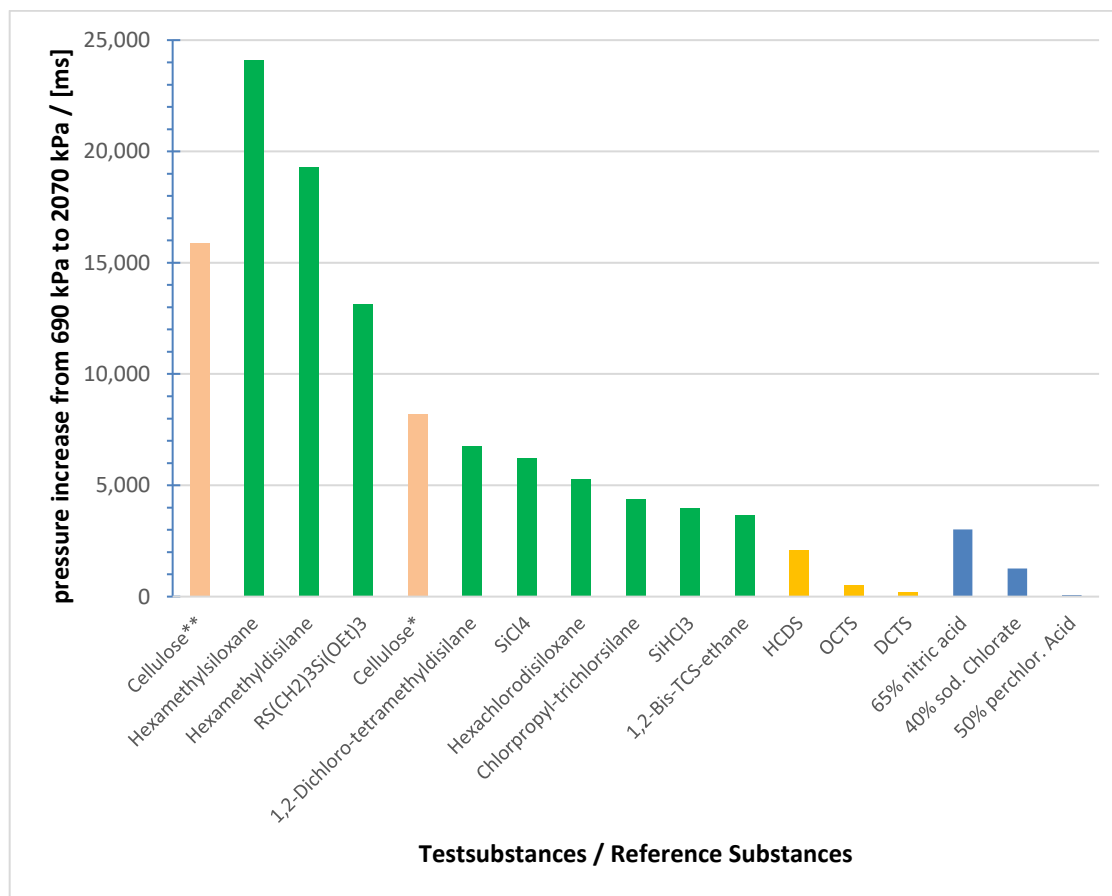
*Figure 1. Graphical illustration of the mean pressure increase time from UN Test O.2 for the reference substances and the silanes (Kroesche et al. 2021; Kroesche 2024); *pure cellulose (5g, single measurement, filled in air), **pure cellulose (2.5g, single measurement, filled in air)*

From a hazardous goods point of view, it is of course sensible to analyze a defined substance weight. To perform mechanistic observations, however, it is a disadvantage of this test specification that 2.5 g of test substance are examined by default – regardless of the molar mass introduced. For the silanes examined, molar quantities over a range from 5 mmol (DCTS) to 18 mmol (SiHCl$_3$) are used.
However, a mathematical consideration of the molar mass used (exemplary calculation: see Table 1) does not significantly change the relative order of the substances (Fig 2).

Table 1: Exemplary calculation to compare the relative reactivity with regard to the molar masses (the division by 100 was only done for reasons of clarity)

	DCTS	OCTS	SiHCl3	HCDS
dp / [ms]	220	531	3987	2106
MM [Da]	467	368	136	269
2.5g=[mol]	0.005	0,007	0.018	0.009
[ms/mol]	41096	78163	216095	226521
./.100	411	782	2161	2265

Only the trichlorosilane would be strongly shifted in the direction of the pressure increase rate of HCDS. Tetrachlorosilane cannot be oxidised because the silicon atom already has the maximum possible oxidation state for silicon. The high reactivity of tri- and tetrachlorosilane with nucleophiles (such as the cellulose here) is well known. This explains the rapid pressure increase for $SiCl_4$ and $SiHCl_3$. This is caused by the significantly higher amount of trichlorosilane used. The effect is further enhanced by the high molar excess of trichlorosilane used.
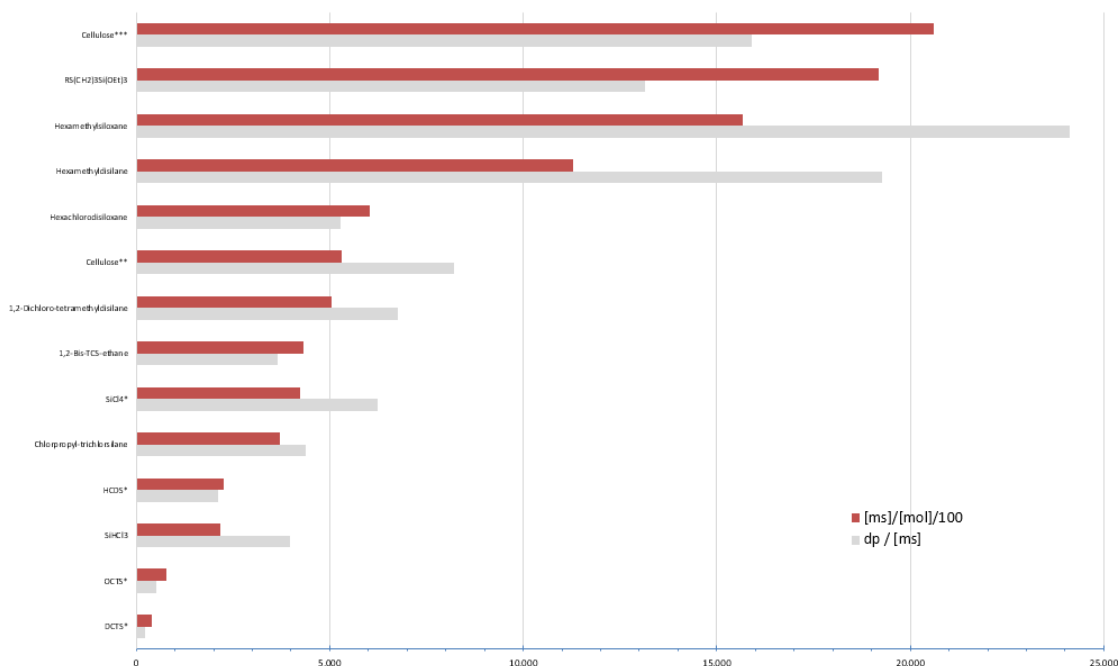
Figure 2. Overview of average rates of pressure increase (690 kPa to 2070 kPa in [ms]/[mol]/100]) in relation to the <u>molar</u> mass used instead of 2.5g weight. Grey shaded barrows dp/[ms]: data from fig. 1.

It is possible to wonder if the increase in pressure of the substances containing chlorine is caused by the release of HCl gas.

Since 2.5 g of the substance is used for the test as specified, the molar amount of HCDS (9 mmol) introduced into the reactor decreases in relation to DCTS (5 mmol) (due to the increasing molar mass), and thus the maximum stoichiometrically possible amount of HCl that can be released also decreases. The measurements show that the rate of pressure increase increases from HCDS to DCTS (Fig 3).
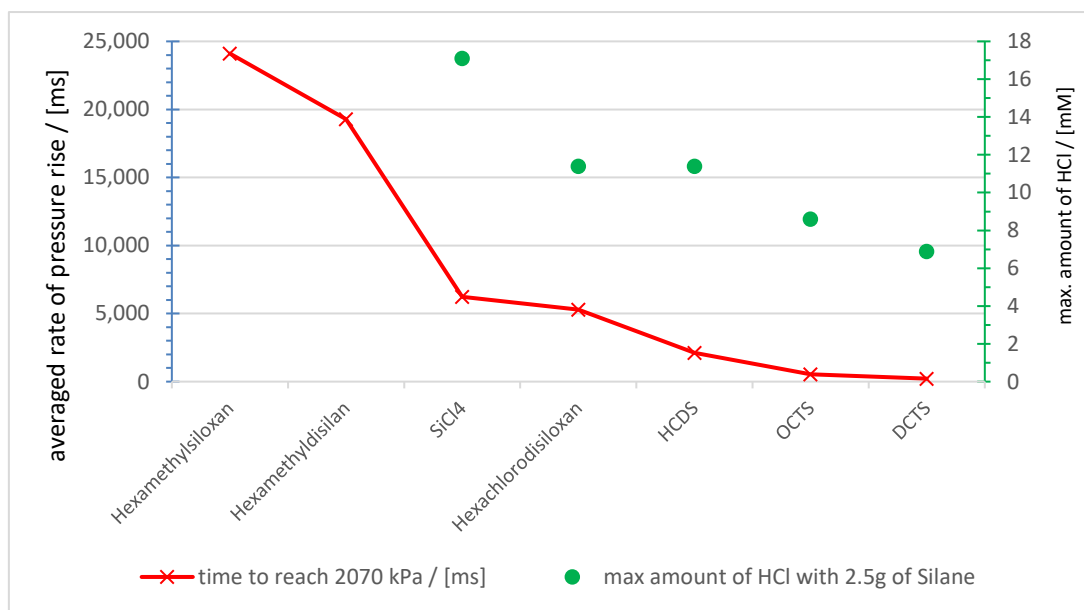
Figure 3. Stoichiometric max. releasable amount of HCl / [mM]. Hexachlorodisiloxane/HCDS: approximately the same maximum releasable amount of HCl, but double the rate of increase of pressure

Hexachlorodisiloxane and hexachlorodisilane (HCDS) can release approximately the same maximum amount of HCl, but the rate of pressure increase is about twice as fast for HCDS as for hexachlorodisiloxane (9 mmol) (Fig. 3). This means that it can be ruled out that the increasing rate of pressure increase is related to the amount of HCl released.

Therefore, the idea that the pressure increase could be caused by HCl formation was rejected.

4. Conclusions

The most important result for handling and transportation in industry is that all silanes investigated were outside the classification threshold for packing group III and classified as "non-oxidizing liquids". Thus all silanes produced the expected result of "non-oxidizing" as required by the theory.

To 'round off' these investigations, silicon powder was examined for possible oxidative properties in both the UN O.1 and UN O.3 tests. In both tests, the result 'not oxidising' was also obtained (EVONIK, 2021).

It can be shown that the pressure increase in the case of the chlorosilanes is not caused by the released chlorine.

The reaction residues were investigated in order to draw conclusions about basic mechanisms. But evaluation by IR, Raman and XPS was not possible, due to the mostly highly heterogeneous reactor reactions.

References

EVONIK 2021. Research-Project on Higher Polychlorosilanes (2015-2021). Unpublished results.

Kroesche, C., 2018. 9th European Silicon Days, Saarbrücken, Germany.

Kroesche, C., Budde, K., Malow, M., 2021. False-positive results of UN test O.2 liquid oxidizer test of polychlorosilanes. Journal of Loss Prevention in the Process Industries, Volume 70, May 2021, 104434; doi.org/10.1016/j.jlp.2021.104434

Kroesche, C, 2024. Comparative investigations of silanes in UN Test O.2 (liquid oxidizer). Results in Chemistry, Volume 10, 2024, 101686, https://doi.org/10.1016/j.rechem.2024.101686.

UN-TDG, 2015. UN Recommendations on the Transport of Dangerous Goods, Manual of Tests & Criteria (6th revised ed.). New York and Geneva: United Nations. Section 34, CLASSIFICATION PROCEDURES; TEST METHODS AND CRITERIA RELATING TO OXIDISING SUBSTANCES OF DIVISION 5.1.

Proposals for Improvements of the UN O.2 Test for Liquid Oxidizer

Matthias Vorwinkel, Christoph Kroesche *

Evonik Operations GmbH, 63457 Hanau, Germany

*christoph.kroesche@evonik.com

1. Introduction

Decachlorotetrasilane, octachlortrisilane and hexachlorodisilane show false-positive results in the UN Test O.2 (liquid oxidizer). The cause of this unexpected result had been explained in former investigations (Kroesche, Budde, Malow, 2021).

To clarify whether it is possible to obtain false-positive test results in this statutory and legally required test also with other silanes, different silanes were compared with each other. The focus was on investigating chlorinated silanes. All silanes produced the expected result "non-oxidizing liquid" as required by the theory showing that the international UN O.2 test for other silanes gives reliable results (Kroesche, 2024).

Nevertheless, while investigating the oxidative properties of these silanes, we discovered some shortcomings of this important UN O.2 test.

Here we describe some of the disadvantages observed and propose possible ways to overcome these disadvantages to improve the UN O.2 test.

2. Methods

The UN Test O.2 describes in detail a method to test liquids for oxidizing properties (UN-TDG, 2015). A substance will be assessed by comparing the relative oxidation strength with known oxidizing agents. Reference oxidizing agents are perchloric acid, aqueous sodium chlorate solution, and aqueous nitric acid, which are mixed with dried cellulose as the reference substance to be oxidized. For the experiments, a pressure vessel with specified dimensions is used (you can find a description of the test procedure used for silanes and a photo of the vessel in Kroesche et al., 2021). The vessel is equipped with a rupture disk, a pressure transducer, and an ignition device.

The mixture of the respective test substance with cellulose or the individual reference substances with cellulose are placed in the pressure vessel. When the ignition source is activated, the time required for the pressure to change from 690 kPa to 2070 kPa is measured.

Ignition wire used: CHRONITHERM 80/20 (Ni/Cr; 0,6 mm; 3,885 Ohm/m [manufacturer's information]; Fa Thyssen, Germany)

Cellulose: Technocel 75; before being used, the cellulose was dried for 8 h at 105 °C; residual moisture content: ≤0.15%.

3. Results and discussion

While investigating the oxidative properties of silanes using the UN O.2 Test we discovered some shortcomings of this important test.

Time and again, the ignition wire melted through getting no test result (Fig. 1).
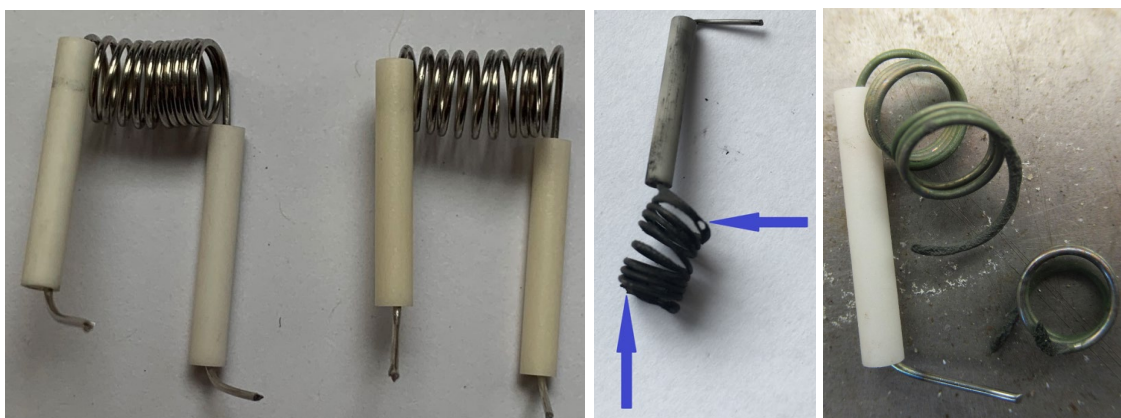
Fig. 1. Left: newly manufactured spirally wound wire. Right: wire that melted (without substance contact) and broke during the test (far right)

It is easy to see in the pictures that even the unused, new wire spirals show different windings. As a rule, without coming into contact any material, the free coils (Fig. 3) can withstand several minutes and a few heating/cooling cycles. Sometimes, however, the filaments melt after about 20-40 seconds even without contact with the material (see picture on the right: breakage in two places (see arrows). According to our observations, the filaments typically break at the point of contact between the ceramic sleeve and the filament. We propose the authorization of alternative wire materials for the test standard and not only Ni/Cr(80/20) (more corrosion-resistant metals like high Ni alloys, thicker wire diameter).

Some residues of the same silane/cellulose mixtures showed great visual differences in some silanes (Fig. 2a) indicating an inhomogeneous reaction.

Fig. 2a. Visual differences of reaction residues of the same silane/cellulose mixture in different test runs (here shown: reaction residue hexamethyldisilane/cellulose)
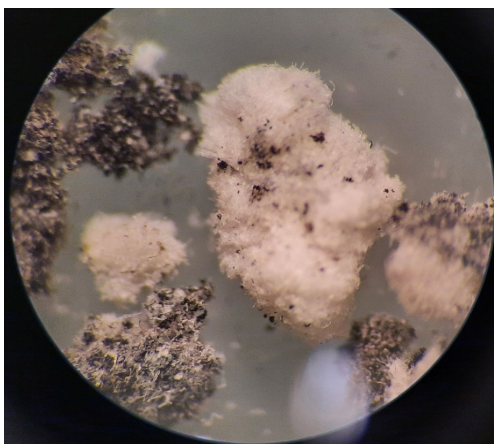
Fig 2b. Light microscopic image of a reaction mixture. The large amounts of unreacted cellulose are easily recognizable.

In our interpretation this is e.g. attributed to varying contact intensity between the spiral-wound filament and the reaction mixture because the reaction mixture of cellulose and liquid silane no longer flows freely and is not always distributed around the filament to the same extent resulting in varying contact intensity between the spiral-wound filament and the reaction mixture. These measurements showing >30% deviation from the mean (according to the legal text) cannot be evaluated and should be disregarded, resulting in laborious repeat tests. This effect could be reduced by using a larger-coiled wire and we suggest the admission of straight wires, without spiral winding (Fig. 3a).
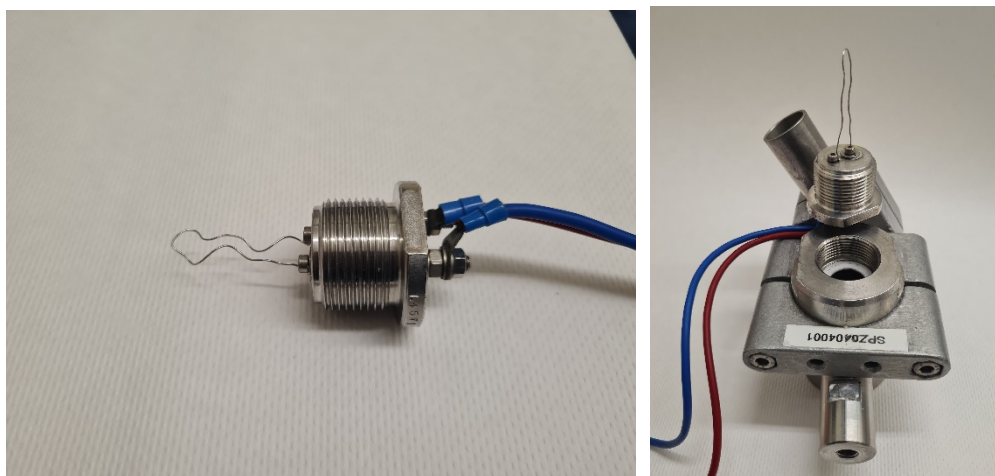
Figure 3a. The ignition wire holder removed from the reactor (right). Ignition wires with a less complex shape than a helix wound wire (left).

Investigations of the temperature of the spiral-wound wire showed no single temperature but a gradient of temperature within and the outer parts of the spiral, subsequently resulting in different heat flow distribution (Fig. 3b, 4).
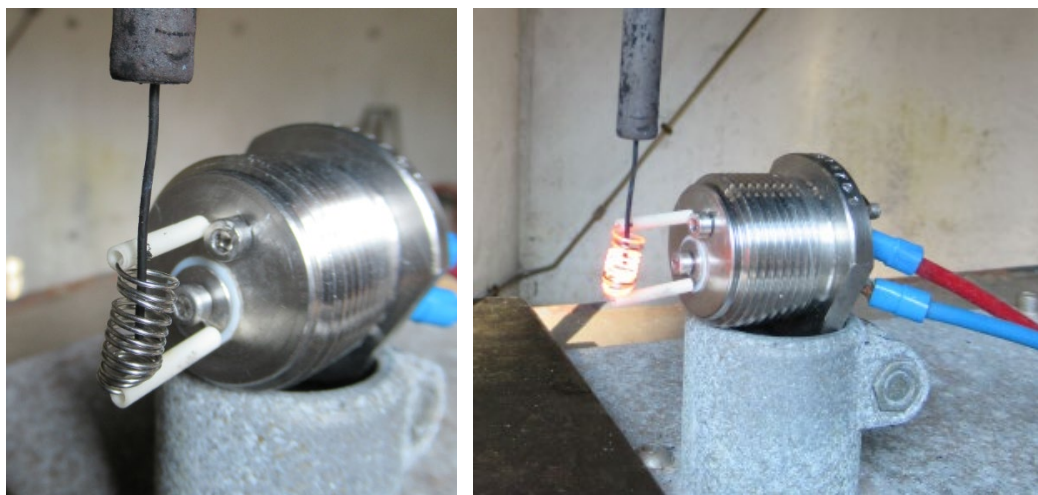
Figure 3b. Removed ignition wire bracket with temperature sensor inserted in the centre of the helix (left). Shortest distance between wire and temperature sensor (PT100): ca. 1mm. Glowing wire (10 Ampere current flow) (right)
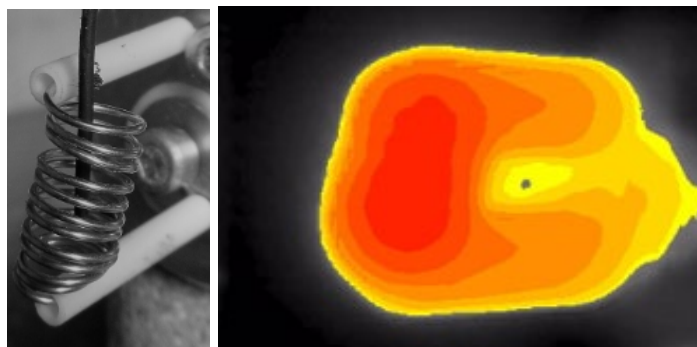
Fig. 4. Photo of the heat flow distribution in the spiral-wound ignition wire (thermal imaging camera). After approx. 18 sec a maximum temperature of 950-980°C was reached in the inner part of the spiral. The outside surface of the wire showed a temperature of around 750°C. In the measurement set-up shown above, a temperature of 300°C after ca 1.5 sec, and 500°C was measured after ca 2.5 sec in 3 tests. Typically, the reaction rates of the oxidation reactions in UNO.2 test system are <5 sec.

The different temperatures inside the pressure vessel are considered to be an additional source of different reaction progressions and incomplete reactions. Here, too, ignition wires with a less complex shape could be advantageous (Fig. 3a).

The UN Test O.2 in its current form ("modified time/pressure test") was established in the 1990s by the Energetic and Oxidizing Substances Working Group (EOS) of the OECD and the Committee of Experts on the Transport of Dangerous Goods of the UN. The focus of the investigation consisted in reactor design, comparative substances, test conditions, method standardization, etc. At that time, the igniter wire was selected from standard igniter wires for heating elements, mainly because of ready availability (Wildner, 2021). Up to now, only little literature in the public domain refers to investigations that look into possible factors influencing the UN test. Important findings were obtained by a major interlaboratory test and detailed statistical evaluation, under the auspices of the Federal Institute for Materials Research and Testing (BAM), Germany (Antoni et al. 2011). Accordingly, the igniter wire was already identified as a factor influencing the pressure increase times. Therefore, we are the opinion that alternative wire materials should be investigated e.g. larger diameter and adjusted current to achieve the required power, and wires made of materials other than NiCr 80/20. This would be an additional advantage in case corrosive intermediates are generated leading to broken wires (Fig. 1)

The required test material to be used according UN TDG (2015) is cellulose as reference testing substance to be oxidized. As shown earlier (Kroesche, Budde, Malow 2021; Kroesche, 2024) it is very difficult to analyze the test residue by e.g. IR- Raman- and XPS-spectroscopy as the residue of the cellulose interfere strongly with the residues of the investigated substance.
Alternatives to the prescribed cellulose should be considered (e.g. activated carbon) if it is necessary to analyze reaction residues (e.g. for an expert judgement as described in the manual), analysis in the presence of cellulose is extremely difficult (strong bands in IR/Raman, impossible evaluation of XPS signals in the carbon-range due to the reaction products of the cellulose. In cases cellulose is an unsuitable material we propose as alternative reference material to establish activated carbon. During the reaction carbon is reacting to carbon dioxide or carbon monoxide no longer influencing any solid state analysis. And, possibly not converted activated carbon is IR-inactive and thus does not complicate the IR spectra evaluation.

4. Conclusions

The UN O.2 test is characterized by relatively large fluctuations in the measurement results (deviations of up to 30% from the mean value of a quintuple measurement are permissible). We assume that the adjustments will also reduce the range of fluctuation of test series and will save the time to repeat test multiple times. We suggest the following points be investigated and updating the UN O.2 test accordingly.

Investigating the influence of winding technology for the wire (larger radius or shorter wire to avoid contact points; using a wire template, better 'flow around' of the helix with cellulose moistened with test substance)

We suggest checking a non-helical, straight, shorter taut wire

Use a thicker wire for the same (or even higher) electrical power (reduced melting of the wire; in the event of possible corrosion reactions: melting of the wire then takes longer → *one commercial laboratory is already doing this and getting more stable results)*

To be checked: is a higher temperature of the wire advantageous?

Check and authorize alternative, additional wire qualities to avoid reaction with the wire in case of corrosive substances or intermediates and thicker wires to reduce premature melting (e.g. high Ni-alloys in case of deliberated HCl)

Approval of (e.g.) activated carbon as an alternative to cellulose to simplify analysis of the reaction residue (oxidation tests with activated carbon instead of cellulose and reference oxidizer already carried out: Kroesche, Budde, Malow, 2021)

Acknowledgments

References

Antoni, S., Kunath, K., Lüth, P., Simon, K., Uhlig, S., 2011. "Evaluation of the interlaboratory test on the method UN O.2 / / EC A.21 - Test for Oxidising liquids", Final Report 31.10.2011; Ed. BAM – Federal Institute for Materials Research and Testing, Berlin, Germany

Kroesche, C., Budde, K., Malow, M., 2021. False-positive results of UN test O.2 liquid oxidizer test of polychlorosilanes. Journal of Loss Prevention in the Process Industries, Volume 70, May 2021, 104434; doi.org/10.1016/j.jlp.2021.104434

Kroesche, C, 2024. Comparative investigations of silanes in UN Test O.2 (liquid oxidizer). Results in Chemistry, Volume 10, 2024, 101686, https://doi.org/10.1016/j.rechem.2024.101686.

UN-TDG, 2015. UN Recommendations on the Transport of Dangerous Goods, Manual of Tests & Criteria (6th revised ed.). New York and Geneva: United Nations. Section 34, CLASSIFICATION PROCEDURES; TEST METHODS AND CRITERIA RELATING TO OXIDISING SUBSTANCES OF DIVISION 5.1.

Wildner, W. 2021. Personal Communication. Former Member of Committee of Experts on the Transport of Dangerous Goods for DEGUSSA AG, Deutschland at UN & OECD-IGUS

Risk Assessment and Consequences Analysis of Accidental Release of Natural Gas in Pipelines by using ALOHA

Nilambar Bariha[1,2,*], Vimal Chandra Srivastava[1], Indra Mani Mishra[1,3]

[1]Department of Chemical Engineering, Indian Institute of Technology Roorkee, Roorkee- 247667, Uttarakhand, India

[2]Assam Energy Institute Sivasagar, Centre of Rajiv Gandhi Institute of Petroleum Technology, Sivasagar- 785697, Assam, India

[3]Department of Chemical Engineering, Indian Institute of Technology (Indian School of Mines), Dhanbad, Dhanbad- 826004, Jharkhand, India

nilambarbariha@gmail.com; vimalcsr@yahoo.co.in (VCS);

immishra49@gmail.com

Introduction

Natural gas is mainly composed of methane which is colorless, odorless and non-toxic gas. It is a wide variation in its composition, depending upon the production source, the level of pretreatment of the gas and the requirements of the end-use. It plays an important role for energy transmission in the field of infrastructure in every country. The composition and properties of natural gas produced from various sources and marketed by various companies in India are shown in Table 1.

Table 1. Typical Composition of natural gas in India.

Components (mol %)	Oil well source unrefined	Refined natural gas with refined	Transport sector	ONGC/GAIL		
				Refined NG	CNG	LNG
Methane (CH_4)	70-90%	85-96.7%	88%	70-100%	82-94%	89.7%
Ethane (C_2H_6)		1.9-8.6%	6%		3-6%	6.1%
Propane (C_3H_8)	0-20%	0.68-4.1%	1.7%	20%	0.1-0.2%	2.35%
Butane (C_4H_{10})		3%	0.3%		0.1-0.7%	1.49%
Pentane (C_5H_{12})	-	-	-		0.1-0.2%	0.06%
Carbon dioxide (CO_2)	0-8%	0.1%	4.5%	0-8%	< 10	-
Oxygen (O_2)	0-0.2%	-		-	-	-
Nitrogen (N_2)	0-5%	0-0.40%		0-1%	< 15	0.22
Hydrogen Sulfide (H_2S)	0-5%	0-0.15%	-	< 5		< 5
Carbon monoxide (CO)	-	-	0.1%	-	-	-
Hydrogen (H_2)	-	-	0.1%	-	-	-
Rare gases (Trace)	Argon, Helium, Neon, etc.	Helium	-	0.2%	0-0.2%	-

Source:[http://www.naturalgas.org/overview/background.asp;

http://petrofed.winwinhosting.net/upload/LNG.pdf;http://www.arb.ca.gov/fuels/altfuels/gti.ppt;

http://petrofed.winwinhosting.net/upload/IAI/17-20mar10/GasProcessing&Valueaddedproducts.pdf]

The NG pipeline networks are laid down in underground it is passes through residential areas, where more safety concerns are needed. Today, the natural gas covers ~40% of

energy requirement in India, with a consumption of ~189 million standard cubic feet per day (MMSCMD). India has a pipeline network of ~23,391 km length operational with 11,615 km length of the gas pipeline to be commissioned by 2025 [NSG, 2024]. Gas transport under compressed mode is very convenient, safe and environment-friendly, and requires much lower maintenance and house-keeping than any other mode of transport. The failure of the gas pipeline leading to leakage and accidents during transmission is generally caused by such factors as corrosion, material and construction defects, damages from external natural causes (such as earthquakes, flood, landslides, etc.), third party intentional/ non-intentional damage, and operator error. NG pipeline incidents occurred due to leakage that affected the production as well as environmental impact [Bi et al., 2022]. These accidents are having potential to pose risks in terms of life and property safety in urban areas [Scasta et al., 2023]. In this study, the leakage and rupture of NG pipeline that occurred in Nagaram, India, on June 27, 2014, it was taken considered for analysis of detailed hazards and risks in urban areas. The release of the gas flowing under pressure (~49 bar) and at about 20°C created a gas cloud with water condensate mist. It would be exploring the various factors responsible for leading to the incident's consequences, including type, injury, fatality, and environment affected. Fire or explosion and dispersion of vapor cloud NG were calculated by using ALOHA software, and risk assessment was done by hazard identification and risk assessment (HIRA) for future suppression of hazards.
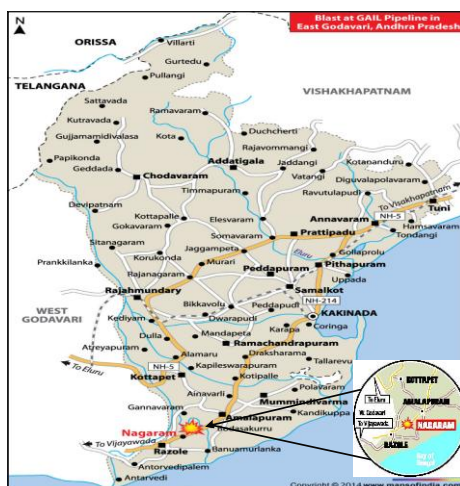
Figure 1. Map shows the natural gas pipeline accident has taken place in East Godavari, Andra Pradesh (India).

Fig.1 shows the accident site on the truncated map, where an accident, took place at about 06:00 AM on 27th June, 2014. The accident took place on a pipeline, in the village Nagaram, in the state of Andhra Pradesh, India. The pipeline was carrying 0.7 million cum per day of natural gas. This ~200 km long pipeline, which was laid in the year 2001, connects the gas treatment plant located at Tatipaka, District East Godavari and the Lenko's gas-based thermal power plant at Kondapalli, District Vijawada, in the State of Andhra Pradesh. It was reported that a number of gas leaks occurred from this pipeline over the years. Around 7-8 leakage incidents have been recorded by the investigating team. The pipeline was reported to be prone to corrosion because of H_2S and water moisture in the gas. The corrosion was detected, about three years before this accident happened, during an inspection of the pipeline. It was, then, recommended to use a corrosion inhibitor to prevent further corrosion of the pipeline. It seems that either no action was taken, or the action taken for the repair of the pipeline, corrosion control, etc. was inadequate to meet the standards of the pipeline

integrity. Therefore, the disaster of such a magnitude was waiting to happen [http://timesofindia.indiatimes.com/india/Nagaram-blast-Probe-nails-GAIL-says-it-ignored-disaster-warnings/articleshow/39775714.cms].

ALOHA software was used to develop the consequences of natural gas pipeline failure scenarios and the estimation of gas release scenarios from crack formation of small leaks leading to pipeline rupture. Two conditions are modelled in this work: (i) leakage of gas from a crack/small sized hole, and (ii) full bore rupture of natural gas pipeline. Modelling and simulation scenarios were discussing that the gas concentration buildup due to leakage, ignition, explosion, rupture, and jet fire. Since the gas pressure in the pipeline decreases with the time of release of the gas, the release rate also decreases with a decrease in the gas pressure. The release rate also depends on the crack/hole size. Calculations were made for three-hole sizes, namely 1mm, 5mm and 50 mm and the gas pressure decreasing from 48 bar to zero bar. To find out the release rate, thermal radiation from jet fire, the probit values and the fatalities likely to occur at the corresponding damage distances. The damage distance of jet fire can be evaluated by simply as follows by using the above equations. The probability of fatalities due the release rate of gas as 99%, 50% and 1% respectively are shown in Fig. 2 (a), (b) and (c) which are corresponding probit values of 7.33, 5 and 2.67.

(a) d_0 = 5 mm
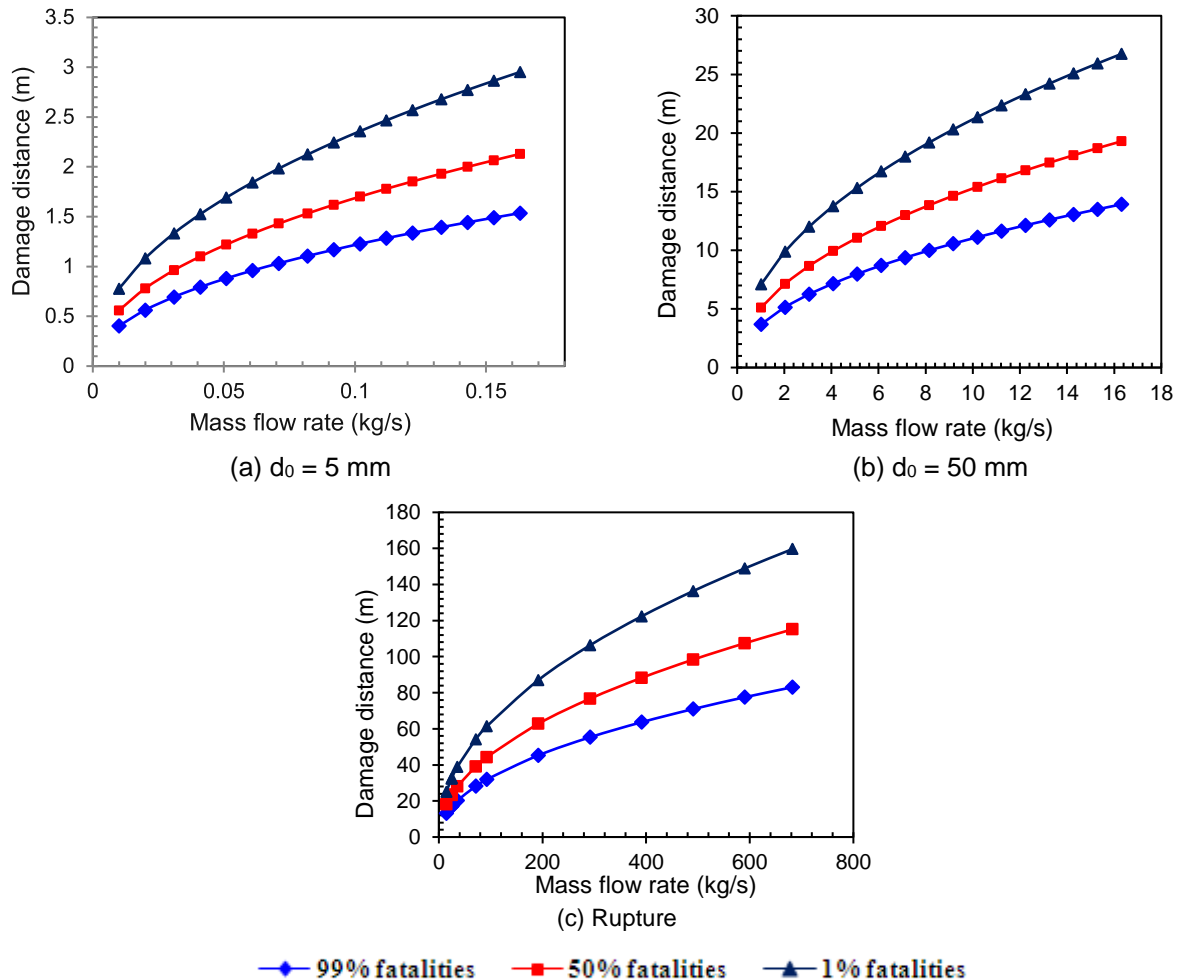
(b) d_0 = 50 mm

(c) Rupture

Figure 2. Damage distances of jet fire with release of natural gas (a) small leakage (d_0 =5 mm), (b) medium leakage (d_0 = 50 mm), and (c) full bore rupture (d = 0.457 m) of pipeline.

In Fig. 2(a) shows the damage distance of jet fire with the release of natural gas from the crack/hole/rupture of the pipeline. The maximum release of natural gas is 0.16 kg/s at a pressure of 49 bar with the 99% fatalities up to 1.54 m radial distance from the release point. At 2.13 m radial distance, 50% fatalities may occur, whereas the 1% fatalities can occur up to 2.95 m radial distance from the release point. Fig. 2(b) shows the release of the gas from the medium hole size of 50 mm and the damage distance. The maximum release of natural gas from the hole size is 16.32 kg/s at a pressure of 49 bar with the 99% fatalities in the radial distance of 13.92 m from the release point. 50% fatalities can occur at 19.29 m radial distance where as 1% fatalities may occur up to 26.75 m radial distance from the release point. Fig. 2(c) shows the release rate and the damage distance in case of full-bore rupture of the pipe. With the maximum release of natural gas at a rate of 682.30 kg/s at 49 bar pressure may cause 99% fatalities up to 83.06 m from the release point. 50% and 1% fatalities may occur up to a distance of 115.15 m and 159.62 m respectively from the release point. Fig. 2(c) shows the actual mass flow rate at the time of full-bore rupture that affects the radial distance of ~160 m from the source point.

It has been reported that 22 people died because of severe burns in an area within 228 m radius around the accident site. Six persons received extensive burns (70-100% total body surface area burns) at a distance of about 64-90 m from the site. The coordinates of the natural gas pipeline failure point are taken as 16° 30´ 3.98´´N and 81° 54´ 38.62´´S. The simulated results of ALOHA are shown in Fig. 3 (a) for a small leak in the pipeline. The red circle shows the thermal intensity of 37.5 kW/m^2 is about 12 m, whereas the orange circle gives the results of thermal intensity of 12.5 kW/m^2, which is 21 m away from the failure point. If the person received second degree burn injuries in the yellow circle, the thermal intensity of 5 kW/m^2 is formed up to 32 m away from the failure point. Fig. 3 (b) shows the simulated results of rupture in natural gas pipeline. The red circle shows the thermal intensity of 37.5 kW/m^2 is upto about 10 m. All persons within this circle will die at the flux for 30 s. The Google Earth image shows the area that some houses and coconut trees come within the range of 10 m radius. The property will also be damaged severely and the vegetation will turn into ashes. The orange circle shows the thermal intensity of 12.5 kW/m^2 at a radius of 47 m, which may cause 1st degree severe burn injuries to those people who could not move away from the failure point. The yellow circle shows the thermal intensity of 5 kW/m^2, spread over 85 m radius which may cause second degree burn injuries to people in the area. The vegetation may get burnt.

| (a) | (b) |

Figure 3. Simulated results (ALOHA) of thermal radiation with the damage distances of jet fire with release of natural gas (a) small leakage (d$_h$ = 0.05 m) and (b) full bore rupture (d = 0.45 m) of pipeline.

In this paper, it provides the description of an accidental release of natural gas due to corrosion in pipeline, during the transportation of natural gas from the gas station that have been analysis the consequences of hazards/risks after the releases with their effects on the

population. The consequence models are simulated in ALOHA and validate with the models available in the literature. Simulation results including the number of fatalities, damages to the property, and the impact on environment of hazards parameters (fire and explosion) generated after the accident of some physical parameter thermal radiation, overpressure, etc. are significance of the presented work. The simulation shows an area of about 90-150 m radius were badly affected which corresponds to actual loss of life and property verified from the ground data. Considering the results acquired from the present study, the following recommendations can be drawn to aware and safety measures reduces such incident for the future:

1. Preventive measures should be taken to avoid corrosion because it diminishes the thickness of natural gas pipeline and reduces the life of transportation.

2. The natural gas pipelines must be quarterly or half yearly examined and certification should be mandatory certificates issued.

3. The minimum distance of natural gas pipelines is maintained from the populated areas.

4. Warning signs such as "No Smoking", "No Fire Burning", etc. are installed/with the minimum safety distance near the natural gas pipeline.

Reference

http://www.naturalgas.org/overview/background.asp; accessed 15 June 2019

http://petrofed.winwinhosting.net/upload/LNG.pdf; accessed 15 June 2019

http://www.arb.ca.gov/fuels/altfuels/gti.ppt; accessed 04 July 2019

http://petrofed.winwinhosting.net/upload/IAI/17-20mar10/GasProcessing&Valueaddedproducts.pdf   accessed 04 July 2019

Gas Statistics Review, Natural Gas Society, July 2024. https://ngsindia.org accessed 10 August 2024

http://timesofindia.indiatimes.com/india/Nagaram-blast-Probe-nails-GAIL-says-it-ignored-disaster-warnings/articleshow/39775714.cms accessed 21 March 2019

Bi, H., Shen, S., Wang, K., Tian, L., Zhang, Q., Shao, H. 2022. Influence of different opening conditions on explosion consequence in a LPG transmission pipeline. Energy Sources, Part A: Recovery, 44(4): 9649-9662. https://doi.org/10.1080/15567036.2022.2136795

Scasta, J.D., Leverkus, S., Tisseur, D. S., Leverkus, G. 2023. Vegetation response to a natural gas pipeline rupture fire in Canada's montane cordillera, Energy, Ecology and Environment, 1-14. https://link.springer.com/article/10.1007/s40974-023-00287-4

Process Safety and Cyber Factors in the Recent Operating Experience at Italian Seveso Sites

Paolo Bragatto [1], Patrizia Agnello [2], Silvia Ansaldi [2] and Roberto Setola[1]

1 Università Campus Bio-Medico. Via Álvaro del Portillo, 21, 00128 Roma
2 Inail – DIT via Fontana Candida, 1 00078 Monteporzio Catone RM Italia
p.bragatto@unicampus.it

1. Introduction

Operational technology systems (OT) refer to the hardware and software used to monitor, manage and control operations like distributed control systems DCS, programmable logic controllers PLC, sensors, and robotics. On the other side, Information Technology systems (IT) are the technological infrastructure handling an organization's data and information-related functions like email, finance and Human Resource. The issue of worker and environmental safety was, consequently, based on OT performance, while the IT part marginally influenced just the management aspects of safety. OT and IT systems in the process industries, were traditionally operated in insulation with separate technology, protocols and organizational units. In the last decade, however, with the Fourth Industrial Revolution and increases in industrial internet of thing (IIoT), OT and IT are integrating more and more. That is assumed to provide large benefits for the profitability, reliability and safety. Unfortunately, the tight integration between OT and IT introduces new risks related to, but not limited to, cybersecurity aspects. In the process industries, these issues are not only about the loss of valuable data or the disclosure of confidential information, but can also compromise control and regulation systems and potentially lead to containment losses, with the release of hazardous substances with related consequences for workers, the environment and assets. This is an emerging risk and it is therefore important to have more numerous and reliable data to monitor the scenario and understand the true extent of the phenomenon in order to define concrete indications to manage the risk well in advance. At the moment there is still little data available, in fact just early warnings rather than clear evidence, but it is important to collect this data, organize the information and extract knowledge that can be useful for those who have to make decisions. In the scientific literature there are some reviews, here are two that have appeared recently: the first (Stergiopoulos et al. 2020) concerns only oil & gas 42 events, between upstream, midstream and downstream. Half with serious consequences Most frequent attacks: Malware and external phishing; Injection Internal. Impact on control logic, availability and property. 10 cascade consequences with major losses. The second review (Iaiani et al. 2021) covers various industries and covers 82 cases. 35 events are accidental, 47 intentional. In estrema sintesi si può dire che a good cyber risk assessment is nowadays a matter of paramount importance for process industries (Nobili et al. 2023) and, in particular, for the establishments under the European Directive Seveso III for the control of major accident hazard.

2. Methods

For this purpose, it is important to continuously gather data about anomalies, near-misses and minor accidents that occur in the operation of the plants and related with cyberspace events. A good source of information comes from INAIL/ EsOpIA, a repository containing

over six thousand reports of accidents and near misses diligently collected in the last twenty years during inspections at the approximately one thousand Seveso plants in Italy. In this archive some 6000 events are collected (Ansaldi et al. 2021). Exploiting such unique repository, we are able to investigate how many events can be traced back to cyber problems. The study discriminates accidents due to hostile intentions and unintentional ones. Among the latter, criticalities are due, in particular, to the poor quality of the software, the unreliability of the hardware, the inadequate management of access, the negligence of the operators and the sloppiness of the operators.

The documents available in the INAIL/EsOpIA repository are of different quality and the causal relationship is not always well described, but the use of machine learning methods makes it possible to extract information that is not so evident to a direct reading. In this way it is possible to build a credible causal model of potential cyber triggered incidents.

For a broader comparison, incidents and accidents reported in another accident databases, including the French Barpi/ARIA and the European eMars.

3. Results

3.1 Operating experience in Italy

The incidents and near misses reported in EsOpIA have been investigated and results are summarized in Table 1. There are no events clearly connected to intentional attacks, but many events show the cyber vulnerability. There are more than 60 of them, all very recent, some are due to trivial errors in the software in the OT systems, the infamous bugs due to the inadequacy of the developers or the specifications provided. But there are also more intriguing cases due to software with outdated or incompatible versions, as well as password leaks. There are also a couple of events attributed to undescribed software crashes. Even though errors and faults in IT systems do not impact directly on physical systems, they can jeopardize safety procedures becoming a remote cause for loss of materials. Thus, also IT relate incidents have been included in the study. As you can see, most of the events reported in EsOpIA are not intentional, but are due to software limitations or incorrect actions, often due to lack of training.

Table 1 Cyber Failure Modes and effects source EsOpIA

↓ Cyber Failure mode	Physical Effects →	block	leakage	rupture	injuries	
Software mistake(bugs)		15	1	8	1	25
Obsolescence		3		1		4
Missing software		2		6		8
IT issues (indirect)		13		8		21
Software misuse		1		4		5
crashes		2				2
TOTAL		36	1	27		64

Analyzing in the detail the content of the reports, the impact of cyber events on different type of physical system have been investigated, and results have been summarized in Table 2. It shows the physical elements that have been affected by the consequences of different cyber failures.

Seveso inspectors insist on reporting near misses, because they believe it is an important opportunity to learn from experience. Thus, in EsOpIA you can also find a lot of information on the corrective actions taken by the company to avoid the recurrence of failures, which can be useful to the entire Seveso community. Table 3 shows the actions taken, as find in EsOpIA.

In conclusion, from the operational experience reported in EsOpIA, the high degree of digitalization of processes appears, leading to the vulnerability of the software that can be the cause of losses and injuries. The problem can be bigger where the resources dedicated to software development and maintenance are scarce.

Table 2 Physical Systems affected by the effects of cyber failures source EsOpIA

↓ Cyber Failure mode	Affected Item →	pipe	vessel	valve	other
Software mistake(bugs)		1	13	4	7
Obsolescence					4
Missing software		1	6	1	
IT issues (indirect)		1	7	3	7
Software misuse			3	2	
Crashes					1
TOTAL		5	30	11	20

Table 3 Actions taken after cyber failures source EsOpIA

↓ Cyber Failure mode	Action Taken →	modify	updating	training	verify
Software mistake(bugs)		20	4	4	1
Obsolescence		3	1		
Missing software		1	7		1
IT issues (indirect)		12	2	2	5
Software misuse		5		2	
Crashes				1	
TOTAL		43	15	10	8

3.2 Operating experience in other European countries

A valuable source of information about accident is the BARPI/ARIA, which covers events that are reported in France and overseas[1]. Among the thousands of accidents, which have been reported for years, some containment losses are beginning to appear that have cyber as their cause. In 2019, an alert was published with four cases, Wastewater treatment plant hit by cryptocurrency malware; alert system failure; Sensor failure caused by old printed circuit; Incorrectly programmed PLC. At the present, in the data base you can find 11 events due to cyber attacks, 1 with major consequences. There are also 16 events due to software misfunction, 3 with severe consequences for workers. The Seveso Directive requires the National Authorities to upload a detailed report of any major accident in the eMars database, a database managed by the JRC Joint research center of EU Commission[2]. At the present there are no accident is related to cyber attacks. There are just in a couple of events where the software inadequacy was included in the causes. It has to be stressed that in eMars there are just accidents with very severe consequences and most actual events have consequences below the limits required for reporting in eMars.

4. Conclusions

One of the purposes of the study of near misses is also to identify emerging problems, which at the moment manifest themselves as minor facts, but which can evolve over time and lead to severe consequences. Software-related events are a novelty that cannot be

---

[1] https://www.aria.developpement-durable.gouv.fr/the-barpi/the-aria-database/?lang=en
[2] https://emars.jrc.ec.europa.eu/en/emars/accident/search

underestimated. In particular, in the risk analysis, and in particular in the fault tree, the reliability of the instrumentation is always considered, but perhaps it would also be necessary to include the reliability of the software as a possible origin of an accident chain. In plants subject to the European Seveso III Directive incidents due to cyber factors (intentional or unintentional) have never had consequences as severe as to be classified as "major accident" within the meaning of Annex VI of the same Directive. However, this are not good reasons to underestimate the risk, which according to the data analysed, seems to be growing, both in Italy and in France.

This study aim to provide, together with the other important research and reviews found in the literature, useful insights for a regulatory updating.

While waiting for a possible update of the Seveso legislation that explicitly considers the risks deriving from the interference between cyber risks and process risks, it is useful that cyber factors are now taken into account in the identification and analysis of risks in security reports. The developed causal model is a good basis to include cyber factors in formal analysis method such as fault-tree or bowtie method.

The policy for the prevention of major incidents should also include explicit references to the cyber issues. The safety management system for the prevention of major accident should include procedures and operating instructions to prevent errors or intentional acts in the cyber field from having repercussions on process safety.

References

Iaiani M., Tugnoli A., Bonvicini S., Cozzani V. (2021) Major accidents triggered by malicious manipulations of the control system in process facilities *Safety Science* 134 105043

Stergiopoulos, G., Gritzalis, D. A., & Limnaios, E. (2020). Cyber-attacks on the Oil & Gas sector: A survey on incident assessment and attack patterns. *IEEE Access*, *8*, 128440-128475.

Nobili, M., Fioravanti, C., Guarino, S., Ansaldi, S. M., Milazzo, M. F., Bragatto, P., & Setola, R. (2023). DRIVERS: A platform for dynamic risk assessment of emergent cyber threats for industrial control systems. In *2023 31st Mediterranean Conference on Control and Automation (MED)* (pp. 395-400). IEEE.

Ansaldi, S. M., Agnello, P., Pirone, A., & Vallerotonda, M. R. (2021). Near miss archive: a Challenge to share knowledge among inspectors and improve Seveso inspections. *Sustainability*, *13*(15), 8456.

Insulations for Cryogenic Tanks in Fire Incidents

Robert Eberwein[1]*, Aliasghar Hajhariri[1]*, Davide Camplese[2], Giordano Emrys Scarponi[2], Valerio Cozzani[2], Frank Otremba[1]

1 Bundesanstalt für Materialforschung und -prüfung (BAM), Unter den Eichen 44 – 46, 12203 Berlin, Germany
2 Alma Mater Studiorum - Università di Bologna, Dipartimento di Ingegneria Chimica, Mineraria e delle Tecnologie Ambientali, via Terracini 28, 40131 Bologna, Italy

* e-mail contact: robert.eberwein@bam.de

In the course of decarbonizing the energy industry, cryogenic energy carriers are seen as having great potential. This is because they allow significantly higher volumetric energy densities to be achieved than when these energy carriers are stored at typical temperatures on Earth. This is important for numerous energy-intensive applications, such as those found in all transport sectors. Important cryogenic energy carriers include liquefied hydrogen (LH2) and liquefied natural gas (LNG).

For all cryogenic transported fluids, cold conditions must be maintained. This can be achieved by minimizing heat leakage from the environment. Therefore, thermal super-insulations (TSI) systems are used, based on e.g. rock wool, perlites, microspheres, multilayer insulations (MLI), and vacuum. However, due to the short period of use in some applications, the small number of documented incidents, and the still few investigations carried out in the field, the exploitation of such systems in the cryogenic fluids transport sector still suffers from insufficient knowledge about the course and consequences of incidents. Accidents involving collisions, fires, and their combination are quite common in the transportation sector and may generate extraordinary loads on the tank and its insulation system, eventually leading to tank failure.

The present study focuses on TSI systems behaviours in tanks when exposed to an external heat source representative of a hydrocarbon fire scenario. This may cause an increase of the heat flow into a tank by several orders of magnitude compared to design conditions, which can damage the TSI, lead to the rapid release of flammable gas, and even a Boiling Liquide Expanding Vapour Explosion (BLEVE).

To study such scenarios a test rig named High Temperature Thermal Vacuum Chamber (HTTVC) was developed at BAM that allows testing of TSI at industrial conditions and enables subsequent analysis of TSI samples. This test rig considers the typical double-walled design of tanks for cryogenic fluids with a vacuum and an additional insulating material in the interspace. Adjustable electrical heating elements simulate the fire on one side of the double wall. This process allows the implementation of repeatable heat loads of up to 100 kW/m². The other side of the double wall is represented by a fluid-supported heat exchanger, which allows the simulation of cold or cryogenic conditions in the test rig, and to determine the heat flow transmitted through the double wall. Thus, the test rig allows thermal loading and performance analysis of TSI samples at the same time.

In the first test series typically MLI-based and bulk insulations combined with vacuum were tested at maximum temperature of 800°C. The worst performance was observed from MLI based on polyester. This insulation degrades when the HTTVC bottom-temperature increases above 400°C. While further increasing the temperature the solid MLI pyrolysis to oligomers which move as a gas in the space of the double-wall. This gas accumulates on cold surfaces as the inner tank wall, or pyrolysis further on warm surfaces as the outer tank wall. The accumulated pyrolysis products change the optical surface properties of the walls which strongly affects the heat transfer by radiation, such that the potential heat flow in the fire scenario is higher than in the same system without MLI. Also, it was observed that the pressure increases and reduces the vacuum. This increases the contribution of gas conduction and convection to the overall heat transfer. The MLI samples which are based on aluminum layers, and glass-fleece, or glass-paper show much better performance under the thermal loading compared to the polyester-based MLI. These samples were partially damaged in the tests and the observed heat flows were much smaller compared to the polyester based MLI. From the tested bulk insulation materials, the microspheres/vacuum insulation shows the best performance. This insulation showed a minor degradation within the test, the pressure development was less compared to the other bulk insulations, and the heat flow by the double wall while testing and after testing was nearly unaffected by the fire scenario. Furthermore, in the Perlites and Rock wool test a similar heat flow was observed which was much lower compared to the tested MLI's, but which was also 20 times higher than the observed heat flow in the Microspheres test. In all tests with bulk insulations, a larger delay between the start of the test and the increase of the heat flow by the double wall was observed compared to the tests with MLI/vacuum insulations.

Based on the worst behavior of polyester-based MLI further tests were performed with this type of insulation. Here the maximum temperature of the external wall was varied by 600°C (leaned on standards as ECE R 110 and GTR13) and 800°C (leaned on ISO 21843-2023), as well as the condition of the space in the double wall was varied regarding vacuum, nitrogen, and air. The last one represents an outer hull rupture of a double-walled tank. The experimental results offers that the course of insulation degradation in case of a fire can be changed means by a strong or full degradation of the vacuum in the double wall and by the maximum temperature of the outer wall attained in a fire scenario. The gas contamination of the double wall changes strongly the accumulation of the MLIs pyrolysis products at the cold inner wall and also its overall distribution within the double wall, which is of great importance for the magnitude of the heat flow during and after the fire event. Furthermore, in the presence of air and combustible MLI, there was no flaming combustion observed in any of the tests, which could result in a sudden failure of the entire thermal insulation.

The results are relevant for the evaluation of accident scenarios involving full-scale cryogenic tanks. They can thus contribute to the improvement of thermal super insulations, the development of safer tank designs, as well as the development and definition of emergency measures for the protection of persons and infrastructures.

Acknowledgments

Waves of Safety - Evaluating Overpressure Risks from Gases in Ductile Equipment

Dariusz Jablonski*, Patrycja Zacharzewska, Michael Kirby, Hans-Jürgen Gross

Bayer AG, Leverkusen

*dariusz.jablonski@bayer.com

1. Introduction

Risk assessment is a fundamental task for process and plant safety experts, commonly referred to as PPS Practitioners at Bayer. This procedure involves systematically evaluating potential hazards to ensure the safety and integrity of operations. Utilizing a risk matrix, practitioners together with a team classify during Hazard and Operability Studies (HAZOPs) the likelihood of various possible initiating events - such as the malfunction of the Basic Process Control System (BPCS) - and assess the severity of the resulting consequences. These assessments play a crucial role in evaluating the reliability requirements for the necessary safety measures. By establishing robust safety concepts, practitioners aim to protect not only human lives but also the environment.

This article focuses on the methodologies employed in risk assessment, particularly regarding hazards associated with gas over-pressurization of equipment made from ductile materials. We will highlight the significance of accurate classification and the implications of these evaluations for reliability requirements of safety measures. By fostering a comprehensive understanding of risk assessment in the context of overpressurized equipment with gases, we aim to significantly reduce efforts for detailed analysis and the costs associated with safety oversights, while promoting the careful application of simplified methods, when appropriate, within the chemical and pharmaceutical industry.

1.1 Methodologies for Severity Classification

The classification of severity levels during HAZOPs is typically based on guiding principles outlined in company policies, procedures, and knowledge documents, supplemented by the individual judgments of practitioners and the HAZOP team members. In complex scenarios, severity assessments will be supplemented by modelling the physical consequences. The severity of harmful and toxic material releases or thermal radiation from fires is typically estimated using simplified methods or consequence modelling. However, modeling the consequences of physical explosions is complex, resource-intensive, and necessitates multiple boundary conditions and assumptions. To enhance this process, we developed a method that effectively correlates equipment design data with the resulting severity classifications. These classifications are based on calculations of gas-generated pressure waves for diverse ductile equipment configurations with underlying conservative assumptions. Based on the results a user-friendly table was developed that enables practitioners to more easily determine the appropriate and comparable severity level for different design and deviation scenarios, ultimately improving safety practices in risk assessment.

1.2 Severity Levels and Classification of Safety Measures According to Bayer Methodology

The severity of consequences is categorized into five levels according to the Bayer risk matrix, ranging from negligible (S5) to very high (S0). In our methodology, we focus on four levels (S1-S4) that are most relevant to overpressure scenarios caused by gas-containing equipment under excessive pressure. For clarity and ease of reference throughout this article, these levels are presented in the table 1 below. Additionally, examples of safety measures classifications are presented in the table 2 below.

Table 1: Severity levels based on Bayer internal methodology

Severity Level	Consequences resulting from the release of energy (specifically, the pressure wave)
S1	Severe injuries leading to fatalities from the release of energy with life-threatening effects inside the site fence, and severe injuries with irreversible health effects outside the main site fence.
S2	Severe injuries with irreversible health effects to a limited number of personnel, where fatalities are unlikely but cannot be entirely ruled out, due to the release of energy.
S3	Moderate injuries with short-term health effects, preventing return to work the following day.
S4	Minor injuries requiring first aid or simple medical treatment, allowing for return to work without a lost workday.

Table 2: Examples of safety measures classification based on Bayer internal methodology for failure frequency: one initiating event per 1 to 10 years

Severity Level	Max. Achievable Measure Class	Examples
S1	**VH** (Very high reliability)	Safety Instrumented Systems in SIL3, certified Pressure Relief Valves
S2	**H** (High reliability)	Safety Instrumented Systems in SIL2, orifice plates
S3	**I** (Increased reliability)	Safety Instrumented Systems in SIL1, non-certified Pressure Relief Valves
S4	**N** (Normal reliability)	Measures in a BPCS with no additional safety related requirements

2. Technical Background and Development

The concept behind our methodology is not new; it is rooted in the German legislation known as the German Ordinance on Industrial Safety and Health (Betriebssicherheitsverordnung, BetrSichV) and in the European Pressure Equipment Directive, which categorize equipment based on design pressure and volume. These regulations identify four categories of equipment based on the product of design pressure (PS in barg) and volume (V in liters). Category I includes small vessels, such as portable gas cylinders and air compressors. Category II encompasses medium-sized boilers, while Category III covers large-scale steam boilers. Finally, Category IV is designated for large industrial pressure vessels like reactors. The requirements for risk assessment, safety measures, and testing vary by category, with lower requirements for the lower categories and the highest for Category IV. Through this framework, the German regulatory authority helps ensure the health and safety of employees working with such equipment.

Based on the fundamental principles of the aforementioned method, we have formulated an equation to correlate the severity with the energy potential of an overpressurized vessel:

Severity Level = Design Pressure (PS) × Volume of Equipment (V) [barg x liters]   (1)

Applying this equation for design conditions the resulting Severity Level is deemed acceptable, as all design parameters remain within specified limits. According to the Pressure Equipment Directive (PED), any exceedance of design parameters is not permitted, necessitating the implementation of appropriate safety measures. For the sake

of simplicity of this method, we did not consider the design temperature of the equipment, assuming it will remain within design limits under all circumstances which is a boundary condition for the application of the tool.

2.1 Boundary Conditions for Applying and Developing the Method

Generally, this method is applicable to all pressure equipment (with a design pressure of 0.5 barg or higher, as the Pressure Equipment Directive (PED) defines 0.5 barg as the threshold for pressure equipment). For equipment with a design pressure below 0.5 barg, severity rankings of S1 or S2 due to pressure waves from rupture can reasonably be excluded.

This method was developed for pressure equipment containing gas phases and introduces a severity classification based on pressure waves generated by overpressurization of those gas phases. Additionally, this classification is applicable only to equipment constructed from ductile materials; its use for equipment made from brittle materials is not allowed. Even in the case of cryogenic media, the construction material must be designed for operational conditions; otherwise, it shall be classified similarly to brittle materials.

Furthermore, these severity ratings are generally intended for outdoor locations or in larger rooms. In smaller spaces or in congested areas, it is possible that pressure waves may be compounded as the initial pressure wave is reflected or that other consequences may arise not directly from the pressure wave, but from debris, such as damaged walls or equipment in the room.

2.2 PS x V Table with Corresponding Severity Levels

Assuming that the energy content of a pressurized vessel can be estimated using Equation 1, which involves multiplying the design pressure by the vessel's volume, we conducted numerous calculations for various ductile vessel volumes and design pressures. For these calculations, we employed a conservative default bursting pressure factor of 5, as historical data indicates that pressure vessels typically fail catastrophically at pressures ranging from 2 to 5 times their design pressure. For example, API 581 assumes an empirical overpressure factor of 4 times the design pressure for vessels designed according to API standards.

The energy of the physical explosion was calculated using the thermodynamic availability method, as described in various sources, primarily D. A. Crowl's work and the CCPS Guidelines. Generally, thermodynamic availability represents the maximum mechanical energy extractable from a compressed gas as it reversibly moves into equilibrium with the environment when released. For simplicity, the following assumptions were made:
- The entire available mechanical energy of the compressed air is used to produce the pressure wave.
- The system involves only inert compressed gases, such as air.
- The vessel is spherical.
- The ambient and content temperatures were assumed to be 20°C.

The following Figure 1 illustrates the results of one example calculation for four vessel volumes all having a design pressure of 6 barg. The Y-axis represents the magnitude of the pressure wave overpressure as a function of distance from the center of the bursting vessel.
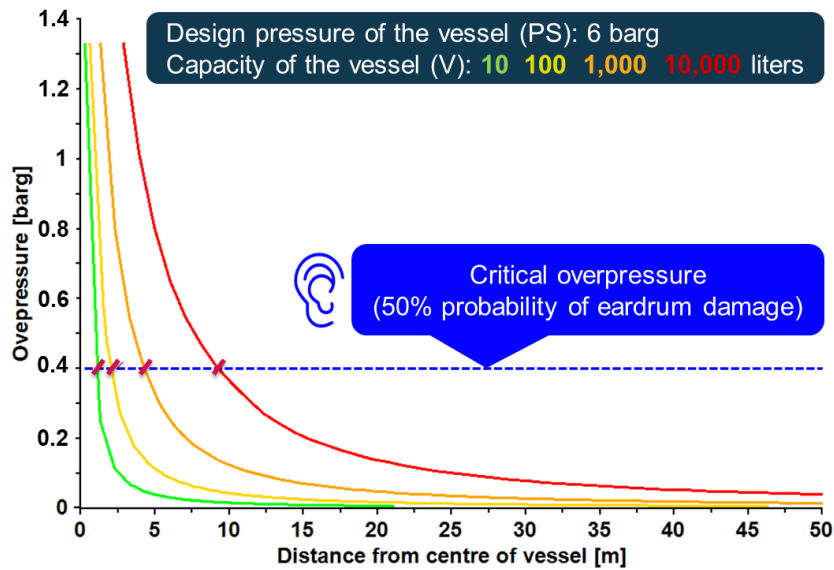
Figure 1. Overpressure history from pressure waves generated by bursting ductile equipment under various design conditions and capacities.

We established a convention based on various vessel configurations to identify critical overpressure distances associated with significant injury risks, such as a 50% probability of eardrum rupture. After analyzing various vessel configurations, we adopted a convention indicating that severity levels S1 to S4 are expected if our defined threshold is exceeded at specific distances from the vessel. This approach enabled us to correlate the energy content of the vessel with different degrees of severity, a relationship confirmed by extensive calculations. Consequently, this led to the development of our new severity table based on PS × V boundaries.

Table 3: PS x V Table - Examples of severity levels based on pressure wave by pressuring of ductile equipment with gas phases (without consideration of physical effects/ consequences)

Severity Level	Design Pressure x Volume Column 1 – **Base Case** (> 3 x PS)	Design Pressure x Volume Column 2 (maximum 3 x PS)	Design Pressure x Volume Column 3 (< 2 x PS)
S1	6,000 < PS x V	18,000 < PS x V	30,000 < PS x V
S2	600 < PS x V < 6,000	1,000 < PS x V < 18,000	2,000 < PS x V < 30,000
S3	200 < PS x V < 600	400 < PS x V < 1,000	600 < PS x V < 2,000
S4	PS x V < 200	PS x V < 400	PS x V < 600

Typically, Column 1 in Table 3 (Base Case) is used to identify the severity of bursting of a pressurized equipment, where the maximum achievable deviation pressure can exceed 3 times the equipment design pressure. But according to the boundary conditions, the conservative calculation is based on rupture at 5 times the design pressure. In cases where the maximum achievable pressure (even in the event of deviations) is intrinsically limited according to high mechanical integrity design principles (HMI) or protected by VH preventative measures to values lower than three times the design pressure, Column 2 can be applied. Additionally, there may be situations where the design pressure can be exceeded, but the pressure source cannot reach twice the original design pressure. In such cases, Column 3 can be utilized, as the pressure wave calculations were based upon rupture at 2 times design pressure.

3. Specific cases and applications

3.1 Standard applications - case studies

The assessment of failure scenarios is a collaborative effort undertaken by the HAZOP team, which comprises both PPS Practitioner and plant operational personnel. As highlighted under section 1, this evaluation is based on internal company policies, procedures, knowledge documents, and the individual experiences of the team.

The internal regulation for Process and Plant Safety describes each severity level in general (see table 1 in section 1.2) and provides examples for the overpressure scenarios that support in classifying the associated risk levels.

Before the PS x V method was developed, the scenario of overpressurizing a "ductile" equipment due to vapor pressure/gaseous pressure (excluding other effects such as toxicity) was assessed in many cases using the following criteria:

  • with volume greater than 10 l: S1 (for high risk),
  • with volume lower than 10 l: S2 (for significant risk).

This estimation neglects the correlation between the equipment's design pressure and volume, as well as the impact of the pressure wave's magnitude. Therefore, the new PS x V method based on calculations of these factors is closer to the reality, which was confirmed by statistical / empirical data of accidents. Furthermore, this method describes 4 categories of severities, in contradiction to the old method where only 2 severity levels could be applied.

In the following sections, examples of the application of the new method are presented. In these cases, the maximum allowable pressure is equal to the design pressure. In the first example (figure 2), a stainless-steel liquid vessel with a volume of 140 liters and a design pressure of 3 barg is considered.
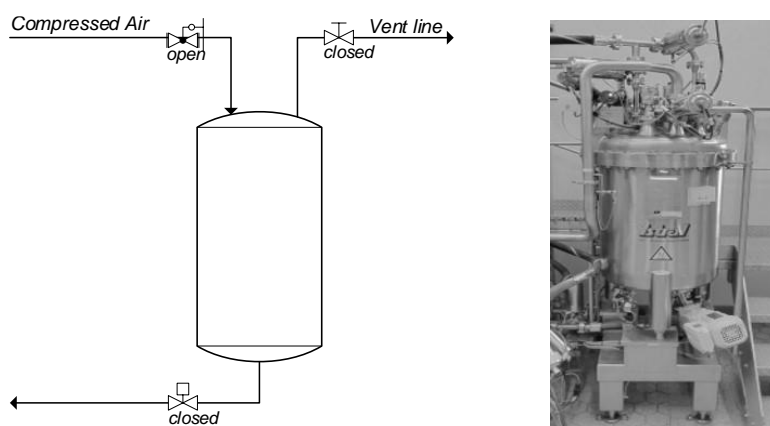
Figure 2: Stainless-Steel Liquid Vessel pressurized with compressed air in failure scenario.

This vessel is emptied using compressed air. The failure scenario involves pressurizing the closed vessel with compressed air up to the maximum achievable protected pressure of 7 barg. This scenario was previously classified as S1. The table below shows how the severity level changes according to the new approach. The calculation is performed for the entire gas volume as the worst case.

Table 4: Estimation of severity for the Liquid Vessel acc. PS x V Table (Example 1)

Volume (V)	Design Pressure (PS)	Max. Pressure (Pmax)	PS x V	Pmax / PS	Severity Level acc. to Table 3. Column 2 (maximum 3 x PS)
140	3	7	420	2.3 times	400 < PS x V < 1,000 => **S3**

Using this method, the severity level could be reduced by two orders of magnitude and now equates to level S3. This can reduce the cost of installing additional pressure safety measures with higher quality, such as a VH rated certified pressure relief valve, with all the required calculations/ documentation and life-cycle management.

The second example (figure 3) is a stainless-steel distillation column, which is also a pressure equipment. The total volume of the column, including the vapor line and condenser, is 2,250 liters, representing the amount of stored energy. The design pressure of the column is 5 barg.
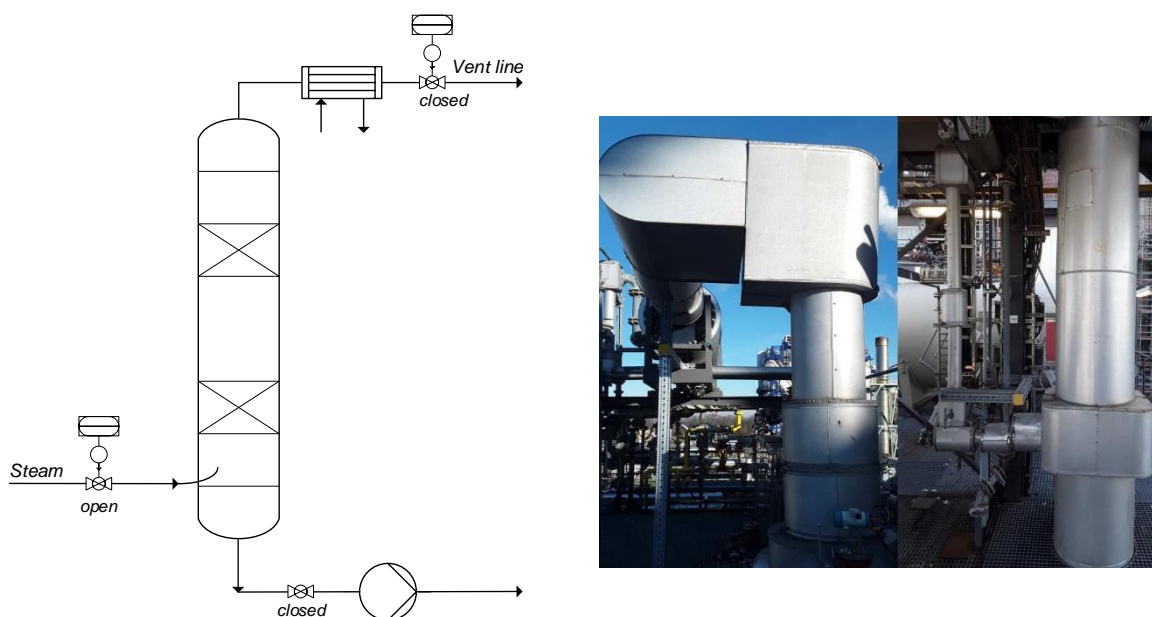
Figure 3: Stainless-Steel Distillation Column pressurized with compressed air in failure scenario.

In this column, steam with a maximum pressure of 6 barg is used for solvent removal. The malfunction scenario where steam is applied to the column with the vent line and outlet line closed. In this case the previous risk was also assessed with severity level S1. The new validation is presented below. The calculation is based on the total system volume as the worst case.

Table 5: Estimation of severity for the Distillation Column acc. PS x V Table (Example 2)

Volume (V)	Design Pressure (PS)	Max. Pressure (Pmax)	PS x V	Pmax / PS	Severity Level acc. to Table 3. Column 3 (< 2 x PS)
2,250	5	6	11,250	1.2 times	2,000 < PS x V < 30,000 => **S2**

In this situation, a detailed calculation and the use of Column 3 enabled the severity level to be reduced by one level. This also had positive impact on the planned safety measures. The planned upgrade PCT installation for the SIL3 pressure interlock was no longer necessary, as the existing SIL2 high pressure interlock was sufficient.

The third example (figure 4) is a stainless-steel filter with a strainer. The function of this filter is to retain deposits, foreign material and fibers. Compared to the examples above, this filter contains both liquid and gas. The total volume of the filter and the directly connected pipes is 300 liters, while the remaining gas volume is 60 liters. The design pressure of the system is 4 barg.
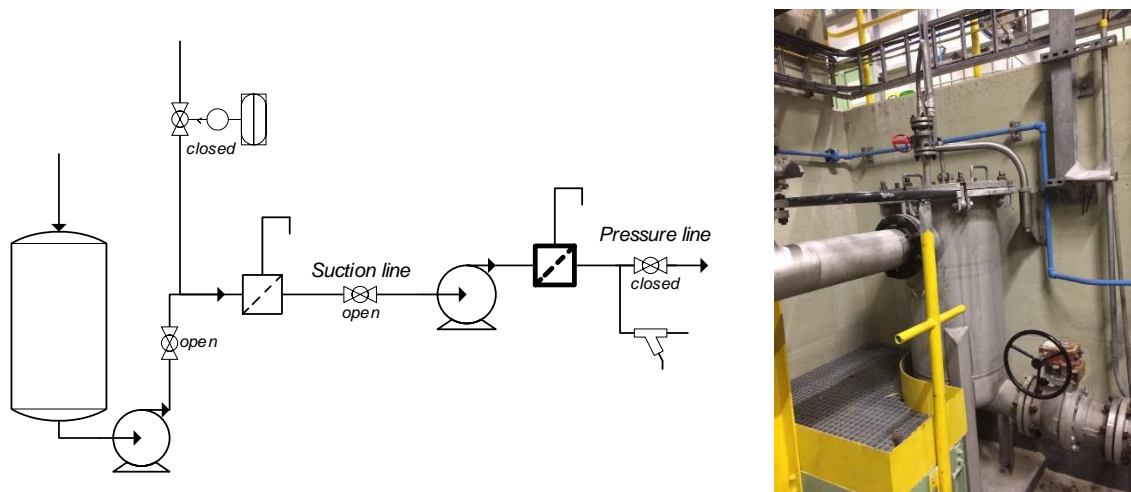
Figure 4: Stainless-steel filter with a strainer pressurized with pumps in failure scenario.

The filter is pressurized by two centrifugal pumps connected in series. When the valve on the pressure side of the filter behind the second pump is closed, a maximum pressure of 15.5 barg is generated by both pumps. The overpressure scenario of this system due to the displaced gas volume of the pump was previously rated as S1. However, the new method gives a different result. The following calculation is applied to the existing gas phase only.

Table 6: Estimation of severity for the filter with a strainer acc. PS x V Table (Example 3)

Volume (V)	Design Pressure (PS)	Max. Pressure (Pmax)	PS x V	Pmax / PS	Severity Level acc. to Table 3. Column 1 (> 3 x PS) Base Case
60	4	15.5	240	3.9 times	200 < PS x V < 600 => **S3**

As in the first case, the severity level is now reduced by two levels with this method and is now equal to S3. In this example, no further safety measures were required as the existing pressure switch-off in SIL 1 was adequate.

3.2 Specific cases – derated pressure

There may be situations where equipment is manufactured to a specific design pressure, but due to process conditions or additional requirements for registering and maintaining equipment as pressure vessels, it is assigned a Maximum Allowable Working Pressure (MAWP) that is lower than the original design pressure. In such cases, the original design pressure cannot be used for the PS x V calculation. Instead, a 'theoretical' design pressure should be determined based on a conservative approach, which assesses the potential severity of equipment failure at the maximum achievable pressure.
Example:
A vessel has a volume of 10,000 liters and a design pressure of 6 barg. In this example, the maximum achievable pressure in the process is 5 barg (limited by VH measure or HMI). The derated pressure (referred to as "Fertiggemeldeter Druck" or MAWP) is set at 0.5 barg. While exceeding the original design pressure is not possible, the MAWP can be exceeded. In this case we need to determine a new 'theoretical' design pressure.
For determining the product "PS x V" a "theoretical" design pressure is calculated by the following formula:

'theoretical' design pressure = max. achievable pressure / 2 = 5 barg / 2 = 2.5 barg   (2)

Factor 2 is to be used in all cases, to then determine the potential severity using column 3 in Table 3.
The Severity Level can be estimated according to the following equation and Table 3 and results in a classification of S2:

Severity Level = 2.5 barg × 10,000 liters = 25,000 (barg × liters)   (3)

Essentially using a max. achievable pressure divided by two, then applying factor 2 means that we determine a severity based on stored energy at the max. protected pressure.
In the upcoming chapters, the practical implementation of this method will be presented for two different equipment types.
A common case in chemical companies where the Maximum Allowable Working Pressure (MAWP) is lower than the design pressure are storage tanks. These are often operated with pressure of equal to or below 0.5 barg, although they are intended for a higher design pressure. The following example (figure 5) refers to a stainless-steel tank with a maximum allowable working pressure of 0.5 barg and a design pressure of 6 barg. The volume of the tank equals 32,000 liters. In this example, the maximum achievable pressure in the process is 5 barg (limited by VH measure or HMI).
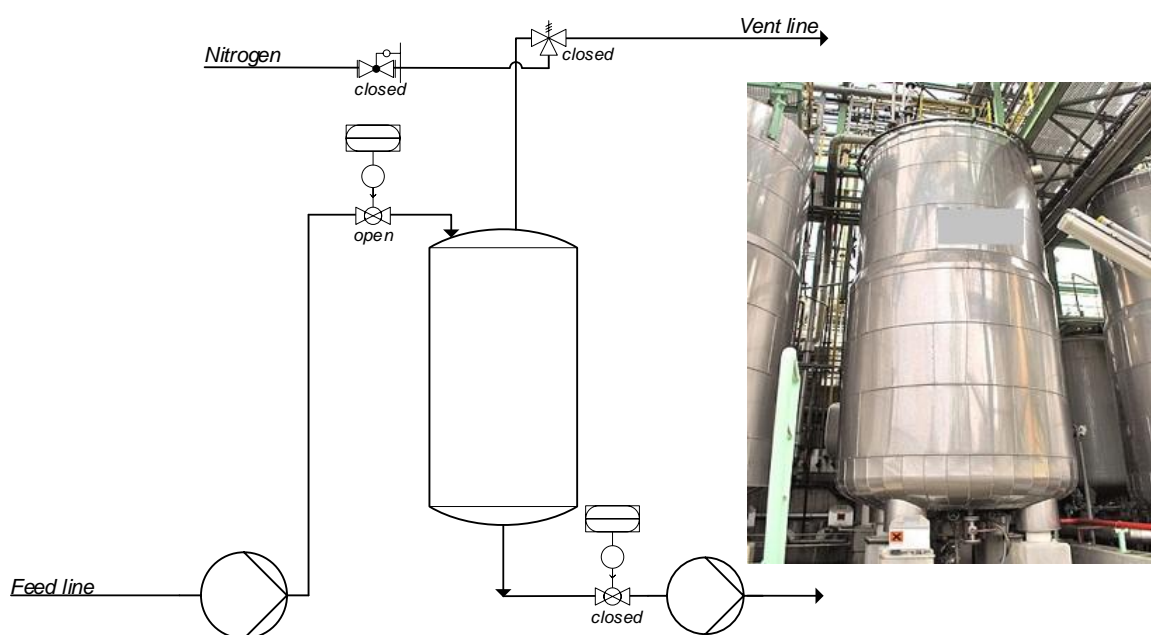
Figure 5: Stainless-Steel Storage Tank pressurized with pump in failure scenario.

Table 7: Estimation of severity for the tank acc. PS x V Table (Example 1)

Volume (V)	Design Pressure (PS)	Derated Pressure (MAWP)	Max. Pressure (Pmax)	New Theoretical Design Pressure (new PS = Pmax / 2)	new PS x V	Severity Level acc. to Table 3. Column 3
32,000	6	0.5	5	2.5	80,000	30,000 < PS x V => **S1**

The result of this calculation shows that the severity level has not changed. This confirms that, as in this case, a non-pressure equipment designed for pressure above 0.5 barg can initially rupture at higher pressures due to its design, which can be life-threatening.

For comparison, a stainless-steel exhaust gas scrubber (figure 6) with a significantly smaller volume of 1,000 liters is considered below. The maximum allowed pressure of this scrubber is 0.5 barg, while the design pressure is 6 barg.
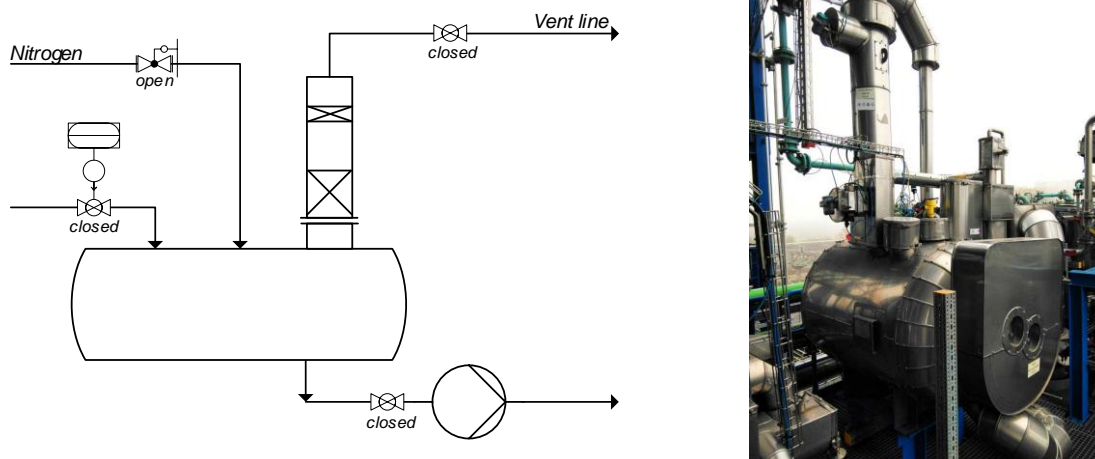
Figure 6: Stainless-Steel Exhaust Gas Scrubber pressurized with nitrogen in failure scenario.

The exhaust gas scrubber is purged with nitrogen, maintaining a protected pressure of 3 barg, In this example, the maximum achievable pressure in the process is 3 barg (limited by VH measure or HMI). With the vent path closed, the apparatus may become overpressurized. This scenario had previously been assessed as S1. The following calculation enables a validation of the severity level using the new method.

Table 8: Estimation of severity for the Exhaust Gas Scrubber acc. PS x V Table (Example 2)

Volume (V)	Design Pressure (PS)	Derated Pressure (MAWP)	Max. Pressure (Pmax)	New Theoretical Design Pressure (new PS = Pmax / 2)	new PS x V	Severity Level acc. to Table 3. Column 3
1,000	6	0.5	3	1.5	1,500	600 < PS x V < 2,000 => **S3**

In this case, the severity of mechanical damage to the apparatus is reduced from S1 to S3. The assessment avoided an upgrade of the interlock to SIL3.

4. Conclusions

In this article, we introduced a user-friendly table that enables PPS Practitioners to easily determine the appropriate severity level for various overpressure scenarios resulting in physical explosions. This innovation not only enhances safety practices in risk assessments but also aims to achieve better harmonization of severity level determination and safety concepts throughout Bayer.

By fostering a comprehensive understanding of risk assessment in the context of overpressurized equipment with gases, we aim to significantly reduce the efforts of HAZOP teams and promote the application of simplified methods within the chemical and pharmaceutical industry. This approach ensures a more consistent and accurate evaluation of risks, leading to improved safety outcomes and optimized resource allocation.

The successful application of this method has been confirmed through examples from Bayer plants, demonstrating the practical benefits and effectiveness of this approach. These case studies validate the advantages of the new methodology, including enhanced efficiency, reduced costs, and improved safety harmonization across the organization.

However, this method does not consider additional consequences that may need to be addressed, such as the release of harmful, toxic, or flammable substances. In such cases, the physical impact of the resulting pressure wave may be significantly less than that associated with the properties of the substances involved. Additionally, this table is not applicable for internal explosions or decomposition/deflagration scenarios. In these situations, the potential generation of debris cannot be excluded, which may result in an underestimation of the overall severity of consequences.

It should be emphasized that local regulation, which may be more stringent, need always be considered and whichever have the higher requirements must be applied.

Acknowledgments

References

American Institute of Chemical Engineers, Center for Chemical Process Safety. Guidelines for Vapor Cloud Explosion, Pressure Vessel Burst, BLEVE, and Flash Fire Hazards. Second Edition (2010).

American Petroleum Institute. (2016). API Recommended Practice 579: Fitness-For-Service. (3rd ed.). Washington, D.C.: American Petroleum Institute.

Betriebssicherheitsverordnung (BetrSichV). (2002). Ordinance on Industrial Safety and Health. Federal Ministry of Labour and Social Affairs, Germany.

Corporate Policy No.: 2055, HSE Management and HSE Key Requirements, April 1, 2021.

D. A. Crowl: Understanding explosions. American Institute of Chemical Engineers, CCPS Publication G-61 (2003).

PED, Pressure Equipment Directive, Directive 2014/68/EU of the European Parliament and Council on pressure equipment.

Procedure No. CHS-PUB-9-300617, Safe Design and Operation of Processes and Plants, Oct 1, 2018.

Challenges of Managing Process Safety in Facilities Operated by Multiple External Service Providers

Filipp Chlebus, Lucas Gianola, Mischa Schwaninger*

Novartis Pharma AG, Novartis Campus, CH-4056 Basel

*mischa.schwaninger@novartis.com

1. Introduction

Process safety management is crucial component in today`s pharmaceutical industry, particularly due to the prevalent externalization of non-core business functions. This typically includes the diligent oversight of process safety-relevant infrastructure, including gas and steam supply installations, solvent distribution systems, refrigeration units, as well as storage facilities for dangerous goods, including tank farms. The process safety risks associated with these facilities, given their operation by multiple external service providers and the connection to essential core processes of the business, presents significant challenges in managing them. These challenges involve the coordination of safety measures among diverse parties and the need for effective communication and collaboration to ensure comprehensive awareness of potential risks and concerted efforts to mitigate them effectively.

2. Methods

The process safety management approach discussed is anchored on the 14 process safety management elements derived from the OSHA Process Safety Management (PSM) Program [OSHA 1992].

3. Results and discussion

The 14 PSM elements were further evolved based on lessons learned from near-misses, incidents, and past experiences to help prioritize the key elements and priorities for process safety measures. These key elements include clearly assigning responsibility for safety-relevant facilities and processes, keeping them separate from other operations. Furthermore, the role of a system operations manager is required, effectively overseeing the process safety requirements, and exercising a pivotal function in maintaining a robust process safety management framework with proper handling of safety information in preventing incidents and continually improvement of safety.

4. Conclusions

The discussed work references several key events, which relate to processes safety on a modern research and development (R&D) campus, employing approximately 10,000 individuals. It demonstrates the experiences gained during the implementation of the process safety management program among various stakeholders. By sharing these experiences, this work aims to contribute to the broader understanding and adoption of effective process safety management practices within the pharmaceutical industry.

References

US Occupational Safety and Health Administration (OSHA), 1992, Process Safety Management Guidelines for Compliance

Early Integration of Safety in Process Design: an Index-based Approach for Streams

Silvia Pelucchi[1,*], Filippo Carretta[1], Federico Galli[2], Paolo Mocellin[1,3]

1 *Università degli Studi di Padova, Dipartimento di Ingegneria Industriale, Via Marzolo 9, 35131 Padova, Italia.*
2 *Département de Génie Chimique et de Génie Biotechnologique, Université de Sherbrooke, 2500, boul. de l'Université,*
Sherbrooke, Québec, J1K 2R1, Canada.
3 *Università degli Studi di Padova, Dipartimento di Ingegneria Civile Edile e Ambientale, Via Marzolo 9, 35131 Padova, Italia.*

* *silvia.pelucchi.1@phd.unipd.it*

1. Introduction

The traditional and most applied way to design a process considers the fulfilment of technical and economic targets as the main objectives, while environmental and safety matters are often addressed after the main process design is concluded, leaving limited room for improvement. This traditional process design protocol can lead to further economic investments to adjust part of the project to meet safety or environmental requirements if deficiencies are identified.

In this context, a research need emerges: including safety considerations during the conceptualisation of a process, when the level of detail available is limited.

The maximization of safety and minimization of environmental burdens must be integral objectives of process design rather than constraints, on par with technical decisions and economics. Safety, in particular, must always take precedence among design objectives. An unsafe plant is not only inherently hazardous but also detrimental to profitability due to the massive potential production and capital losses resulting from accidents. For these reasons, safety considerations should shape design decisions from the initial stages of a project (Heikkilä, 1999; Rahman et al., 2005). An alternative and beneficial approach is to integrate inherent safety principles during the chemical process design stage. An inherently safer design avoids hazards rather than controlling them, particularly by reducing the amount of hazardous material and the number of hazardous operations in the plant. When safety is inherent, it is built into the process or product rather than added on later.

In this framework, implementing inherent safety principles is most effective during the early stages of design when adjustments can be readily made to incorporate safer features. Applying these strategies after the design is finalized necessitates additional investment compared to modifications made during the preliminary design phase.

The objective is to introduce some metrics or indexes that provide immediate feedback on the safety performance of a process flowsheet under development, in the same way that ROI, IRR, and productivity do for economic and technical aspects.

Over the past few decades, the use of inherent safety metrics for measuring, ranking, and selecting inherently safer process alternatives has increased. These metrics have been gaining popularity because they are fast, easy to implement and require limited information, making them appropriate for the conceptual stage of design. These metrics can be classified into four categories: consequence-based metrics, graphical assessments, risk-

based metrics, and index-based metrics. This work focuses on index-based metrics, which are the most targeted because they consist of mathematical models that output a numerical value, usually ranging over a scale (Park et al., 2020). Although an assessment conducted by a team of experts can never be fully replaced by an automated method, linking the safety assessment to process simulation simplifies, systematizes, and speeds up the design process (Mohammadi et al., 2023).

Despite significant advancements in developing safety indexes and considerable efforts in the field, no unified metric exists for assessing inherent safety (Gao et al., 2021; Qian et al., 2024; Zhu et al., 2022). Therefore, there remains a demand for new, simple indices to evaluate different process alternatives during the conceptual design phase, whether for new or retrofitting processes (Ordouei et al., 2016).

A key challenge highlighted in the literature is that many indexes lack a standardized scale (e.g., from 0 to 10), making it difficult to interpret the index without direct comparison with alternatives, and they often use step functions. Another prominent issue is subjectivity and the absence of automatization, which makes the calculation of such indexes slow and tedious.

In this work, we develop and implement an index capable of evaluating the safety of a generic process stream, incorporating all the possible information available at the conceptual stage. The index ranges over a simple scale (from 0 to 10) and uses continuous functions rather than steps.

The proposed code is fully automated in MATLAB, as it receives all the required information from the simulator or a built-in database and immediately computes the index for each stream. The index provides immediate feedback about the safety of the stream. When process conditions change, the index is recalculated, allowing users to quickly understand how different choices impact the overall safety of the process.   This study introduces a new pattern, starting from the analysis of process streams rather than units. Process simulators, like Aspen Plus, provide the user with extensive information about streams rather than units, and once the indexes for the streams are available, they can be combined to calculate the indexes for the units.

2. Methods

The index was developed as a MATLAB code coupled with Aspen Plus, which calculates mass and energy balances. The database was constructed using a Python code capable of retrieving all relevant chemical properties from the CAMEO Chemicals database. The Phyton code extracts the properties of interest and exports the, into an Excel sheet.

The algorithm evaluates the safety performance of a stream, whether it carries a liquid, a gas, or a liquid-gas mixture. We introduced a standardized, easy-to-understand scale from 0 to 10: the higher the index, the better the safety performance. Our objective is to develop an index that is both comprehensive and user-friendly.

The Stream Safety Index (SSI) is the result of the combination of seven different sub-indexes, each covering key properties areas available at conceptual design stage: I_P (pressure index), I_{EN} (temperature and internal energy index), I_{AT} (autoignition temperature index), I_{FL} (flammability limits index), I_{FP} (flash point index), I_{TOX} (toxicity index), $I_{FL,cloud}$ (index for the flammability limits of the cloud).

For clarity, the algorithm is divided into two sections (Figure 1). In the first section, the indexes are calculated using the properties as computed and provided by Aspen Plus, and so we analyze aspects such as operative temperature, pressure and flammability. In the second section, we consider the possibility of experiencing a loss of containment. In this situation, the pressure decreases and part of the liquid (if present) vaporizes. A code based on thermodynamic formulas computes the new composition of both the cloud released in

air and the liquid puddle. Here we analyze two more relevant aspects such as toxicity of the cloud and its flammability. The indexes are computed considering the newly computed composition.
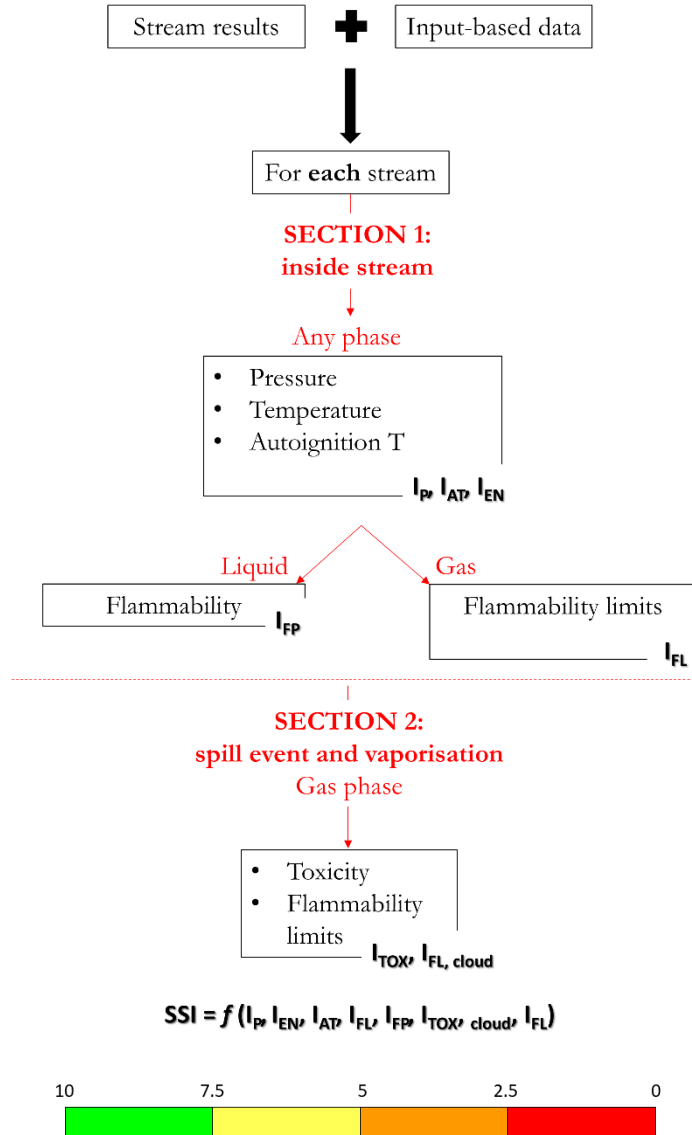
Figure 1. Structure of the algorithm that computes the Stream Safety Index (SSI).

This work proposes an alternative to traditional approaches presented in the literature, where safety indexes are built based on penalties assigned using step functions (Athar et al., 2022; Gangadharan et al., 2013; Heikkilä, 1999). The main limitation of the step-function approach is that it assigns the same penalty value across a wide range of values. For instance, a vessel operated at 0.5 bar and one operated at 5 bar may receive the same hazard rating, despite the significant difference in operating conditions.

To address this limitation, continuous mathematical functions were developed to represent trends based on key reference points. These functions have a fixed y-axis ranging from 0 to 10 (corresponding to the index value), while the x-axis represents the property under study.

The reference points were selected based on literature sources (Gangadharan et al., 2013; Heikkilä, 1999; Park et al., 2020; Qian et al., 2024), expert opinions, or a combination of both.

The functions used include logistic, logarithmic, and power functions, and were intentionally designed to be parametric. For each function, an optimization algorithm was implemented in MATLAB to determine the optimal parameters that best fit the desired curve.

This methodology eliminates the need for step functions and predefined ranges, resulting in a cleaner and more efficient computation of the safety index.

We applied our index to a case study of the partial oxidation (POX) process (Figure 2), which converts shale gas into methanol. This process is comprehensively descrived in the work by Julian-Duran et al. (Julián-Durán et al., 2014). Aspen Plus was used to solve mass and energy balances, and stream summary results served as input for the safety index calculation. In the POX process, oxygen is supplied by an air separation unit and mixed with the shale gas feed. The feed is preheated to 300 °C. Partial oxidation occurs at 1350 °C and 30 bar in a reactor modelled using an RGibbs reactor in Aspen Plus. Subsequently, a water gas shift reactor, modelled as an RStoic reactor, is employed to increase the H_2/CO ratio from 1.8 to 2. The product stream is then cooled and passed through a flash drum to remove water. Afterward, tea separator removes 99.8% of CO_2. Finally, the syngas is compressed to 83 bar before entering the methanol reactor, which operates at 260 °C.
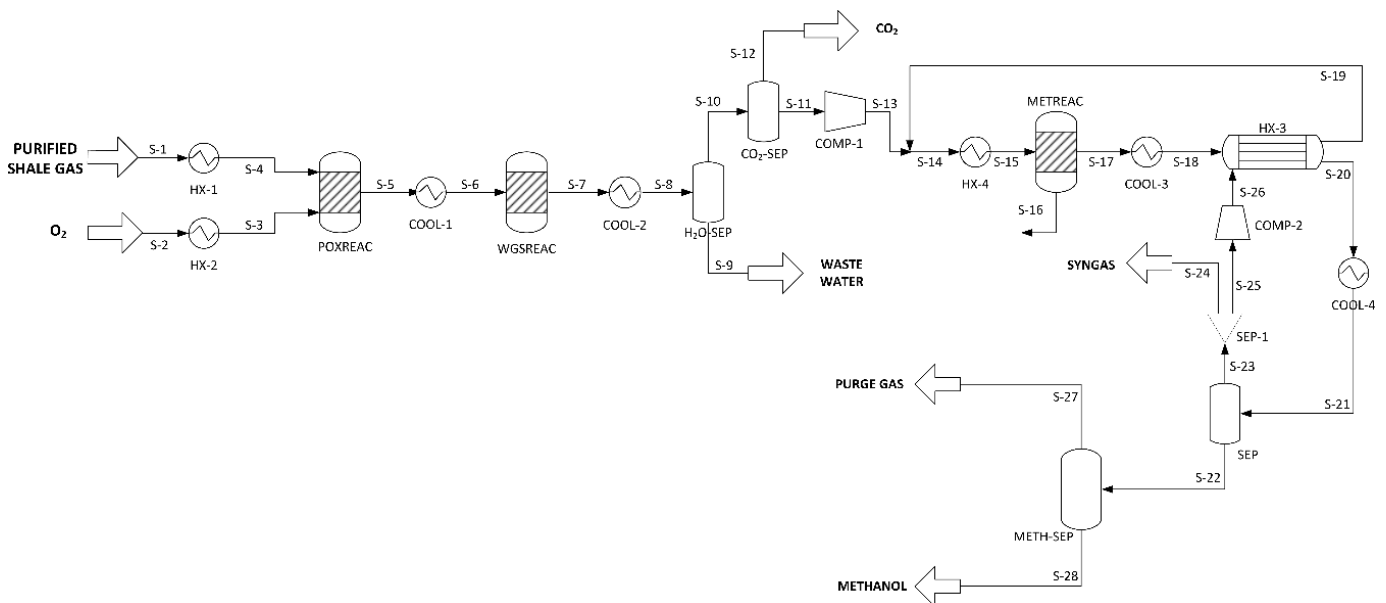
Figure 2. Simplified process flow diagram of the partial oxidation process used as a case study.

3. Results and discussion

When the code is run, it produces first the results for each stream. The code is then iterated for the number of streams in the flowsheet to produce at the end an overall Stream Safety Matrix for the process (Figure 3).
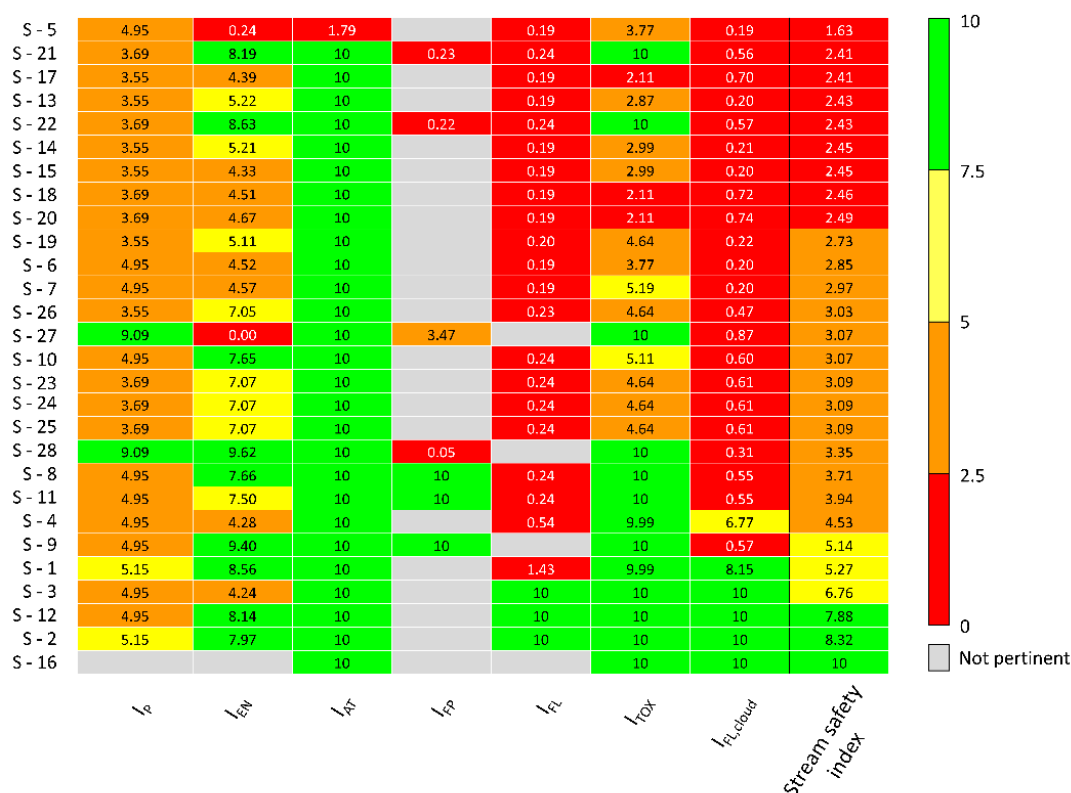
Figure 3. Stream Safety Matrix of the POX process here used as a case study.

According to the matrix, S-5 has the lowest safety performance overall (Stream Safety Index = 1.63) (Figure 3, 4). S-5 exits the partial oxidation reactor, which operates at 1350 °C and 30 bar. The sub-indexes I_{EN}, I_{FL} and $I_{FL,cloud}$ are very low (< 1) due to the extremely high operating temperature (1350 °C), and the presence of H_2 in the stream, which is characterized by a wide flammability range. Additionally, most of the components have autoignition temperatures lower than the operating temperature of the stream.

Figure 4. PFD of the partial oxidation process with SSI labels for each stream.

The safest part of the flowsheet under study is the cluster comprising the H_2O and CO_2 separators.

On the other hand, the cluster consisting of COMP-1, HX-4, METREAC and COOL-3 requires attention due to the low index values of the streams involved. Although the evaluation of individual units has not yet been considered, the stream index alone already highlights the most sensitive parts in the flowsheet.

Only 3 streams out of 28 fall within the green zone, and one of these, S-16, is a placeholder used for calculation purposes. Most of the streams have an overall index below 6.8, reflecting the fact that the process operates at high pressures (> 30 bar) and handles flammable components such as CH_4, C_2H_6, C_3H_8 and H_2.

The automation offered by the SSI distinguishes it from other proposed indexes. Although automation may not be a primary concern during the conceptual design stage, we believe it enhances the usability and dissemination of such tools. The POX process analyzed here consists 28 streams, making manual computation of an index feasible but time-consuming. In larger flowsheets (e.g., 40 + streams), manual calculation becomes impractical due to the required time and cost. Additionally, any minor adjustment in the process simulator necessitates recalculating the safety index. Without automation, this involves re-copying simulation results into the Excel file, further prolonging the process.

The proposed code addresses this issue by linking the database, the MATLAB script, and the simulator properties, allowing the computation to be accomplished in seconds. For the current 28-streams flowsheet, the matrix is generated in around 20 seconds (with the time depending on the computer's RAM). This speed enables users to quickly recalculate the index after making process modifications. Furthermore, the SSI gives a comprehensive overview of the most property areas available at conceptual stage, unlike other indexes that focus solely on flammability or explosiveness. The SSI also returns information on flammability and toxicity conditions in the event a loss of containment occurs and the stream gets in contact with air.

4. Conclusions

The traditional approach to process design prioritizes technical and economic targets, often addressing safety considerations later in the process. This can undermine the overall performance of the technology and lead to additional investments to address safety gaps. Safety should be a primary consideration from the early stages of process design, despite the limited information available during the conceptual phase. Safety indexes provide a quick, generally easy-to-implement tool that offers immediate feedback on the safety performance of the process. Significant advancements have been made in this field, with numerous indexes developed in the recent years. However, there remains room for improvement in aspects such as reducing subjectivity, using continuous rather than stepwise functions, automating calculations, and establishing a standardized scale.

In this work we presented the new Stream Safety Index (SSI), designed to assess the safety performance of a generic individual process stream of a flowsheet under development. The SSI uses data from process simulators and retrieves missing properties from a database built using Python and CAMEO Chemicals. The SSI evaluates the safety performance of liquid, gas or liquid-gas streams and, ranging from 0 to 10 on a standardized scale. The SSI comprises seven sub-indexes that cover different property areas, such as pressure, enthalpy, autoignition temperature, flash point, flammability limits, and toxicity. Continuous functions interpolated over a specific combination of data are used to build each sub-index, eliminating the need for stepwise penalty. The index was tested on a case study involving the partial oxidation process for methanol production, demonstrating its practicality and advantages. A key benefit of the SSI is its automation, which significantly reduces computation time compared to manual methods. While this advantage may seem less critical in small flowsheets, it becomes essential for larger ones. For the 28-streams case study, the index matrix was computer in just 20 seconds. Automation also allows for rapid recalculation following changes in the process simulator.

Although the SSI improves safety assessment in many ways, some level of subjectivity remains. However, the code's parametric structure allows users to customize data inputs to optimize parameters based on their specific needs.

Future work includes the development of unit-level safety indexes derived from stream-level indexes, which can be aggregated to assess the overall safety performance of a flowsheet. Additionally, a key objective is to develop an environmental safety index, as current approaches primarily focus on personnel safety.

References

Athar, M., Shariff, A. M., Buang, A., Umer, A., & Zaini, D. (2022). Inherently safer process route ranking index (ISPRRI) for sustainable process design. Journal of Loss Prevention in the Process Industries, 104909. https://doi.org/10.1016/j.jlp.2022.104909

Gangadharan, P., Singh, R., Cheng, F., & Lou, H. H. (2013). Novel methodology for inherent safety assessment in the process design stage. Industrial and Engineering Chemistry Research, 52(17), 5921–5933. https://doi.org/10.1021/ie303163y

Gao, X., Abdul Raman, A. A., Hizaddin, H. F., Bello, M. M., & Buthiyappan, A. (2021). Review on the Inherently Safer Design for chemical processes: Past, present and future. Journal of Cleaner Production, 305, 127154. https://doi.org/10.1016/j.jclepro.2021.127154

Heikkilä, A. (1999). Inherent safety in process plant design, Technical research center of Finland. 1–132.

Julián-Durán, L. M., Ortiz-Espinoza, A. P., El-Halwagi, M. M., & Jiménez-Gutiérrez, A. (2014). Techno-economic assessment and environmental impact of shale gas alternatives to methanol. ACS Sustainable Chemistry and Engineering, 2(10), 2338–2344. https://doi.org/10.1021/sc500330g

Mohammadi, H., Jafari, M. J., Pouyakian, M., Keighobadi, E., & Moradi Hanifi, S. (2023). Development of a new index for assessing the inherent safety level of chemical processes using a multi-criteria fuzzy decision-making approach. Journal of Loss Prevention in the Process Industries, 105238. https://doi.org/10.1016/j.jlp.2023.105238

Ordouei, M. H., Elsholkami, M., Elkamel, A., & Croiset, E. (2016). New composite sustainability indices for the assessment of a chemical process in the conceptual design stage: Case study on hydrogenation plant. Journal of Cleaner Production, 124, 132–141. https://doi.org/10.1016/j.jclepro.2016.02.107

Park, S., Xu, S., Rogers, W., Pasman, H., & El-Halwagi, M. M. (2020). Incorporating inherent safety during the conceptual process design stage: A literature review. In Journal of Loss Prevention in the Process Industries (Vol. 63). Elsevier Ltd. https://doi.org/10.1016/j.jlp.2019.104040

Qian, Y., Vaddiraju, S., & Khan, F. (2024). Inherent Process Risk Index (IPRI) – A tool for analyzing Inherently Safer Design using Aspen Plus simulation. Process Safety and Environmental Protection. https://doi.org/10.1016/j.psep.2023.12.070

Rahman, M., Heikkilä, A. M., & Hurme, M. (2005). Comparison of inherent safety indices in process concept evaluation. Journal of Loss Prevention in the Process Industries, 18(4–6), 327–334. https://doi.org/10.1016/j.jlp.2005.06.015

Zhu, J., Liu, Z., Cao, Z., Han, X., Hao, L., & Wei, H. (2022). Development of a general inherent safety assessment tool at early design stage of chemical process. Process Safety and Environmental Protection, 167, 356–367. https://doi.org/10.1016/j.psep.2022.09.004

Data-Driven Vulnerability Assessment Method for Industrial Cyber-Physical Systems

Yimeng Zhao, Guohua Chen[*], Qiming Xu, Yihong Huang, Honghao Chen

Institute of Safety Science & Engineering, South China University of Technology, Guangzhou, 510640, Guangdong, China

*mmghchen@scut.edu.cn

1. Introduction

Industrial cyber-physical systems (ICPSs), as a key technology of the Industry 4.0 era, have been widely applied across various industrial sectors, including manufacturing, energy, power, chemicals, and transportation. By integrating operational technology (OT) with information technology (IT), ICPSs achieve a high level of interconnectivity and coordination between devices, systems, humans, and data, driving the intelligent transformation of industries. However, despite the immense potential of ICPSs, their implementation also introduces several risks and challenges.Attackers can infiltrate the network, disrupt normal system operations, and even cause severe cyber-physical (C2P) incidents. There were as many as 36 cyber-attacks in the oil, chemical, and energy sectors worldwide between 2006 and 2014 (Iaiani et al., 2021).

ICPSs are composed of multiple components, including sensors, actuators, logic controllers, human-machine Interface, engineering stations, and data servers. This inherently means that ICPSs typically contain numerous vulnerabilities. In practice, however, it is often unrealistic for practitioners to address and patch all vulnerabilities. Furthermore, during the pre-risk assessment phase of a system, considering all possible attack pathways stemming from these vulnerabilities could lead to a combinatorial explosion of accident scenarios. Therefore, conducting vulnerability assessment research and identifying critical vulnerabilities in ICPSs is of paramount importance. Common Weakness Enumeration (CWE), as a collection of Common Vulnerabilities and Exposures (CVE), provides a detailed classification of CVEs. The MITRE CWE database annually lists the top 25 most common CWE types to guide cybersecurity professionals (MITRE CWE database). However, this statistical result is not specific to ICPSs. Currently, the most widely used vulnerability assessment tool is the Common Vulnerability Scoring System (CVSS). However, Nayak et al. demonstrated that the CVSS exploitability and impact scores are only applicable at the software level, failing to account for the subsequent physical consequences in ICPSs. As a result, CVSS scores do not align with the actual exploitation rates of vulnerabilities. Therefore, some researchers have since proposed modifications to the CVSS to address this limitation. Wang et al. (2023) considered the impact of exploited vulnerabilities and enhanced the original CVSS model by incorporating metrics for safety, finance, operations, and privacy. Zhu et al. (2023) optimized the Access Vector (AV) and Access Complexity (AC) parameters by considering factors such as property safety, life safety, functional safety, and privacy safety, addressing some of the limitations within the CVSS framework. However, the effectiveness of most improved CVSS models remains unvalidated by empirical evidence. Falco et al. (2018) analyzed the density of Common Weakness Enumeration (CWE) within ICPS vulnerabilities and examined the real-world exploitation of these vulnerabilities using open-source databases such as CWE, ExploitDB, and CVEDetails. Based on their findings, they proposed a data-driven vulnerability

prioritization method to objectively assess systemic risk. Nevertheless, this method has limitations. In practice, incident data is often scarce, and accident reports are typically too brief, making it difficult to map these descriptions effectively to current CWE types.

In summary, this study will improve traditional vulnerability assessment model and, using a data-driven approach, validate the correlation between the vulnerability assessment index system and the actual exploitation frequency of vulnerabilities. Furthermore, the proposed vulnerability prioritization method can significantly simplify the risk assessment process for complex ICPSs while ensuring the objectivity and accuracy of the evaluation results.

2. Methods

2.1 Research flowchart
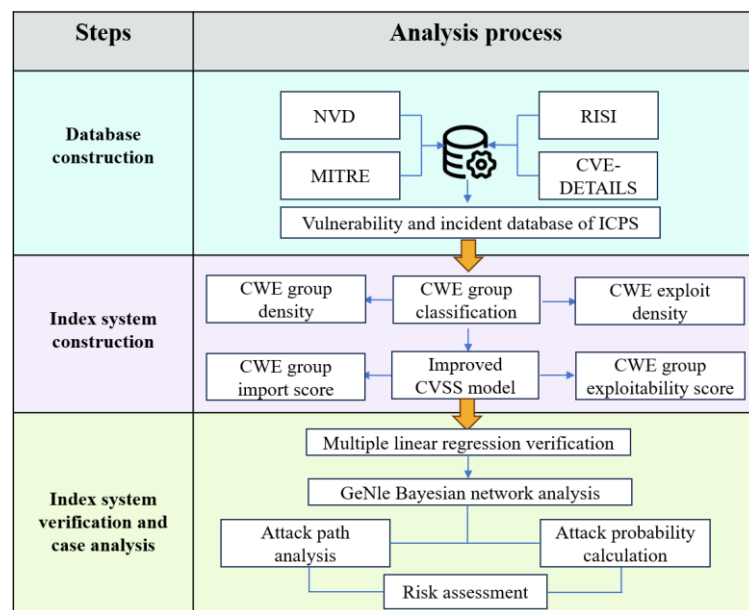
Figure 1: Framework of the analysis process in the study.

As shown in Figure 1, this study consists of three parts: First, a database of vulnerabilities and cyber-attack incidents related to ICPSs is established. Then, based on the CWE groups classification principle, the density of CWE groups and the real-world exploitation density of CWE groups are calculated. An improved CVSS model, which considers the consequences of subsequent incidents, is proposed to compute the average impact and exploitability scores for each CWE group, thus constructing a vulnerability prioritization assessment index system. Finally, multiple linear regression is used to validate the effectiveness of the index parameters, and the method is applied to the tank level control system for risk analysis.

2.2 Database construction

Based on the key devices in ICPSs, a search was conducted in the MITRE CVE database, resulting in the collection of 1,053 vulnerabilities. The corresponding CVE identifiers and base scores were retrieved from the National Vulnerability Database (NVD). Additionally, 19 relevant incident cases were collected from the RISI cybersecurity incident database (RISI database), encompassing various industrial sectors such as chemicals,

electricity, manufacturing, and transportation. Furthermore, 48 currently exploited vulnerabilities were obtained from the CVEDetails database. The above data together constitute the ICPS-specific vulnerability and cyber-attack incident database, which provides data support for the vulnerability priority assessment.

2.3 CWE group classification principle

Thomas et al. (2020) proposed a novel CWE groups classification approach specifically for ICPSs, which encompass 95% of the vulnerabilities in the database. Unlike previous studies, this classification approach, while still based on CWE, avoids the definitional ambiguity of the traditional CWE classification approach and provides a clearer reflection of how vulnerabilities manifest in ICPS. As mentioned in the introduction, the currently available cybersecurity incident reports for ICPS are often too brief, making it challenging to map incident causes using the conventional CWE classification approach. In this study, the new CWE group classification approach ensures accurate mapping of cybersecurity incident reports to CWE groups, thereby better reflecting the actual exploitation of vulnerabilities. The detailed definitions of each CWE group are outlined below.

1) Web-Based Weaknesses: Attackers exploit vulnerabilities or flaws exposed in web applications to gain unauthorized access. 2)Default Credentials: Attackers use default system passwords or hardcoded sensitive credentials to infiltrate the system. 3)Denial of Service and Resource Exhaustion: Attackers overwhelm the target system with large volumes of requests or data, rendering the system or service unresponsive to legitimate user requests. 4)Exposed Sensitive Data: These vulnerabilities allow unauthorized attackers to access sensitive information, leading to the leakage of user credentials or other sensitive data. 5)Weak and Broken Cryptography: Attackers exploit weak encryption techniques or incorrectly apply strong encryption to gain unauthorized access. 6)Memory and Buffer Management: Attackers input data exceeding the buffer size of a program, causing memory overwrites that can result in the execution of malicious code. 7)Permissions and Resource Access Control: Attackers exploit incorrect privilege allocation or lack of proper access control to perform arbitrary operations on the system. 8)Privilege Escalation and Authentication Weaknesses: Attackers bypass authentication mechanisms by exploiting system vulnerabilities, and gaining elevated privileges to perform unauthorized actions.

Based on the above CWE group classification approach and the data from Section 2.2 on ICPS-specific vulnerabilities and cyber-attack incidents, the CWE group density and actual exploit density for each CWE group are calculated, as shown in Figure 2. It is evident that there is a clear positive linear relationship between the top five CWE group densities and exploit densities. This means that the more frequent occurrence of a particular type of vulnerability increases its exposure rate and makes it more susceptible to exploitation by attackers.
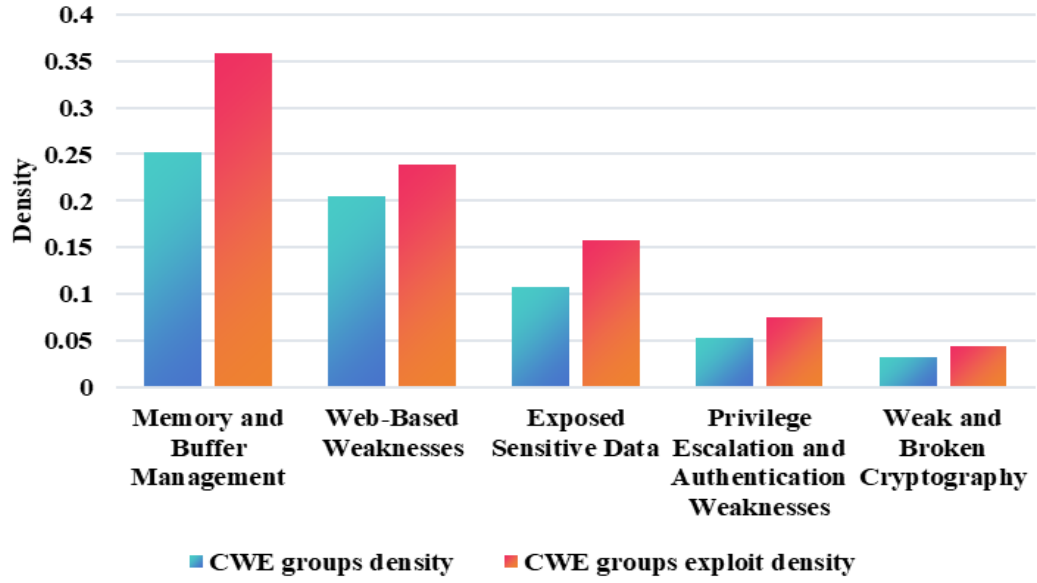
Figure 2: The CWE groups density and exploit density of top 5 CWE groups.

2.4 Improved CVSS model

To more objectively quantify the prioritization of vulnerability importance, this section takes into account the impact of subsequent incidents on the significance of vulnerabilities. Therefore, on the basis of the CVSS 3.1 framework, additional nodes have been introduced, including operational error, privacy leakage, and C2P Risk. The operation node is determined by the Integrity and Availability scores of the vulnerability, while the C2P risk level is influenced by both the operation and privacy nodes. These nodes are connected through OR gates, and the H, L, and N thresholds for each node are calculated separately. The improved CVSS model is illustrated in Figure 3, and using Eq. (1-4), the impact score, exploitability score, the condition probability of successful attacks, and risk level of the vulnerability are calculated (Zhang et al. 2017).

$$ISS = 1 - \left[(1-C)(1-I)(1-A)(1-P)(1-O)(1-C2P) \right]$$

$$impact\ score =$$

$$if\ scope\ is\ Unchanged\quad 6.42 \times ISS$$

$$if\ scope\ is\ changed\quad 7.52 \times (ISS - 0.029) - 3.25 \times (ISS - 0.02)^{15}$$

$$\text{(1)}$$

$$Exploitability\ score = 8.22 \times AV \times AC \times PR \times UI \quad \text{(2)}$$

$$P_{attack\ success} = 2.11 \times AV \times AC \times PR \times UI \quad \text{(3)}$$

$$R = P_{attack\ success} \times S(management\ layer = 1, \sup ervisory\ layer = 2, control\ layer = 3) \quad \text{(4)}$$
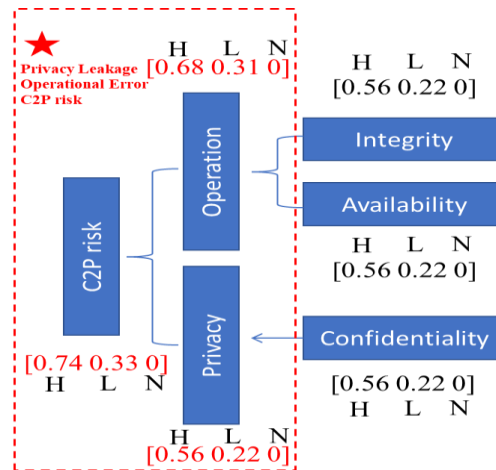
Figure 3: Improved CVSS model

2.5 Index system verification

In this section, the MATLAB multiple linear regression tool is used to calculate the standard error, and R^2 of the regression parameters between CWE group density, average impact score, average exploitability score, and CWE group exploit density, in order to verify the effectiveness of the index system. As shown in Table 1, there is a significant correlation between CWE group density and exploit density. Moreover, after applying the improved CVSS model, the R^2 value increased from 0.955 to 0.994, demonstrating the effectiveness of the vulnerability assessment index system.

Table 1: Results of Multiple Linear Regression

Traditional CVSS model	Estimate	Standard error
Intercept	-0.119	0.283
CWE group density	1.004	0.734
average impact score	0.021	0.029
average exploitability score	0.021	0.095
R^2	0.955	
Improved CVSS model	**Estimate**	**Standard error**
Intercept	-0.634	0.257
CWE group density	0.167	0.013
average impact score	0.185	0.067
average exploitability score	0.044	0.034
R^2	0.992	

3. Case study: an application to tank level control system

3.1 Construction of tank level control system

This section takes the real tank level control system as an example to conduct vulnerability prioritization and risk level analysis. As shown in Figure 4, the tank level control system is composed of the management layer, monitoring layer, and control layer. Key equipment includes the Administrator host, HMI, Data server, and PLC. In the control layer, three PLCs are responsible for controlling the level gauge, pump, level interlock device, and control valve
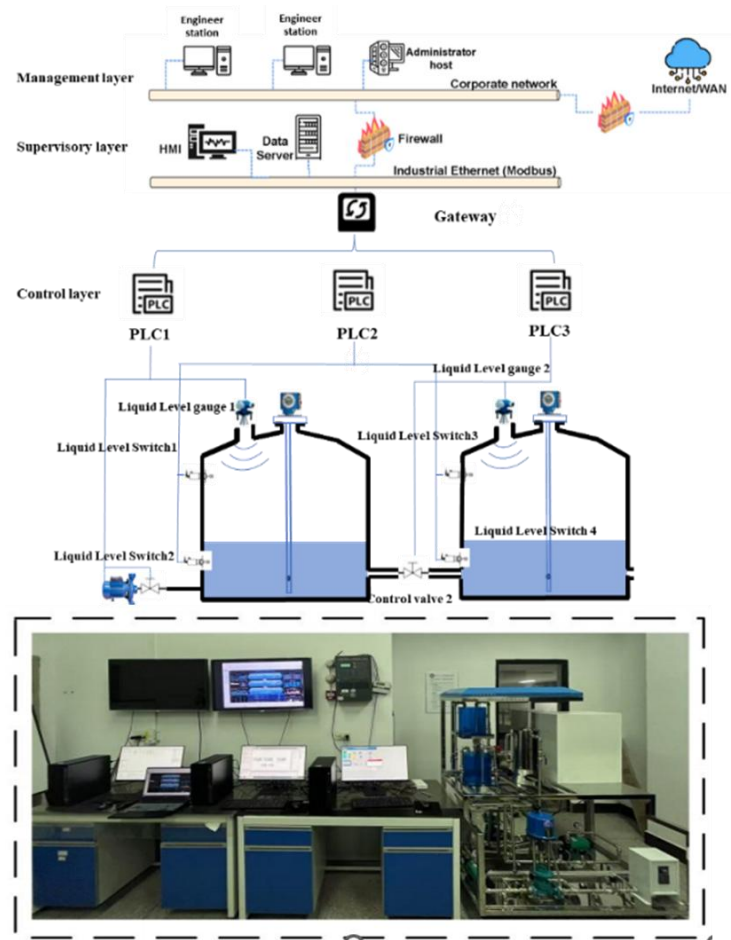
Figure 4: The tank level control system

3.2 Risk analysis

Based on the methods outlined in Section 2, an attack graph was established for vulnerabilities in the top 5 CWE groups with an average impact score and exploitability score sum greater than 7. The results of the high-risk vulnerability screening are shown in Table 2, which displays the CVE ID, corresponding device name, the sum of the average impact score and exploitability score, and the associated probability of the successful attack.

Table 2：Result of high-risk vulnerability screening

CWE group	CVE number	NO.	Equipment	ES+IS	Pattack success
Memory and Buffer	CVE-2022-47393	V1	HMI	9.1	0.727
Management	CVE-2022-4046	V2	HMI	12.2	0.727
Web-Based Weaknesses	CVE-2016-8673	V3	PLC	12.1	0.727
	CVE-2018-8997	V4	PLC	12.2	0.345
	CVE-2017-1498	V5	AH	7.2	0.531
Exposed Sensitive Data	CVE-2018-1994	V6	DS	8.5	0.727
Privilege Escalation and	CVE-2017-0283	V7	ES	12.2	0.727
Authentication	CVE-2017-8692	V8	AH	12.1	0.416
Weaknesses					
Weak and Broken	CVE-2018-6618	V9	DS	12.2	0.471
Cryptography					

Using the GeNIe software, the attack graph is converted into a Bayesian Network (BN), quantifying the probability of successful attack and risk level for each device node, as shown in Figure 5. In this representation, circles denote vulnerability nodes, while squares represent device nodes. The attack success probabilities for the Administrator host, HMI, Data server, and PLC are 0.73, 0.67, 0.62, 0.53, and 0.59, respectively, and the risk level increases with the penetration of attack levels.

Figure 5: The risk calculation result based Bayesian Network

4. Conclusions

This study developed a vulnerability prioritization assessment method tailored for ICPSs based on an improved CVSS model and a novel CWE) groups classification approach and verified the effectiveness of the assessment index system by applying the incident case-driven. Finally, a case study on a tank level control system was conducted to quantify attack paths and risk levels. The application of this vulnerability assessment method can significantly reduce the complexity of security assessments in ICPSs while ensuring the objectivity of the assessment results to some extent.

Acknowledgments

References

Iaiani, M., Tugnoli, A., Bonvicini, S., Cozzani, V., 2021, Analysis of Cybersecurity-related Incidents in the Process Industry. Reliability Engineering & System Safety. 209, 107485.

Wang, Y., Yu, B., Yu, H., Xiao, L., Ji, H., Zhao, Y., 2023, Automotive Cybersecurity Vulnerability Assessment Using the Common Vulnerability Scoring System and Bayesian Network Model. IEEE Systems Journal. 17(2), 2880-2891.

Zhu, Q., 2023, Enhancing vulnerability scoring for information security in intelligent computers. International Journal of Intelligent Networks. 4, 253-260.

Falco, G., et al. 2018, CALDERA C, SHROBE H. IIoT Cybersecurity Risk Modeling for SCADA Systems. IEEE Internet of Things Journal. 5(6), 4486−4495.

Thomas, R.J., Chothia, T., 2020, Learning from vulnerabilities - categorising, understanding and detecting weaknesses in industrial control systems. In: Computer Security. Springer International Publishing, Cham.

Nayak, K., Marino, D., Efstathopoulos, P., Dumitras, T., 2014, Some vulnerabilities are different than others. In: Research in Attacks, Intrusions and Defenses. Springer International Publishing, Cham.

RISI - The Repository of Industrial Security Incidents. https://www.risidata.com/. [dataset].

Common vulnerability enumeration (CVE). MITRE, https://www.cve.org/. [dataset].

Zhang, H., Lou, F., Fu, Y., Tian, Z., 2017, A conditional probability computation method for vulnerability exploitation based on CVSS. 2017 IEEE 2nd International Conference on Data Science in Cyberspace, 238−241.

Development of a Support System for the Analysis of Human Factors in Chemical Plant Accidents

Masaki Nakagawa, Mamiko Takahara

Mitsubishi Chemical Co., 1-1, Marunouch 1 Chome, Chiyoda-ku, Tokyo 100-8251, JAPAN

masaki.nakagawa.ma@mcgc.com; mamiko.takahara.md@mcgc.com

1. Introduction

Variation Tree Analysis (VTA) and Why-Why analysis are methods for analysing the causes of accidents caused by human behaviour during manufacturing processes and maintenance work at chemical plants. VTA and Why-Why analysis are often used as a set. VTA is a method of analysing the circumstances of an accident in time order, with particular emphasis on human behaviour and judgment (Figure 1). The progression of an accident is shown along a time series (the flow of time can be from top to bottom or bottom to top). In VTA, situations, tasks, judgments, or actions that deviate from normal conditions are picked up as variation factors. Among the variation factors, those that would not have caused the accident without this factor are specifically called elimination nodes This elimination node is the starting point of the Why-Why analysis.

Why-Why analysis is a method of continuously questioning the causes of an accident in a logical manner to identify the root causes of the accident and take countermeasures (Figure 2). Why-Why analysis is conducted through discussions among participants. The procedure of Why-Why analysis when used in combination with VTA is as follows,

    1. Starting from the elimination node of the VTA, ask "why" it occurred.
    2. Then turning the answer to the first question into a second "why" question.
    3. After that, the next answer becomes the third "why" question, and so on.
    4. Repeating the "why" until the root cause is identified, and appropriate measures are taken.

The process of deriving answers and putting them into writing in the conventional Why-Why analysis was very time-consuming. This is because in this analysis method, answers are listed one by one, referring to all information related to the occurrence of mistakes and problems. For this reason, the writing process varied from analyst to analyst in the analysis. In other words, the conventional analysis method had the problem that the results of the analysis varied depending on the analysts conducting the analysis, even if the analysis was conducted for the same accident.

To solve these problems, Nakagawa and Shibata (2016) describe a method that was devised to create templates for Why-Why analysis in advance from the viewpoint of human factors, and to efficiently perform Why-Why analysis by referring to these templates. However, in this method, the wording of the templates did not always facilitate the analysis. It is also failed to determine the accuracy of the logical structure of the Why-Why analysis when deviating from the structure of the template. Furthermore, there were problems such as the time and effort required to modify the template once it was created.

Therefore, there is a need to develop a tool that could ensure the quality of analysis, reduce analysis time and manpower, provide support that is in line with actual analysis, and provide flexible support according to the accident conditions.
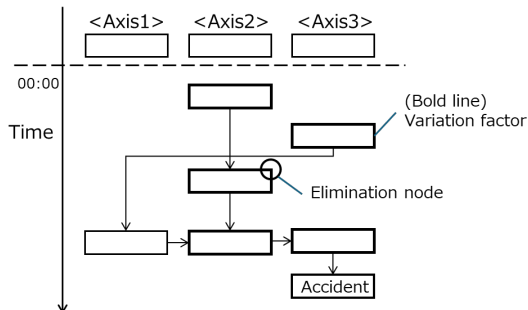
Figure 1. VTA.
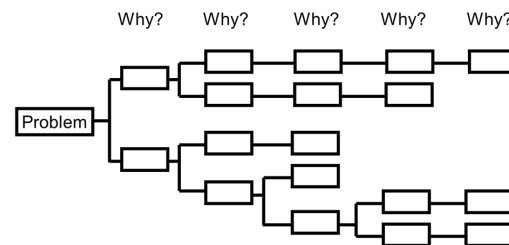
Figure 2. Why-Why Analysis.

2. Methods

In this study, to support Why-Why analysis, methods that patterns accident analysis results and supports Why-Why analysis using the patterned data are developed. This support methods have functions to accumulate the analysis results of Why-Why analysis, to learn new analysis results, to support the analyst in suggesting candidates for the next "why", and to check the logical consistency of the Why-Why analysis results.

2.1 Patterned accident analysis results

Why-Why analysis consists of a series of short sentences, and each short sentence has a "cause" and "effect" relationship with each other. In this study, a method to organize each sentence that constitutes the result of Why-Why analysis in the form of abstracted words (concepts) is proposed. By implementing this approach, the Why-Why analysis is transformed from "the connection of short sentences" to "the connection of concepts" (Figure 3). Since the event that initiates the Why-Why analysis is the elimination node of the VTA, it is separately conceptualized as a problem event to facilitate ease of understanding and usability for analysts. The "why concept" and the next "why concept" are connected in terms of cause and effect. When the results of numerous Why-Why analyses are organized and tabulated in terms of the connection between "causes" and "effects" of "why concepts", a tree-like diagram can be created (Figure 4). This diagram organizes the patterns of accident analysis results into a tree-like structure. In addition, if the tree is organized by a business field, it is useful to understand the trend of accidents and occupational injuries in each business field.

By organizing the results of the Why-Why analysis in the form of a concept tree, it is possible to visually grasp the patterns of accident analysis. This method allows the analyst to efficiently understand the relationship between cause and effect and to propose candidates for the next "why".

2.2 Development of a support program

A support program is developed to facilitate Why-Why analysis by utilizing accident analysis data organized into a conceptual tree structure. This support program has the following functions as follows,

a) Accumulation function of analysis results: The results of past Why-Why analyses are accumulated in a database so that they can be utilized in later analyses.

b) Learning function for new analysis results: The newly obtained analysis results are learned and added to the database to modify the concept tree each time and improve the accuracy of the support program.

c) Next "why" candidate suggestion function: This function enhances the efficiency of analysis by proposing candidates for the next "why" to the analyst.

d) Logical consistency check function: This function checks the logical consistency of Why-Why analysis results by detecting contradictions and inconsistencies.

Figure 3. Example of rewriting to the why concept.

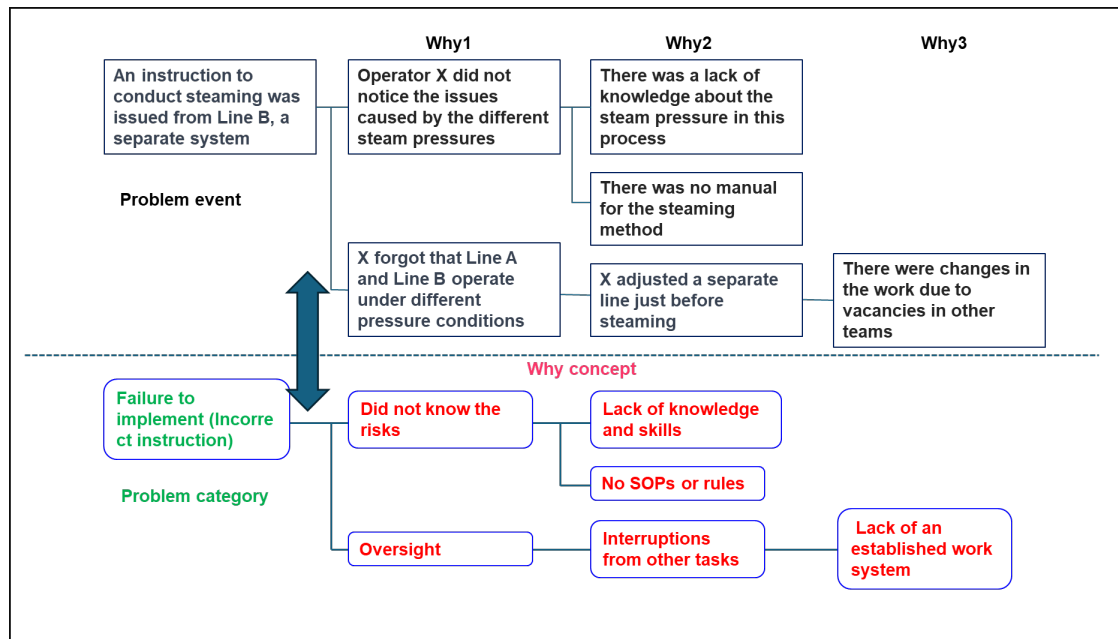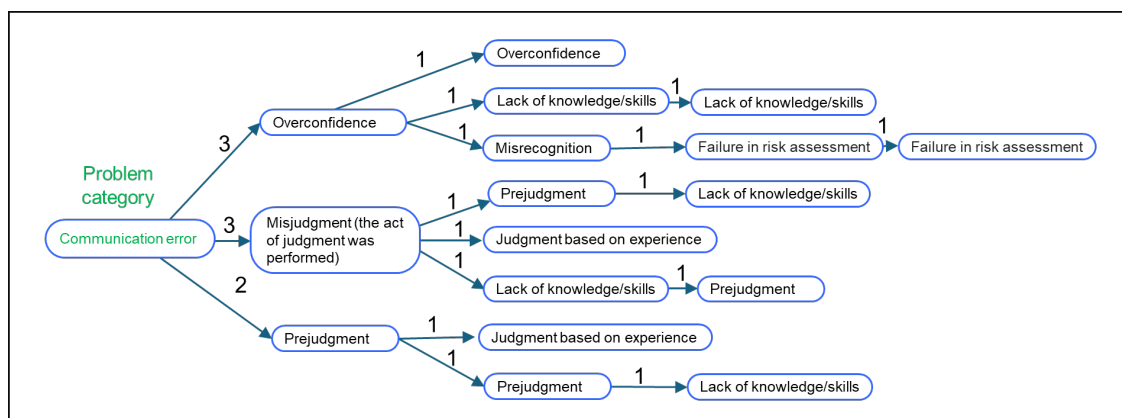*Figure 4. Part of the concept tree. The numbers in the diagram indicate the aggregated values of the relationships between the "why concepts".*

Analysis Methods Using Support Programs are as follows,

(1) Classification of problem categories

Problem categories are abstracted terms grouped as the starting points (problem events) of the Why-Why analysis. These terms are extracted from past accident analysis data and include around a dozen types, such as "Failure to respond" and "Equipment malfunction." When the analyst inputs the starting point of the Why-Why analysis, the AI predicts the appropriate problem category based on the words of the problem event and presents them in order of increasing certainty. For example, as shown in Figure 5, if the starting point of Why-Why analysis is the VTA elimination node "Operator X instructed to conduct steaming from Line B, a separate system", the problem category is classified in terms of what kind of problem this problem event is in general. The analyst selects the problem category that finally seems to fit the content of this sentence from the presented problem categories (if there is no word to be selected, add it as appropriate). "Failure to respond (incorrect instruction)" is selected in this example.

(2) Classification into why concepts

The "why concepts" are grouped as abstract words, such as "Oversight", "Inadvertent error", and "Insufficient knowledge and skills", for the answers to the "why" in the Why-Why analysis. Approximately 200 types are prepared from past accident analysis data. The AI predicts the "why concepts" that will be the causes of the next "why" from past data, based on the first problem category selected, and presents them as candidates in order of their high probability. In this case, the analyst selects "Oversight", as in (2).

(3) Determining the why factor

When the analyst selects a "why concept", specific examples of events corresponding to the "why concept" are presented. A concrete example related to "Oversight" is presented. The analyst uses this as a reference to describe the next "why" factor. In (3), the analyst stated, "X forgot that Line A and B have different pressures".

(4) Why-Why reasoning and countermeasure planning

Next, the AI predicts the next "why concept" from past data based on the event described in the "why", and then analyst describes the next "why" factor using the predicted concept and specific examples as ideas. The analysis is continued repeatedly until specific measures are taken. For example, from the "Why 1 event", "I forgot that Line A and B have different pressures", AI presents the concept of "Why 2". If "Interruption from other tasks", "Information overload", or "Work stress" is selected, several more specific examples will be presented. The analyst should refer to this and describe the following why factors as in (2). In (4), "X adjusted a separate line just before steaming" is described. The analyst repeats this process to arrive at the root cause in the "Why n" event and considers countermeasures.

The above reasoning part was divided into four steps (1) through (4), and algorithms were constructed for each of these steps. These can provide more appropriate support by using machine-learned models of accident analysis data for each business field. Furthermore, generative AI is utilized to verify the theoretical correctness of the connections between "Why n" event and "Why n+1" event in the Why-Why analysis.

		Support by AI	Analyzer(User) Action
(1)		List potential problem categories	Select the problem category relevant to the event
(2)		List potential "Why1 concepts" related to the problem category	Select the most suitable Why1 concept
(3)		List examples of past events involving the Why1 concept.	Refer to the provided examples and freely input a related Why1 event
(4)		List potential Why2 concepts as causes of the Why1 event	Select the most suitable Why2 concept after further analysis

Figure 5. The various inference parts of Why-Why analysis.

3. Results and discussion

Although the support program proposed in this study contributes to improving the efficiency and accuracy of Why-Why analysis, several issues remain to be addressed.

3.1 Issues related to granularity of "why concepts"

Setting detailed "why concepts" related to SOPs may affect the accuracy of machine learning. This is because the corresponding examples will be dispersed and the number of examples corresponding to each "why concept" will decrease. On the other hand, if the concepts are set too broadly, the amount of data for each "why concept" will be biased and may require appropriate subdivision. Therefore, it is necessary to check the examples corresponding to the "why concepts", subdivide the concepts for those that occur frequently, and if there are only a few examples, integrate those that can be lumped together and create "why concepts" as needed (Figure 6).
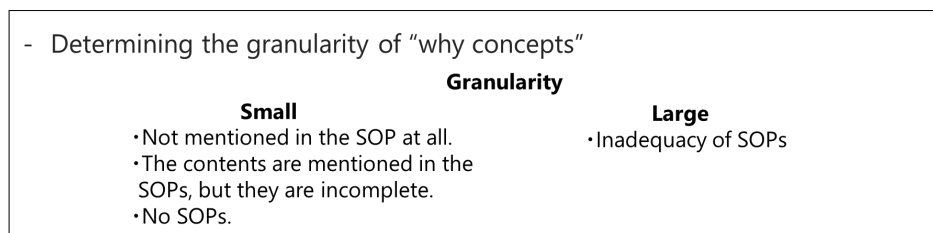
Figure 6. Issues related to why concept granularity.

3.2 Issues related to the wording of concept

Synonyms and indistinguishable terms may confuse analysts. To clarify these differences, terms are rewritten using alternative expressions (Figure 7). For example, "Did not understand" is revised to "Did not understand something", and "Did not know" is revised to "Was unaware of the information". These adjustments are made to ensure that the expressions are clear and comprehensible to the analysts.

- Defining the meaning of "why concepts" (e.g., addressing synonymous terms)

Rewriting "why concepts"

・Didn't understand.	⟹	・Didn't understand the writing
・Didn't know.		・Didn't know the information
・Didn't notice.		・Didn't recognize the issue(or detail)

Figure 7. Issues related to why concept granularity.

3.3 Future work

The "why concepts" are being modified by using generative AI for more efficient study. Figure 8 shows some of the "why concepts" being organized, and the concepts themselves are being organized using the generative AI and modified to make them easier to reason about. The more data on these concepts is accumulated, the more room there will be for reexamination. Future research will continue to explore these concepts. Currently, this program has completed the machine learning component and is being developed as an application that can be used by anyone. When the application completed, it is expected that more data will be accumulated, and accuracy will be improved by having employees use the application.

(e.g.) List of concepts related to communication

Before revision by generative AI	After revision by generative AI
The provider of the information was misinformed.	The provider of the information was misinformed.
Didn't get the information right.	Didn't get the information right.
Didn't have the proper documentation.	Didn't have the proper documentation.
A failure to communicate.	A failure to communicate.
Poor communication.	Poor communication.
Be indifferent to others.	Be indifferent to others.
Only had verbal communication.	Only had verbal communication.
Didn't make it known.	Didn't make it known.
Didn't give them the right information.	The information given (text, pictures, cues) was difficult to understand or comprehend
They didn't share information.	They made a mistake in the way they conveyed information.
They made a mistake in the way they conveyed information.	An assumption that they understood.
There were inadequate methods of communicating information.	Difficult to understand the instructed work procedures.
Didn't give them the information.	Relationships were not smooth.
I had an assumption that they understood.	Inadequacies in the education and training system.
It was difficult to understand the instructed work procedures.	For sharing incorrect information.
Relationships were not smooth.	The information given (text, pictures, cues) was difficult to understand or comprehend
Inadequacies in the education and training system.	The information (text, picture, cue) given was incorrect.
For sharing incorrect information.	There was a lack of communication.
There wasn't enough sharing of information.	Inadequate communication tools.
They didn't share information.	A lack of emergency communication channels.
The information given (text, pictures, cues) was difficult to understand or comprehend	Communication protocols for emergencies were unclear.
The information (text, picture, cue) given was incorrect.	The timing of communication was not right.
	Communication skills were lacking.

New

Figure 8. Organizing "why concept" with generative AI

4. Conclusions

This study involves the patterning of accident analysis results to support Why-Why analysis, leading to the development of the support program utilizing these patterned data. This support program has a function to accumulate the analysis results of Why-Why analysis, a function to learn new analysis results, a support function to suggest candidates for the next "why" to the analyst, and a function to check the logical consistency of the Why-Why analysis results.The method proposed in this study contributes to improving the efficiency and accuracy of Why-Why analysis. Future work is required to apply the method to actual accident analysis and to verify its effectiveness.

References

Nakagawa M., Shibata T., 2016. Analysis Methods for Human Factors in C
hemical Plant Accidents, CHEMICAL ENGINEERING TRANSACTIONS 48, 781-786.

Apparatus Effects on Calorimetric Safety Parameters and Their Impact on Operation Limits

Adrian Zentel[1], Dominik Ohlig, Jana Sartorius, Johannes Schröder[1], Marc-André Serrer*[1], Markus Gödde[2], Robert John Blanchard[1]

[1] *Safety Assessment & Testing (BASF SE, Carl-Bosch-Straße 38, 67056 Ludwigshafen, Germany*

[2] *Process Safety (BASF SE, Carl-Bosch-Straße 38, 67056 Ludwigshafen, Germany*

*marc-andre.serrer@basf.com

1. Introduction

In the chemical process industry, it is essential to minimize accident risks to protect human life, the environment, and assets. Process safety experts advocate for a balanced approach between economic efficiency and necessary risk reduction measures. Conservative safety characteristics can negatively impact overall process economics, as they are closely linked to data quality and the sensitivity of the chosen characterization methods. A comprehensive understanding of these methods, including their sensitivities and uncertainties, is essential for reducing potentially overly conservative safety margins, thereby allowing for increased process temperatures and enhanced production capabilities. For instance, even a small rise in the maximum allowable process temperature can yield significant benefits for a production plant.

One of the key safety characteristics is the TMR_{24}, the temperature at which the time to the maximum decomposition rate is 24 hours under adiabatic conditions. The TMR_{24} can be derived from differential scanning calorimetry (DSC) by distance rules or kinetic evaluation or directly measured by adiabatic calorimetry. The maximum allowable process temperature T_{exo} correlates directly with the TMR_{24} by $T_{exo} = TMR_{24} - 10$ K.[1] The correlation between TMR_{24} and the onset temperature (T_{Onset}) for non-autocatalytic thermal decomposition reactions is defined as $TMR_{24} = T_{Onset, DSC} - 100$ K for DSC or $TMR_{24} = T_{0,1W/kg} - 10$ K. Therefore, both characteristics are influenced by the uncertainties of the respective calorimetric method. To determine the TMR_{24} by kinetic evaluation of dynamic DSC scans especially the tau lag and the time constants of the DSC device are the critical apparatus effects which must be considered. Tau lag comprises the heating rate dependent temperature offset between the oven temperature and the respective temperature inside the reference cell. The time constants describe the thermal relaxation of the crucible and sensor as well as the sample and crucible. If the TMR_{24} is directly measured by adiabatic calorimetry the critical apparatus effects are the phi-factor and the detection limit of the measuring system.

To explore and mitigate these uncertainties, a detailed study on apparatus effects impacting TMR_{24} determination was conducted using a known model system of 40 wt.% dicumyl peroxide (DCP) in ethylbenzene.[2]

2. Methods

To assess the apparatus effects of differential scanning calorimetry (DSC) and adiabatic calorimetry impacting the determination of TMR_{24}, a comprehensive study was conducted based on the thermal behaviour of 40 wt.% dicumyl peroxide (DCP) in ethylbenzene (EB).

DSC measurements were performed on Mettler Toledo DSC-1 and DSC-3 instruments. To determine the tau lag and time constants melting peaks of indium and zinc were measured in V4A, V2A, HC, gold, and glass crucibles (in-house). The heating rate dependent shift of the melting point was used to calibrate for tau lag. The time constants were derived from the relaxation curve of the heat signal after melting was completed. Measurements of DCP/EB in V4A and Glass crucibles were conducted with devices calibrated for the respective crucible types and compared to those calibrated solely with V4A crucibles. Subsequently, a formal kinetic model was developed utilizing the software *"Thermal Safety Series-Advanced Reaction Kinetics Simulation (TSS-ARKS)"* from *Cheminform St. Petersburg Ltd.* The DSC data of runs conducted at 1-5 K/min underwent several corrections, including adjustments for thermal resistance of the measurement cell, normalization, smoothing, background subtraction, and data thinning. The heat capacity was conservatively estimated at 2.00 J g^{-1} K^{-1}. The optimal model was derived from a reaction of n-th order (A → B), characterized by the equation $r_i = k_0 e^{-E/RT} (1-\alpha)^n$. An example of the kinetics derived from the corrected measurements will be presented in the following. However, all conducted measurements were evaluated analogously to determine the overall influence of the mentioned parameters.

Table 1: Formal Kinetics derived from DSC measurements of the 40 wt.% dicumyl peroxide (DCP) in ethylbenzene.

$\ln(k_0)$	E_a	n	Q
[$\ln(s^{-1})$]	[kJ mol^{-1}]	[-]	[kJ kg^{-1}]
36.7	153.30	1.03	356.60

The determined parameters are presented in Table 1, with a comparison between model predictions and experimental results illustrated in Figure 1.
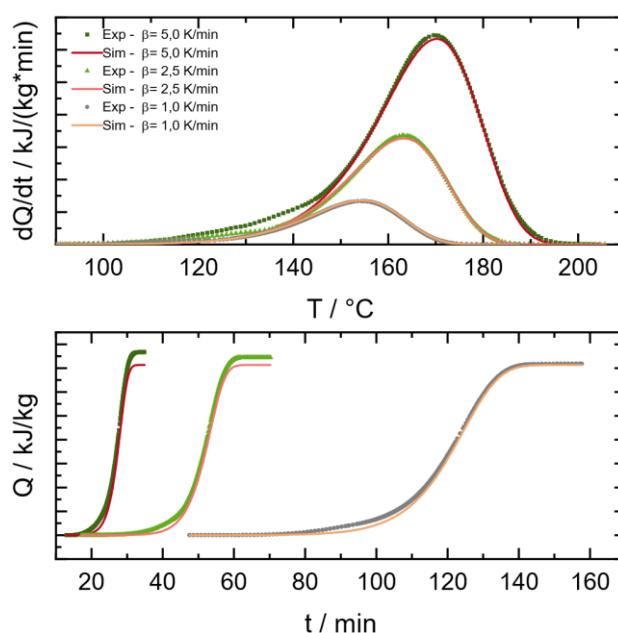
Figure 1: Comparison of experimental DSC data (points) of the 40 wt.% dicumyl peroxide (DCP) in ethylbenzene with the fit of the formal kinetic model (line).

The comparison depicted in Figure 1 reveals a satisfactory alignment between the experimental DSC data (points) and the model (line), indicating the model's applicability for calculating temperature-dependent heat flows and TMR.

2.1 Heat accumulation pressure vessel test

The apparatus employed for these investigations was developed in-house by BASF. The temperature-dependent detection limit of the apparatus was determined as follows: An inert heating oil with a known heat capacity was utilized, and a defined power input was applied to the system through electrical impulses. This established a measurement curve, as illustrated in Figure 2.
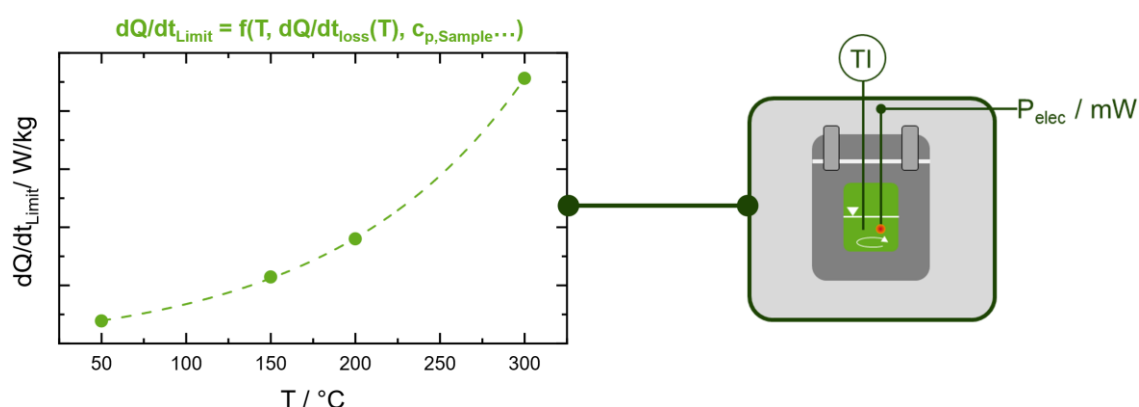
Figure 2: Temperature dependent detection limit of the in-house heat accumulation pressure vessel test.

Based on the determined detection limit, two measurements were conducted using the model system: The first measurement was performed at 75 °C for three days, remaining below the detection limit, followed by a temperature increase to 87 °C, just above the detection limit. The second measurement commenced directly at 90 °C, above the detection limit. Subsequently, the TMR_{24} for the conducted experiments was calculated using the aforementioned methodology and the software code from *Cheminform St. Petersburg*.

3. Results and discussion

First, the impact of the crucible material on the tau lag of the DSC device was investigated.
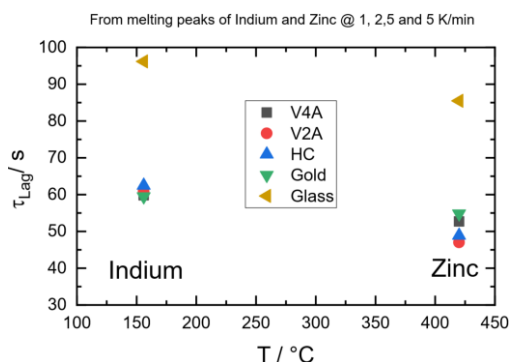
Figure 3: Impact of different crucible materials (V4A, V2A, HC, Gold and Glass) on the tau lag.

The results in Figure 3 show for both reference materials, *i.e.* indium and zinc, that the metal crucibles resulted in similar tau lag values while for the glass crucibles a tau lag of approximately 30 seconds higher was obtained. Using a DSC device calibrated with a tau lag of a metal crucible with a glass crucible led to an onset temperature shift of up to 5 K (at a heating rate of 10 K/min) as well as a loss of about 9% in the detected enthalpy due to wrong enthalpy calibration. Hence, it can be concluded that when applying new measurement crucibles, the tau lag needs to be determined to check whether the use of the same tau lag for all crucibles is sufficient, or a separate tau lag calibration must be applied.
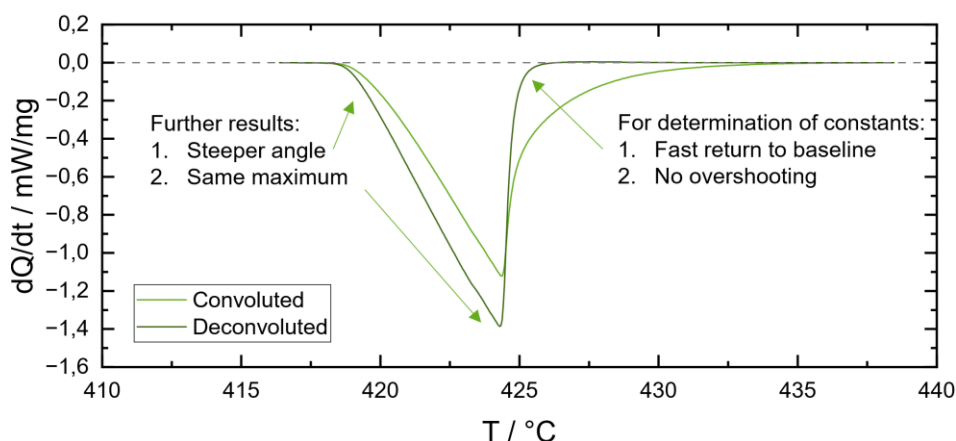
Figure 4: Effect of deconvolution on a DSC Peak.

Other parameters that impact the TMR are time constants. To investigate their impact on the activation energy (that significantly impacts the determination of the TMR), the data was deconvoluted, *i.e.* corrected by these time constants. The impact of the deconvolution is shown in Figure 4: The slope of the peak is corrected. As the activation energy of the thermal decomposition is derived from the slope of the peak, the deconvolution has a direct impact thereon.
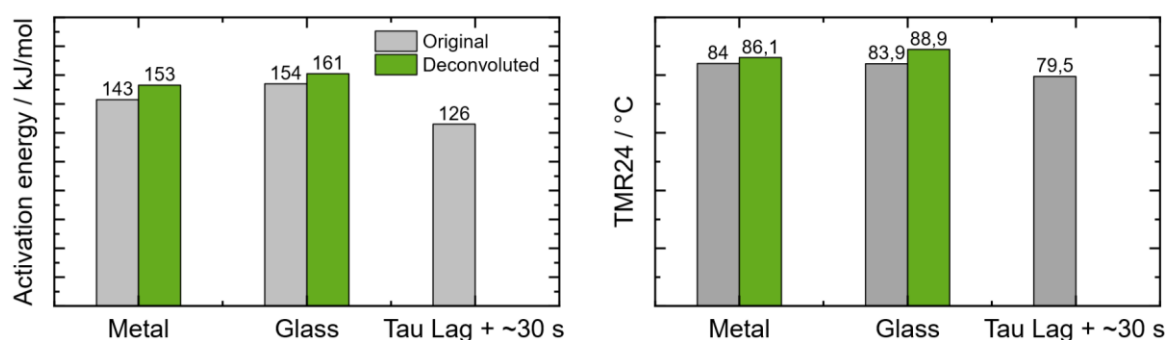
Figure 5: Influence of the deconvolution of DSC data on the activation energy (left) and the TMR_{24} (right) for metal and glass crucibles. The original data is depicted in grey, the corresponding deconvoluted data in green. Tau lag + ~30 s depicts a glass vial on a DSC device calibrated with a metal vessel and without deconvolution.

According to the results shown in Figure 5, the deconvolution resulted in an increase in activation energy by approximately 10 kJ/mol, which corresponds to an increase in TMR_{24} of 2 to 5 K. Conversely, uncorrected DSC data from inadequately calibrated instruments

(*e.g.* glass crucibles measured on a device calibrated for metal crucibles) significantly underestimated the TMR_{24}, compromising economic potential (*cf.* Figure 5, Tau Lag + ~30 s).

Hence, the tau lag as well as the time constants tau for the relaxation of crucible/sensor relaxation and sample/crucible, have a significant influence on the measurement results and the uncertainties in the thereof derived TMR_{24}.
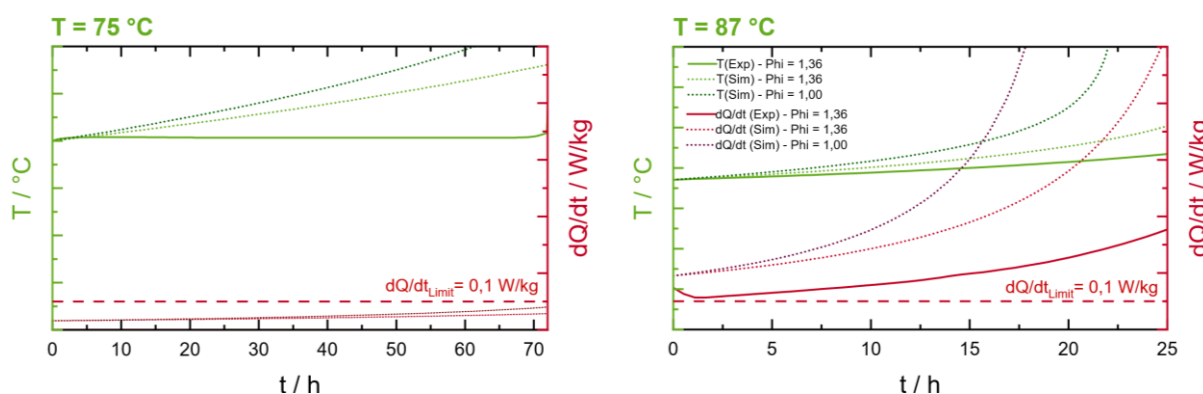
Figure 6: Comparison of a non-optimized experimental run (left) started at 75 °C with a model-based optimized experimental design (right) started at 87 °C of an adiabatic measurement of 40 wt.% dicumyl peroxide (DCP) in ethylbenzene.

Adiabatic calorimetry is a technique employed to directly measure TMR_{24}. This requires a precise sensitivity calibration, which can be achieved using an external heat source and/or known reference materials, as elaborated in section 2.2. To analyse the effects of detection limits and experimental design on results, a kinetic model derived from differential scanning calorimetry (DSC) was utilized to simulate the adiabatic behaviour of a 40 wt.% DCP in an ethylbenzene solution across various initial temperatures. This simulation aimed to identify the temperature at which the heat release during the onset of thermal decomposition reaches the sensitivity threshold of the adiabatic calorimeter.

Adiabatic experiments were subsequently performed at temperatures both below and above this detection limit. At 75 °C, which is beneath the detection threshold of 0.1 W/kg (*cf.* Figure 6, left), the simulated initial heat generation rate was lower than this limit, suggesting that heat loss surpassed the heat generated by thermal decomposition (dQ/dt). Consequently, no measurable temperature increase was observed, indicating a no exothermic reaction. The dotted curves in the results illustrate the temperature profiles that would have been observed if the calorimetric setup had a detection limit of 0 W/kg (pale green dotted curve) and if the phi-factor were 1 (dark green dotted curve), implying no heat loss to the reactor walls. These findings demonstrate that measuring a sample with unknown thermal kinetics may lead to an underestimation of its energetic potential, particularly critical when used for scale-up where low surface-to-volume ratios of reactors approach almost adiabatic conditions.

In the next phase, the aged sample was heated to 87 °C, a temperature predicted by the simulation to yield heat generation exceeding the detection limit (*cf.* Figure 6, right). Hence, the measurement program follows the widely known heat-wait-search method. It is essential to note that the simulation did not comprise the thermal history of the sample, thus neglecting the energy losses due to previous storage at 75 °C during heat-wait-search. This results in artificially elevated temperature and energy generation curves in the simulated data. This demonstrates that the implications of thermal aging on samples, particularly

regarding heat generation below detection limits, necessitates further investigation concerning their impact on the final TMR_{24}. To achieve this, the phi-corrected TMR_{24} was calculated using three methodologies.

Table 2: Formal Kinetics derived from DSC measurements of the 40 wt.% dicumyl peroxide (DCP) in ethylbenzene.

Kinetic	DSC	Adiabatic Calorimetry	Method	TMR_{24}
Kinetic 1	X		Dynamic	86,1 °C
Kinetic 2	X	X	One Step	86,3 °C
Kinetic 3	X	X	HWS	88,6 °C

Kinetic 1 is derived from data generated on a well calibrated DSC device including all aforementioned corrections (*cf.* Figure 1). Kinetic 2 is based on the DSC data from Kinetic 1 and further supplemented by an adiabatic experiment that was directly started with a fresh sample above the detection limit of the setup (not shown). Kinetic 3 is based on the DSC data from Kinetic 1 and further supplemented with the adiabatic experiment from the heat-wait search experiment shown in Figure 6. The results are summarized in Table 2. It is shown that using the data from an adiabatic calorimetry with thermal history below the detection limit of the setup, *e.g.* due to heat-wait search method or due to long heat up phases, might result in a TMR_{24} that is not conservative.

4. Conclusions

In conclusion, precise characterization of calorimetric measurement devices is essential for accurately determining safety-relevant characteristics in thermal process safety. The study underscores that uncorrected data from poorly calibrated instruments (DSC) or prolonged measuring times close to the detection limit (adiabatic calorimetry) can lead to significant variation in TMR_{24}, resulting in overly conservative and uneconomic or even underestimated safety margins. Integrating kinetic modelling supports accurate and cost-efficient experimental planning while simultaneously reducing experimental uncertainties. This study demonstrates that a careful attention to apparatus effects and data processing might significantly influence the quality of derived safety characteristics. Furthermore, an optimization and minimization of such uncertainties facilitates the reduction of conservative safety margins and provides economic benefits in the operation of exothermic chemical processes while ensuring consistent safety levels.

References

1. Bundesministerium für Umwelt, Naturschutz und Reaktorsicherheit, **2021**. *Technische Regel für Anlagensicherheit (TRAS) 410*, Kommission für Anlagensicherheit, Bundesanzeiger.
2. Duerrstein S. H., Kappler C., Neuhaus I., Malow M., Michael-Schulz H., Goedde M., **2016**. *Model-Based Prediction of the Adiabatic Induction Period and SADT of Dicumyl Peroxide Solution and Comparison to Large-Scale Experiments Performed Using 216.5-Liter Steel Drums in the UN-Test H.1*, Chemical Engineering Transactions, *48*, 475-480. DOI:10.3303/CET1648080.

Impact of Near-Wall Particle Concentration on Dust Explosion in the 20 L Sphere Through Numerical Simulation

Kasun Weerasekara[1,2*], Stefan H. Spitzer[3], Sabine Zakel[1], Holger Grosshans[1,2]

[1] *Physikalisch-Technische Bundesanstalt, Bundesallee 100, Braunschweig, 38116, Germany;*
[2] *Otto von Guericke University of Magdeburg, Universit¨atspl. 2, Magdeburg, 39106, Germany*
[3] *ElfI-Tech, Universit¨atspark 1/1, Schw¨abisch Gm¨und, 73525, Germany.*

*kasun.weerasekara@ptb.de

1. Introduction

A dust explosion is a hazardous chemical explosion that can occur in process industries such as flour mills, grain silos, textile industries, etc. Dust explosions occur when ignition starts in the confinement of combustible dust. Dust explosions can cause significant harm to human lives sna physical resources. Therefore, understanding and regulating dust explosions is essential to minimize the damage.

In laboratory level 20 L, the Siwek apparatus is used to investigate the explosion pressure (P_{ex}) and the explosion pressure rise ((dP/dt)$_{ex}$) for a particular dust type. The Siwek is a 20 L sphere with two chemical igniters at the center. Dust is conveyed through a nozzle into the sphere. A commonly used nozzle type is a rebound nozzle. Two pressure sensors measure the pressure development inside the sphere, which is the main finding of the experiment.

A uniform dust distribution inside the sphere is required to determine the dust's minimum explosible concentration (MEC) and other safety characteristics. However, particles are more concentrated near the wall before the ignition. Kalejaiye O. et al. built a Siwek apparatus with six optical probes in different locations inside the sphere. They have found that the concentration of particles near the wall is higher than in other locations. Du B. et al. observed similar detailed results using a transparent 20 L Siwek sphere and shadowgraphy technique. They have suggested a new nozzle arrangement for better dust distribution before the ignition. However, experimental methods are minimal for visualizing dust distribution and movements inside the sphere. Well-validated computational fluid dynamic (CFD) simulation can provide more insight into dust distribution inside the sphere. Di Benedetto A. et al. simulated dust dispersion inside the 20 L sphere through the rebound nozzle using the ANSYS-Fluent cfd package. They have observed that particles are not uniform and are more converted near the wall. Beauce, when particles disperse into the sphere, it creates two counter-rotating vortexes inside the sphere. Later, particles settle down and reduce the turbulence inside.

In summary, both experiments and simulation confirm that particles are more concentrated near the wall and inhomogeneous. This study presents the near particle concentration impact on the explosion pressure and explosion pressure rise in the side 20 L sphere through the numerical simulation.

2. Methodology

2.1 Dust Explosion Modelling

Dust explosion is a multiphase problem involving solid and fluid phases. The Euler-Lagrangian approach was selected because the solid phase has a lower volume fraction. The numerical simulation uses the OpenFOAM open-source package and the "coalChemistryFoam" Euler-Lagrangian solver, which can also solve chemical reactions and radiation.

The Euler-Lagranian approach has separate sets of governing equations for each phase. The fluid/continuous phase consists of four equations based on Reynolds Average Navier-Stokes (RANS) equations and the conservation of species and energy. Each conservation equation has source terms coupled with the governing equations of the solid phase, which also consists of conservation energy of mass momentum and energy.

In dust explosion modeling, we assume that a particle includes solid, liquid, and gas phases. The solid phase consists of char and ash. The liquid phase consists of water (moisture), and the gas phase consists of volatile gases such as CH_4 and H_2. When the particle is heated from ignition, moisture evaporation starts first, followed by the devolatilization of gases and, finally, char combustion. Figure 1 shows an overview of modeling the combustion of a dust particle.

Moisture evaporation and devolatilization absorb energy from the surrounding fluid, and char combustion generates heat. These devolatile gases, evaporated moisture, and combustion products will be source terms for the fluid phase mass and species conservation equation, and absorbed or generated heat will be the source term for the fluid phase energy equation. While particles move in the fluid phase, they are subjected to drag, buoyancy, and gravity forces. The reaction of each force will be the source term for the momentum equation of the gas phase.
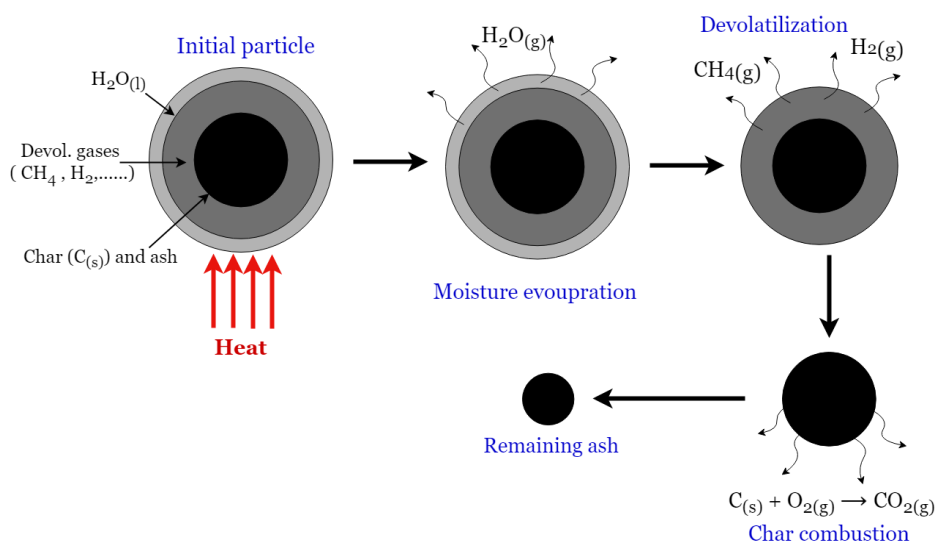

Figure 1. Overview of a dust particle combustion process

2.1 Case Set-Up and Benchmark Test

We selected the lycopodium dust explosion experiment to validate the numerical solver due to its comparatively uniform distribution compared to other dust types. The experiment uses the "Janovsky" nozzle to ensure a total dust mass inside the sphere. The numerical simulation required several material properties of the lycopodium dust and experiment parameters.

Sartorius MA35 test determined the composition of the dust, yielding a 3.4% weight percentage of moisture and a 3.8% weight percentage of volatile matter. We assume that CH_4 is only a volatile gas and that the solid part is pure carbon, according to the study by Rasam H. et al. Lycopodium has a narrow size distribution of d_{50} = 30.6 µm, d_{10} = 25.3 µm, and d_{90} = 30.6 µm measure, and we assumed all particles are spheres with d_{50} as the particle diameter. The material density of lycopodium is ρ = 100 kg/m3, and the specific heat capacity is C_p = 1005 J/kgK. The devolatilazation temperature is T_{dev} = 483 K and devolatzilzation latent heat is $\Delta H_{dev} = 3.07 \times 105$ J/kg (Portarapillo M. et al).

The geometry is a sphere with a 0.168 m radius equivalent to 20 L volume. All the internal components, like the ignition mechanism nozzle, are neglected for simplicity. Dust particles are initially placed uniformly inside. The simulation domain has a single wall boundary. We set wall temperature to 294 K, velocity as no slip, and pressure as zero gradients as boundary conditions. Initially, the internal domain was set to uniform 294K temperature, 1 bar of pressure, and zero velocity field. Ignition is modeled as a temperature patch inside the sphere, adopted by Pan Y's doctoral thesis. Ignition volume contains two spheres, a 4 cm radius each, and the center-to-center distance is 8cm at the sphere's center. Temperature is modeled as a first-order polynomial function $T(t) = 2 \times 10^5$ t + 294 K with ignition duration of t = 20 ms. For the stability of the simulation, the CFL number is set to 0.1 with first-order Euler time integration. We used the k-ε turbulence model, which is a commonly used turbulence model in combustion problems.

The mesh convergence test involved six meshes ranging from 2.5 $\times 10^4$ to 1.6 $\times 10^6$ elements. A structured mesh with all hexagonal elements was generated, and Figure 2 compares the pressure development curve of each mesh case with the experimental results. Figure 3 illustrates the relationship between P_{ex}, $(dP/dt)_{ex}$, with the number of elements. After considering both computational time and accuracy, the mesh with 8 $\times 10^5$ elements was selected, as it had a 3.5% and 2.5% error relative to the experimental value for P_{ex} and $(dP/dt)_{ex}$, respectively. Additionally, we use 5 $\times 10^5$ no of particles.

3. Particle Concentration Analysis and Results

As discussed in the introduction section, the distribution of particles within a 20 L sphere is not uniform and is more concentrated near the wall. This study aims to investigate the impact of dust particle distribution on explosion characteristics. To achieve this, we simulate dust explosions of lycopodium for different particle distributions. Spherical coordinates, including radial distance, polar angle, and azimuthal angle can define the position of a particle. To alter the radial homogeneity of the particles, we apply a power law function to the radial distances of the particles without changing the two angles of each particle. The coefficient of the power law, defined as the radial homogeneity of the distribution, is denoted as ϕ.
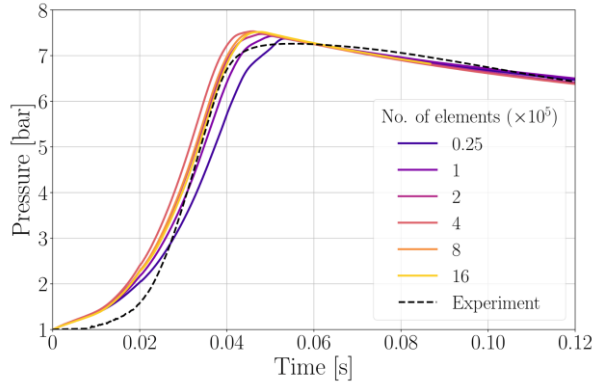
Figure 2. Pressure curves of simulations with different mesh sizes compared to experimental data
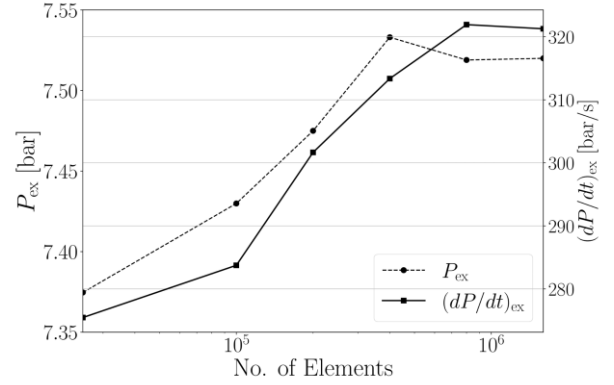
Figure 3. P_{ex} and $(dP/dt)_{ex}$ for different mesh sizes

The analysis begins with generating a uniform dust distribution within a unit radius sphere, with the radial distance of a particle denoted as r_{uni}. We then define the new radial distance of the particle with inhomogeneity (wall concentrated) as $r_\phi = R(r_{uni})^\phi$. Here, R represents the scale of the sphere's radius, which is 0.166 m. The parameter ϕ varies between 0 and 1, with $\phi = 1$ indicating a uniform distribution of particles and $\phi = 0$ indicating all particles are on the wall. Figure 1 illustrates the uniform distribution ($\phi = 1$), and Figure 2 illustrates $\phi = 0.5$ of particle distribution. For this study, we simulated 10 cases for $\phi = 0.1, 0.2, 0.3,...,1$ while maintaining all parameters constant.

Figure 6 presents the pressure development curves for each particle distribution. As ϕ decreases from 1 to 0.4, the explosion delays and the time to reach the P_{ex} increases. However, after 0.4, the time to reach the P_{ex} is decreasing. When particles are uniformly distributed, immediate particle combustion begins once the ignition is initiated. However, when particles are more concentrated towards the wall, the flame front takes some time to reach the dust particles, thereby delaying the explosion. Moreover, when particles are extensively concentrated near a wall ($\phi < 0.4$), the flame front propagates towards the wall rapidly and encounters higher particle concentration, leading to an intense explosion. Figure 7 confirms these observations.
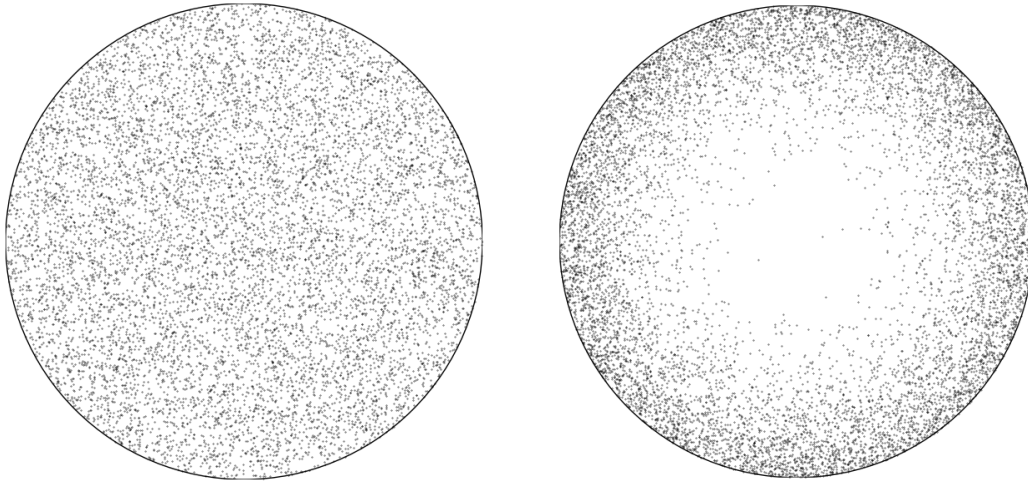
Figure 4. Initial particle distribution for $\phi = 1$

Figure 5. Initial particle distribution for $\phi = 0.5$

Figure 7 shows the variation in the pressure gradient over the time for each distribution. This trend is similar to the pressure development curve in Figure 6. The highest pressure gradient occurs when particles are extensively concentrated near the wall. When ϕ is decreasing, the time to reach $(dP/dt)_{ex}$ increases while the value of $(dP/dt)_{ex}$ also decreases. Still, the time to reach $(dP/dt)_{ex}$ is increasing until $\phi = 0.4$, similar to Figure 6. However, $(dP/dt)_{ex}$ rises after the $\phi < 0.7$. The highest value for P_{ex} and $(dP/dt)_{ex}$ are reached when $\phi = 0.1$, and they are 1.75% and 10% higher than when particles are uniformly distributed, respectively. The lowest value of P_{ex} was reached when $\phi = 0.8$ and for $(dP/dt)_{ex}$, reached when $\phi = 0.7$ are 0.25% and 5.6% lower compared to the uniform distribution (see Figure 8).
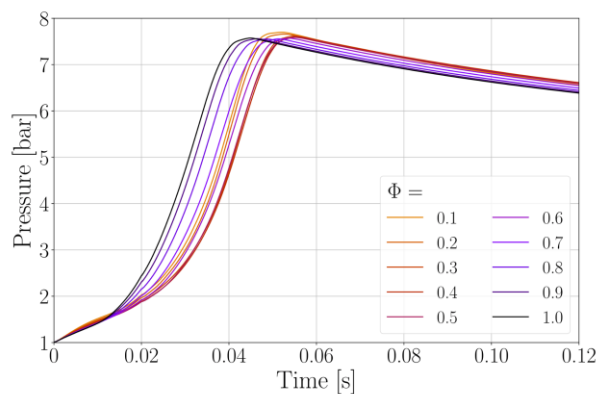
Figure 6. Pressure development curve for each particle distribution
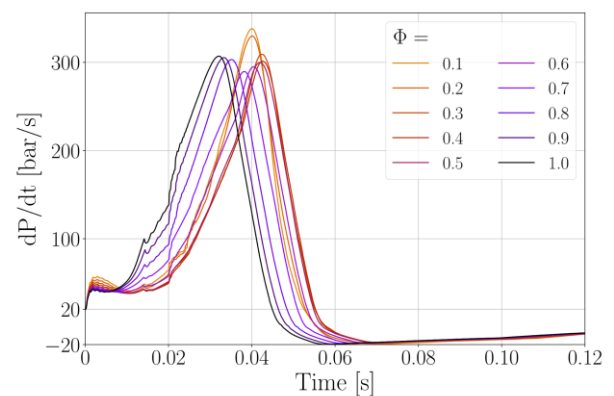
Figure 7. Pressure gradient curve for each particle distribution
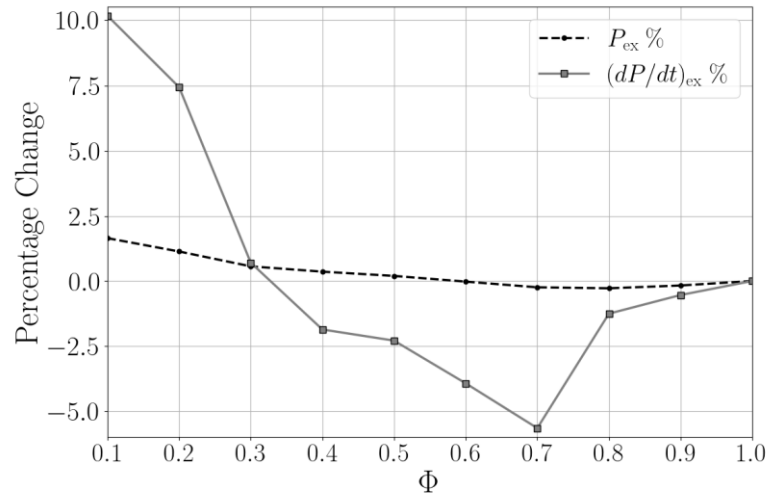
Figure 8. Percentage of variation of P_{ex} and $(dP/dt)_{ex}$ compared to uniform distribution for each ϕ value

4. Conclusions

Uniform particle distribution is essential for accurate measurement of the safety characteristics of the 20 L sphere. However, in practice, particles are not uniform and are more concentrated near the wall. This study investigated the influence of particle distribution on the explosion characteristics of the 20 L sphere. The results indicate that the explosion is more intense when particles are concentrated near the chamber wall. The highest P_{ex} and $(dP/dt)_{ex}$ are reached when the particles are most concentrated near the wall ($\phi = 0.1$), and the lowest values are reached for moderate wall concentration distributions ($\phi = 0.8$ and $\phi = 0.7$, respectively). These findings have practical implications for safety engineering, highlighting the importance of considering particle distribution in safety assessments. As a future study, developing a correction factor for the safety characteristics of the 20 L sphere will be important due to the influence of wall particle concentration. Furthermore, this study can extend to different dust types and geometries like 1m^3 explosion chamber, silos, and dust conveying pipes.

References

Du, Bing, Weixing Huang, Long Liu, Tan Zhang, Hao Li, Yidan Ren & HanlinWang. 2015. Visualization and analysis of dispersion process of combustible dust in a transparent Siwek 20-l chamber. Journal of Loss Prevention in the Process Industries 33. 213–221.

Kalejaiye, Omotayo, Paul R. Amyotte, Michael J. Pegg & Kenneth L. Cashdollar.2010. Effectiveness of dust dispersion in the 20 L Siwek chamber. Journal of Loss Prevention in the Process Industries 23(1). 46–59.

Pan, Yangyue. 2023. Flame behavior of coal dust explosion considering internal particle effects: Montanuniversitaet Leoben dissertation.

Portarapillo, M., R. Sanchirico, G. Luciani & A. Di Benedetto. 2023. Flame propagation of combustible dust: A Mallard-Le Chatelier inspired model. Combustion and Flame 251. 112737.

Rasam, Hamed, Maryam Nematollahi, Sadegh Sadeghi & Mehdi Bidabadi. 2019.An asymptotic assessment of non-premixed flames fed with porous biomass particles in counter-flow configuration considering the effects of thermal radiation and thermophoresis. Fuel 239. 747–763.

Predicting Pressure Effects of Delayed Ignition in Gas Free Jets: Model Development and Validation with CFD Approach

Fabian Krieg[1,*], Jens Denecke[2,3], Lukas Bohlender[1,2], Jürgen Schmidt[2], Oliver Odenwald[1]

1 BASF SE, Carl-Bosch-Str. 38, 67056 Ludwigshafen, Germany;
2 CSE Center of Safety Excellence (CSE-Institut), Joseph-von-Fraunhofer-Str. 9, 76327 Pfinztal, Germany
3 University of Applied Sciences, Moltkestrasse 30, 76133 Karlsruhe, Germany

*Fabian.krieg@basf.com

1. Introduction

In the chemical industry, overpressure protection for equipment and plant components is typically achieved through mechanical safety devices such as safety valves and rupture discs. When gaseous or vapor releases occur, the gas is often released into the atmosphere with high momentum, potentially resulting in an ignitable free jet. Despite adherence to regulatory design standards for the outlet, ignition of the free jet cannot be entirely excluded. In such instances, the flame front propagates more rapidly due to the turbulence within the free jet compared to passive gas clouds. This results in higher pressure effects relative to a passive gas cloud with the same explosive mass (Sail, Blancheterie, Osman, Daubech, & Jamois, 2018).

Common models for evaluating the pressure effects of gas cloud explosions, such as the Baker-Strehlow-Tang (BST) (Pierorazio, Thomas, Baker, & Ketchum, 2005) and the TNO Multi-Energy Method (MEM) (van den Berg, 1985), account for turbulence caused by obstacles but do not consider the turbulence in the ignitable mixture due to high-momentum releases. Consequently, these models may not always provide conservative estimations of the pressure effects when applied to ignitable free jets.

The objective is to develop a model that offers conservative estimations of the pressure effects, including pressure and pressure impulse, for the ignition of gas free jets. This model should incorporate outlet conditions, substance-dependent properties, and represent the conservative case for other influencing factors such as ignition point, weather conditions, and time of ignition. The interaction of the free jet with objects will be investigated at a later stage. For validation, the model is compared to literature experiments on explosion pressures of horizontal free jets including ground interaction.

2. Methods

Firstly, the influencing variables of the parameters in the models for the pressure effect of the gas cloud explosion were analysed. The following were considered:

1) The Concentration on the free jet axis according to Schefer (Schefer, Houf, & Williams, 2008)
2) The mean velocity on the free jet axis according to Birch (Birch, Hughes, & Swaffield, 1987)
3) For the turbulence on the free jet axis, the approach by Hinze (Hinze, 1975)
4) For the turbulent flame velocity, the models to Bray (Bray, 1990), Bradley (Bradley, Lau, & Lawes, 1992), Peters (Peters, 2010)

5) Complete short-cut models such as BST (Pierorazio, Thomas, Baker, & Ketchum, 2005), MEM (van den Berg, 1985), Giesbrecht (Giesbrecht, 1987)

Experiments of an appropriate scale were identified based on these models and the industrial requirements (Jallais, Vyazmina, Miller, & Thomas, 2018), (Sail, Blancheterie, Osman, Daubech, & Jamois, 2018), (Miller, Eastwood, & K., 2015). Using these experiments, a suitable setup was developed using the CFD software FLACS from Gexcon to reproduce the pressure effects during the ignition of a free jet. This setup facilitated a comprehensive parameter study, from which the pressure effects during the delayed ignition of turbulent gas free jets were evaluated. Specifically, the substances methane, propane, ethylene, acetylene, and hydrogen were assessed within a mass flow range of 0.06 kg/s to 12 kg/s.

3. Results and discussion

The validation of the setup in FLACS has demonstrated that the experimental findings regarding the pressure effect during free jet explosions can be reproduced. The discrepancies between experimental data and simulation results are within a factor of two (figure 1, left). Deviations of the same order of magnitude are observed in repeated experimental trials (Chaineaux, 1993).
The extensive parameter study reveals that the pressure effect is significantly influenced by the type of medium and the released mass flow rate (figure 1, right).
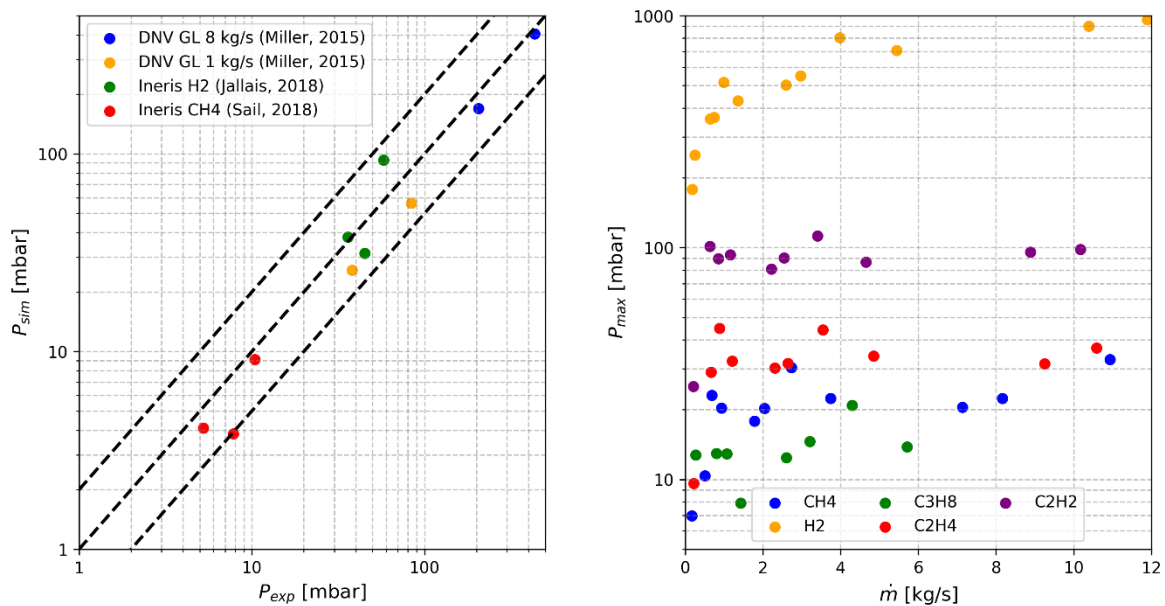
Figure 1. Comparison of the experimentally and simulatively measured peak overpressures for experiments in a technically relevant order of magnitude (left) and maximum peak overpressures on the jet axis as a function of the mass flow rate for several media (right).

4. Conclusions

The validation process has confirmed that the effects of free jet ignition can be simulated with an accuracy comparable to that of experimental results. A comprehensive parameter study, involving variations in the released medium and outlet conditions, reveals significant dependencies between pressure effects, medium properties, and outlet geometrical

dimensions. These observed dependencies present an opportunity to develop an empirical model capable of predicting pressure and pressure impulse based on the specific properties of the released medium and the outlet conditions. The potential of an empirical model based on the findings from the simulations and experiments is discussed.

References

Birch, A. D., Hughes, D., & Swaffield, F. (1987). Velocity Decay of High Pressure Jets. *Combustion science and technology*, 161-171.

Bradley, D., Lau, A. K., & Lawes, M. (1992). Flame stretch rate as a determinant of turbulent burning velocity. *Philosophical Transactions of the Royal Society of London. Series A: Physical and Engineering Science, 338*, 359-387.

Bray, K. N. (1990). Studies of the turbulent burning velocity. *Proceedings of the Royal Society of London. Series A: Mathematical and Physical Sciences, 431*, 315-335.

Chaineaux, J. (1993). *Projet MERGE - Rapport Final.* L'Institut national de l'environnement industriel et des risques (Ineris).

Giesbrecht. (1987). *Gefahren durch Druckwellen und Wärmestrahlung beim Zünden von Brenngasstrahlen - BASF internal.*

Hinze, J. (1975). *Turbulence.* McGraw-Hill.

Jallais, S., Vyazmina, E., Miller, D., & Thomas, J. K. (2018). Hydrogen Jet Vapor Cloud Explosion: A Model for Predicting Blast Size and Application to Risk Assessment. *Process safety progress*, 397-410.

Miller, D., Eastwood, C. D., & K., T. J. (2015). Hydrogen Jet Vapor Cloud Explosion: Test Data and Comparison with Predictions. *11th Global Congress on Process Safety, AIChE Annual Meeting*.

Peters, N. (2010). *Technische Verbrennung.* University of Aachen: Course Material (2006).

Pierorazio, A., Thomas, J., Baker, Q., & Ketchum, D. (2005). An update to the Baker–Strehlow–Tang vapor cloud explosion prediction methodology flame speed table. *Process Safety Progress*, 59-65.

Sail, J., Blancheterie, V., Osman, K., Daubech, J., & Jamois, D. (2018). *Review of knowledge and recent works on the influence of initial turbulence in methane explosion.* L'Institut national de l'environnement industriel et des risques (Ineris).

Schefer, R. W., Houf, W. G., & Williams, T. (2008). Investigation of small-scale unintended releases of hydrogen: momentum-dominated regime. *International Journal of Hydrogen Energy, 33*(21), 6373-6384.

van den Berg, A. C. (1985). The multi-energy method: a framework for vapour cloud explosion blast prediction. *Journal of Hazardous materials, 12*(1), 1-10.

Optimal SIL Configuration Selection: a graph-theoretic Approach

Abdulqader Bin Sahl, Sidra Beg, Moreno Johan, Senithi Lorensuhewa, Cesare Baca, Maurizio Truscello, Francesco Perrone*

Igeam Consulting S.r.l., Via Fara, 35 – 20124 Milano

*f.perrone@igeam.it

1. Introduction

The increasing awareness of industrial accidents, including property damage, injuries, and loss of life, has driven significant growth in functional process safety applications. Companies are legally and ethically obligated to mitigate operational risks, and the rising costs of mitigation have reinforced the importance of prioritizing reliability and safety. As a result, process industries are actively aligning with national and international safety standards, such as IEC 61508 and IEC 61511. To prevent accidents, industries implement multiple layers of protection, with Safety Instrumented Systems (SISs) being one of the most widely used. SISs are specifically designed to execute Safety Instrumented Functions (SIFs), to detect hazardous conditions and ensure the process remains in a safe state (Cheraghi & Taghipour, 2024). A SIS is composed of a combination of sensors, controllers, and final elements that work together to enhance process safety. Each SIF is designed to mitigate a specific process hazard or dangerous event, ensuring that the required Safety Integrity Level (SIL) is achieved. SIL defines the effectiveness and reliability of a SIF in reducing risks for a defined scenario, to an acceptable level. The appropriate SIL rating is determined by the Risk Reduction Factor (RRF), which quantifies the gap between the existing risk and the acceptable risk threshold. SIL are defined across four distinct levels of integrity. As the SIL level increases, the probability of failure on demand (PFD) decreases, reflecting enhanced system reliability and performance. However, higher SIL levels are generally accompanied by increased costs and complexity. SIL values are typically assigned within the range of 1 to 4, with Level 1 representing the lowest (least reliable) and Level 4 the highest (most reliable) level of safety. Table 1 presents the SIL ratings along with the corresponding ranges of RRF and Probability of Failure of Demand (PFD), where PFD is the inverse value of RRF, for a SIF functioning in demand mode (IEC 61511, 2016; IEC 61508a, 2010).

Table 1: SIL and the respective PFD and RRF (IEC 61511, 2016; IEC 61508a, 2010).

Safety Integrity Level (SIL)	Probability of Failure of Demand Avg (PFD_{AVG})	Risk Reduction Factor (RRF)
SIL 4	$\geq 10^{-5}$ to $< 10^{-4}$	$> 10\,000$ to $\leq 100\,000$
SIL 3	$\geq 10^{-4}$ to $< 10^{-3}$	$> 1\,000$ to $\leq 10\,000$
SIL 2	$\geq 10^{-3}$ to $< 10^{-2}$	> 100 to ≤ 1000
SIL 1	$\geq 10^{-2}$ to $< 10^{-1}$	> 10 to ≤ 100

Achieving the desired SIL after the allocation of SIFs, such as through methods like Layers of Protection Analysis (LOPA) or Risk Graph, involves a thorough and strategic selection of system components. Furthermore, the integration of these components into a SIS must consider potential failure scenarios, response times, and the overall reliability of the system. In some cases, it may involve incorporating redundancy (e.g., multiple sensors or controllers) to ensure that a failure in one component does not compromise the system's ability to meet the required SIL. Selecting the optimal SIL configuration involves balancing cost, reliability, and operational feasibility, as compliance can be achieved through various system architectures. While industry standards and company policies often mandate fixed configurations, such as three SIL 2 transmitters, these may not always be the most cost-effective or efficient solutions. Redundant architectures, as opposed to the traditional one-out-of-one (1oo1), i.e., one-out-of-two (1oo2) or two-out-of-three (2oo3) (Figure 1), enhance system reliability but also lead to higher costs and increased complexity.
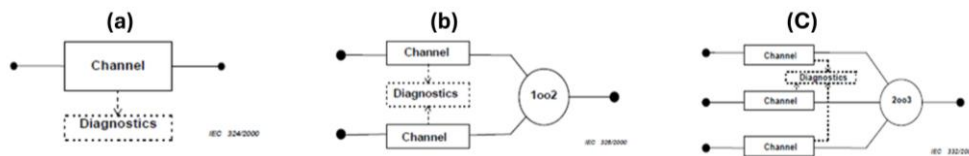
Figure 1: Block Diagram for voting logics: (a) 1oo1, (b) 1oo2 and (c) 2oo3 (IEC 61508b, 2010)

In SIL selection, Hardware Fault Tolerance (HFT) is a key parameter that defines the ability of a system to continue functioning despite hardware failures. It represents the number of failures a system can tolerate before losing its safety function, meaning an HFT of 0 implies a single component with no redundancy, while HFT = 1 means one redundant component is available, and so forth. Additionally, it is crucial to consider that each component of a SIS has a maximum achievable architectural SIL, constrained by HFT and Safe Failure Fraction (SFF). While redundancy improves system reliability, the maximum SIL that can be achieved is also dependent on the SFF of the individual components, meaning that even with increased HFT, certain components may still be limited in the SIL they can achieve due to their inherent failure characteristics. Table 2 and Table 3 present the required HFT and SFF for thresholds for achieving different SIL levels for Type A and Type B components route 1H approach, respectively. Type A components, being less complex with well-understood failure modes, generally require lower SFF values to achieve a given SIL. In contrast, Type B components, which include microprocessor-based or software-driven devices with more unpredictable failure characteristics, require higher SFF values to compensate for their increased uncertainty in failure behavior.

Table 3: Maximum allowable SIL for a safety function carried out by a type A element (IEC 61508c, 2010).

Safe failure fraction of an Element	Hardware Fault Tolerance		
	0	1	2
< 60 %	SIL 1	SIL 2	SIL 3
60 % - < 90 %	SIL 2	SIL 3	SIL 4
90 % - < 99%	SIL3	SIL 4	SIL 4
≥ 99%	SIL 3	SIL 4	SIL 4

Table 4: Maximum allowable SIL for a safety function carried out by a type B element (IEC 61508c, 2010).

Safe failure fraction of an Element	Hardware Fault Tolerance		
	0	1	2
< 60 %	Not Allowed	SIL 1	SIL 2
60 % - < 90 %	SIL 1	SIL 2	SIL 3
90 % - < 99%	SIL 2	SIL 3	SIL 4
≥ 99%	SIL3	SIL 4	SIL 4

For optimal SIL configuration selection, decision-makers must carefully assess multiple feasible options, ensuring that safety requirements are met while optimizing compliance and economic viability. Conventional SIL configuration selection methods typically reply on engineering judgment or predefined standards and guidelines, which can sometimes overlook cost-effective or optimal solutions. Graph-theoretic approaches, such as P-graph, offer a structured and computational means to systematically evaluate all feasible solutions for a problem. P-graph, introduced by Friedler et al. (1979), has been a power tool to solve process network synthesis (PNS) problems given its capable mathematical algorithms, computational efficiency, and flexibility. As opposed to conventional mathematical programming (MP) methods, P-graph has a user-friendly interface which does not require prior programming knowledge (Friedler et al., 1998). Additionally, P-graph is capable of generating all optimal and near-optimal solutions, which provides decision-makers with the flexibility to choose the most optimal solution for their scenario. As such, P-graph has been implemented in several applications such as supply chain synthesis (How et al., 2016), resource conservation optimization (Sahl et al., 2023), multi-objective energy planning (Sahl et al., 2024), reliability and risk analysis (Süle et al., 2019), and non-engineering problems (Aviso et al., 2017).

However, to the best of the authors' knowledge, P-graph has not been previously applied to optimize SIL selection. Therefore, this work presents a novel P-graph approach to determine the optimal SIL configuration, leveraging its ability to systematically generate all optimal and near-optimal solutions. This capability ensures that decision-makers can evaluate multiple feasible configurations, allowing for flexibility in aligning with company guidelines, internal policies, and supplier restrictions. Since SIL compliance can often be achieved through different architectural setups, the ability to explore various alternatives while optimizing for cost, reliability, and operational feasibility makes P-graph a particularly valuable tool in SIS design and SIL allocation.

2. Methods

The methodology framework adopted for this work is shown in Figure 2. SIS data is collected in Step 1, which includes data for the transmitter, logic, and final element. All relevant data to calculate the PFD and is to be collected from manufacturer certificates. Similarly, SFF and cost data for the SIS is also collected. Following that, in Step 2, the P-graph structure is developed, and the collected data is used as input. Based on the desired SIL, the data constraints are entered in the model (e.g., Total PFD for SIL 2 ≤ 1 x 10^{-1}). In Step 3, the P-graph model is used to generate all the feasible SIS configurations that meet the desired SIL requirement for the total PFD while also meeting the maximum allowable architectural SIL. Finally, in Step 4, the results are analyzed in terms of Cost and Total PFD.
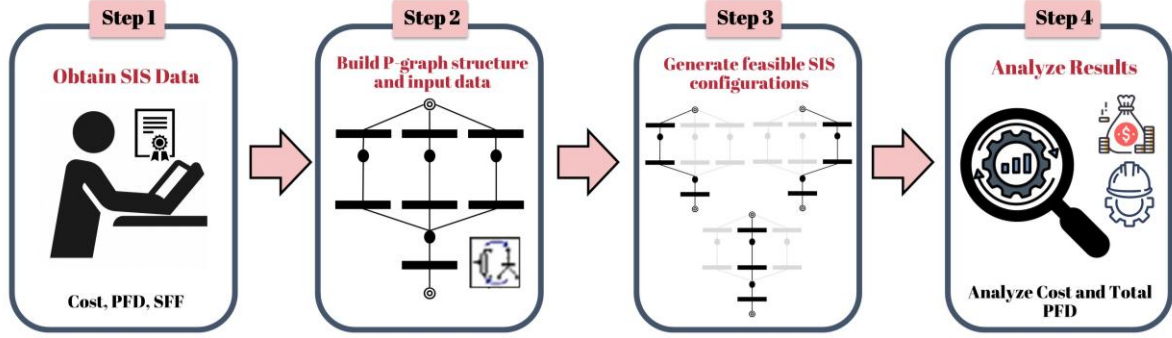
Figure 2. Methodology framework.

2.1 Mathematical Modelling

The mathematical formulations that are represented in the P-graph framework are discussed in this section, which consist of the objective function and model constraints based on a mixed integer linear programming (MILP) approach.

The objective function of this work is to minimize the total cost of the SIS (C_{SIS}), which is c which is calculated as the sum of the costs of transmitter (C_T), logic solver (C_{LS}), and final element (C_{FE}) The objective function is expressed as:

$$Minimize \ C_{SIS} = \ C_T + \ C_{LS} + \ C_{FE} \qquad \text{Eq. (1)}$$

where the cost of the transmitter varies based on the selected voting logic.

To satisfy the SIL requirement of the SIS, the total PFD (PFD_{TOTAL}) of the SIS must be determined, which is done by summing the PFD contributions from all system components, including the transmitter (PFD_T), logic solver (PFD_{LS}), and final element (PFD_{FE}). The total PFD is calculated as:

$$PFD_{TOTAL} = \ PFD_T + \ PFD_{LS} + \ PFD_{FE} \qquad \text{Eq. (2)}$$

The probability of failure of the transmitters differs based on the selected voting logic and is computed according to IEC 61508 standards. For a 1oo1 voting logic, the probability of failure is estimated by:

$$PFD_T^{1oo1} = \frac{\lambda_{DU} \cdot T}{2} \qquad \text{Eq. (3)}$$

For a 1oo2 voting logic, the PFD is calculated as:

$$PFD_T^{1oo2} = \ \frac{\lambda_{DU,1} \cdot \lambda_{DU,2} \cdot ([1-\beta] \cdot T)^2}{3} + \frac{\beta \cdot \lambda_{DU}^{min} \cdot T}{2} \qquad \text{Eq. (4)}$$

For a 2oo3 voting logic, the probability of failure is expressed as

$$PFD_T^{2oo3} = \ PFD_{AVG} = \frac{(\lambda_{DU,1} \cdot \lambda_{DU,2} + \lambda_{DU,2} \cdot \lambda_{DU,3} + \lambda_{DU,1} \cdot \lambda_{DU,3})([1-\beta] \cdot T)^2}{3} + \frac{\beta \cdot \lambda_{DU}^{min} \cdot T}{2} \quad \text{Eq. (5)}$$

where $\lambda_{DU,n}$ represents the dangerous undetected failure rate of a channel in a subsystem, λ_{DU}^{min} is the smallest of all dangerous undetected failure rates, β is the fraction of undetected failures that have a common cause, and T denotes the test period in years.

Once the total PFD is determined, the achievable RRF can be calculated also to facilitate the SIL selection process. The RRF is given by:

$$RRF = \frac{1}{PFD_{TOTAL}}$$ Eq. (6)

The maximum allowable SIL is constrained by the architectural limitations of the system component, which depend on the HFT and SFF. Thus, the system must satisfy the constraint:

$$SIL_{achievable} \leq SIL_{max}$$ Eq. (7)

2.2 P-graph Model

A SIS that can adopt one of 3 transmitters with different voting logics (i.e., 1oo1, 1oo2, 2oo3), logic solver, and final element can be represented in P-graph as shown in Figure 3. P-graph nodes are classified to two classes, i.e., materials and operating units, where material nodes consist of raw material, intermediate, and product nodes. A detailed foundation of P-graph fundamentals is discussed in literature (Friedler et al., 1993; Friedler et al., 2022). The displayed P-graph model must follow the mathematical constrains outlined in Section 2.1. For Figure 3, the red colored nodes are for a transmitter of voting logic 1oo1, the grey color is for a transmitter of voting logic 1oo2, while the blue color represents the transmitter for a voting logic 2oo3. The respective PFD_T and C_T of each transmitter is inserted into the operating unit node. Similarly, the PFD_{LS}, PFD_{FE}, C_{LS}, C_{LS} are input into the operating unit nodes for the logic solver (represented in green) and final element (represented in yellow), respectively. The desired outputs of this model are the PFD_{TOTAL} and $SFF_{T,achievable}$, which are represented as product nodes in pink. The respective PFD_{TOTAL} of the required SIL (based on Table 1) is to be inserted in the PFD_{TOTAL} node. In addition, $PFD_{T,N}$ and $SFF_{T,N}$ must be added as a value on the connecting arcs of the intermediate material node and the operating unit, which are facilitated by imaginary operating units, as shown in Figure 3. Finally, the maximum architectural allowable SIL SFF range for each transmitter is inserted in a respective operating unit before being connected to the final $SFF_{T,achievable}$ product node.
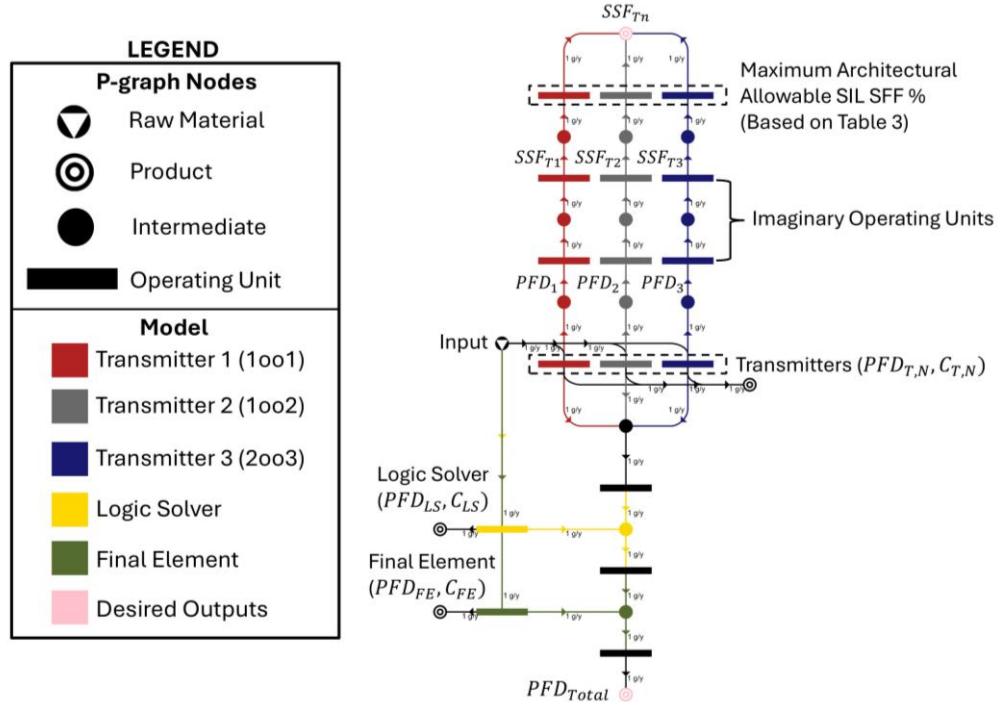

Figure 3. P-graph representation of a SIS with transmitters of different voting logic options.

3. Results and discussion

3.1 Case Study Description

A case study of a generic SIS is adopted to demonstrate the proposed P-graph methodology. The SIS under consideration consists of temperature transmitters (TTs), a fixed logic solver, and a fixed final element. The system is designed to accommodate three different voting logics for the transmitters: 1oo1, 1oo2, and 2oo3. To evaluate different system configurations, three distinct temperature transmitter (TT) models are considered, denoted as TT1, TT2, and TT3. These models are based on industry data from available manufacturer safety certificates and specification sheets. Table 4 shows the data obtained for this case study, which consist of the PFD, SFF, and cost of each SIS component. It is worth noting that the test period for all the SIS components is taken as 1 year, which aligns with main industry best practices for safety system maintenance and inspection intervals. The objective of this SIS is to achieve a minimum requirement of SIL 2, which includes the verification in terms of maximum achievable architectural SIL. A SIL 2 verified (in terms of architectural constraints) logic solver and final element is used for this case study and thus they do not need to go through maximum achievable architectural SIL verification, unlike the TTs.

Table 4: Case study data.

SIS Component	PFD	SFF (%)	Cost ($)
TT1 (1oo1)	3.07×10^{-4}	86	1195
TT1 (1oo2)	3.08×10^{-5}	86	2390
TT1 (2oo3)	1.57×10^{-5}	86	3585
TT2 (1oo1)	2.76×10^{-4}	87	1935
TT2 (1oo2)	2.77×10^{-5}	87	3870
TT2 (2oo3)	1.41×10^{-5}	87	5805
TT3 (1oo1)	1.49×10^{-4}	90	2200
TT3 (1oo2)	1.49×10^{-5}	90	4400
TT3 (2oo3)	7.53×10^{-6}	90	6600
Logic Solver 1 (1oo2)	4.69×10^{-4}	80	3702
Final Element 1 (1oo1)	1.10×10^{-3}	60	718

3.2 P-graph Model

The P-graph model is developed based on the proposed case study as shown in Figure 4 with labels of each TT voting logic, logic solver, and final element. The P-graph model resulted in the generation of 7 total SIS configurations, and the solution details are shown in Table 4. In the proposed case study, 2 transmitters (i.e., TT1 (1oo1) and TT2 (1oo1)) were not selected as a possible configuration as their architectural requirements does not meet SIL 2 (SFF less than 90%). Among the seven solutions, the three most cost-effective configurations (refer to P-graph solution structure in Figure 5) are Solution 1 (TT3 (1oo1)) with a total cost of $6620, Solution 2 (TT1 (1oo2)) with a total cost of $6810, and Solution 3 (TT1 (2oo3)) with a total cost of $8005. The corresponding RRF values for these solutions are 582, 625, and 631, respectively, indicating an increasing level of reliability. Comparing Solution 1 and Solution 2, the latter is 2.87% more expensive but offers a 43-point increase in RRF, improving the system's fault tolerance. Similarly, Solution 3, which implements a 2oo3 voting logic, is 17.6% more expensive than Solution 2, with a minor RRF improvement

of 6 points. Compared to the lowest-cost configuration (Solution 1), Solution 3 is 20.9% more expensive but provides a 49-point improvement in RRF, demonstrating enhanced system reliability. From a decision-making perspective, the selection of an optimal configuration depends on company policies and specific safety requirements. If a 2oo3 voting logic is required by company standards, Solution 3 (TT1 (2oo3)) would be a suitable choice, as it meets the redundancy requirement while maintaining a reasonable trade-off between cost and performance. However, if no strict voting logic constraints are imposed, Solution 1 (TT3 (1oo1)) offers the most cost-effective option while still achieving SIL 2 compliance. The results highlight the flexibility of the P-graph optimization model, enabling users to evaluate multiple configurations based on their respective cost, reliability, and safety performance. This flexibility will become even more apparent when additional transmitter options are introduced, as the model would be able to identify the most cost-effective choices from a broader set of alternatives. The P-graph framework thus serves as a powerful decision-support tool, enabling structured evaluation of safety instrumented system configurations while ensuring compliance with SIL requirements and minimizing costs.
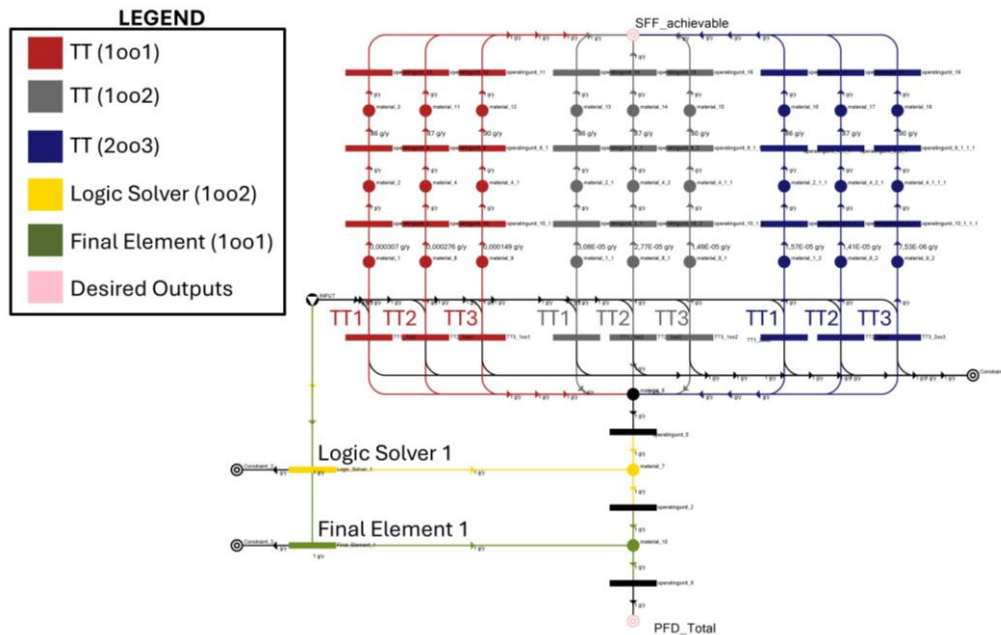
Figure 4. P-graph model for the case study's SIS.

Table 4: P-graph solution results.

Solution No.	Selected TT	Total PFD (x 10^{-3})	RRF	Total Cost ($)	SFF (%)
1	TT3 (1oo1)	1.7180	582	6620	90
2	TT1 (1oo2)	1.5998	625	6810	86
3	TT1 (2oo3)	1.5847	631	8005	86
4	TT2 (1oo2)	1.5967	626	8290	87
5	TT3 (1oo2)	1.5839	631	8820	90
6	TT2 (2oo3)	1.5831	632	10225	87
7	TT3 (2oo3)	1.5765	634	11020	90
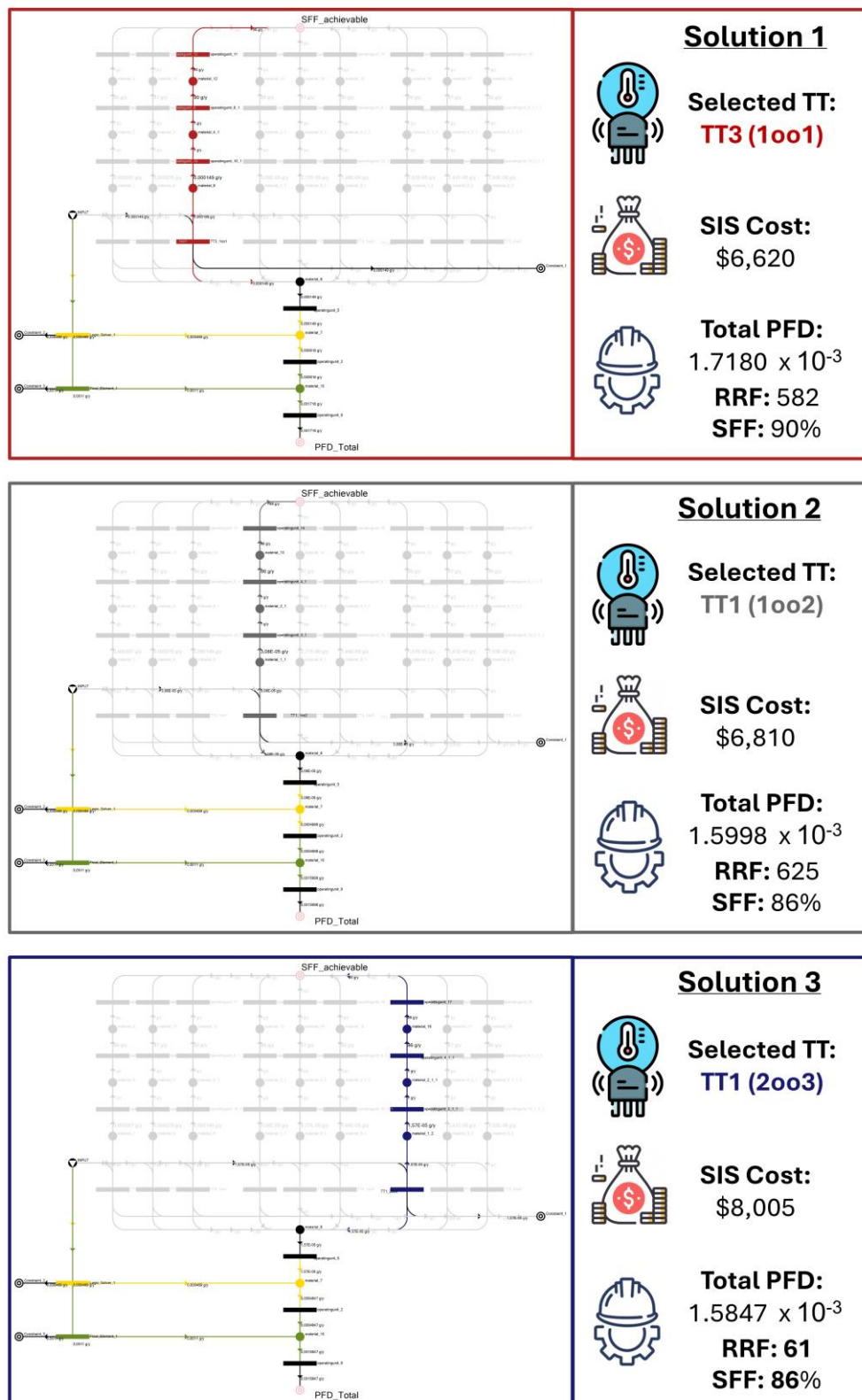
Figure 5. Top 3 SIS configuration solutions from P-graph.

4. Conclusions

This study presented a novel P-graph approach for optimizing SIL configuration selection, addressing the challenge of balancing cost, reliability, and compliance in SISs. The proposed model systematically generates all optimal and near-optimal solutions, allowing decision-makers to evaluate feasible configurations while considering architectural constraints, redundancy levels, and economic feasibility. The case study demonstrated that among the seven feasible solutions, the three most cost-effective configurations were Solution 1 (TT3 (1oo1)) at $6620, Solution 2 (TT1 (1oo2)) at $6810, and Solution 3 (TT1 (2oo3)) at $8005, with corresponding RRF of 582, 625, and 631, respectively. The results highlighted the trade-off between cost and reliability, where Solution 3 (2oo3 configuration) offers the highest reliability but at a 20.9% higher cost compared to the cheapest option (Solution 1, TT3 1oo1). By integrating SFF and HFT constraints, the model ensures that selected configurations are both technically feasible and compliant with SIL architectural limitations. The P-graph methodology proved to be a computationally efficient and scalable tool, enabling users to systematically explore different SIS configurations and select an optimal or near-optimal solution based on budget, safety requirements, and regulatory constraints. This flexibility will become even more apparent as additional transmitter options, logic solvers, and final elements are introduced, allowing for broader optimization in future applications. A natural extension of this work would be to incorporate a wider selection of SIS components (i.e., transmitters, logic solvers, and final elements), enabling more complex configurations while maintaining optimal SIL configuration selection. The proposed P-graph approach serves as a structured decision-support tool, allowing SIS engineers and process safety practitioners to achieve cost-effective and compliant SIL configuration selection while enhancing industrial safety and reliability.

Acknowledgments

References

Cheraghi, M., Taghipour, S., 2024. A mathematical optimization model for determining safety integrity levels in process facilities. Reliab. Eng. Syst. Saf. 109896.

Friedler, F., Blicket, T., Gyenis, J., Tarján, K., 1979. Computerized generation of technological structures. Comput. Chem. Eng. 3 (1–4), 241–249. https://doi.org/10.1016/0098-1354(79)80042-3.

Friedler, F., Fan, L., Imreh, B., 1998. Process network synthesis: problem definition. Networks Int. J. 31 (2), 119–124.

Friedler, F., Tarjan, K., Huang, Y., Fan, L., 1993. Graph-theoretic approach to process synthesis: polynomial algorithm for maximal structure generation.

Friedler, F., Orosz, A., Losada, J.P., 2022. P-Graphs for Process Systems Engineering. Springer.

How, B.S., Lam, H.L., 2017. Novel evaluation approach for biomass supply chain: an extended application of PCA. Chem. Eng. Trans. 61, 1591–1596. https://doi.org/10.3303/CET1761263.

IEC 61508a, 2010. IEC 61508 Functional Safety of electrical, electronic and programmable electronic (E/E/PE) safety-related system - Part 1: General requirements. International Electrotechnical Commission.

IEC 61508b, 2010. IEC 61508 Functional Safety of electrical, electronic and programmable electronic (E/E/PE) safety-related systems - Part 6: Guidelines on the application of parts 2 and 3. International Electrotechnical Commission.

IEC 61508c, 2010. IEC 61508 Functional Safety of electrical, electronic and programmable electronic (E/E/PE) safety-related systems - Part 2: Requirements for electrical/electronic/programmable electronic safety-related systems. International Electrotechnical Commission.

IEC 61511, 2016. IEC 61511 Functional Safety - Safety Instrumented Systems for the Process Industry Sector - Part 1: Framework, definitions, system, hardware and application programming requirements. International Electrotechnical Commission.

Sahl, A.B., Loy, A.C.M., Lim, J.Y., Orosz, A., Friedler, F., How, B.S., 2023. Exploring N-best solution space for heat integrated hydrogen regeneration network using sequential graph-theoretic approach. Int. J. Hydrogen Energy 48 (13), 4943–4959. https://doi.org/10.1016/j.ijhydene.2022.10.196.

Sahl, A.B., Orosz, Á., How, B.S., Friedler, F., Teng, S.Y., 2024. Electrification of oil refineries through multi-objective multi-period graph-theoretical planning: A crude distillation unit case study. J. Clean. Prod. 434, 140179. https://doi.org/10.1016/j.jclepro.2023.140179.

Süle, Z., Baumgartner, J., Dörgő, G., Abonyi, J., 2019. P-graph-based multi-objective risk analysis and redundancy allocation in safety-critical energy systems. Energy 179, 989–1003. https://doi.org/10.1016/j.energy.2019.05.043.

Aviso, K.B., Cayamanda, C.D., Mayol, A.P., Tan, R.R., 2017. P-graph approach to human resource reallocation in industrial plants under crisis conditions. In: 2017 6th International Symposium on Advanced Control of Industrial Processes (AdCONIP), pp. 131–136. IEEE.

A Systematic Literature Review on Safety of Methanol as a Marine Fuel

Marko Gerbec[1*], David Levovnik[1], Olga Aneziris[2], Vladimir Maras[3], Ernesto Salzano[4]

1 Department for inorganic chemistry and technology, Jožef Stefan Institute, Jamova 39, 1000 Ljubljana, Slovenia;
2 NCSR "DEMOKRITOS", Agia Paraskevi Attikis, Greece;
3 Faculty of Transport and Traffic Engineering, University of Belgrade, Vojvode Stepe 305, 11000 Belgrade, Serbia;
4 Department of Civil, Chemical, Environmental and Materials Engineering, University of Bologna, Bologna 40131, Italy;

* marko.gerbec@ijs.si

1. Introduction

This paper summarizes the intermediate results of a literature review on safety and risk assessment at ports that store, handle, and provide methanol for ship refueling. This is the first review that attempts to cover the available standards organizations, international and regional organizations, IMO regulations, classification societies for the applicable rules and guidelines for assessing hazards and risk of the methanol storage at ports and during bunkering (refueling procedure at ships).

A further review is conducted on literature related to the safe use of methanol as an alternative marine fuel, together with risk assessment studies performed in the last 10 years. The aim of this review is to investigate scientific and harmonization gaps of methanol bunkering safety within the EU.

2. Methods

The review covered scientific literature, standards, regulations, white papers, guidelines and examples of best practices. During the reviewer process, the following parameters were considered:

- Information sources: citation databases (Web of Science, Scopus), registers, websites of international organizations (IMO, IAPH, SGMF, IMPCA, MI), classification societies (ISO, DIN, DNV, ABS, BV, Lloyds), regulators national/multi-national (EU, EMSA, UN).
- Main keyword: methanol.
- The language of publications was limited to English.
- Search context limitations: a.) safety/process safety; b.) maritime or bunkering; c.) fuel; d.) storage; e.) operational procedures.

Search hits were compiled and examined each one in a detail for the applicability of the context limitations.

3. Results and discussion

The review identified 184 scientific papers (combined results from Scopus and Web of Science). The 184 papers were reviewed in two steps. First, papers were briefly reviewed,

focusing on the title, keywords, and abstract. Papers that, for example, only indirectly addressed safety or methanol were excluded. In the second step, the remaining papers were manually reviewed, focusing on how the use of methanol was explored (focusing on safety, environmental and economic aspects) and in which context (focusing on the maritime application, specifically on the use of methanol in ports). The papers that, for example, focused on the life cycle assessment of alternative fuels and only briefly mentioned the use of methanol in ports or bunkering processes were excluded. The review process highlighted 12 papers. The papers explored methanol as an alternative marine fuel from both environmental and economic perspective (e.g., Deniz & Zincir, 2016; Jesus et al., 2024), evaluated the readiness to bunker alternative marine fuels (Wei et al., 2023), discussed how to assure their availability (Kloppot et al., 2023), provided decision support system for bunkering operations (Sheng, 2024), developed training scenarios for safe bunkering (Liu, et al., 2024), and addressed the views of various stakeholders on bunkering operations (Kolakowski et al., 2024).

The review of standards, regulations, white papers, guidelines and examples of best practices identified 51 documents, contents of which are discussed as follows:

The Methanol Institute, IMPCA and ISO documents cover the quality and safe handling aspects of the methanol as a maritime fuel (Methanol Institute, 2020; IMPCA, 2021; ISO, 2024).

Regarding the design and operation of the methanol fueled ships, there is a plethora of documents at various organizations, which can be summarized to the interim IMO's guidelines (IMO, 2020) based on the IGF requirements for low flashpoint fuels (IMO, 2015). The guidelines cover the methanol/ethanol use, e.g., ship design and arrangement, fuel containment system, material and general pipe design, bunkering, fuel supply to consumers, power generation incl. propulsion, fire safety, explosion prevention and area classification, ventilation, electrical installations, control, monitoring and safety systems, operation.

The classification societies adapted the IMO guidelines and published more specific rules and regulations on the ships using methanol or ethanol for propulsion (ABS, 2024a; ABS, 2024b; BV, 2024; Lloyds, 2024a; Lloyds, 2024b). While those rules and regulations cover also the bunkering, the bunkering procedure, requirements, safety measures are prescribed in addition in a form of detailed checklists by the classification societies (Lloyds, 2020) and specific regulators and ports/associations (EMSA, 2023; IAPH, 2023; SGMF, 2024; Port of Gothenburg, 2022). DNV prepared also a competence requirements reference (DNV, 2024).

Regarding the specific national legislation, we did not find anything.

At the specific port level, we found two risk assessment reports, both related to the Amsterdam and external safety of the bunkering operations (DNV, 2021; AVIV, 2023). Both reports are interesting as they cover different bunkering modes and different fuels (LNG, methanol, ammonia, hydrogen and their operational combinations).

In addition, we found that within the GreenVoyage 2050 project[1] a regulatory mapping exercise was prepared. Regarding the methanol mainly high regulatory readiness was assigned, but low readiness regarding the potential marine pollution and human health hazards. As the web site mentions marine standards in progress that are today (end of 2024) already available, the gap analysis seems a bit outdated in mentioned details.

---

[1] https://greenvoyage2050.imo.org/alternative-marine-fuels-regulatory-mapping/ (accessed 18.11.2024)

4. Conclusions

The use of methanol as a maritime fuel appears to be covered by the IMO regulations and other international organizations, classification societies and port authorities, however, there is no specific national legislation within the ADRION countries.

There is also a scarcity of papers in the scientific literature that would holistically address all the aspects (e.g., safety, environmental, and economic) of using methanol as a marine fuel in ports. A more in-depth analysis is needed to address the research landscape further, highlight potential gaps in the literature and explore how the research on the use of methanol as a marine field is developing compared to research on other alternative fuels.

Acknowledgments

References

ABS, 2024a. Requirements for Methanol and Ethanol Fueled Vessels. July 2024. https://pub-rm20.apps.eagle.org/r/4/2024-07-01/Methanol-and-Ethanol-Fueled-Vessel

ABS, 2024b. Methanol bunkering: technical and operational advisory, April 2024. https://ww2.eagle.org/content/dam/eagle/advisories-and-debriefs/methanol-bunkering-advisory.pdf

AVIV, 2023. Adviesgroep AVIV BV, Risk analysis / Bunkering of alternative fuels in the port of Amsterdam. https://www.portofamsterdam.com/sites/default/files/2023-05/Rap224962def.pdf

BV, 2024. BV NR670 DT R02 July 2024, Methanol and ethanol – fuelled ships. https://erules.veristar.com/dy/data/bv/pdf/670-NR_2024-07.pdf

Deniz, C., Zincir, B., 2016, Environmental and economical assessment of alternative marine fuels, Journal of Cleaner Production, 113, 438-449. https://doi.org/10.1016/j.jclepro.2015.11.08

DNV, 2021. External safety study - bunkering of alternative marine fuel for seagoing vessels (Port of Amsterdam). https://sustainableworldports.org/wp-content/uploads/DNV-POA-Final-Report_External-safety-study-bunkering-of-alternative-marine-fuels-for-seagoing-vessels_Rev0_2021-04-19.pdf

DNV, 2024. Standard DNV-ST-0687, Competence related to the use of methanol as fuel. https://standards.dnv.com/explorer/

EMSA, 2023. Safe bunkering of biofuels. Bunkering of biofuels in maritime: characteristics, regulatory landscape and safety assessment. Rev. 1.0, 15.12.2023. https://www.emsa.europa.eu/component/flexicontent/download/7727/5119/23.html

IAPH, 2023. Bunker Checklist Alcohol Based Series Ship to Ship bunker operations. AB STS A Version 1.0. https://sustainableworldports.org/wp-content/uploads/IAPH-Alcohol-Based-Bunker-Checklist-STS-A-v1.0.pdf

IMO, 2020. Resolution MSC.1/Circ. 1621, Interim guidelines for the safety of ships using methyl/ethyl alcohol as fuel. https://www.register-iri.com/wp-content/uploads/MSC.1-Circ.1621.pdf

IMO, 2015. Resolution MSC.391(95), Adoption of the International Code of Safety for Ships Using Gases or Other Low-Flashpoint Fuels (IGF Code). London, UK: International Maritime Organization.

IMPCA, 2021. International methanol producers consumers association, IMPCA methanol reference specifications, version 9. https://www.methanol.org/wp-content/uploads/2016/07/IMPCA-Ref-Spec-08-December-2015.pdf

ISO, Standard ISO 6583. Methanol as a fuel for marine applications — General requirements and specifications. Under publication, 2024. https://www.iso.org/standard/82340.html

Jesus, B., Ferreira, A., I., Carreira, A., Erikstad, o., S., Godina, R., 2024, Economic framework for green shipping corridors: Evaluating cost-effective transition from fossil fuels towards hydrogen, International Journal of Hydrogen Energy, 83, 1429-1447. https://doi.org/10.1016/j.ijhydene.2024.08.147.

Klopott, M., Popek, M., Urbanyi-Popiołek, I., 2023. Seaports' Role in Ensuring the Availability of Alternative Marine Fuels—A Multi-Faceted Analysis, Energies, 16, 3055. https://doi.org/10.3390/en16073055

Kołakowski, P., Gil, M., Wróbel, K., Stakeholders' view on selecting a prospective location for marine alternative fuels bunkering station, 2024, Marine Policy, 164, 106164. https://doi.org/10.1016/j.marpol.2024.106164.

Liu Y., Onn T.C., Lim E., Chua R., Tantawi M.A.B.A., Hui N.Y., 2024, An Immersive VR Training Scenario for Safe Methanol Bunkering in the Maritime Industry, Journal of Physics: Conference Series, 2867 (1), 012001. doi:10.1088/1742-6596/2867/1/012001

Lloyds, 2020. Introduction to Methanol Bunkering Technical Reference. Lloyd's Register, https://www.methanol.org/wp-content/uploads/2020/04/Introduction-to-Methanol-Bunkering-Technical-Reference-1.5.pdf

Lloyds, 2024a. LR-GN-047 Guidance notes for the methyl and ethyl alcohol fuels, July 2024. https://r4s.oneocean.com/regulation/page/275381

Lloyds, 2024b. LR-RU-012 Rules and regulations for the classification of ships using gases or other low-flashpoint fuels, July 2024. https://r4s.oneocean.com/regulation/page/271903

Methanol Institute, 2020. Methanol safe handling manual 5th Edition. https://www.methanol.org/wp-content/uploads/2020/03/Safe-Handling-Manual_5th-Edition_Final.pdf

Port of Gothenburg, 2022. METHANOL BUNKER OPERATING REGULATIONS. https://safety4sea.com/wp-content/uploads/2022/04/Port-of-Gothenburg-Methanol-bunker-operating-regulations-2022_04.pdf

SGMF, 2024. Methanol as a marine fuel safety and operational guidelines – bunkering. FP22-01 Ver 1, ISBN: 978-1-7395354-6-9.

Sheng B.L.K., Tkalich P., Chow J.H., Sasmal K., 2024, Envisioning a decision support system for the planning of alternative fuel bunkering operations in Singapore, Journal of Physics: Conference Series, 2867 (1), 012013. doi:10.1088/1742-6596/2867/1/012013

Wei, H., Müller-Casseres, E., Belchior, C.R.P., Szklo, A., 2023, Evaluating the Readiness of Ships and Ports to Bunker and Use Alternative Fuels: A Case Study from Brazil. Journal of Marine Science and Engineering, 11, 1856. https://doi.org/10.3390/jmse11101856

On the NO$_x$ Production of Ammonia, Hydrogen and Methanol Fuels for Shipping Purposes

Gianmaria Pio[1], Olga Aneziris[2], David Levovnik[3], Vladislav Maras[4], Ernesto Salzano[1,*]

1 Dep. of Civil, Chemical, Environmental, and Materials Eng., University of Bologna, Bologna, Italy;
2 NCSR "DEMOKRITOS", Agia Paraskevi Attikis, Greece;
3 Department for Inorganic Chemistry and Technology, Jozef Stefan Institute, Ljubljana, Slovenia
4 Faculty of Transport and Traffic Engineering, University of Belgrade, Belgrade, Serbia

*ernesto.salzano@unibo.it

1. Introduction

The International Maritime Organization (IMO) has adopted a strategy for reducing greenhouse gas (GHG) emissions from ships, proposing to reduce carbon emissions in the global shipping industry by 50% by 2050 and to achieve zero carbon emissions in the global shipping industry in the 21st century. To this aim, the transition toward cleaner fuels, particularly for short-distance routes, port operations and long-term docking in urban harbours is necessary. Possible candidates are ammonia (NH_3), hydrogen (H_2) and methanol (CH_3OH) (if produced from renewable sources). However, the transition to sustainable power requires careful consideration of multiple factors to ensure successful implementation, including safety, economic and environmental aspects (Aneziris et al., 2023; Zanobetti et al., 2023). In the EU Adrion project SUPERALFUEL, Key Performance Indicators (KPI) for the quantitative assessment of the sustainability of the cited three fuels, in the specific framework of harbour system, will be developed. For what concern the environmental indicators three main parameters should be considered. The first indicator is related to the total amount of NO_x produced by any fuel per kWh of energy produced (KPI-ENV1), defined often as the NO_x emission rate. This data can be compared with Nitrogen Oxides (NO_x) – Regulation 13 - Tier III, which allows for a total weighted cycle emission limit of 2.0 g/KWh (for diesel ships) (Shaw & Van Heyst, 2022). The second parameter (KPI-ENV2) is related to the total amount of CO_2 per kWh produced by the energy production, to evaluate the Global Warming Potential (GWP). In this regard, the N_2O should be considered for comparison, as NH_3) and H_2 are intrinsically carbon-free on a tank-to-wake basis rather than a well-to-wake. For the calculation of the KPIs, a detailed kinetic model KIBO (Pio et al., 2024; Salzano et al., 2018) developed at the University of Bologna has been adopted for the above-cited fuels after extensive validation.

2. Methods

The detailed kinetic mechanism KIBO, which includes nitrogen-based chemistry was used. The adopted kinetic mechanism includes 172 species and 488 reactions. The design of KIBO prioritizes computational efficiency for practical implementation while maintaining accuracy, as evidenced by thorough validation documented in existing literature. A zero-dimensional reactor implemented in the open-source software Cantera (Goodwin, 2009),

was utilized to represent the adiabatic conditions in a transient mode and to evaluate the composition of products either by using a pure thermodynamic approach based on the minimization of Gibbs-free energy or by assessing the laminar burning velocity. For details, the reader can refer to Pio et al. (2022). Results are given in terms of the molar fraction (composition) of combustion products (NO, N_2O and NO_2) for the three fuels by varying the stoichiometric fraction φ:

$$\varphi = \frac{\frac{fuel}{O_2}}{\left(\frac{fuel}{O_2}\right)_{st}} \tag{1}$$

Also, for each fuel, the amount of NO_x produced per kWh is given. Finally, for the sake of comparison, the emission index $E_{NO_x,fuel}$, for each fuel, was evaluated as the following ratio:

$$EI_{NO_x} = \frac{g_{NO_x}}{kg_{fuel}} \tag{2}$$

The following Table 1 reports the three fuels' analysed composition and main properties.

Table 1: Composition, heat of combustion, storage (st) conditions of fuels analysed in this work.

Fuel	T_{st} K	P_{st} bar	$-\Delta H^o_{c,298\,K}$ kJ/mol	ρ_{T_s,P_s} kg/m^3	φ	x_{fuel}	x_{O_2}	x_{N_2}
H_2 (liq)	298	700	285.8 (gas)	39.6	0.8	0.183	0.172	0.645
					1.0	0.251	0.157	0.591
					1.2	0.101	0.189	0.710
NH_3 (liq)	298	10.0	382 (gas)	609	0.8	0.219	0.164	0.617
					1.0	0.296	0.190	0.715
					1.2	0.123	0.184	0.693
CH_3OH (liq)	298	1.13	763.7 (gas)	792	0.8	0.251	0.157	0.591
					1.0	0.335	0.140	0.525
					1.2	0.144	0.180	0.676

3. Results and discussion

Figure 1 shows the molar fraction of NO_x for the three fuels at stoichiometric, rich, and lean fuel compositions, as calculated by KIBO by using the purely thermodynamic-based approach and the kinetic-based methodology.
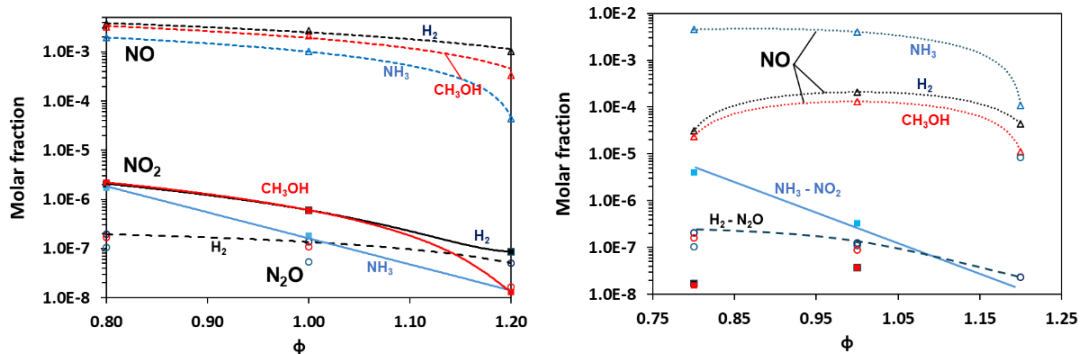

Figure 1. Molar fraction of NO_x (NO – Δ, dotted line; N_2O – O, dashed line, NO_2 – continuous line, square) produced by NH_3, H_2 and CH_3OH by a pure thermodynamic model (left) and by the kinetic model (right) vs equivalence ratio φ as calculated by the KIBO model.

Quite clearly, the molar fraction of nitrogen monoxide NO prevails over the other oxides, even if NO_2 shows some relevance in lean conditions. Besides, N_2O is almost negligible in all conditions, as expected. Once the Gibbs-free energy model is considered, NH_3, H_2 and CH_3OH produce a comparable amount of NO_x, whereas the adoption of the kinetic model results in a significantly larger content of NO_x in the case of NH_3. This trend can be attributed to the variation in nitrogen content due to the different stoichiometric coefficients, acting as a thermal and kinetic diluent. This aspect can have a significant impact on the overall reactivity, as well. Hence, meaningful considerations can be obtained by comparing the emissions per unit of energy (in kWh) produced by combustion and the consumption rate, i.e. the total amount of fuel required to produce 1 kWh (Figure 2).
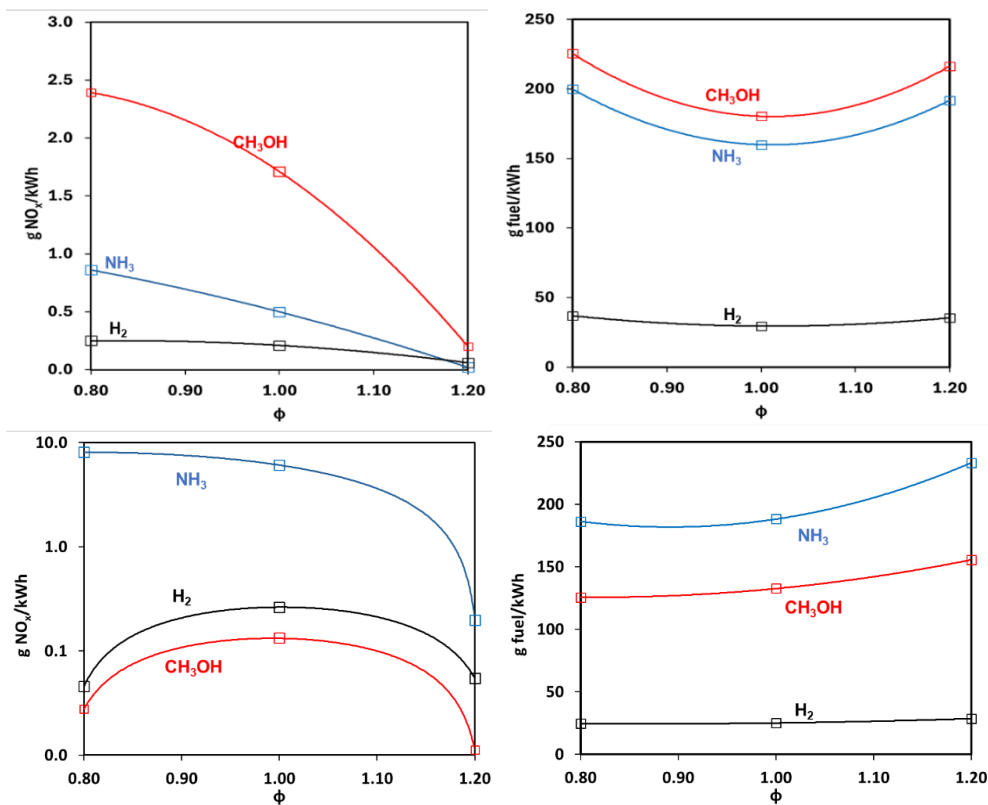
Figure 2. Mass of NO_x emitted per unit of energy (left) and mass of fuel required for the production of 1 kWh of energy (right) for the investigated fuels vs the equivalence ratio φ, as calculated by the KIBO code. Top: thermodynamic equilibrium, Bottom: kinetic model.

The figure shows clearly that both the amount of fuel and the amount of NO_x per kWh are consistently low in the case of H_2 either thermodynamically or kinetically. Besides, the NH_3 shows a very high consumption rate and a larger amount of NO_x if the detailed chemistry is considered. If considering the kinetic approach, H_2 and CH_3OH produce less NO_x/kWh than Tier III – IMO, at any condition.

The calculated emission index (Eq. 2), based on the grams of fuel and grams of NO_x produced per kWh is shown in Figure 3. In the figure, the emission index EI_{NO_x} decreases almost linearly with the equivalence ratio for NH_3. That is quite important in the framework

of advanced combustion technologies, e.g. the MILD (Moderate or Intense Low oxygen Dilution) combustion or other ultra-lean conditions for Low-NO_x energy production, which uses recirculated heat and exhaust gases to reduce the flame temperature, thus reducing the amount of pollutants and increasing thermal efficiency. In this regard, it is worth mentioning that MILD combustion produces a dramatic decrease in NO_x emissions but is still far from being adopted for shipping purposes.

As for previous results, the thermodynamic approach shows a large difference with respect to the kinetic model; NH_3 seems relevant in terms of NO_x emission with a dramatic increase at lean conditions if the kinetic model is considered.
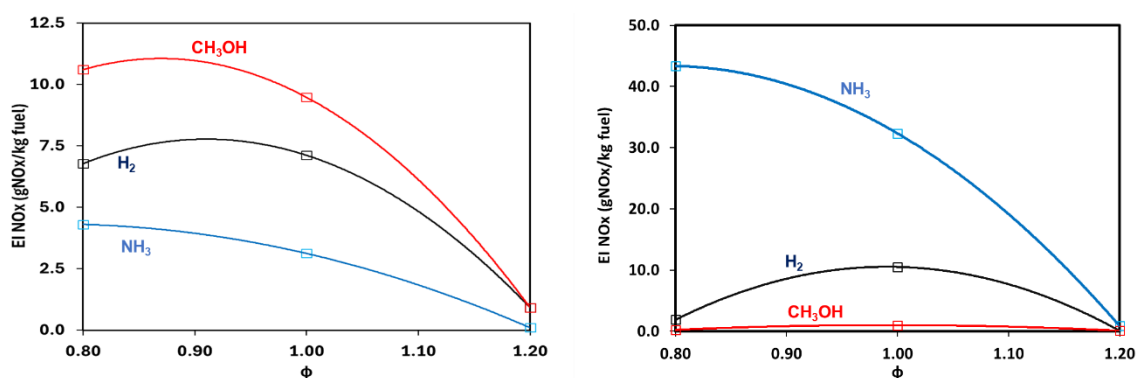
Figure 3. Emission index (Eq. 2) based on NO_x produced per kg of fuel vs equivalence ratio φ by using a Gibbs-free energy approach (left) and by using a kinetic approach (right).

The emission index EI_{NO_x} shows that NH_3 is the best option if considering a pure thermodynamic analysis based on the Gibbs-free energy approach whereas a dramatic increase in the NO_x is shown if a kinetic model is adopted.

4. Conclusions

The NO_x emissions are over 95% from anthropogenic (mainly industrial and transportation) sources, so a key performance indicator for environmental sustainability based on these oxides is strongly recommended. Nevertheless, a comprehensive database on the experimental characterization of this parameter is missing. Numerical analyses conducted in this work show the sensitivity to the implemented approach, suggesting the implementation of kinetic models within a simplified layout and geometry of real case scenarios of interest.

Acknowledgements

References

Aneziris, O., Koromila, I.A., Gerbec, M., Nivolianitou, Z., Salzano, E., 2023. A Comparison of Alternative Cryogenic Fuels for Regional Marine Transportation from the Perspective of Safety, Chemical Engineering Transactions, 100, 25-30.

Zanobetti, F., Pio, G., Jafarzadeh, S., Ortiz, M.M., Cozzani, V., 2023. Inherent safety of clean fuels for maritime transport, Process Safety and Environmental Protection, 174, 1044-1055.

Pio, G., Dong, X., Salzano, E., Green, W.H., 2022. Automatically generated model for light alkene combustion. Combust Flame. 241, 112080.

Pio, G., Eckart, S., Richter, A., Krause, H., Salzano, E., 2024. Detailed kinetic analysis of synthetic fuels containing ammonia. Fuel. 362, 130747.

Salzano, E., Pio, G., Ricca, A., Palma, V., 2018. The effect of a hydrogen addition to the premixed flame structure of light alkanes. Fuel. 234, 1064-1070.

Goodwin, D.G., 2009. Cantera: An object-oriented software toolkit for chemical kinetics, thermodynamics, and transport processes, Caltech, Pasadena.

Shaw, S.B., Van Heyst, B., 2022. Nitrogen Oxide (NOx) emissions as an indicator for sustainability. Environmental and Sustainability Indicators. 15, 100188.

A Systematic Literature Review on the Safety and Risk Assessment of Alternative Fuels in Inland Waterway Transport

Vladislav Maraš[1*], Danijela Pjevčević [1], Aleksandar Radonjić[1], Anita Abođi[1], Olga Aneziris[2], Ernesto Salzano[3], Marko Gerbec[4]

1 Faculty of Transport and Traffic Engineering, University of Belgrade, Vojvode Stepe 305, 11000 Belgrade, Serbia
2 NCSR "DEMOKRITOS", Agia Paraskevi Attikis, Greece;
3 Department of Civil, Chemical, Environmental and Materials Engineering, University of Bologna, Bologna 40131, Italy;
4 Department for inorganic chemistry and technology, Jožef Stefan Institute, Jamova 39, 61000 Ljubljana, Slovenia

* v.maras@sf.bg.ac.rs

A systematic literature review on the safety and risk assessment of alternative fuels, i.e. hydrogen, ammonia, and methanol in inland waterway transport is given in this paper. This review is based on three types of relevant sources: EU policies and regulations, publications, guidelines and methodologies of classification societies as well as outcomes of research projects. European Green Deal [EC, 2021a], belonging to the European Union's ambitious decarbonisation policies, aims to achieve net zero greenhouse gas emissions by 2050 and a 55% reduction by 2030 (as formalized in the European Climate Law [EC, 2020a]). Further, the European Commission's Fit-for-55 legislative package [EC, 2021b] and the Sustainable and Smart Mobility Strategy [EC, 2020b] underscore the commitment to reducing greenhouse gas emissions in the transport sector, including inland navigation, by promoting alternative, low-emission fuels. The NAIADES III initiative [EC, 2021c], central to the EU's strategy for inland navigation, emphasizes the need for zero-emission vessels, the development of an EU energy index to assess carbon intensity, and funding opportunities for vessels utilizing alternative fuels. Furthermore, recent EU regulations, such as Regulation (EU) 2023/1804, mandate shore-side electricity infrastructure at core inland waterway ports by 2024 and comprehensive ports by 2029, while the Renewable Energy Directive (RED III) [Directive (EU) 2023/2413] sets renewable energy targets for transport, promoting a 29% share of renewables by 2030. Additionally, the EU's Alternative Fuels Infrastructure Facility (AFIF) provides financial support for infrastructure that enables alternative fuels like methanol, ammonia, and hydrogen, enhancing compliance with the Alternative Fuels Infrastructure Regulation (AFIR) objectives [Directive (EU) 2023/2413].

Methanol, ammonia, and hydrogen are considered technically promising for inland waterway vessels due to their potential for reducing emissions, though they present unique safety and technical challenges. This review includes an evaluation of safety guidelines and risk methodologies published by classification societies, alongside the European Commission's alternative fuel regulations. Further insights from the research projects, such as PLATINA3 [PLATINA3 project D2.1, 2021; D4.2, 2022; D1.5, 2023; D2.7, 2023] and

SYNERGETICS [SYNERGETICS project D1.1, 2024; SYNERGETICS project 2024a and 2024b], emphasize the need for robust safety standards and regulatory harmonization to enable the sustainable integration of these alternative fuels into the inland waterway sector. This study aims to identify and highlight gaps in safety standards and regulatory harmonization and therefore to offer insights into the current EU regulatory landscape for safe and sustainable fuel transitions in inland waterway transport.

Acknowledgements

References

1. EC, 2020a. The European climate law, European Commission, Directorate-General for Communication, Publications Office, 2020, https://data.europa.eu/doi/10.2775/790913.
2. EC, 2020b. Sustainable and Smart Mobility Strategy – putting European transport on track for the future, European Commission, COM(2020) 789, SWD(2020) 331 final, 9 December 2020.
3. EC, 2021a. European Green Deal: research & innovation call, European Commission, Directorate-General for Research and Innovation, Publications Office of the European Union, 2021, https://data.europa.eu/doi/10.2777/33415.
4. EC, 2021b. 'Fit for 55': delivering the EU's 2030 Climate Target on the way to climate neutrality. Communication from the Commission to the European Parliament, the Council, the European Economic and Social Committee and the Committee of the Regions, COM(2021) 550 final, Brussels
5. EC, 2021c. NAIADES III: Boosting future-proof European inland waterway transport, European Commission, Directorate-General for Mobility and Transport, Publications Office of the European Union, 2021, COM(2021)324 final.
6. Regulation (EU) 2023/1804 of the European Parliament and of the Council of 13 September 2023 on the deployment of alternative fuels infrastructure, and repealing Directive 2014/94/EU, Official Journal of the European Union, Vol. 66, L234, ISSN 1977-0677.
7. Directive (EU) 2023/2413 of the European Parliament and of the Council of 18 October 2023 amending Directive (EU) 2018/2001, Regulation (EU) 2018/1999 and Directive 98/70/EC as regards the promotion of energy from renewable sources, and repealing Council Directive (EU) 2015/652, Official Journal of the European Union, 2023/2413.
8. PLATINA3 project D2.1, 2021. Report on the zero – emission strategy IWT update of STEERER work, https://platina3.eu/download/zero-emission-iwt-strategy/# .
9. PLATINA3 project D4.2, 2022. Report on findings, perspectives and recommendations on clean energy along waterways and ports, https://platina3.eu/download/clean-energy-infrastructure/# .
10. PLATINA3 project D1.5, 2023. Report on recommendations for policy measures which result into higher use of green IWT, https://platina3.eu/download/policy-measures-for-green-iwt/# .
11. PLATINA3 project D2.7, 2023. Report on policy recommendations on regulatory pathway towards zero emission fleet, https://platina3.eu/download/towards-zero-emission-fleet/# .
12. SYNERGETICS project D1.1, 2024. Relevant identified technical solutions, https://www.synergetics-project.eu/wp-content/uploads/2024/09/SYNERGETICS_D1.1_Relevant-identified-technical-solutions_FINAL.pdf .
13. SYNERGETICS project 2024a, Catalogue of Greening Technologies – Fact Sheet No. 1 – Methanol ICE, https://www.synergetics-project.eu/Fact_Sheet_1/ .
14. SYNERGETICS project 2024b, Catalogue of Greening Technologies – Fact Sheet No. 2 – H2 ICE, https://www.synergetics-project.eu/Fact_Sheet_2/ .

Explosion and Ignition Behavior of NH$_3$/H$_2$ Mixtures in the 20-liter Sphere

Dieter Gabel*, Ulrich Krause

Otto-von-Guericke University, Magdeburg, Germany

* dieter.gabel@ovgu.de

1. Introduction

Ammonia is one of the possible future energy carriers for transporting (green) hydrogen or it will be used as fuel directly. In both cases mixtures of NH3 and H2 in air can occur during normal operation or accidental release. To ensure the uphold of the explosion protection principles the explosion and ignition behavior of such mixtures need to be known.

In this ongoing project the ignition limits and explosions characteristics of mixtures of Ammonia and Hydrogen in air are systematically determined in the 20-l-sphere. Unlike the standard procedure (DIN EN 1839) all measurements were conducted in a closed vessel, recording the time sequence of the pressure rise. Besides the ignition limits, the maximum explosion pressure and the pressure rise velocity are determined for the complete explosion range.

The advantage of the closed setup is that in all cases a release of Ammonia into the environment can be avoided. Therefore, the operation procedure was adapted in a way that mixtures that could not be ignited were forced to react in a second step. This is possible by either adding additional fuel or Oxygen (air) and force an ignition before releasing the exhaust gases.

Furthermore, the 20-l-sphere enables to test for different conditions and ignition sources. Besides the quiescent mixture with electrical spark ignition test are conducted in turbulent mode, comparable to the dust explosion standard (DIN EN 14034). In addition, the influence of the ignition source is punctually tested by applying pyrotechnical igniters with 2 kJ and 10 kJ.

2. Background

Whether an unintended release of a combustible gas in air leads to an ignition or not depends mostly on the concentration of that substance. For gas ignition in most cases it can be assumed that a strong enough ignition source is present. The ignition regions of many pure gases are well known and published (Molnárné 2003). To represent the dependency on the Oxygen content triangle diagrams are used as shown in Figure 1 für pure Hydrogen and Ammonia.

The availability of such data for mixtures of combustible gases is much less. Already almost a century ago explosion ranges of Ammonia/Hydrogen/Oxygen and Ammonia/Hydrogen/Air mixtures were published (Jorissen,1926). The current project aims in renewing the findings presented in Figure 2 utilizing a standardized setup. Additionally, the maximum explosion pressures and pressure rise velocities are determined as well to be able to judge the severity of the ignitions.
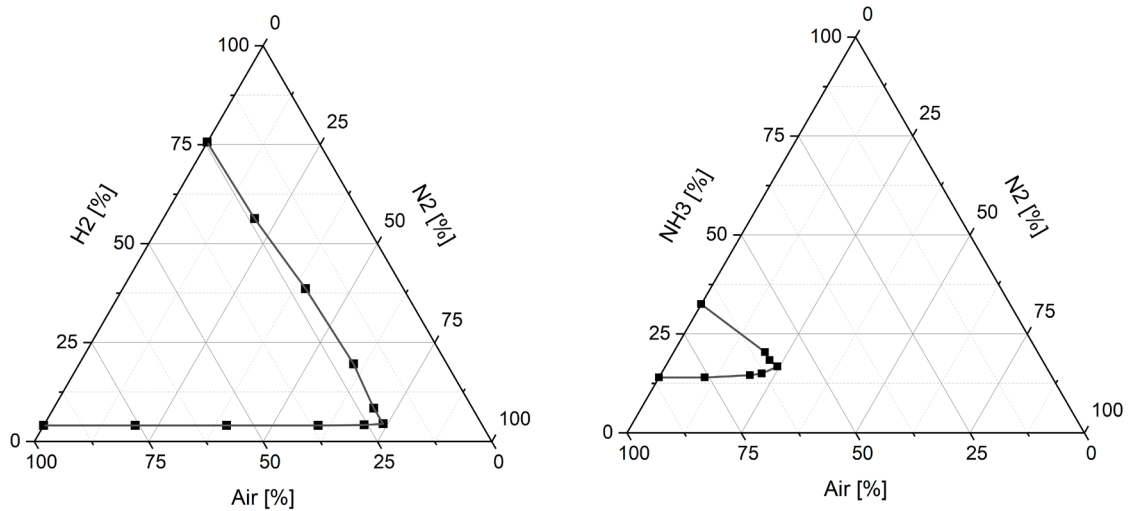
Figure 1. Ignition area of pure Hydrogen (left) and Ammonia (right) in Air and Nitrogen (Molnárné 2003).
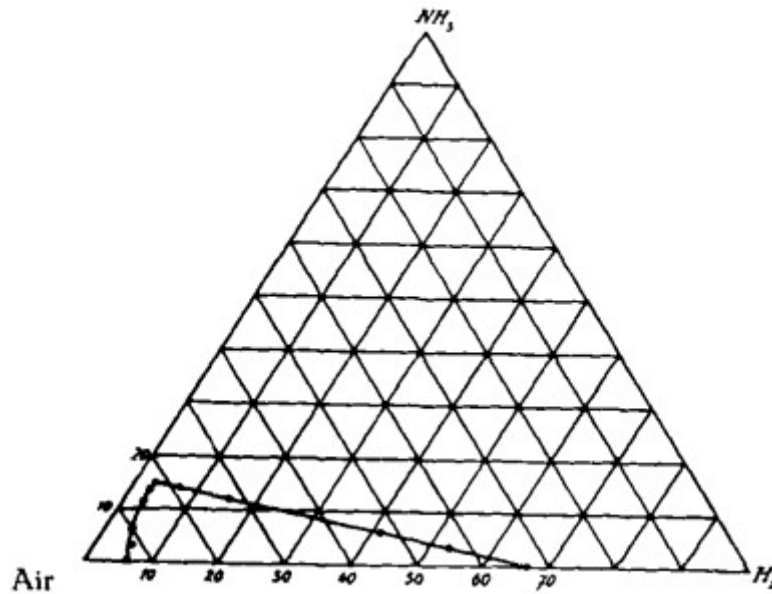
Figure 2. Explosions range of Ammonia/Hydrogen/Air mixtures (Jorissen,1926)

3. Method

The experimental setup used is the 20 Liter sphere known from the dust explosion standard DIN EN 14034. If used for gases the setup complies to the procedure B – Bomb method of the gas standard DIN EN 1839. For the experiments the extensions of the dust standard for hybrid mixtures published as DIN/TS 31018-1. The validity of this procedure was proven in two international round robin tests (Spitzer 2023). The schematic of the setup is shown in Figure 3.
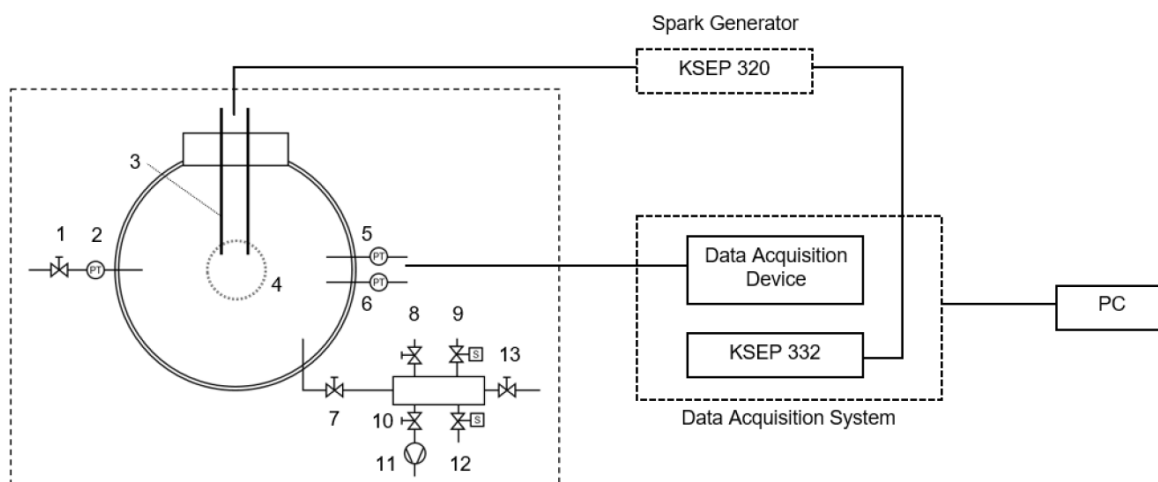
Figure 3. Schematic diagram of the experimental setup with

1	Valve out	8	Manual valve to ammonia source
2	Pressure sensor	9	Solenoid valve to hydrogen source
3	Ignition source	10	Manual valve to vacuum pump
4	Observation window	11	Vacuum pump
5	Pressure sensor P1	12	Solenoid valve to surrounding
6	Pressure sensor P3	13	Valve for flushing air
7	Valve in prior to chamber		

Additionally, the spark ignition source can be replaced by the pyrotechnical igniters used for dust explosions experiments. With energies of 2kJ or 10kJ the available ignition potential is much higher. This might influence the ignition boundaries as well as maximum values of the explosion pressures and pressure rise velocities.

4. Results and discussion

The focus of this ongoing project in the beginning was on the regions of the lower explosion limits with spark ignitions. Due to safety and environmental considerations mixtures with low content of Hydrogen and Ammonia a better to handle. A procedure to consequently reignite unignited mixtures was applied before releasing the mixtures into the exhaust system.

The outcome so far is represented in Figure 4. These ternary diagrams with contour plots show the explosions limits as well as the developments of the explosion pressure and pressure rise velocity for Ammonia/Hydrogen/Air mixtures with spark ignition.

The data behind these diagrams is quite extensive and needs to be discussed in detail. A much smaller dataset for ignition with pyrotechnical igniters exists, too.
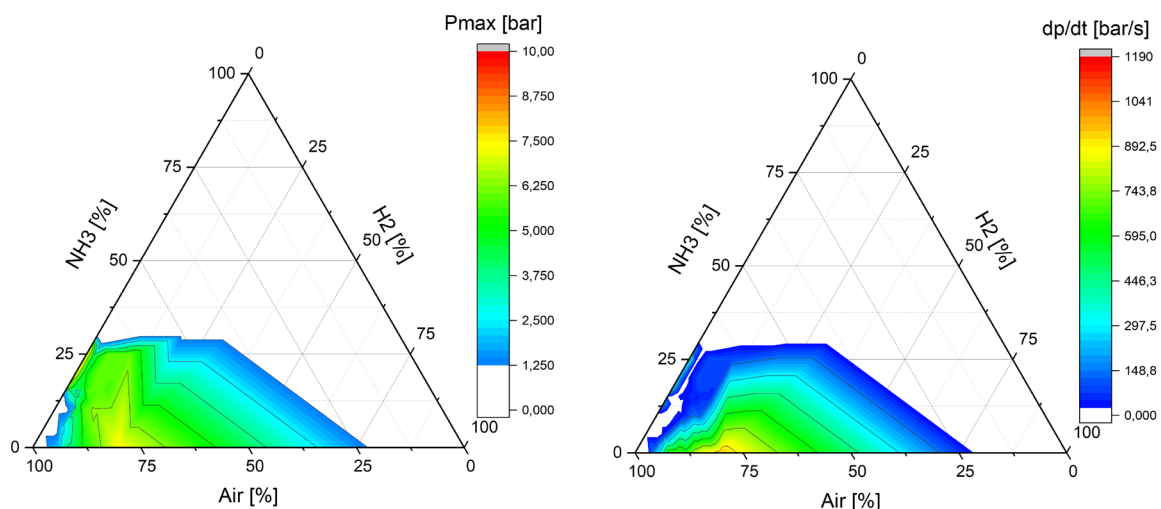
Figure 4. Ternary diagrams of the explosion pressure (left) and pressure rise velocity (right) for Ammonia/Hydrogen/Air mixtures with spark ignition.

4. Conclusions

The knowledge of the ignition and explosion behavior of mixtures of Hydrogen and Ammonia in air will be essential to ensure a reasonable design of safety measure in the emerging Hydrogen society, were Ammonia might be used as an energy carrier or storage. The use of the 20 Liter Sphere enables for a variety of conditions to be tested, that can better reflect real accidental release situations.

References

DIN/TS 31018-1:2024. Bestimmungsverfahren für sicherheitstechnische Kenngrößen des Explosionsschutzes für hybride Stoffgemische - Teil 1: Gase

DIN EN 1839:2012. Determination of explosion limits of gases and vapours; German version

DIN EN 14034-1:2011. Determination of explosion characteristics of dust clouds - Part 1: Determination of the maximum explosion pressure p_{max} of dust clouds

Jorissen, W. P., Ongkiehong, B. L, 1926. Explosion regions, VIII: The explosion regions of hydrogen-ammonia-air and hydrogen-ammonia-oxygen mixtures. In: Recueil des Travaux Chimiques des Pays-Bas 45, 224–231. https://doi.org/10.1002/recl.19260450312

Molnárné, Maria, Schendler, Thomas, Schröder, Volkmar, 2003. Sicherheitstechnische Kenngrößen: Band 2: Explosionsbereiche von Gasgemischen. Bremerhaven : Wirtschaftsverl. NW, Verl. für Neue Wiss – ISBN 3–89701–746–6

Spitzer, Stefan H. et. Al., 2023. 1st International Round Robin Test on Safety Characteristics of Hybrid Mixtures, Journal of Loss Prevention in the Process Industries. Verfügbar unter: https://doi.org/10.1016/j.jlp.2022.104947

Safety Risk Management of Ammonia Fuelled Ships

Marta Bucelli[1,*], Simon Gant[2], Valerio Cozzani[3]

[1] *SINTEF Energy Research, Norway*
[2] *Health and Safety Executive, United Kingdom*
[3] *University of Bologna, Italy*

*marta.bucelli@sintef.no

1. Introduction

Ammonia is deemed to be a promising fuel to reduce carbon emissions from shipping as well as a viable alternative solution as a global hydrogen carrier. Several initiatives are ongoing to demonstrate the use of ammonia in fuel cells and internal combustion engines for use on offshore vessels. While the interest in ammonia increases, so do the concerns regarding its safety. Ammonia is toxic to humans and to marine life, and, at certain concentrations, when mixed with air, could ignite resulting in explosions. Although safely transported as a chemical and fertilizer for decades, ammonia has always been stored in dedicated carriers and handled by highly skilled personnel, crews and operators. The potential large-scale implementation of ammonia as a fuel in the maritime environment and its handling by different users introduces emerging risks and a potential need for further guidance. This work presents a bibliographic approach for the definition of accidental scenarios for safety risk management of ammonia fuelled offshore vessels and ammonia carriers. A screening of historical accidental events potentially resulting in ammonia released to sea is performed to identify key safety risk management aspects.

2. Methods

This analysis was conducted as a bibliographic literature review of past accidents involving refrigerated liquid ammonia. Both storage and transfer operations were considered as well as different industrial domains, such as fertilizer industry, process industry and food industry, including also fishing vessels which use ammonia as a refrigerant. The study focuses on storage conditions and operations that can provide valuable insight into the use of ammonia as ship fuel.

3. Results and discussion

Ammonia as a ship fuel is likely to be stored on board as refrigerated liquid, slightly pressurized above atmospheric pressure. Compared to ammonia as cargo, guidelines and procedures for the use of ammonia as a fuel are still under development (IMO, 2024; DNV, 2024). Furthermore, the operational experience with ammonia as ship fuel is limited and not established (ABS, 2024). Mitigation measures are therefore of foremost importance. Compared to Liquefied Natural Gas (LNG), for which the requirements are set by the IGF code, when ammonia is used as ship fuel, a comprehensive risk assessment is required. Therefore, the definition of risk assessment scenarios for the quantitative analysis of risk for ammonia as ship fuel is of outmost importance.

Three incident tiers can be considered to define the safety risk management and emergency preparedness strategy for ammonia releases *at sea* (GCMD, 2024):

1. First tier incidents: releases from connection and flanges, contained on board. These are releases that are contained within a specific area;
2. Second tier incidents: medium and large releases of ammonia, potentially spreading beyond operational area and activating the emergency release system that might cause overboard spillage; and
3. Third tier incidents: catastrophic releases resulting in overboard leaks, including hose rupture.

From this categorization as well as from the analysis of the reported ammonia accidents from different databases sources (such as the analyses presented by Gant et al. 2024, Bucelli et al., 2025), two key considerations are to be made.

Firstly, the operational conditions and the release scenario should be considered, and especially the rate, duration and location. Secondly, the potential impact and effects of the ammonia release should be assessed. Ammonia is toxic to human and its dispersion can result in clouds within dangerous thresholds in the atmosphere. Dispersion studies should be carried out to identify mitigation measures for different stakeholders.

Different ammonia storage conditions on the ship can also play a significant role in the fate of ammonia upon release. Releases from deck-mounted tanks and hull-located tanks have some differences that need to be considered (see Masia et al., 2024). These two cases may require different containment and integrity management.

For the case of ammonia onboard ships as marine fuel, safety assessments should consider dispersion of ammonia, both in terms of toxic and flammable hazards (including the potential for confined explosions in some areas). Also, releases of ammonia onto the deck, onto the sea, and below the sea (e.g., from a ship collision). These can potentially impact both human health and the environment. From the investigation by Bucelli et al. (2024), based on the ARIA database, 10% of documented incidents resulted in environmental impact including effects on vegetation, water contamination, and aquatic species. This is of concern when *directly* using and transferring ammonia over water.

It should also be noted that fires and explosions are less frequent outcomes of ammonia releases (Bucelli et al., 2025), but could represent a risk when the ammonia gas is indoors and confined and exposed to ignition sources (e.g., hot surfaces), as is potentially the case in engine rooms for maritime applications.

The lesson learnt from the analysed incidents and accidents involving refrigerated liquid ammonia that can be relevant in the context of using it as ship fuel can be summarised in Table 1

Table 1. Key safety aspects in implementing ammonia as ship fuel.

Key safety aspect	Description
Material selection	Materials used in presence of ammonia should be compatible and suitable. Their compatibility should be considered for both new-built and retrofits.
Equipment integrity	In addition to standard equipment integrity issues, the potential for stress corrosion cracking and corrosion under insulation should be addressed when handling ammonia, with suitable procedures for inspection and maintenance to reduce the potential for loss of integrity. Cold spill protection may also need to be considered in some areas.
Maintenance	Maintenance errors and component failures are one of the drivers for ammonia accidents and incidents. Protocols, procedures and training for

Key safety aspect	Description
	maintenance and inspection should reduce the risk and the potential exposure to ammonia gas.
Gas detection systems	Suitable gas detection systems for ammonia should be in place. The gas detection system can be a part of the leakage detection system, together with low temperature measurements and other operational monitoring parameters (such as temperature and pressure on lines and storage vessels). The ammonia gas detection system should provide quick and reliable detection of ammonia releases, issue warnings and *automatically* initiate safety actions (such as emergency shut down and automatic isolation of leakages to reduce their consequences). (Green Shipping Program, 2023).
Ammonia tank location onboard	The location of the tank on board is proven to be critical for different tier release scenarios. Hull-located tanks are less prone to catastrophic release scenarios upon collision.
Personal Protection Equipment (PPE)	Different PPE should be planned for operations, maintenance and emergency response, based on the type and amount of potential exposure to ammonia. Consideration should be given to toxic inhalation protection, thermal protection (cold spills and fire) and protection from corrosive burns.
Effect distances	Understanding the potential extent of ammonia effect distances can support the development of dedicated handling procedures and emergency response. Consideration should be given to whether the ammonia release will impact trained and equipped operators or third parties and members of the public. Several stakeholders may be involved in the case of refuelling operations at ports. Risk analysis and quantification can support the identification of access-controlled zones. Tools that can dynamically estimate the ammonia effect distances could support the evacuation and mitigation procedures in case of large ammonia releases, considering also the wind direction and speed.
Emergency preparedness	Emergency response to ammonia releases at sea requires modification of the conventional chemical spill emergency response plans (ERPs), mostly related to its toxicity.
Environmental damage	The environmental effects of ammonia on the marine life should be understood and handled accordingly. Ammonia can be a threat to fish, vegetation and marine life.
Regulation and certification	The ongoing development of regulations and certification requirements should support the safe introduction of ammonia as an alternative marine fuel for decarbonization. There are many stakeholders involved in this process: ship designers, operators, port authorities, regulators and certification bodies. Collaboration is key to successful implementation.

4. Conclusions

This study presents a series of key factors for the safety risk management of ammonia used onboard ships as *decarbonised* fuel. The study is based on a literature reviews and findings from incident investigations. A total of nine factors were identified as being important safety considerations. These included maintenance and emergency response procedures, as well as operational procedures for carrying out critical operations, such as, bunkering. Some of these topics, notably effect distances, are the subject of ongoing research projects.

Acknowledgments

References

ABS. 2024. Ammonia bunkering: Technical and Operational Advisory, https://ww2.eagle.org/content/dam/eagle/advisories-and-debriefs/ammonia-bunkering-advisory.pdf

Bucelli, M., Zanobetti, F., Schiaroli, A.,Cozzani, V. Accident scenarios for safety risk management of ammonia fuelled ships. In proceedings of the European Safety And Reliability Conference ESREL. Stavanger, Norway. 15-19 June 2025. *In Press.*

Yang, M., & Lam, J. S. L. 2024. Risk assessment of ammonia bunkering operations: Perspectives on different release scales. Journal of Hazardous Materials, 468, Article 133757, https://doi.org/10.1016/j.jhazmat.2024.133757

Gant, S., Pearson, A., Sullivan, E. 2024. Review of ammonia incidents and update on ongoing research activities on ammonia safety. Presented at FABIG Technical Meeting on "Harnessing history: safe design and operation of future energy systems". London, UK. 23-24 October 2024, https://www.gant.org.uk/research/241023%20HSE%20at%20FABIG%20ammonia%20v9.pdf

Global Centre for Maritime Decarbonization GCMD. 2024. How do we respond to an ammonia release at sea? https://www.gcformd.org/how-do-we-respond-to-an-ammonia-release-at-sea/

Green Shipping Program. 2023. Ammonia as a marine fuel safety handbook. Accessed: 24.03.2025. Available at: https://grontskipsfartsprogram.no/wp-content/uploads/2023/06/Ammonia-as-a-Marine-Fuel-Safety-Handbook-Rev.02-1.pdf

IMO. 2024. Sub-Committee on Carriage of Cargoes and Containers, 10th session (CCC 10), 16-20 September 2024. Accessed: 24.03.2025. https://www.imo.org/en/MediaCentre/MeetingSummaries/Pages/ccc-10th-session.aspx

DNV. 2024. IMO CCC 10: Interim guidelines for ammonia and hydrogen as fuel. Accessed: 24.03.2025. https://www.dnv.com/news/imo-ccc-10-interim-guidelines-for-ammonia-and-hydrogen-as-fuel/

Masia, B., Yang, M., Cozzani, V. 2024. Risk Assessment of ammonia fueled ships: consequences on human health of ammonia releases from damaged fuel storage tanks, ACS Chemical Health and Safety, 31(6), p502-520, https://doi.org/10.1021/acs.chas.4c00044

Factors Affecting the Thermal Behavior of Butyl Acrylate for Thermal Hazard Evaluation and Safe Handling

Mahoko Ando , Motohiko Sumino

Safety Engineering Technology Development Office, Production Technology Department,
Mitsubishi Chemical Corporation,
1000 Kamoshida-cho, Aoba-ku, Yokohama-shi, Kanagawa 227-8502, Japan

* mahoko.ando.ma @mcgc.com

1. Introduction

Monomers are widely used in the chemical industry as materials for plastics, paints, film, etc. On the other hand, they can generate radicals through self-initiation reactions, which may lead to runaway polymerization. In Japan, the explosion and fire occurred in the acrylic acid storage tank in 2012. Since then, it has been recognized that proper thermal hazard evaluation is important for safe handling of monomers.

During the storage process of monomers, inhibitors are typically added to avoid self-polymerization reactions. Commonly used hydroquinone type inhibitors require oxygen to be effective, so they are stored in an atmosphere where oxygen present. The effect of these inhibitors depends on both their concentration and the dissolved oxygen concentration. The interaction between these parameters complicates the measurement and prediction of the thermal behavior of the monomers [1]. If thermal analysis is performed under inappropriate conditions without considering these effects, it can lead to incorrect thermal hazard assessments. Therefore, it is important to reveal the influence of these parameters on the thermal behavior of monomers.

The purpose of this study is to investigate the impact of these parameters on the thermal behavior of monomers. Butyl acrylate with 15 ppm 4-methoxyphenol (MEHQ) was used as a model monomer. The work examined factors affecting the thermal behavior, such as the atmosphere in the gas phase and the liquid level height. The effects of these factors were discussed in terms of the polymerization reaction mechanism and the change in dissolved oxygen concentration.

2. Methods

2.1 Theory

2.1.1 Polymerization reaction mechanism

The radical polymerization of a butyl acrylate is started by self-initiation reaction as shown in Eq. (1) [2].

$$M \rightarrow R\cdot \qquad (1)$$

where M is a monomer, R· is a primary radical.
In the presence of oxygen, R· react with oxygen to form peroxy radicals as shown in Eq.(3), instead of the normal radical reaction as shown in Eq.(2) [3].

$$R\cdot + M \rightarrow RM\cdot \qquad (2)$$
$$R\cdot + O_2 \rightarrow RO_2\cdot \qquad (3)$$

These peroxy radicals react slowly with monomer as shown in Eq. (4) and copolymer is generated as shown in Eq. (5) [4].

$$RO_2 \cdot + M \rightarrow RO_2M \cdot \qquad (4)$$

$$RO_2M \cdot + O_2 \rightarrow RO_2MO_2 \cdot \qquad (5)$$

Inhibitors can stabilize radicals, but hydroquinone type such as MEHQ react much more rapidly with polyperoxy radicals as shown in Eq. (6), than with radicals (R•) [5].

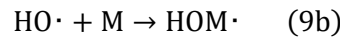$$RO_2MO_2 \cdot + IH \rightarrow RO_2MOOH \qquad (6)$$
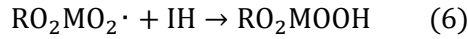
where IH is inhibitor. This is why the oxygen is necessary for the hydroquinone type inhibitors.

Also, in the presence of oxygen, the auto-oxidation of the monomer also occurs as shown in Eq. (7) [6].

$$M + O_2 \rightarrow MOOH \qquad (7)$$

Furthermore, the peroxides formed in Eq. (6) and (7) decompose to produce radicals at high temperatures as shown in Eq. (8) [7]. These radicals then react with the monomer, as shown in Eq. (9a) and (9b).

$$MOOH \rightarrow MO \cdot + \cdot OH \qquad (8)$$

$$MO \cdot + M \rightarrow MOM \cdot \qquad (9a)$$

$$HO \cdot + M \rightarrow HOM \cdot \qquad (9b)$$
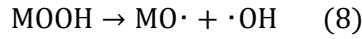
2.1.2 Change in the dissolved oxygen concentration

The rate of the consumption of dissolved oxygen concentration in butyl acrylate with 15ppm MEHQ is expressed by Eq. (10), based on the study by Holger et al. [4].

$$C_{cons.} = -kt \qquad (10)$$

where $C_{cons.}$ is the dissolved oxygen concentration [ppm], k is the rate constant [ppm s^{-1}], t is time [s]. The rate constant k at 90°C is 4.63×10^{-5} ppm s^{-1}[4].

For the diffusion of dissolved oxygen concentration, it is assumed to diffuse in one direction. The analysis was performed using the Finite Volume Method, as shown in Figure 1. C is the dissolved oxygen concentration in each cell, subscript t is time, and i represents the i-th cell. Δx is the distance between cells, and S is the contact area between cells.

Figure 1. Unsteady-state diffusion analysis using the Finite Volume Method.

According to Fick's law of diffusion, the diffusion flux J is given by:

$$J = -D\frac{\partial C}{\partial x} \qquad (11)$$

where J is the diffusion flux [mol m^{-2} s^{-1}], D is the diffusion coefficient [m^2 s^{-1}], C is the dissolved oxygen concentration [mol m^{-3}], x is position [m].

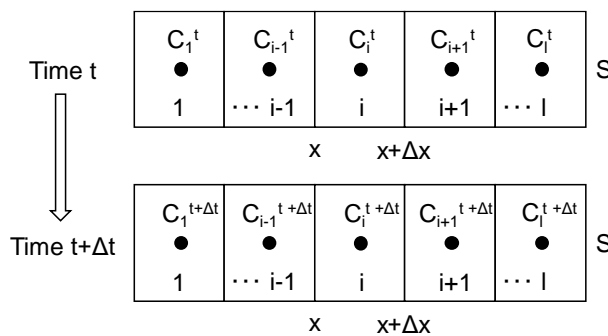Considering the change in the dissolved oxygen concentration in the small volume $S\Delta x$ between positions x and x+Δx, the difference in diffusion flux at each position is equal to the diffusion flux accumulated in cell i. This can be expressed by Eq. (12).

$$S\Delta x \frac{\partial C_i}{\partial t} = J(x)S - J(x+\Delta x)S \quad (12)$$

where S is the contact area between cells [m^2], t is time [s].
Dividing by both side Δx, Eq. (13) is given:

$$\frac{\partial C_i}{\partial t} = -\frac{\partial J}{\partial x} \quad (13)$$

When Eq. (11) is substituted into Eq. (13), Eq. (14) is given:

$$\frac{\partial C_i}{\partial t} = \frac{\partial}{\partial x}\left(D\frac{\partial C}{\partial x}\right) \quad (14)$$

To solve for C, integrating both sides over the interval from x to x+Δx yields Eq. (16):

$$\int_x^{x+\Delta x} \frac{\partial C_i}{\partial t} dx = \int_x^{x+\Delta x} \frac{\partial}{\partial x}\left(D\frac{\partial C}{\partial x}\right) dx \quad (15)$$

$$\frac{\partial C_i}{\partial t}\Delta x = D\left(\frac{\partial C}{\partial x}\bigg|_{x+\Delta x} - \frac{\partial C}{\partial x}\bigg|_x\right) \quad (16)$$

When solving for each analysis step Δt, Eq. (16) can be transformed as follows:

$$\frac{C^{t+\Delta t}_i - C^t_i}{\Delta t} = \frac{D}{\Delta x}\left(\frac{\partial C}{\partial x}\bigg|_{x+\Delta x} - \frac{\partial C}{\partial x}\bigg|_x\right) \quad (17)$$

The concentration gradients at positions x+Δx and x on the right-hand side of Eq. (16) are represented by equations (18) and (19).

$$\frac{\partial C}{\partial x}\bigg|_{x+\Delta x} = \frac{C^t_{i+1} - C^t_i}{\Delta x} \quad (18)$$

$$\frac{\partial C}{\partial x}\bigg|_x = \frac{C^t_i - C^t_{i-1}}{\Delta x} \quad (19)$$

Eq. (17) can be transformed as follows:

$$C^{t+\Delta t}_i = C^t_i + \frac{D\Delta t}{\Delta x}\left(\frac{C^t_{i+1} - 2C^t_i + C^t_{i-1}}{\Delta x}\right) \quad (20)$$

From Eq. (20) and (11), the dissolved oxygen concentration of the i-th cell at time t+Δt can be expressed by Eq. (21).

$$C^{t+\Delta t}_i = C^t_i + \frac{D\Delta t}{\Delta x}\left(\frac{C^t_{i+1} - 2C^t_i + C^t_{i-1}}{\Delta x}\right) - k\Delta t \quad (21)$$

As boundary conditions, at t=0, C=C$_0$, and at x=0, C=C$_s$, where C$_0$ is the initial oxygen concentration and C$_s$ is the saturated oxygen concentration. The diffusion coefficient is set to D=2.42$\times$10^{-5} cm^2 s^{-1}, and the analysis is performed with Δt=30s, Δx=0.1cm.

2.2 Experiment

Isothermal measurements were conducted using a high-sensitivity calorimeter (C80). This experiment aimed to examine the effect of the atmosphere in the gas phase and the liquid level height on the thermal behavior. The gas phase atmosphere is estimated to influence the saturated dissolved oxygen concentration in the monomer. The liquid level height is estimated to affect the ease of oxygen diffusion from the gas phase to the bottom. The atmosphere were Air and 2% O_2/N_2, and the liquid levels were 3.1 cm, 1.2 cm, and 0.3 cm. All measurements were performed at 90°C. Stainless steel pressure-resistant cells were used, and a glass liner was inserted to prevent reaction between the butyl acrylate and the metal. Table 1 presents the measurement conditions of C80.

Table 1: The measurement conditions of C80 for butyl acrylate

The gas phase atmosphere	The liquid level height [cm]	Sample mass [g]	The liquid fill level [%]	Temperature [℃]
Air	3.1	2.5	44	90
	1.2	1	18	
	0.3	0.2	4	
2%O$_2$/N$_2$	3.1	2.5	44	
	1.2	1	18	
	0.3	0.2	4	

3. Results and discussion

3.1 Results of the thermal behavior under an air atmosphere

According to the experimental data by Holger et al. [4], the saturated dissolved oxygen concentration butyl acrylate at 90°C is 66 ppm. Figure 2 shows the C80 results of butyl acrylate at 90°C under an air atmosphere. It suggests that as the liquid level decrease, the time until polymerization starts becomes shorter. Figure 3 shows the estimation results of the change in dissolved oxygen concentration at each liquid level. It indicates that as the liquid level decrease, the dissolved oxygen concentration at the bottom is higher because the diffusion of oxygen to the bottom is faster. These results imply that when the liquid level is lower, the concentration of peroxides formed by Eq. (7) in section 2.1.1 is higher due to the increased oxygen concentration. Consequently, more radicals are generated through the decomposition of peroxides, as shown in Eq. (8) in section 2.1.1, leading to a short time to polymerization initiation. However, since the reproducibility of the C80 experiments was low, it is necessary to increase the number of measurements in future studies.
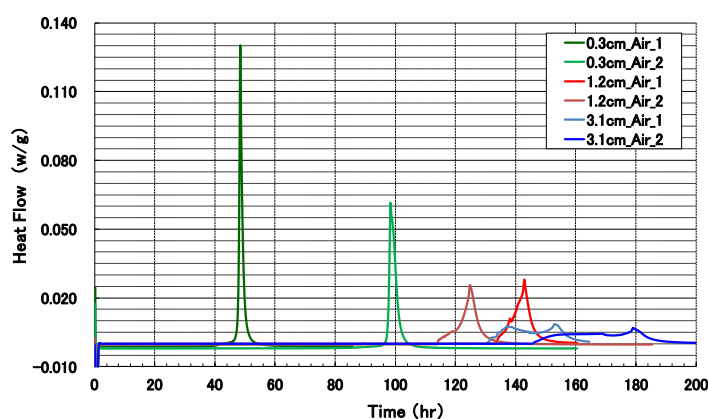

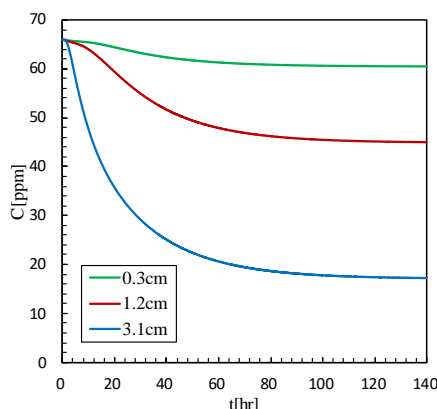*Figure 2. The C80 results of butyl acrylate at 90℃ under an air atmosphere.*

Figure 3. The estimation results of the change in dissolved oxygen concentration at each liquid level under an air atmosphere.

3.2 The results of thermal behavior under a 2% O_2/N_2 atmosphere

Since the experimentally measured saturated dissolved oxygen concentration of butyl acrylate at 90°C under air is 66 ppm [4], it is estimated to be 6.6 ppm under 2% O_2/N_2. Given that the inhibitor can stabilize two polyperoxy radicals [5], 15 ppm concentration of inhibitor is excessive relative to the 6.6 ppm of the dissolved oxygen. Once the initial dissolved oxygen is consumed, the diffusion from the gas phase becomes important. Figure 4 shows the C80 results of butyl acrylate at 90°C under a 2% O_2/N_2 atmosphere. It suggests that as the liquid level increase, the time until polymerization started becomes shorter. Figure 5 shows the estimation results of the change in dissolved oxygen concentration at each liquid level. It indicates that as the liquid level increase, the dissolved oxygen concentration at the bottom is lower because the diffusion of oxygen to the bottom is slower. These results imply that when the liquid level is higher, oxygen is insufficient at the bottom, leading to the start of radical polymerization as shown in Eq. (1) in section 2.1.1. However, since the reproducibility of the C80 experiments was low, it is necessary to increase the number of measurements in future studies.

Next, the cause of the different relationships between the liquid level and the time to polymerization initiation under air and 2% O_2/N_2 atmospheres will be discussed. This is suggested to be due to the different effects of oxygen on the monomer. Oxygen acts as an inhibitor for the monomer, as shown in Eq. (3) to (5) in section 2.1.1. On the other hand, oxygen also contributes to the initiation of polymerization by generating radicals through the decomposition of peroxide, as shown in Eq. (7)–(9b) in section 2.1.1. In the case of the air atmosphere, the saturated dissolved oxygen concentration is higher than 2% O_2/N_2. Under conditions of higher dissolved oxygen concentration, peroxide increases, and the effect of oxygen on polymerization initiation becomes greater. On the other hand, under 2% O_2/N_2, the impact of oxygen as an inhibitor is likely more significant. Under the air atmosphere with a higher saturated dissolved oxygen concentration, the peroxide concentration increased, leading to a greater effect of oxygen in initiating polymerization. On the other hand, under the 2% O_2/N_2 with a lower dissolved oxygen concentration, it is suggested that the effect of oxygen as an inhibitor is more significant.
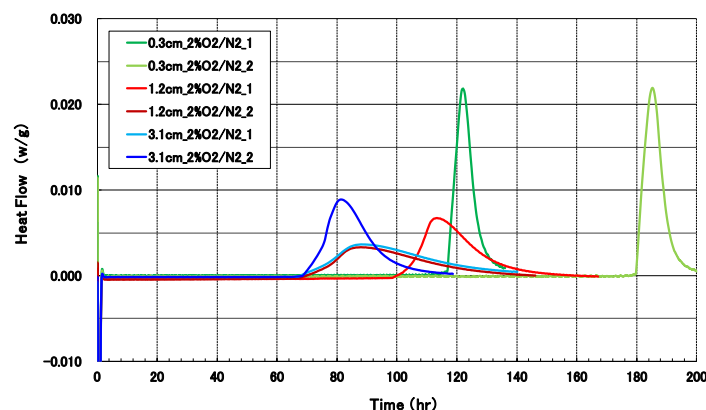
Figure 4. The C80 results of butyl acrylate at 90℃ under a 2% O₂/N₂ atmosphere.
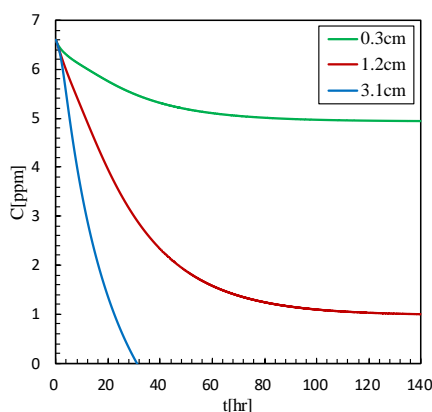
Figure 5. The estimation results of the change in dissolved oxygen concentration at each liquid level under a 2% O₂/N₂ atmosphere.

4. Conclusions

This study investigated the effect of the atmosphere in the gas phase and the liquid level height on the thermal behavior of butyl acrylate. The results suggest that as the liquid level decreases, the time until polymerization starts becomes shorter under an air atmosphere. This is because more radicals are generated through the decomposition of peroxides in the lower liquid level. On the other hand, as the liquid level increase, the time until polymerization started becomes shorter under a 2% O₂/N₂ atmosphere. This is due to the insufficient oxygen at the bottom in the higher liquid level. The different relationships between the liquid level and the time to polymerization initiation were suggested to be due to the different effects of oxygen on the monomer. These findings highlight the complex interaction between the atmosphere, the liquid level, and the dissolved oxygen concentration in determining the thermal behavior of monomers. Proper understanding and consideration of these factors are essential for accurate thermal hazard assessments and safe handling of monomers.

References

[1] Min, S., Florin, D., Steve, H., Robert, B., Marabeth, H., Travis, S., Stephan, W., Alan, S.,2019. Calorimetric Method To Determine Self-Accelerating Polymerization Temperature (SAPT) for Monomer Transportation Regulation: Kinetics and Screening Criteria. Org. Process Res. Dev. 23, 737-749.

[2] Ahmad, A. S., Nazanin, M., Sriraj, S., Patrick, C., Michael, C. G., Andrew, M. R., Masoud, S., 2016. Study of n-Butyl Acrylate Self-Initiation Reaction Experimentally and via Macroscopic Mechanistic Modeling. Processes, 4(2), 15.

[3] Stefanie, S., Herbert, V., 1998. Aspects of the Safe Storage of Acrylic Monomers: Kinetics of the Oxygen Consumption, Chem. Eng. Technol., 21, 10, 829-837.

[4] Holger, B., Herbert, V., 2004. Stabilization of Acrylic Esters, Chem. Eng. Technol., 27, 10, 1122-1126.

[5] Leon, B. L., 1987. Inhibitor-Oxygen Interactions in Acrylic Acid Stabilization, Plant/Operations Progress, 6, 4, 188-189.

[6] Basic Acrylic Monomer Manufacturers, Inc.,2020, Acrylic esters - a summary of safety and handling, 4th ed, Basic Acrylic Monomer Manufacturers, Inc.

[7] Liu. X., Zhai, Z., 2015. Thermally induced aerobic autopolymerization of methyl methacrylate in amide-type solvents: simultaneous polymerization during induction via direct in situ O2 activation, *Macromolecular Chemistry and Physics*, 216, 1201-1211.

Simulation of Decomposition Reactions considering the Residual Cooling Capacity of Industrial Reactors

Adrian Zentel*[1], Marc-André Serrer[1], Steffen Salg[2], Markus Gödde[3], Johannes Schröder[1,], Robert John Blanchard[1]

[1] *Safety Assessment & Testing (BASF SE, Carl-Bosch-Straße 38, 67056 Ludwigshafen, Germany)*

[2] *Pluriol Plant (BASF SE, Carl-Bosch-Straße 38, 67056 Ludwigshafen, Germany)*

[3] *Process Safety (BASF SE, Carl-Bosch-Straße 38, 67056 Ludwigshafen, Germany)*

*adrian.zentel@basf.com

1. Introduction

In chemical production plants, process safety is one of the key aspects of process development. A basic scenario within the field of thermal process safety to safeguard exothermal decomposition reactions is the total loss of cooling event with the simplified assumption of adiabatic conditions [1], see Figure 1. Within this scenario the reaction temperature T_R, the maximum temperature of the synthesis reaction (MTSR) and the adiabatic decomposition temperature (ADT24) are essential characteristics. Knowing the ADT24, the maximum allowable temperature for the process T_{Exo} can be derived. The technical rule for plant safety (German: Technische Regel für Anlagensicherheit (TRAS) 410) suggests limiting the T_{Exo} 10 K below the ADT24 [2].
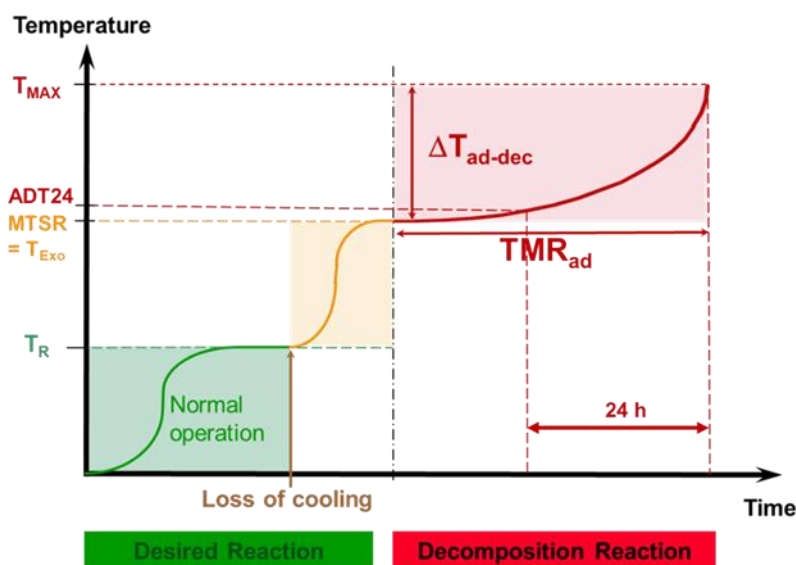

Figure 1: Temperature development in the scenario of a total loss of cooling event with the simplified assumption of adiabatic conditions [1].

The TRAS 410 also emphasizes to consider the heat loss of the system when determining the maximum allowable temperature T_{Exo}. Within this frame a study has been performed, investigating the impact of the residual cooling capacity of industrial reactors on the T_{Exo}. The residual cooling capacity describes the passive cooling capability of the system after failure of active cooling, particularly due to the heat loss to the environment, i. e. ambient convective cooling.

In this study, alkoxylation reactions were investigated with respect to the scenario of a cooling failure. In alkoxylation processes, a nucleophilic compound like an alcohol or amine is reacted with an alkylene oxide, e. g. ethylene oxide or propylene oxide. The reaction can be catalyzed by Bronsted bases such as sodium hydroxide or potassium hydroxide. Within the alkoxylation process there are significant hazards to be safeguarded: high toxicity of alkylene oxides, gas phase decomposition of ethylene oxide, high reaction enthalpy of - 95 kJ/mol ethylene oxide (l) or - 121 kJ/mol ethylene oxide (g) and exothermal decomposition reactions of educts, intermediates and products [3, 4].

2. Methods

At BASF, a model-based concept is used to safeguard the aforementioned hazards of the alkoxylation processes [4 - 6]. The model calculates the free oxide concentration in the reactor in every moment of the reaction based on temperature, pressure and known substance properties. The oxide dosage is regulated such that in case of a cooling failure the runaway of the synthesis reaction is limited to the maximum allowed temperature T_{Exo}. At this temperature, the decomposition of the reaction mixture starts slowly with a rather small heat release rate. In alkoxylation processes, a slightly different definition of the ADT24 is used, which is more conservative than the definition given in TRAS 410. According to TRAS 410, the ADT24 is the temperature at which the time to maximum rate (TMR) at adiabatic conditions equals 24 hours [2]. Following this approach, the $T_{24\_TDesign}$ is defined as the temperature, at which it takes at least 24 hours to reach the reactor design temperature. This period is long enough to deploy suitable countermeasures against thermal runaway, i. e. external emergency cooling by the fire department. The maximum rate of the decomposition reaction is usually observed at temperatures larger than 250 °C, which is a common reactor design temperature. Because of this conservative definition and after having conducted sophisticated thermal analyses of the decomposition reaction for each polyether polyol, the $T_{24\_TDesign}$ is implemented as maximum allowed temperature T_{Exo}.

To investigate the impact of the residual cooling capacity on the alkoxylation process, the process-limiting exothermal decomposition reaction was investigated by calorimetric methods and formal kinetic models were generated describing the decomposition reactions. In addition, for various industrial reactors the specific heat loss due to ambient cooling was determined experimentally and numerical reactor models were developed. The models describing decomposition kinetics and the reactor models were used to perform numerical simulations for the prediction of the thermal behaviour for various product-reactor-combinations. For modelling and simulation, the software code from Cheminform St. Petersburg "Thermal Safety Series-Advanced Reaction Kinetics Simulation (TSS-ARKS)" was used. The concept of simulating the thermal behaviour of a peroxide decomposition reaction under non-adiabatic conditions with the software code and the validating 1:1 experiments were published by our group at Loss Prevention in 2016 [7].

3. Results and discussion

The numerical simulations of the thermal behaviour of the decomposition reactions within the reactor models representing the industrial scale reactors were applied to derive the maximum allowed temperature T_{Exo} with an induction time of at least 24 hours under process relevant conditions. Depending on the product-reactor-combination the T_{Exo} may be 10 K to 20 K higher when considering ambient cooling than the T_{Exo} in the ideal adiabatic case. These benefits of additional temperature increase are strongly dependant on the criticality of the decomposition reaction and the specific heat loss of the reactor. If a decomposition reaction generates heat at a slow rate and the reactor can dissipate heat at a high rate the resulting temperature benefit will be large. For fast decomposition reactions in large reactors with low surface area to volume ratios the benefit will be small, since the system will behave close to the ideal adiabatic case. If additional countermeasures, like independent emergency cooling or drainage/quench systems, are provided, the T_{Exo} may be increased by approximately 50 K compared to the ideal adiabatic case, see Figure 2
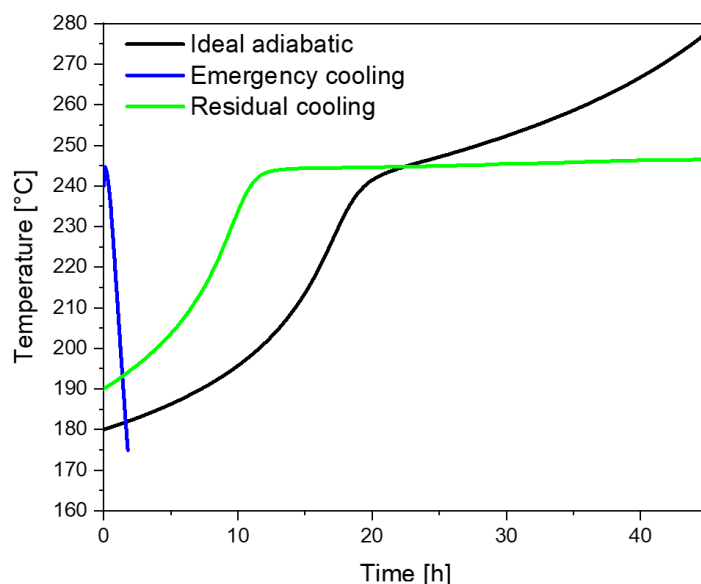
Figure 2: Simulation of the temperature-time curves of the decomposition reaction of a polyether polyol for 3 cases: ideal adiabatic, residual cooling and active emergency cooling (starting at 180 °C, 190 °C and 245 °C respectively (reactor model: 35 m³ reactor with insulation). The initial temperature of each curve corresponds to the maximum allowed temperature T_{Exo}.

4. Conclusions

The findings of these studies show that it can be highly beneficial to consider the process under process relevant conditions when setting up the safeguarding concept. The additional temperature increases of 10 K to 20 K by considering the residual cooling and the up to 50 K temperature increase when active emergency cooling is available can be directly transferred to additional plant capacity while keeping the same safety level as in the conservative worst-case scenario. This highlights that safety engineering and economical production can go hand in hand when the safety assessment is done in a smart way with advanced analytical methods based on high quality and robust caloric data.

References

1. Gygax R., 1988. Chemical reaction engineering for safety. Chemical Engineering Science. 43(8), 1759-1771. https://doi.org/10.1016/0009-2509(88)87040-4
2. Bundesministerium für Umwelt, Naturschutz und Reaktorsicherheit, 2021. Technische Regel für Anlagensicherheit (TRAS) 410. Kommission für Anlagensicherheit, Bundesanzeiger.
3. BG RCI, 2022. R 009 - Reaktionen mit Ethylenoxid und andere Alkoxylierungen. Merkblätter der R-Reihe Anlagensicherheit.
4. Loetgering-Lin O., Salg S., Koenig C., Buchholz H., Goedde M., Odenwald O., Sager W., Brodhagen A., Heitz T., Ries R., 2023. *Knowing and Controlling the Risks of Semi-batch Alkoxylation Reactions*, Chemical Engineering Transactions, 98, 51-56. https://doi.org/10.3303/CET2398009.
5. Reiser M., Salg S., Loetgering-Lin O., Buchholz H., Hohendorf S. Fischer J., Fath W., Odenwald O., Goedde M., 2019. Modellbasierte Absicherungskonzepte für Semi-Batch-Alkoxylierungen. 14. Fachtagung Anlagen-, Arbeits- und Umweltsicherheit. Köthen: Dechema
6. Loetgering-Lin O., Salg S., Buchholz H., Odenwald O., Goedde M., 2020. Modellbasierte Absicherungskonzepte für Semi-Batch-Alkoxylierungen. Chemie Ingenieur Technik. https://doi.org/10.1002/cite.202055061.
7. Duerrstein S. H., Kappler C., Neuhaus I., Malow M., Michael-Schulz H., Goedde M., 2016. Model-Based Prediction of the Adiabatic Induction Period and SADT of Dicumyl Peroxide Solution and Comparison to Large-Scale Experiments Performed Using 216.5-Liter Steel Drums in the UN-Test H.1. Chemical Engineering Transactions, 48, 475-480. DOI:10.3303/CET1648080.

Introduction of Quantitative Approaches Supporting Cybersecurity Risk Assessment in the Chemical and Process Industry

Matteo Iaiani*, Alessandro Tugnoli, Valerio Cozzani

LISES - Dipartimento di Ingegneria Civile, Chimica, Ambientale e dei Materiali, Alma Mater Studiorum - Università di Bologna, via Terracini n.28, 40131 Bologna (Italy)

*matteo.iaiani@unibo.it

1. Introduction

Cyber-attacks to Industrial Automation and Control Systems (IACS) such as the Basic Process Control System (BPCS) and the Safety Instrumented System (SIS) in chemical and petrochemical facilities are of major concern due to the potential severity of consequences on humans, property, and the surrounding environment, which are comparable to those of the major accident scenarios caused by safety-related causes (Iaiani et al., 2021). The ISA/IEC 62443 series of standards offer a systematic and practical framework to address cybersecurity challenges in IACS. Implementing this framework requires identifying all potential impacts of deliberate malicious attacks on the BPCS and SIS, evaluating the consequences on the physical plant, and assessing their likelihood. However, the standards do not provide specific methods or guidelines to support these activities, highlighting a critical research gap that demands further investigation.

2. Proposed approaches supporting cyber-risk assessment

The proposed set of tools supporting cyber-risk assessment (e.g., ISA/IEC 62443) is graphically represented in Figure 1. In particular, the contribution covers:

- *Identification of critical events*. This step focuses on determining major events (release of hazardous materials, fire, explosion, etc.) or production outages that could be initiated by cyber-attacks targeting the BPCS and SIS. The POROS 2.0 (Process Operability Analysis of Remote manipulations through the cOntrol System) methodology developed by the authors is suggested for this purpose. Details can be found in Iaiani et al. (2023a), together with an example of application.
- *Identification of cyber-attacks*. This step focuses on determining potential attack pathways within the IT (Information Technology) – OT (Operational Technology) system that adversaries might exploit to access the target elements of BPCS and SIS. The new tool called Cyber – Adversary Sequence Diagram (Cyber-ASD) is suggested for this purpose. It consists in a schematic representation of the IT-OT network structure (e.g., cyber areas such as IT intranet, BPCS, SIS, and cyber path elements such as firewalls and switches) through which it is possible to systematically identify all cyber pathways to access a certain target element. The formal conceptualization of the cyber-ASD is part of future work; however, application of the ASD in the context of the physical security of chemical and process plants can be found in Iaiani et al. (2023b). Moreover, this step requires identification of the specific set of manipulations of the BPCS and SIS target elements (e.g., PID controllers, PLCs) to initiate the critical events identified in the previous step. This can be systematically performed through the application of POROS 2.0 methodology.
- *Evaluation of consequences*. In this step, the consequences of identified critical events are quantified in terms of their impact on people, assets, the environment, and reputation.

The score-based approach provided in the POROS 2.0 methodology is suggested for this purpose

- *Evaluation of likelihood.* This step requires the evaluation of the probability of success of the identified cyber-attacks. This is given by the product of the probability of attempted attack and the conditional probability of successful execution given the attempt. While quantification of the first contribution requires expertise of intelligent and socio-political analysts, the evaluation of the second term falls within the background of risk analysts. To this purpose, a Bayesian Network (BN)-based approach, leveraging the Estimate of Adversary Sequence Interruption (EASI) model developed by the Sandia National Laboratory in the context of nuclear security, is proposed. The formal conceptualization of the method is part of future work; however, an application in the context of physical security of offshore Oil&Gas platform is provided in Iaiani et al. (2023b).
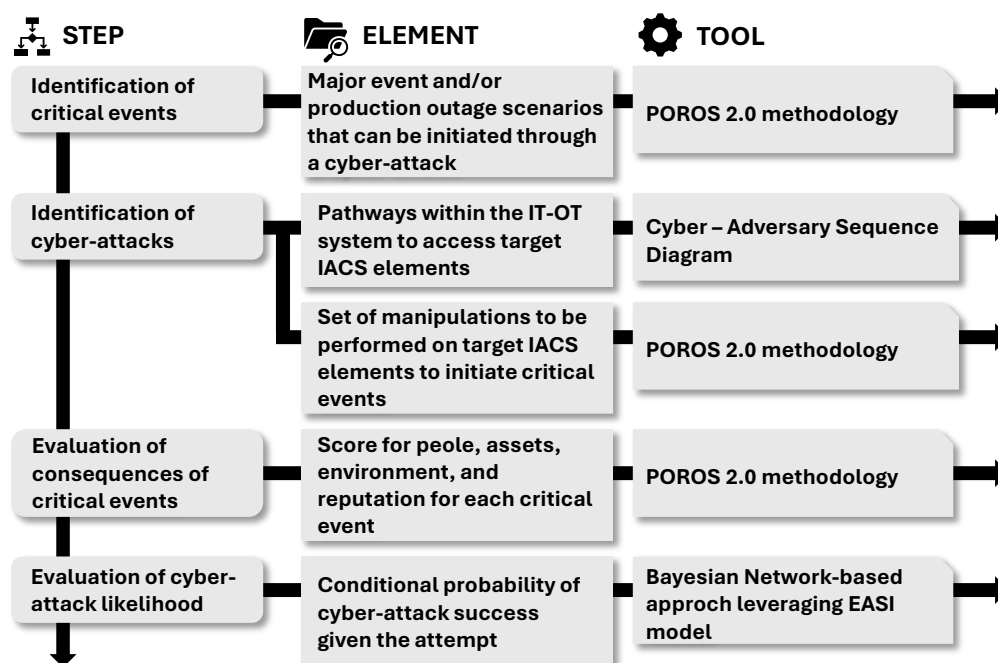
Figure 1. Tools proposed to support different steps of the quantitative cyber-risk assessment.

3. Conclusions

A set of novel approaches is proposed to enhance the identification of critical cybersecurity events and cyber-attack pathways, the evaluation of potential consequences, and the assessment of attack likelihood. These approaches aim to improve the reproducibility and accuracy of cyber-risk assessments in chemical and process facilities.

Acknowledgments

References

Iaiani, M., Tugnoli, A., Bonvicini, S., Cozzani, V., 2021. Analysis of Cybersecurity-related Incidents in the Process Industry. Reliab Eng Syst Saf. 209, 107485. https://doi.org/10.1016/j.ress.2021.107485

Iaiani, M., Tugnoli, A., Cozzani, V., 2023a. Process hazard and operability analysis of BPCS and SIS malicious manipulations by POROS 2.0. Proc Saf Env Prot. 176, 226–237. https://doi.org/10.1016/j.psep.2023.06.024

Iaiani, M., Tugnoli, A., Cozzani, V., Reniers, G., Yang, M., 2023b. A Bayesian-network approach for assessing the probability of success of physical security attacks to offshore Oil&Gas facilities. Ocean Eng. 273, 114010. https://doi.org/10.1016/J.OCEANENG.2023.114010

Introduction to Digital Twins for Supporting Quantitative Cybersecurity Risk Assessment

Antonio Manzi, Matteo Iaiani, Alessandro Tugnoli*, Giacomo Antonioni, Valerio Cozzani

LISES - Dipartimento di Ingegneria Civile, Chimica, Ambientale e dei Materiali, Alma Mater Studiorum - Università di Bologna, via Terracini n.28, 40131 Bologna (Italy)

*a.tugnoli@unibo.it

1. Introduction

With the increasing digitalization of the chemical, process, Oil&Gas, and energy production industries, cybersecurity has emerged as a critical issue (Center for Chemical Process Safety, 2022). This is particularly evident in scenarios where cyber attackers gain access to and manipulate Operational Technology (OT) systems, including the Basic Process Control System (BPCS) and the Safety Instrumented System (SIS). In fact, historical evidence demonstrates that such malicious interferences can initiate events with consequences comparable to scenarios arising from conventional equipment failures (Iaiani et al., 2023a).

A key phase in quantitative cybersecurity risk assessment (QCRA) involves understanding and modeling the dynamics of plants when BPCS and SIS are maliciously manipulated through cyber-attacks, alongside evaluating the response performance of the adopted protection strategies (e.g., inherent/passive safeguards such as pressure safety valves, and procedural/active safeguards such as shutdown procedures), to identify vulnerabilities, quantify potential consequences, and prioritize mitigation measures.

In this regard, the present study investigates the use of digital twins—digital replicas of physical plants implemented in dynamic process simulation environments—as a tool to support the quantitative assessment of cybersecurity risks. The conditioning section of a green hydrogen production plant was taken as case study.

2. Method

The method employed in this study is outlined in Figure 1.
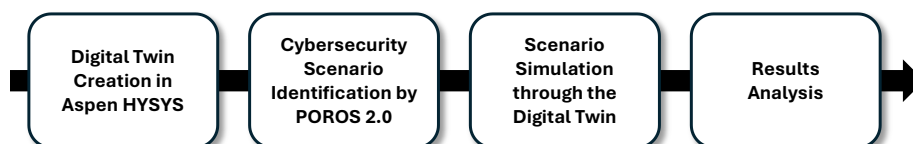
Figure 1. Method adopted in the present study.

Firstly, the digital twin of the plant section analyzed was created using aspen HYSIS software in dynamic mode. Then, the cybersecurity scenarios to be simulated (e.g., those relevant in the context of quantitative cyber risk assessment) were identified

using POROS 2.0 (Process Operability analysis of Remote manipulations through the cOntrol System) methodology, developed by the authors in a previous study (Iaiani et al.,

2023b). The methodology provides the sequence of manipulations of BPCS and SIS components that can initiate process-related critical events such as major events or operation outages.

The identified scenarios were individually simulated using the developed digital twin, and the resulting data—including pressure, temperature, level, and flow plots—were analysed to extract information relevant to quantitative risk assessment, such as response times and the capability of the installed pressure safety valves in managing the pressurization induced by the scenario.

3. Case Study

3.1 Description

Figure 2 shows Process Flow Diagram (PFD) of the plant section analysed in the case study. The section represents one of the parallel conditioning lines in a green hydrogen production plant utilizing AEL electrolysers. Specifically, the produced hydrogen is first dehydrated in V-100 after being cooled in HE-100, where water condenses. Subsequently, the small amount of oxygen present in the stream is converted into water within the deoxidizer (CRV-100). This water is then separated in V-101, and the hydrogen is compressed to meet transport specifications.
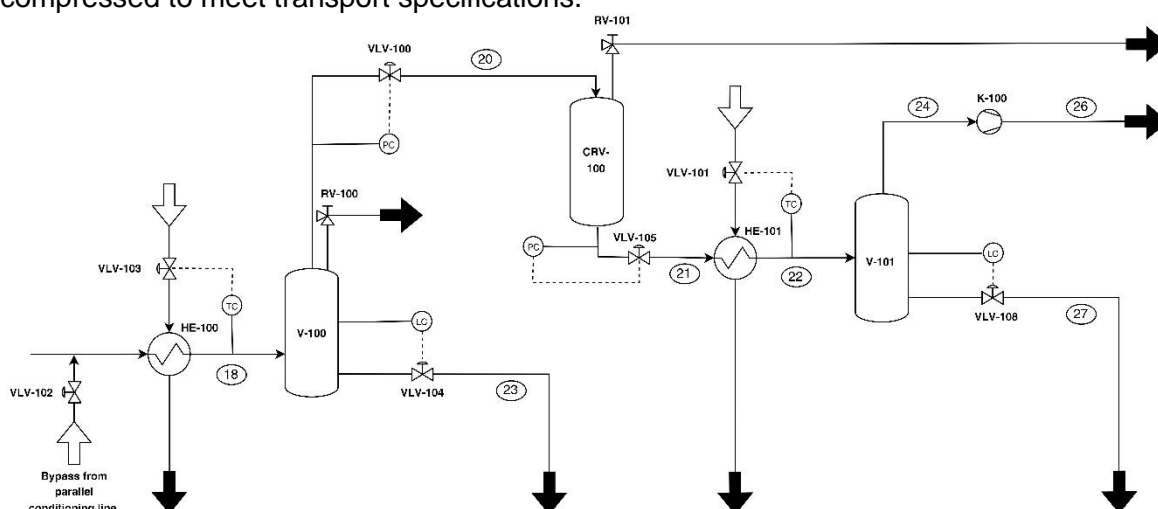
Figure 2. Process Flow Diagram (PFD) of the section analysed (green H$_2$ conditioning)

3.2 Results and discussion

The digital twin corresponding to the plant section depicted in Figure 2 was developed using Aspen HYSYS in dynamic mode. This process involved designing all equipment and valves, as well as implementing the necessary control loops.

POROS 2.0 was subsequently applied to identify relevant cybersecurity scenarios. For the sake of brevity, the results are presented for a single scenario: the simultaneous opening of the bypass stream between the conditioning line under assessment and the adjacent line (via manipulation of the BPCS controller managing valve VLV-102) and the closure of the gas outlet stream from V-100 (via manipulation of the pressure controller managing VLV-100). This scenario is designed to over-pressurize the dryer V-100, potentially causing a breach and the subsequent release of hydrogen (highly flammable gas). It was then simulated using the digital twin to assess the adequacy of the PSV installed on V-100, which was designed for a closed outlet configuration, and to evaluate the system's response time. Figure 3 illustrates the pressure response within the separator V-100 under the simulated cybersecurity scenario. The pressure exceeds the Maximum Allowable Accumulated

Pressure (35 bar), reaching a peak of 40 bar (black curve) after 17 s after the second manipulation (pressurization time to be used in QCRA). This highlights that the PSV installed on V-100, with an orifice area of 29 mm², is unable to provide adequate relief for the overpressure induced by the described manipulations. As previously stated, this scenario is critical, as the excessive pressure could compromise the structural integrity of the separator and lead to a potential release of hydrogen, warranting consideration within cybersecurity risk assessment.

To address this criticality, the installation of a type D PSV (orifice area of 70.97 mm^2), as specified in API standard 526, is proposed to enhance the system's overpressure protection capabilities against this cybersecurity scenario.
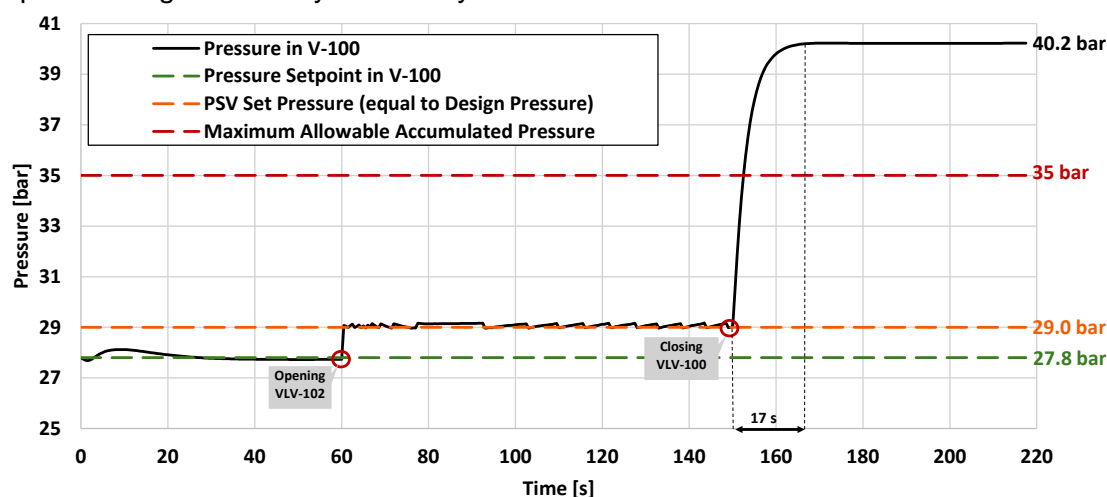
Figure 3. Pressure trend in dryer V-100 obtained with Aspen HYSYS simulation.

4. Conclusions

The present study investigates the role of digital twins in supporting quantitative cybersecurity risk assessment (QCRA). The dynamic Aspen HYSYS-based digital twin of the conditioning section of a green hydrogen production plant, considered as a case study, demonstrated the effectiveness of digital twins in checking the adequacy of passive safeguards (such as PSVs) in preventing or mitigating the cyber malicious interference with the BPCS and SIS and in evaluating the system's response time, information required in QCRA. Future developments will explore the use of digital twins to simulate more complex scenarios and to assess whether the order of manipulations affects the extent of consequences.

Acknowledgments

References

Center for Chemical Process Safety (CCPS), 2022. Managing Cybersecurity in the Process Industries - A Risk-based Approach. Wiley.

Iaiani, M., Tugnoli, A., & Cozzani, V., 2023a. Identification of cyber-risks for the control and safety instrumented systems: a synergic framework for the process industry. Proc Saf Env Prot. 172, 69–82. https://doi.org/10.1016/j.psep.2023.01.078

Iaiani, M., Tugnoli, A., & Cozzani, V., 2023b. Process hazard and operability analysis of BPCS and SIS malicious manipulations by POROS 2.0. Proc Saf Env Prot. 176, 226–237. https://doi.org/10.1016/j.psep.2023.06.024

The 'Human as a Barrier' in Cybersecurity Incident Response

Chidera Winifred Amazu[*], Gabriele Baldissone, Micaela Demichela

Politecnico di Torino, Corso Duca degli Abruzzi, 24, 10129, Turin, Italy

* chidera.amazu@polito.it

1. Introduction

In safety-critical facilities like the process industries, cybersecurity is of grave importance, considering the magnitude of the consequences of a cyberattack, which seems to be somewhat similar to those of physical attacks (Iaiani et al., 2021). In many cases, there are huge losses, environmental, health and economic impacts, for example, due to data theft or loss, plant shutdowns, and so on (Boring et al., 2019; Iaiani et al., 2021). Therefore, it is generally safe to say that prevention of the attack itself is the best line of action.

A systematic review by Iaiani et al. (2021) shows that the attacks in such facilities, which can either be premeditated (internal or external) or accidental (internal attacks), are usually targeted at not only the information technology (IT) system but also the operational technologies from the physical plant systems to higher level management devices. For example, in their review, it was reported that while IT systems were largely infected, the number of operational technology (OT) systems affected was higher. A key OT vulnerability for such attackers involves monitoring and supervision systems, for example, the HMI workstations in control rooms. Out of 23 OT infection attack cases reported, 12 were on the monitoring systems, while those on the control systems and the safety and alarm systems were 8 and 3, respectively.

An attack on important systems as the monitoring and control systems are vulnerabilities as it is possible to infiltrate such OT system making information unavailable as in the case of denial of service (Iaiani et al., 2021) or fills the system with wrong information on process parameter presented to the operators as in the case of man-in-the-middle attacks (Nystad et al., 2020) or where same information is presented over and over like in the replay attacks (Nystad et al., 2021). These have been some of the notable forms of attacks on the monitoring and control systems. In these situations, operators can, through their behaviour and actions, introduce vulnerabilities.

The intention of the attacker, towards operators, is to deceive and ensure poor situational awareness, leading to poor detection and errors in interpretation and response to events. Operators during these times are generally reported to have been observed to assume technical or safety issues in such cases and dire cases resorting to using procedures meant for emergency responses involving eventual plant shutdowns (Nystad et al., 2020). While IT measures are largely introduced to curb such human vulnerabilities, such as the use of passwords, single or two-factor authentication, firewalls, and other company policies etc, certain cognitive, behavioural and correct response targeted measures have been neglected (Boring et al., 2019).

Though the 'human' has been cited as a weak link because of the vulnerabilities they introduce and can become a source of premeditated internal attacks (Harper, 2023), their potential to detect, communicate, and perform further roles, as represented in Figure 1, would be advantageous for the industry. However, just like in any human-in-the-loop setup requiring operator involvement, there ought to be a combination of the right set of factors, including dynamic or traditional factors that can make operators' responses effective. For example, typical factors like the HMI, training, experience, procedures, etc and dynamic ones related to cognition (workload, situational awareness, and so on). Typically, these factors interplay with each other, especially organisational and technical factors on individual factors like behaviour, cognition, etc. There has been a mention of the practical role of factors such as situational awareness, trust in one's capability, communication, training, and procedures in supporting operators and how the combination of these factors can get the operator

to be more confident and take ownership (Nystad et al., 2020; Harper, 2023). This is better illustrated in the incidence response chart on Figure 1, where, as shown in the internal illustration, the operator could have a perception of a possible threat, but would need a combination of cognitive activities like recall from memory on training or procedures to be more confident in taking decisions and communicating effectively and would eventually require a experience or some sort of manual to effectively take actions. It is not merely a simple single factor role, but a combination of extrinsic and intrinsic factors, dynamic or static.
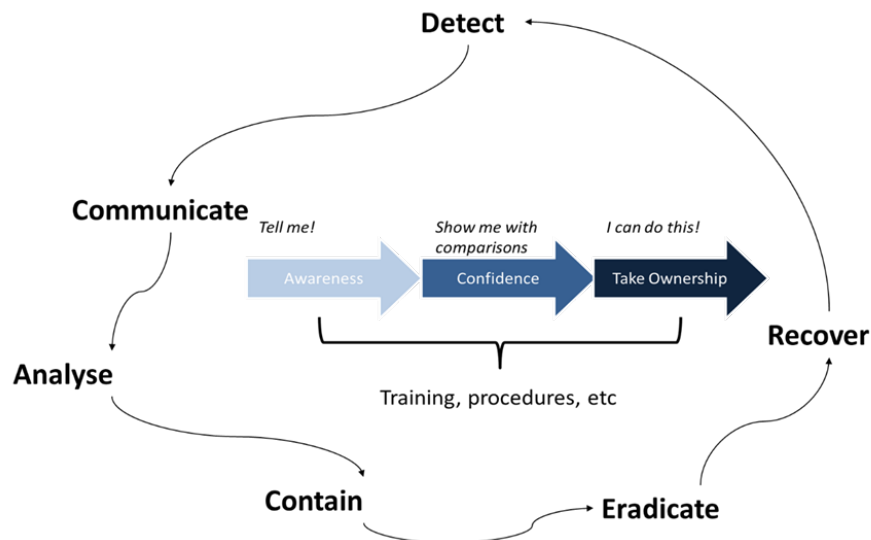
Figure 1. Incidence response flow and the role of factors like procedures, etc. Adapted and represented from Cichonski P. et al., 2012 and Harper, 2023.

Despite the need to understand how these factors put together can be of aid to operators for effective intervention and to minimise the vulnerabilities they introduce, there is little out there particularly investigating the aspect of the 'human' as a barrier in incidence response during cyber-attacks. This paper briefly discusses two current grey yet important areas in incidence response to understand operator behaviour and factors that shape this and the type of aids that should be included as standard. These areas further form key future exploration topics for exploration, design and eventual testing via an experimental and observatory approach.

2. Exploring the role of operators

The areas to be explored by the authors are briefly mapped in Figure 2 and are discussed briefly below. The top left figure shows the research areas of interest, which includes, firstly, comprehensive research on the key factors acting interchangeably and impacting particularly when operators are included as actors and involved in any of the roles mentioned in Figure 1. The idea is to address questions such as the role of such factors in influencing cognition, behaviour and eventually success, which factors stand out in each of the 6-incidence response roles, and so on. Secondly, an exploration of a couple of operator aids augmented on the interface displays, procedures, or independent aids to facilitate support at different stages, as shown in figure 1, but also to support training and learning on cyber-attacks. It seeks to address the questions of the suitability of current displays, display elements and procedures for intervention in cyber events, the type of elements, tools or agents that can facilitate teaming for detection, communication, analysis and so on.

Figure 2.

The actors, cybersecurity, have been added because, in some facilities, these persons are present and usually communicate events with the control room operators and vice versa. According to Nystad et al. (2020), in the situation of cyber-attacks, both control room operators and cyber/IT security teams are to maintain communication and possibl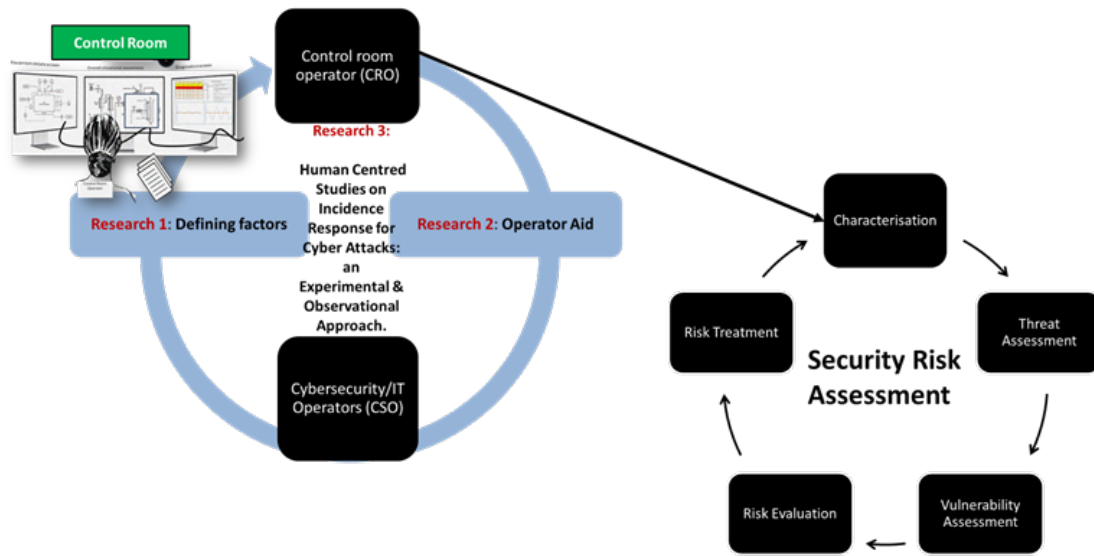y have a similar display overview of what is happening, resolution actions, etc. The bottom right loop shows the different stages of the security risk assessment of the API RP 780 methodology. The idea of mapping the two is to show that this research work eventually explores security risk assessment but factors in an important yet unexplored area in security risk assessment of process industries, which is the operator reliability.

2.1 Defining Factors

The need for understanding key behaviour and performance-shaping factors in cyber-attack scenarios has already been established in the introductory section of this paper. Some factors highlighted so far from the reviewed literature to the best of the authors' knowledge, are quite common in the control room setting, for example, experience, training, procedures, etc. (Nystad et al., 2020; Harper, 2023). There are some others that, though commonly mentioned, are not very much included in many of the pre-defined factors for human reliability assessment, for example, communication, which is very paramount between cyber and control room operators as investigated by (Nystad et al., 2020). In addition, some factors have been identified as peculiar, especially for such scenarios such as Confusion, Trust in the HMI display elements as observed by Nystad et al. (2020), and Trust and Confidence in one's ability to intervene as highlighted by Harper (2023). The inner picture in Figure 1 depicts the role of confidence in launching operators to the point of action, which can be supported by factors like procedures, training, and so on.

A nuclear control room experimental study by Nystad et al. (2020) comes in handy to illustrate further the role of factors and perhaps aids in such settings. It was observed from their study that despite the experience of turbine operators, the operators assumed the events to be due to instrumentation failure until further communication with the cyber-IT team. Feedback from the cyber team, however, made them lose trust in the instrumentation and control (I&C's) on the HMI. Typically, the attacker took the man-in-the-middle approach in this study. There was no situational awareness, which, according to the authors, would not have been the case with proper training accompanied by response procedures, which should not be used independently of one another. Therefore, the following points and questions should be needfully explored regarding the defining factor in cyber-attack scenarios:

> ➢ What factors are defining factors in such human-in-the-loop configurations? The concept of human-in-the-loop in process control rooms has been explained by Amazu et al. (2022).
> ➢ How can some of these less commonly mentioned factors be measured and included in the eventual evaluation of operator response capability?
> ➢ What role does the interplay between these factors play in shaping behaviour and successful incidence response?
> ➢ How can these factors harness or drive the development of operator aids?

2.2 Operator Aids

The most common aids or decision and action support aids in control rooms are the human system interfaces comprising the interface and their display and display elements, procedures and alarm systems (Amazu et al., 2024). However, there are new AI support introductions mentioned or already tested to explore their capabilities in aiding operators at different points of their tasks. For example, use of adaptive interfaces (Hinss et al., 2022), AI recommendation system (Mietkiewicz et al., 2023), virtual reality sets (Roldán et al., 2017), presentation of playbacks or timelines of events with bookmarks (Scott et al., 2006), and temporal image/object presentation and removal (Peysakhovich et al., 2018). The last three have been specifically cited to be effective in increasing situational awareness and interruption recovery.

Situational awareness (SA) can be enhanced through experience or expertise, as this leads to greater activation of long-term memory — particularly procedural and semantic memory. However, for beginners, it is often more effective to provide support for their working memory (Sohn and Doane, 2004). Regular simulation-based training can also play a key role by allowing operators to practice tasks that may not occur frequently but must remain readily accessible in their working memory. A comparable example can be found in aviation, where pilots undergo routine simulations to reinforce emergency procedures and ensure quick, accurate recall when needed. Again, the above examples reinforce training, experience and procedures for situational awareness. How about the capability of these aids or potential aids to minimize confusion or reinforce confidence? Therefore, in developing aids, it is important to understand the defining factors with some of these very common aids already a part of them. It is also vital to propose aids that target experienced versus novice operators. Despite the mention of aids that can come in the form of elements embedded on the HMI, procedures, training tools, etc, there is not a lot out there on the development of such for incidence response with the operators in mind.

The authors, through further research, explore the following points relating to operator aids during cyber attacks

What type of elements and tools can be adapted on the HSI or asides the HMI to aid operators?

What should the eventual outlook of training, procedures and other human system interfaces be?

How do these aids address negative tipping points from the defining factors influencing economy, health, and safety?

What are the pros and cons of potential teaming agents or other support agents in such scenarios?

2.3 Human Centered Studies

Improving how operators respond during cyber incidents starts with understanding their actual experiences, not just what systems expect of them. The way people act in high-pressure situations, especially when dealing with unfamiliar problems or incomplete information, often depends on more than just training or procedures. The way operators respond often comes down to how tools are laid out, what kind of information is actually visible to them, and whether they feel confident enough to make a quick call under pressure.

Because of that, this study keeps the focus on the people who are using the systems. Instead of assuming what might work in theory, it looks at how operators behave in real situations: what they notice, how they react, and where things get difficult. Their input is not just helpful; it is necessary to build anything that will truly work in practice. Their insights help shape the direction of any improvements, ensuring that solutions are actually practical and not just theoretical.

The goal is to identify which factors really matter when it comes to operator performance during cyber-attacks: things like confidence, trust in displays, or even confusion. It's one thing to notice when things don't go as planned, but the harder part is figuring out what helps operators make good decisions under pressure. That is where the real value is — understanding what gets in their way and what genuinely supports them in the moment.

This is not something that can be worked out just by looking at data from a distance. That is why the approach here involves watching people in action: how they respond, what they miss, where they hesitate. What is good or bad behaviour and how can this be guided? It is about learning from the way both new and experienced operators deal with realistic situations, not just ideal ones. It brings in operators with different backgrounds—from those just starting to others with years of experience. Watching how they handle different scenarios gives a clearer picture of what works, what confuses them, and where extra support might be needed.

At the core, it is about designing systems that actually fit the way people think and work. Operators are a critical line of defense. But to do that job well, they need tools and training that make sense in the moment, not just on paper.

2.3.1 Future Experiments

The SERICS project, through a human centred observational and experimental study, aims to investigate operators' behaviour and decision-support potentials for correct incidence response during cyber-attacks. To address the posed questions in this work, the experimental design will involve different human in the loop configurations that:

follows a similar process industry case study as previously applied by Amazu et al. (2024). This will comprise scenarios of easy to high complexity levels driven, in this case, by both process and cyber-attack complexity. The varying of task complexity serves two purposes: 1. to evaluate operators' states: cognition, behaviour, readiness, etc, and tipping points for targeted support, 2.   t   o evaluates the impact of the type of support during different cyber situations.

will be shaped by a couple of the identified defining independent factors, especially decision-support factors/aids like training and procedures. Training will be defined at different levels of training aids – videos, manuals, serious games, etc, while procedures will be paper, digital and in different procedure formats – listed or flow charts.

3. Conclusion

The potential of operators as preventive and protective barriers is often overlooked, especially during cyber-attacks. Rather, much attention is placed on technical defences.

This paper outlined key areas where further research is needed: identifying the factors that shape operator behaviour and successful response in high-stress cyber scenarios and developing aids that genuinely support them in making timely, informed decisions and taking correct actions. Aids that are well-designed and based on how people behave can make a meaningful difference in reducing risk.

By taking a human-centred approach and involving operators directly in the development, design and testing of these tools, this work aims to shift the narrative from seeing the human as a weak link to recognising them as an active line of defence.

Acknowledgments

References

Amazu, C. W., & Demichela, M., Fissore, D., 2022. Human-in-the-Loop Configurations in Process and Energy Industries; A Systematic Review. 3234-3241. 10.3850/978-981-18-5183-4_S33-04-572.

Amazu, C. W., Mietkiewicz, J., Abbas, A. N., Briwa, H., Alonso-Perez, A., Baldissone, G., Fissore, D., Demichela, M., Leva, M. C., 2024. Exploring the Influence of Human System Interfaces: Introducing Support

Tools and an Experimental Study. International Journal of Human–Computer Interaction, 1–18. https://doi.org/10.1080/10447318.2024.2376354

Boring, R., Ulrich, T., Medema, H., Lew, R., 2019. Operator Resilience to Cyber Interdictions in Nuclear Power Plants. 247-251. 10.1109/RWS47064.2019.8971820.

Cichonski, P., Millar, T., Grance, T., & Scarfone, K., 2012. Computer Security Incident Handling Guide : Recommendations of the National Institute of Standards and Technology. https://doi.org/10.6028/nist.sp.800-61r2

Harper, W., 2023. Cybersecurity: a review of human-based behavior and best practices to mitigate risk. Issues in Information Systems, 24(4), 247–254. https://doi.org/10.48009/4_iis_2023_119

Hinss, M. F., Brock, A. M., Roy, R. N., 2022. Cognitive effects of prolonged continuous human-machine interaction: The case for mental state-based adaptive interfaces. Frontiers in neuroergonomics, 3, 935092. https://doi.org/10.3389/fnrgo.2022.935092

Iaiani, M., Tugnoli, A., Bonvicini, S., Cozzani, V., 2021. Analysis of Cybersecurity-related Incidents in the Process Industry. Reliability Engineering & System Safety. 209. 107485. 10.1016/j.ress.2021.107485.

Mietkiewicz, J., Abbas, A. N., Amazu, C. W., Baldissone, G., Madsen, A. L., Demichela, M., & Leva, M. C., 2024. Enhancing Control Room Operator Decision Making. Processes, 12(2), 328. https://doi.org/10.3390/pr12020328

Nystad, E., Katta, V., Simensen, J., 2020. What happens in a control room during a cybersecurity attack?: Preliminary observations from a pilot study. 10.1145/3387940.3391454.

Nystad, E., Simensen, J., Raspotnig, C., 2022. Investigating operative cybersecurity awareness in air traffic control. 10.1109/SIN54109.2021.9699158.

Peysakhovich, V., Lefrançois, O., Dehais, F., and Causse, M., 2018. The neuroergonomics of aircraft cockpits: the four stages of eye-tracking integration to enhance flight safety. Safety 4, 8. doi: 10.3390/safety4010008

Roldán, J. J., Peña-Tapia, E., Martín-Barrio, A., Olivares-Méndez, M. A., Del Cerro, J., and Barrientos, A., 2017. Multi-robot interfaces and operator situational awareness: study of the impact of immersion and prediction. Sensors 17, 1720. doi: 10.3390/s17081720

Scott, S. D., Mercier, S., Cummings, M. L., and Wang, E., 2006. Assisting interruption recovery in supervisory control of multiple uavs. Proc. Hum. Factors Ergon. Soc. Ann. Meet. 50, 699–703. doi: 10.1177/154193120605000518

Sohn, Y. W., Doane, S. M., 2004. Memory Processes of Flight Situation Awareness: Interactive Roles of Working Memory Capacity, Long-Term Working Memory, and Expertise. Human Factors, 46(3), 461-475. https://doi.org/10.1518/hfes.46.3.461.50392

Machine Learning for Efficient CFD-based Quantitative Risk Analysis: Progress and Practical Insights

Muchen Zhang, Pascale Vacca, Eulàlia Planas*

Centre for Technological Risk Studies (CERTEC), Universitat Politècnica de Catalunya · Barcelona Tech, Barcelona East School of Engineering (EEBE). Avinguda Eduard Maristany, 16, 08019 Barcelona, Spain

* eulalia.planas@upc.edu

1. Introduction

In chemical process industry, the presence of large quantities of hazardous materials necessitates quantitative risk assessment (QRA) as a powerful tool for reducing risks. QRA is a systematic approach to evaluate risk levels, probabilities, and consequences of hazardous events in complex technological systems (Arora et al., 2021). Over the decades, regulatory bodies worldwide have established many QRA standards and guidelines (American Institute of Chemical Engineers, 2007; Health and Safety Executive (HSE), 2001; European Union Directive, 2012; API, 2016), providing frameworks to systematically evaluate and mitigate risks from hazardous processes. As pointed out by Apostolakis (2004), QRA is not simply about "getting the number right", it is the impact on decision-making that matters. In order to understand how the system can fail and to prevent such events, both academia and industry are actively developing new methodologies and tools to enhance the robustness of QRA.

A key component of QRA is analysing the consequences of accidents such as fires, explosions, and hazardous substances releases, which can provide high level of confidence in results and robust justification for risk-based decision making, if done adequately (UNECE, 2023). Traditionally, consequence analysis methods often rely on integral models, which are usually fast and easy-to-implement, but may often oversimplify the physics of complex scenarios (Mannan, 2012; Pappalardo et al., 2021). This limitation has driven the increasing use of computational fluid dynamics (CFD) in modelling accident effects in these cases.

In recent years, advancements in high-performance computing have significantly enhanced the feasibility of deploying CFD for consequence analysis in geometrically complex industrial environments (Runchal and Rao, 2020). Shen et al. (2020) systematically reviewed the application of CFD in consequence analysis for the process industries, demonstrating its implementation in fire, explosion, and hazardous material dispersion modelling with improved predictive capabilities compared to traditional methods. However, the time-consuming nature of CFD persists as a critical barrier to its widespread adoption in QRAs.

Recent advances in machine learning (ML) offer strategies to mitigate the computational burden of CFD, this integration can enhance CFD through accelerating direct numerical simulations (DNS), improving turbulence models, and developing reduced-order models (ROM) (Vinuesa and Brunton, 2022). Existing reviews have explored ML's role in enhancing CFD (Caron et al., 2025; Panchigar et al., 2022; Rahman et al., 2024) and its adaptability across various domains of safety and reliability (Tamascelli et al., 2024). Nonetheless, the

specific use of ML-accelerated CFD in the context of QRA –especially in complex industrial settings– has not been thoroughly examined.

This extended abstract reviews diverse strategies for integrating ML with CFD to enhance QRA in process industry, with a focus on recent progress in balancing the efficiency and accuracy regarding the consequence modelling in complex environments. To address the importance of introducing ML into this framework, challenges and current practices regarding the use of CFD in QRA are discussed based on results from an online survey presented in Section 2. ML's ability to streamline CFD processes for QRA is analysed and compared in detail through a literature review in Section 3. Finally, conclusions and future research trends are given in Section 4.

2. Challenges in CFD-based QRA

While the role of CFD tools in consequence analysis is very clear, their contribution in the entire QRA framework is less addressed in the literature. In fact, CFD tools are much more computationally expensive than those simplified integral models, thus limiting the practical application in QRAs (Patel et al., 2024). To better understand the practical application of CFD in QRA, the authors conducted an anonymous survey examining the stages, scenarios, and conditions under which CFD is utilized, as well as the challenges faced in its application.
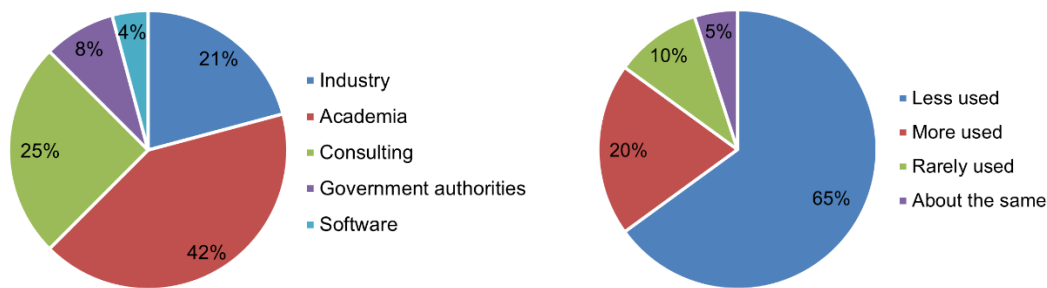
(a) Work fields of the participants.

(b) Frequency of using CFD compared to other models during QRAs.
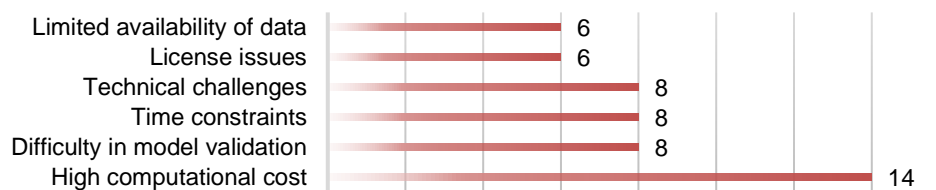
(c) Key challenges in using CFD for QRA.
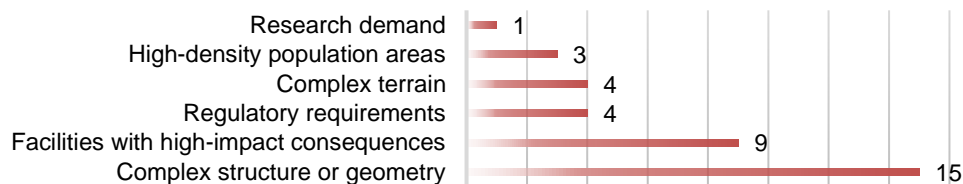
(d) Conditions for choosing CFD over simpler models.

Figure 1: Survey results.

The survey was publicized through two main channels: direct emails were sent to domain experts and colleagues with relevant experience in risk assessment and CFD, and the survey was also shared publicly via LinkedIn posts to engage a broader professional audience involved in safety engineering, process design, and regulatory bodies. A total of 24 responses were collected, of which 20 participants had either directly used CFD or observed its use in QRA projects. As shown in Figure 1 (a), the majority of respondents (42%) identified as working in academia, while the rest were from industry or regulatory bodies, reflecting a diverse perspective on CFD practices across sectors. The survey revealed that most participants (75%) believe CFD is used less frequently than simpler models in QRA workflows, as illustrated in Figure 1 (b). This was attributed primarily to high computational cost, technical complexity, tight project timelines, and the difficulty of model validation (Figure 1 (c)). The reason for respondents to choose CFD over simpler models, as shown in Figure 1 (d), is primarily due to the presence of complex geometries, high-consequence scenarios, or regulatory requirements. These findings are consistent with observations in the literature, where the benefits of CFD in terms of accuracy and detail are often constrained by practical usability and resource limitations, thus hindering its broader adoption. Other insights from the survey include preferred CFD software tools, such as ANSYS Fluent, FLACS, and FDS, and the typical project phases where CFD is applied – most commonly during detailed design or post–incident analysis. Respondents also shared the specific types of risk scenarios modelled using CFD through a multiple-choice question, with fire (70%), explosion (65%), and gas dispersion (55%) being the most frequent applications.

The survey results, aligned with existing literature (Patel et al., 2024; Shen et al., 2020), highlight key barriers of using CFD in QRA. Most notably the high computational cost, the ease of use and validation challenges significantly restrict the routine application of CFD in the QRA. In order to adress these issues, the next section reviews how ML techniques are being integrated with CFD to overcome these specific barriers.

3. ML-CFD integration strategies for efficient QRA

This section presents a purpose-driven overview of how ML has been integrated with CFD to improve its applicability in QRA. Recent research efforts are grouped into three main purposes that reflect the needs of QRA practice: 1) surrogate modelling and acceleration, 2) parameter and model calibration, and 3) real-time prediction. Some relevant areas of each category are listed in Table 1. Despite some overlaps, note that the technical implementation of ML algorithms is beyond the scope of this work, as the structure aims to reflect practical utility in risk assessment.

Table 1: Relevant areas of ML-CFD integration strategies for QRA.

Surrogate modelling and acceleration	Parameter and model calibration	Real-time prediction
Reduced-order models	ML-enhanced turbulence closures	Digital twins
Regression-based surrogates	Uncertainty quantification	Sensor-data integration
Dimensionality reduction	Bayesian parameter optimization	Physics-informed neural
Physics-informed surrogate models	Data assimilation for model refinement	networks (PINNs)

3.1 Surrogate modelling and acceleration

To make CFD more feasible within risk-based frameworks, many recent studies have focused on constructing surrogate models that approximate high-fidelity simulations at a fraction of the cost. Early works (Loy et al., 2017, 2018) demonstrated the potential of support vector machines and interpolation-based models to estimate net radiation flux from LNG pool fires, enabling faster consequence assessments in facility design and siting.

Similar surrogate strategies have been adopted in explosion modelling. For example, Jung and Shin (2024) trained an XGBoost model on FLACS simulation data to predict overpressures from hydrogen leaks, showing excellent accuracy and speed suitable for scenario screening in QRA.

More advanced approaches integrate dimensionality reduction and deep learning. Burela et al. (2025) combined POD-based (Proper Orthogonal Decomposition) reduction with neural networks to simulate wildfire spread, achieving near-instant front prediction, offering promising solutions for the consequence analysis of Natech (Natural Hazard Triggering Technological Accidents) scenarios. Kashefi et al. (2021) developed a novel point-cloud deep learning approach that directly predicts flow fields around complex geometries by processing unstructured mesh vertices, enabling accurate predictions for unseen shapes while maintaining physical conservation laws. Abrate et al. (2023) proposed a bootstrapped POD-RBF (Radial Basis Function) model for offshore gas releases, cutting simulation time by orders of magnitude with minimal error. Meanwhile, Usman et al. (2021) applied deep learning to accelerate large-eddy simulations of atmospheric dispersion, achieving fast and generalizable plume predictions across different source terms and conditions.

In parallel, physics-informed neural networks (PINNs) have emerged as an alternative way to build surrogates that embed governing equations directly into the training process. Comparing to conventional data-driven approaches, PINNs are especially effective for inverse problems and data-scarce scenarios where traditional supervised learning struggles (Wong et al., 2021). Several studies highlight their potential: PINNs have shown up to 25% improvement in accuracy over data-driven approaches (Donnelly et al., 2024), achieved speedups of up to fivefold compared to conventional CFD solvers (Ang and Ng, 2022), and even reduced computational effort by a factor of eight (Sousa et al., 2024). Studies by Wang et al. (2021) and Fernández et al. (2023) further illustrate their potential as lightweight, generalizable CFD surrogates, while limitations such as training instability and accuracy degradation still exist. As surrogate modelling techniques continue to evolve, combining data-driven learning with physical constraints and uncertainty estimation will be key in fluid dynamics simulations and risk analysis.

3.2 Parameter and model calibration

Turbulence modelling remains one of the most challenging aspects of CFD, particularly in the context of Reynolds-Averaged Navier–Stokes (RANS) and Large Eddy Simulation (LES) approaches (Vinuesa and Brunton, 2022). The integration of ML and turbulence modelling has shown the potential in overcoming the limitations of conventional closure models. Instead of relying solely on empirical coefficients or fixed eddy-viscosity formulations, recent studies have explored learning turbulence behavior directly from high-fidelity data. For instance, Maulik et al. (2021) developed surrogate models for turbulent eddy viscosity in RANS, enabling steady-state solutions by accelerating convergence by a factor of 5. While Ling et al. (2016) introduced a tensor-basis neural network (TBNN) to model Reynolds stress in a way that respects physical invariances. These approaches enhance the expressiveness of RANS models, especially in flow regions where traditional closures fail. The PINN-based frameworks proposed by Zhou et al. (2024) and Jang et al. (2024) further offer flexible alternatives by embedding the governing equations directly into the training process, bypassing the need for explicit turbulence models in certain scenarios. Uncertainty quantification and model calibration are also gaining attention, particularly through Bayesian methods. Maruyama et al. (2021) used Bayesian inference to infer turbulence model coefficients and quantify uncertainty using limited experimental data, demonstrating improved prediction and reliability for CFD applications. Similarly, Both et al. (2019) proposed a surrogate-assisted Bayesian optimization approach to calibrate model parameters using explosion test data. For system-level modeling, Berghe et al. (2023)

proposed a machine learning framework to calibrate parameters in reduced-order ejector models by combining data-driven and physics-integrated approaches These techniques not only improve model fidelity but also help quantify the confidence bounds of predictions, providing valuable inputs for risk assessment frameworks.

These above-mentioned studies show that ML-enhanced parameter and model calibration have potential to make CFD more accurate, adaptive, and uncertainty-aware —three qualities that are essential for advancing consequence modeling and scenario analysis in QRA. Future work will need to further explore model transferability, hybrid learning strategies, and the integration of real-time data for continuous model refinement.

3.3 Real-time prediction

The demand for real-time consequence assessment in dynamic risk scenarios has driven increasing interest in integrating machine learning with CFD for fast and adaptive predictions. Digital Twins represent a new paradigm in computational modelling, where ML is used to expand CFD simulation databases for rapid response across a wide range of operational conditions. This hybrid physics-informed and data-driven approach, termed simulation digital twin (SDT), enables real-time prediction and decision support (Molinaro et al., 2021). Thomas et al. (2021) developed accelerated digital twins using lattice Boltzmann algorithms and graphics card-based computing to predict real-time fluid mechanics in mixing tanks, providing insights into stratified two-fluid mixing processes.

Another emerging research focus is sensor-driven integration, which connects physical systems with computational models to enhance real-time monitoring and predictive capabilities. Kim et al. (2019) combined long short-term memory recurrent neural network （LSTM-RNN) with CFD simulations to accurately localize hazardous material leaks in chemical plants using sparse sensor inputs, by training on CFD-generated datasets. Similarly, Li et al. (2024) developed a deep probabilistic learning model for real-time hydrogen dispersion prediction, emphasizing uncertainty estimation and boundary accuracy, which could support future digital twin implementations for emergency management. Also focused on real-time hydrogen leak monitoring at hydrogen refueling stations (HRS), Wang et al. (2024) proposed another regression model based on temporal convolutional networks (TCN) and multimodal sensor fusion, by integrating wind and concentration data, it outperforms conventional models like LSTM, offering guidance for sensor layout and provide a reliable real-time solution for large-scale HRS safety monitoring.

Besides the widely adoption of PINNs in surrogate modelling and parameter calibration, in the comprehensive survey on ML for CFD (H. Wang et al., 2024), PINNs are also highlighted as a key methodology for solving inverse problems while maintaining physical consistency. For example, Shi et al. (2023) integrated variational Bayesian inference with deep learning to predict spatial explosion overpressures in offshore platforms, achieving real-time accuracy (R^2 = 0.955) by combining sparse sensor data with physics-based constraints. These integrations enable rapid and reliable risk assessment such as flammable gas leaks and explosions, thus allowing real-time decision-making with improved efficiency.

4. Conclusions

This review summarized the current state of integrating ML techniques with CFD for enhancing QRA in process industry. Focusing on three application-driven categories: surrogate modelling and acceleration, parameter and model calibration, and real-time prediction, we identified representative studies, categorized typical ML approaches, and discussed their relevance to key QRA challenges such as simulation cost, model uncertainty, and decision-making speed.

It is found that methods such as surrogate modelling and parameter optimization show promise in balancing computational efficiency and predictive rigor, meanwhile ML-facilitated real-time prediction can provide valuable insights for dynamic risk assessment. Despite its potential, the integration of ML and CFD in QRA still faces challenges such as insufficient high-quality training data, compatibility issues across software tools, and the case-specific nature in terms of complex environments. Future research trends include establishing shared CFD databases, exploring real-time risk assessment frameworks and promoting industry standards to ensure the reliability of ML-CFD in QRA.

Acknowledgments

References

Abrate, N., Moscatello, A., Ledda, G., Pedroni, N., Carbone, F., Maffia, E., Carpignano, A., 2023. A novel approach combining bootstrapped non-intrusive reduced order models and unscented transform for the robust and efficient CFD analysis of accidental gas releases in congested plants. J. Loss Prev. Process Ind. 83, 105015. https://doi.org/10.1016/j.jlp.2023.105015

American Institute of Chemical Engineers (Ed.), 2007. Guidelines for risk-based process safety, CCPS Guidelines series. Wiley-Interscience, Hoboken, N.J. https://doi.org/10.1002/9780470925119

Ang, E., Ng, B.F., 2022. Physics-Informed Neural Networks for Flow Around Airfoil, in: AIAA SCITECH 2022 Forum. Presented at the AIAA SCITECH 2022 Forum, American Institute of Aeronautics and Astronautics, San Diego, CA & Virtual. https://doi.org/10.2514/6.2022-0187

API, 2016. API 581: risk-based inspection methodology. American Petroleum Institute.

Apostolakis, G.E., 2004. How Useful Is Quantitative Risk Assessment? Risk Anal. 24, 515–520. https://doi.org/10.1111/j.0272-4332.2004.00455.x

Arora, A.S., Changotra, R., Rajput, H., 2021. An Overview to Quantitative Risk Assessment Methodologies, in: Bow Ties in Process Safety and Environmental Management. CRC Press, Boca Raton, pp. 211–218. https://doi.org/10.1201/9781003140382-12

Both, A.-L., Hisken, H., Rückmann, J.-J., Steihaug, T., 2019. Surrogate-based model parameter optimization based on gas explosion experimental data. Eng. Optim. 51, 301–316. https://doi.org/10.1080/0305215X.2018.1450399

Burela, S., Krah, P., Reiss, J., 2025. Parametric model order reduction for a wildland fire model via the shifted POD-based deep learning method. Adv. Comput. Math. 51, 1–43. https://doi.org/10.1007/s10444-025-10220-4

Caron, C., Lauret, P., Bastide, A., 2025. Machine Learning to speed up Computational Fluid Dynamics engineering simulations for built environments: A review. Build. Environ. 267, 112229. https://doi.org/10.1016/j.buildenv.2024.112229

Donnelly, J., Daneshkhah, A., Abolfathi, S., 2024. Physics-informed neural networks as surrogate models of hydrodynamic simulators. Sci. Total Environ. 912, 168814. https://doi.org/10.1016/j.scitotenv.2023.168814

European Union Directive, 2012. Seveso III Directive 2012/18/EU, on the control of major-accident hazards involving dangerous substances.

Fernández De La Mata, F., Gijón, A., Molina-Solana, M., Gómez-Romero, J., 2023. Physics-informed neural networks for data-driven simulation: Advantages, limitations, and opportunities. Phys. Stat. Mech. Its Appl. 610, 128415. https://doi.org/10.1016/j.physa.2022.128415

Health and Safety Executive (HSE), 2001. ALARP. HSE Books, Sudbury.

Jang, S., Jadidi, M., Mahmoudi, Y., 2024. Physics Informed Neural Network in Turbulent Porous Flow: Pore-scale Flow Reconstruction. Presented at the the 9th World Congress on Momentum, Heat and Mass Transfer. https://doi.org/10.11159/icmfht24.122

Jung, Y.M., Shin, D., 2024. CFD Simulation and Machine Learning Surrogate Modeling for Consequence and Risk Assessment of Leakage, Dispersion, Fire, and Explosion of FCEV Hydrogen Storage Tanks, in: 2024 Spring Meeting and 20th Global Congress on Process Safety.

Kashefi, A., Rempe, D., Guibas, L.J., 2021. A Point-Cloud Deep Learning Framework for Prediction of Fluid Flow Fields on Irregular Geometries. Phys. Fluids 33, 027104. https://doi.org/10.1063/5.0033376

Kim, H., Park, M., Kim, C.W., Shin, D., 2019. Source localization for hazardous material release in an outdoor chemical plant via a combination of LSTM-RNN and CFD simulation. Comput. Chem. Eng. 125, 476–489. https://doi.org/10.1016/j.compchemeng.2019.03.012

Li, J., Xie, W., Li, H., Qian, X., Shi, J., Xie, Z., Wang, Q., Zhang, X., Chen, G., 2024. Real-time hydrogen release and dispersion modelling of hydrogen refuelling station by using deep learning probability approach. Int. J. Hydrog. Energy 51, 794–806. https://doi.org/10.1016/j.ijhydene.2023.04.126

Ling, J., Kurzawski, A., Templeton, J., 2016. Reynolds averaged turbulence modelling using deep neural networks with embedded invariance. J. Fluid Mech. 807, 155–166. https://doi.org/10.1017/jfm.2016.615

Loy, Y.Y., Rangaiah, G.P., Lakshminarayanan, S., 2017. Surrogate modelling for enhancing consequence analysis based on computational fluid dynamics. J. Loss Prev. Process Ind. 48, 173–185. https://doi.org/10.1016/j.jlp.2017.04.027

Loy, Y.Y., Rangaiah, G.P., S., L., 2018. Surrogate modelling of net radiation flux from pool fires in a hydrocarbon storage facility. Process Saf. Environ. Prot. 114, 296–309. https://doi.org/10.1016/j.psep.2017.12.024

Mannan, S. (Ed.), 2012. Lee's loss prevention in the process industries: hazard identification, assessment, and control, Fourth edition. ed. Elsevier Butterworth-Heinemann, Amsterdam.

Maruyama, D., Bekemeyer, P., Görtz, S., Coggon, S., Sharma, S., 2021. Data-driven Bayesian inference of turbulence model closure coefficients incorporating epistemic uncertainty. Acta Mech. Sin. 37, 1812–1838. https://doi.org/10.1007/s10409-021-01152-5

Maulik, R., Sharma, H., Patel, S., Lusch, B., Jennings, E., 2021. A turbulent eddy-viscosity surrogate modeling framework for Reynolds-averaged Navier-Stokes simulations. Comput. Fluids 227, 104777. https://doi.org/10.1016/j.compfluid.2020.104777

Molinaro, R., Singh, J.-S., Catsoulis, S., Narayanan, C., Lakehal, D., 2021. Embedding data analytics and CFD into the digital twin concept. Comput. Fluids 214, 104759. https://doi.org/10.1016/j.compfluid.2020.104759

Panchigar, D., Kar, K., Shukla, S., Mathew, R.M., Chadha, U., Selvaraj, S.K., 2022. Machine learning-based CFD simulations: a review, models, open threats, and future tactics. Neural Comput. Appl. 34, 21677–21700. https://doi.org/10.1007/s00521-022-07838-6

Pappalardo, F., Moscatello, A., Ledda, G., Uggenti, A.C., Gerboni, R., Carpignano, A., Di Maio, F., Mereu, R., Zio, E., 2021. Quantification of Uncertainty in CFD Simulation of Accidental Gas Release for O & G Quantitative Risk Assessment. Energies 14, 8117. https://doi.org/10.3390/en14238117

Patel, P., Garaniya, V., Baalisampang, T., Arzaghi, E., Abbassi, R., Salehi, F., 2024. A technical review on quantitative risk analysis for hydrogen infrastructure. J. Loss Prev. Process Ind. 91, 105403. https://doi.org/10.1016/j.jlp.2024.105403

Rahman, M.S., Hazra, S., Chowdhury, I.A., 2024. Advancing Computational Fluid Dynamics through Machine Learning: A Review of Data-Driven Innovations and Applications. J. Fluid Mech. Mech. Des. 42–51.

Runchal, A.K., Rao, M.M., 2020. CFD of the Future: Year 2025 and Beyond, in: 50 Years of CFD in Engineering Sciences. Springer, Singapore, pp. 779–795. https://doi.org/10.1007/978-981-15-2670-1_22

Shen, R., Jiao, Z., Parker, T., Sun, Y., Wang, Q., 2020. Recent application of Computational Fluid Dynamics (CFD) in process safety and loss prevention: A review. J. Loss Prev. Process Ind. 67, 104252. https://doi.org/10.1016/j.jlp.2020.104252

Shi, J., Zhang, H., Li, J., Xie, W., Zhao, W., Usmani, A.S., Chen, G., 2023. Real-time natural gas explosion modeling of offshore platforms by using deep learning probability approach. Ocean Eng. 276, 114244. https://doi.org/10.1016/j.oceaneng.2023.114244

Sousa, P., Rodrigues, C.V., Afonso, A., 2024. Enhancing CFD solver with Machine Learning techniques. Comput. Methods Appl. Mech. Eng. 429, 117133. https://doi.org/10.1016/j.cma.2024.117133

Tamascelli, N., Campari, A., Parhizkar, T., Paltrinieri, N., 2024. Artificial Intelligence for safety and reliability: A descriptive, bibliometric and interpretative review on machine learning. J. Loss Prev. Process Ind. 90, 105343. https://doi.org/10.1016/j.jlp.2024.105343

Thomas, J., Sinha, K., Shivkumar, G., Cao, L., Funck, M., Shang, S., Nere, N.K., 2021. A CFD Digital Twin to Understand Miscible Fluid Blending. AAPS PharmSciTech 22, 91. https://doi.org/10.1208/s12249-021-01972-5

UNECE, 2023. Risk assessment for industrial accident prevention: an overview of risk assessment methods, selected case studies and available software. United Nations, Geneva.

Usman, A., Rafiq, M., Saeed, M., Nauman, A., Almqvist, A., Liwicki, M., 2021. Machine Learning Computational Fluid Dynamics, in: 2021 Swedish Artificial Intelligence Society Workshop (SAIS). Presented at the 2021

Swedish Artificial Intelligence Society Workshop (SAIS), IEEE, Sweden, pp. 1–4. https://doi.org/10.1109/SAIS53221.2021.9483997

Van Den Berghe, J., Vemula, J.B., Bartosiewicz, Y., Mendez, M.A., 2023. A Machine Learning-Based Calibration of a 1D Ejector Model from CFD, in: 36th International Conference on Efficiency, Cost, Optimization, Simulation and Environmental Impact of Energy Systems (ECOS 2023). Presented at the 36th International Conference on Efficiency, Cost, Optimization, Simulation and Environmental Impact of Energy Systems (ECOS 2023), ECOS 2023, Las Palmas De Gran Canaria, Spain, pp. 424–435. https://doi.org/10.52202/069564-0039

Vinuesa, R., Brunton, S.L., 2022. Enhancing computational fluid dynamics with machine learning. Nat. Comput. Sci. 2, 358–366. https://doi.org/10.1038/s43588-022-00264-7

Wang, H., Cao, Y., Huang, Z., Liu, Y., Hu, P., Luo, X., Song, Z., Zhao, W., Liu, J., Sun, J., Zhang, S., Wei, L., Wang, Y., Wu, T., Ma, Z.-M., Sun, Y., 2024. Recent Advances on Machine Learning for Computational Fluid Dynamics: A Survey. https://doi.org/10.48550/ARXIV.2408.12171

Wang, S., Bi, Y., Shi, J., Wu, Q., Zhang, C., Huang, S., Gao, W., Bi, M., 2024. Deep learning-based hydrogen leakage localization prediction considering sensor layout optimization in hydrogen refueling stations. Process Saf. Environ. Prot. 189, 549–560. https://doi.org/10.1016/j.psep.2024.06.122

Wang, S., Teng, Y., Perdikaris, P., 2021. Understanding and Mitigating Gradient Flow Pathologies in Physics-Informed Neural Networks. SIAM J. Sci. Comput. 43, A3055–A3081. https://doi.org/10.1137/20M1318043

Wong, J.C., Ooi, C., Chiu, P., Dao, M., 2021. Improved Surrogate Modeling of Fluid Dynamics with Physics-Informed Neural Networks. ArXiv.

Zhou, W., Miwa, S., Okamoto, K., 2024. Advancing fluid dynamics simulations: A comprehensive approach to optimizing physics-informed neural networks. Phys. Fluids 36. https://doi.org/10.1063/5.0180770

Surrogates for Health Aware Control Cost-to-Go

Eden Ngowi[*], Rafael de Olivera, Johannes Jäschke

Department of Chemical Engineering, Norwegian University of Science and Technology, Sem Sælandsvei 4, Trondheim, 7491, Norway

*eden.ngowi@ntnu.no

1. Introduction

Maintenance strategies have been evolving over the years from reactive (fix upon break-down) towards a predictive maintenance paradigm where one anticipates the degradation and plans operations accordingly [1].

In the recent years, prognostics and health monitoring techniques have been integrated with advanced control methods for creating automatic control systems which can be used to realize optimally the balance between maximizing instantaneous profit and prolonging the equipment's remaining useful life (RUL) [1]. Model Predictive Controllers (MPCs) have been shown to be a promising framework for achieving this trade-off. This has also been referred to as Health-Aware Control (HAC) [2].

HACs usually require an accurate degradation model to predict the system's health evolution. Moreover, the time scale difference between degradation and control dynamics is very large: the former and latter differing in orders of magnitude of weeks and minutes respectively [2]. Naively including the very long degradation time-scale of weeks and months into the model predictive controller results in optimization problems that are too large to be solved on the fast time-scale required for control [3]. Therefore, the idea of this contribution is to create a simple surrogate model that takes the long-term effects into account, and to add it as the "cost-to-go" in the short-term MPC control problem [4]. The surrogate will approximate the long-term effects of the short-term control actions and allow to solve the short-term MPC problem sufficiently fast.

A case study of a gas-lifted oil well network is used to evaluate this strategy as seen in Figure 1. Here, the optimal operation of the gas-lift choke valves is being sought to maximize profit and extend the RUL of oil production chokes undergoing sand erosion, which is typical in brown fields [5].
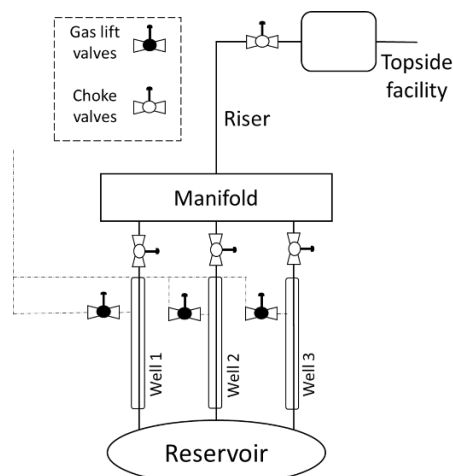

Figure 1: A Schematic Diagram of Gas-lifted Well Network [5]

This is important as most of these subsea facilities are difficult to access and require costly maintenance intervention to restore the plant back to operation after breakdown [5]. Thus, our learning-assisted MPC uses the surrogate to take into consideration the long-term degradation effects, while not substantially increasing the computational cost of solving the short-time MPC problem.

2. Methods

All simulations are done using MATLAB with CasADi add-on which contains algorithms for solving non-linear programming (NLP) problems. A surrogate model is trained to approximate the long-term effects related to degradation. This model is included as arrival cost in the short-term model predictive control problem. As such, the MPC problem remains small and easy to solve, while still taking the long-term degradation into account.

3. Results and Discussion

An online open-loop simulation by [5] can be seen in *Figure 2*. Each well has different sand rates with Well 1 and Well 3 having the highest and lowest sand rates respectively. The HAC adjusts accordingly the gas-lift rate to avoid reaching the maximum erosion limit before the next planned maintenance while simultaneously achieving the maximum possible oil production rate. However, these simulations are computationally expensive, bearing in mind the long prediction horizon of degradation processes. Surrogate models are used for speeding up the computations.
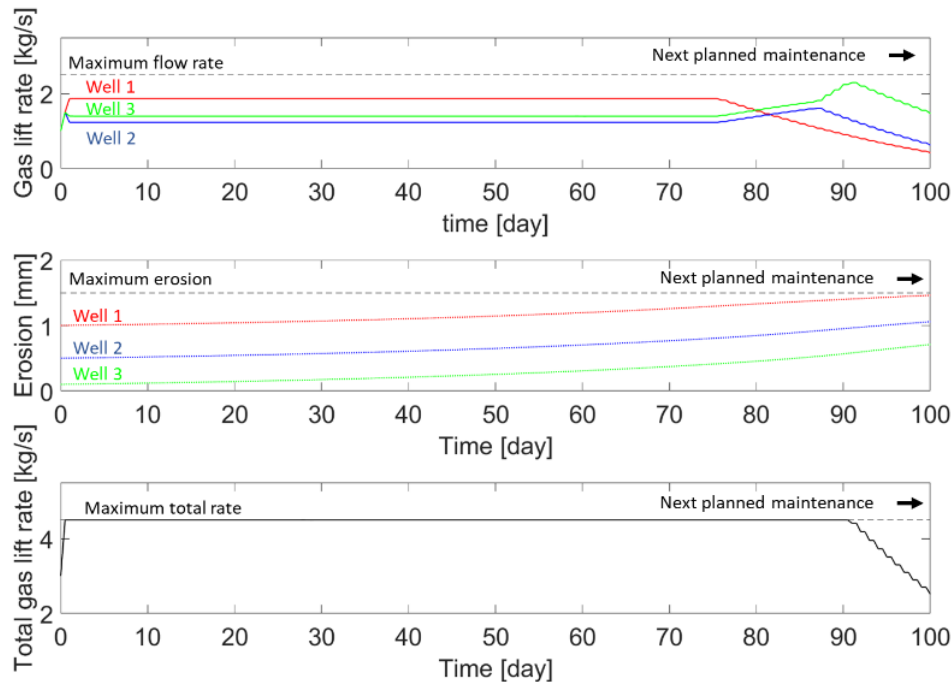
Figure 2: Online Open-loop Simulations for the Whole Gas-lift Oil Network [5].

4. Conclusions

Quicker HAC actions are being envisioned for varying prediction horizons using an offline surrogate model.
This work addresses the challenges that arise in Health-Aware Control, where the control action happens on a fast time scale, while the degradation phenomena occur on a much slower time scale.

References

Escobet, T., Puig, V., & Nejjari, F. (2012). Health aware control and model-based prognosis. In 2012 20th Mediterranean Conference on Control & Automation (MED) (pp. 691-696). IEEE.

De Oliveira, R. D.& Jäschke, J. (2024). Integration of Time Scales in Health-Aware Control. IFAC-PapersOnLine, 58(14): p. 227-227, 2024. ISSN 2405-8963. https://doi.org/10.1016/j.ifacol.2024.08.340

Abdufattokhov, S., Zanon, M., & Bemporad, A. (2021). Learning convex terminal costs for complexity reduction in MPC. In 2021 60th IEEE Conference on Decision and Control (CDC) (pp. 2163-2168). IEEE.

Turan, E. M., Mdoe, Z., & Jäschke, J. (2023). Learning a convex cost-to-go for single step model predictive control. arXiv preprint arXiv:2312.02650.

José Matias, Joachim Ågotnes, and Johannes Jäschke (2020). Health-Aware Advanced Control Applied to a Gas-Lifted Oil Well Network, IFAC-PapersOnLine, 53(3): p. 301-306. ISSN 2405-8963. https://doi.org/10.1016/j.ifacol.2020.11.048

ProSafe: Smart Integration of Process Systems Engineering & Machine Learning for Improved Process Safety

Gürkan Sin[1]*, Merlin Alvarado-Morales[1], Eulàlia Planas[2], Elsa Pastor[2], Johannes Jäschke[3], Idelfonso Nogueira[3], Miguel Muñoz[4], Çan Erkey[5], Erdal Aydin[5], Alessandra Russo[6]

[1]*Department of Chemical and Biochemical Engineering, Technical University of Denmark (DTU), 2800, Kgs. Lyngby/Denmark;*

[2]*Department of Chemical Engineering, Universitat Politecnica De Catalunya (UPC), 08034, Barcelona/Spain;*

[3]*Department of Chemical Engineering, Norwegian University of Science and Technology (NTNU), 7491, Trondheim/Norway;*

[4]*Novotec, 08193, Cerdanyola del Vallés Barcelona/Spain;*

[5]*Chemical and Biochemical Engineering Department, Koç University, 34450, Istanbul/Turkey;*
[6]*Department of Computing, Faculty of Engineering, Imperial College, SW7 2AZ, London/England*

* *gsi@kt.dtu.dk*

1. Introduction

ProSafe is a novel interdisciplinary initiative (Figure 1) aiming to make a step change and reinforce the process safety effectiveness with new methods and skills exploiting emerging digital transformation opportunities (Big Data, ML, AI) in alignment with the EU digitalization roadmap of the European manufacturing industry initiative.
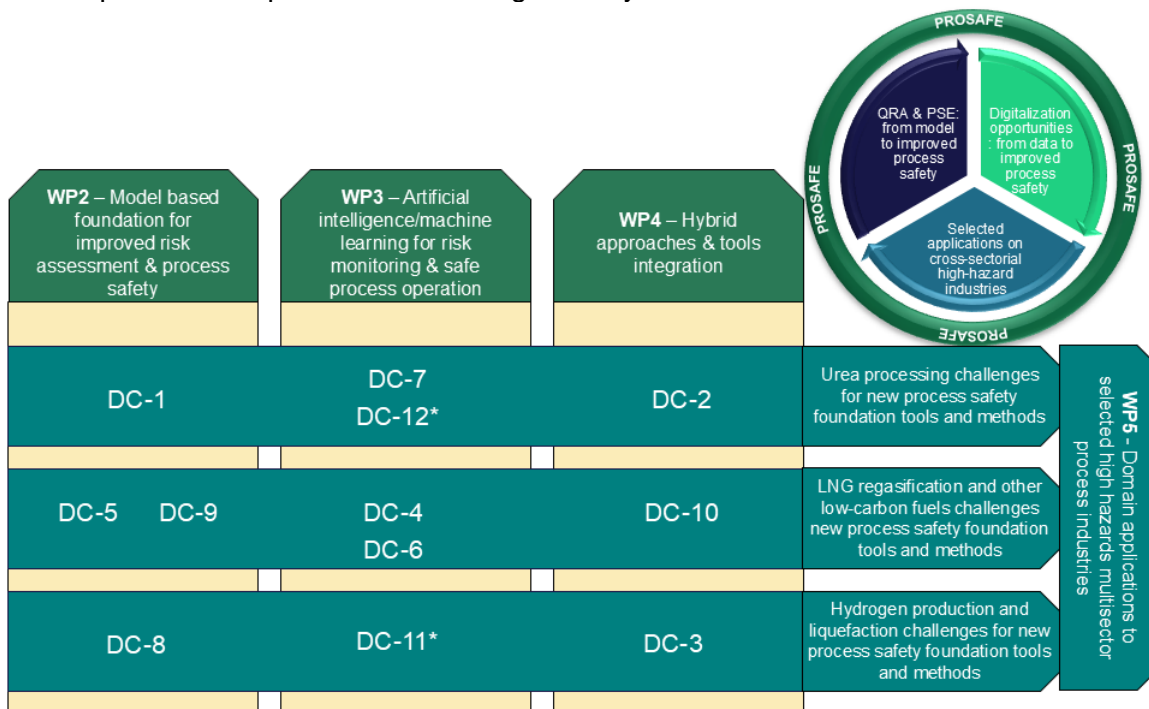

Figure 1. Integration of the doctoral candidates (DCs) into the research program.

Successful process safety enhancement in high-hazard industries calls for the development of new high-level process safety research. In this regard, the synergy between process safety, process systems engineering, machine learning, and artificial intelligence, which is usurping the new era of industry, has not yet been exploited. The underlying reasons are, among others, segregated research, and development efforts at different academic and non-academic centers in EU combined with the complexity of the problem, which makes it too big to tackle alone with a single discipline/research center. Thus, there is a strong need for a European doctoral training program bringing together complementary disciplines in research and training, which sets the motivation for ProSafe.

1.1 Project objectives

ProSafe aims to bring together a critical mass of partners with interdisciplinary expertise and competencies to undertake original research and train next-generation engineers able to combine machine learning, artificial intelligence, and process systems engineering with domain knowledge of process industry and process safety, to significantly improve safety and productivity in high hazard industries. ProSafe will pioneer new foundations by integrating Quantitative Risk Assessment (QRA), Process Systems Engineering (PSE) (model-based approach) with interpretable machine learning (ML) and artificial intelligence (AI) disciplines (data- and knowledge-based approaches) as targeted breakthroughs to achieve the objectives. Through this research and training program, ProSafe will contribute to realizing the promising potential of the new artificial intelligence paradigm with a particular focus on process safety. To this end, ProSafe will develop new synergistic tools and train skilled professionals to address this very important societal, economic, and environmental challenge of safe and sustainable process industries. In the next section the ***research objectives (RO), training objectives (TO),*** and their associated WPs (Table 3.1a) are described.

1.2 Research Objectives (RO)

- ➢ **RO1:** Harmonize robust QRA methods and implementation strategies for effective and improved risk assessment and process safety (from model to improved process risk assessment and safety; top-down approach) (WP2).
- ➢ **RO2:** Develop AI and ML (especially interpretable ML) models using domain knowledge for efficient, safe, and reliable process operations (from data to improved process, operation, and safety; bottom-up approach) (WP3)
- ➢ **RO3:** Develop synergistic integration of model-based with data-based methods for improved process safety operation and monitoring (from model & data to improved process safety; a hybrid approach) (WP4).
- ➢ **RO4:** Identify roadmap and efficient implementation strategies for AI and ML for improved process operation and safety: demonstration and validation of ProSafe novel concepts and methods (RO1, RO2, RO3) on industrial relevant case studies for safer operation (WP5).

1.3 Training Objectives (TO)

- ➢ **TO1:** Training of DCs through individual projects combining multidisciplinary competencies in AI, ML, and PSE within the domain of process safety (WP2-5).
- ➢ **TO2:** Create a new generation of multidisciplinary professionals to pioneer new process safety for the future digital industry: Recruit top candidates with a strategic blend of scientific backgrounds from engineering to AI/ML disciplines (WP1).
- ➢ **TO3:** Establish and pilot the concept of a truly interdisciplinary European multicenter training program in AI/ML, QRA, and PSE areas within the domain of safety in process industries through relevant network-wide events, courses, workshops, and on-site

industry training that complement training in soft skills for effective communication and entrepreneurship (WP6).

By realizing the ambitious training and research objectives, ProSafe is expected to have a transformative impact on the larger sector of European process industries and reinforce their competitiveness thanks to timely alignment with the broader transformation of European process industries under the Industry 4.0 trend.

1.4 ProSafe Consortium

This multidisciplinary consortium comprises a complementary set of 1) university departments very active in research on Hazard identification and quantitative risk analysis (UPC), process systems engineering (DTU, NTNU, KU, COL), process control and automation (DTU, NTNU, KU, COL), Computer Science and model-based AI (IMPERIAL, COL), Machine learning/Big Data analytics (IMPERIAL, DTU, NTNU, KU, COL), Open science practices (IMPERIAL) and 2) non-academic partners within process and plant operation from high hazard process industries (PdB), industrial QRA engineering providers (NOVOTEC, RISKTEC), software providers for process safety (KAIROS), process risk management and safety training (RISKTEC). Thus, we cover the full range of academic skills needed to advance the tools, training, and implementation required to upgrade the performance of risk analysis and monitoring, operation and maintenance planning in an integrated way, and the range of developers, service users, and clients to define, validate and exploit the research questions and outputs.

Table 1: ProSafe Consortium composition

Partner	Name	Country
1 (Coordinator)	Technical University of Denmark (DTU)	Denmark
2	Universitat Politecnica De Catalunya (UPC)	Spain
3	Norwegian University of Science and Technology (NTNU)	Norway
4	Novotec Consultores SA (NOVOTEC)	Spain
5	Koç University (KU)	Turkey
6	Kairos Technology (KAIROS)	Denmark
7	Risktec Solutions (RISKTEC)	UK
8	Port de Barcelona (PdB)	Spain
9	Columbia University	USA
10	Imperial College London (IMPERIAL)	UK

2. Methods

2.1 Overall methodology

PROSAFE´s research program divides the 12 doctoral student projects into 4 technical WPs. The interrelation between the WPs (see Figure 1) is as follows: in WP2, the doctoral candidate (DC) projects (1, 5, 8, 9) contribute to the advancement of the model-based methods by leveraging QRA with PSE methods for harmonized and robust quantitative risk assessment for improving safety; inWP3, the DC projects (4, 6, 7, 11, 12), focus primarily on the systematic study of the data for safety approach by developing neuro-symbolic learning methods that exploit domain knowledge and AI/ML algorithms for online risk monitoring and safe process operation; in WP4, the DC projects (2, 3, 10) undertake research for synergistic integration of model-based with data-based methods (WP3) for improved process safety; in WP5, the research of DC projects converges in three themes

to demonstrate and test improved process safety on selected cases from multi-sectorial industries (e.g., urea, LNG, renewable hydrogen). WP5 will provide the platform for the cross-fertilization of different ideas and concepts for interactive and synergistic improvement and validation of new methods and skills from model-based, data-driven, and hybrid approaches. In this way, PROSAFE overcomes the disadvantages associated with each separate approach. Indeed, the model-based approach relies on first principles and mechanistic modeling of systems dynamics, which makes them often overly reductive given the complexity of the problem. On the other hand, data-based approaches (such as AI and ML) very much depend on the quantity and quality of the data (as in garbage in =garbage out), which may not necessarily be available in sufficient context to enable complete system description and knowledge. Therefore, through smart hybrid integration and recent advancements in data and knowledge-driven ML technologies, ProSafe presents a powerful and complementary research program for DC students to undertake cutting-edge research. The research has also a promising potential and relevance to reinforce safer process operations in alignment with the needs of future digital process industries.

2.2 Integration of methods and disciplines

The research methodology is based on combining top-down and bottom-up approaches to comprehensively address complex aspects of process safety challenges.

- ➢ *In our top-down approach*, we go from model to improved process safety, in which we employ model-based methods that are used in QRA and PSE domains to identify and evaluate risk, make better decisions, and develop methods for improved risk assessment and process safety (WP2).
- ➢ *In our bottom-up approach*, we go from data to improved process safety (WP3). We build upon and expand the knowledge and understanding of risk achieved in top-down methods (WP2) with data-driven methods, employing both numeric AI and knowledge-driven symbolic ML (WP3).
- ➢ *In the hybrid approach*, we combine a model-based approach (WP2) with a data-based approach (WP3) to study the synergistic integration of these approaches for improved understanding and mitigation of process safety risks in high-hazard process industries (WP4).

The integration of these approaches and disciplines will be demonstrated with three high-hazard industry sectors (WP5). These case studies will be crosslinked with interdisciplinary work on model-based (WP2), data-based (WP3), and the synergistic integration of these into hybrid approaches (WP4). DCs working on the same case study but cutting across multiple WPs (e.g., DC-1, -7, -2) will benefit from exchange with the other DCs working on that system, as they use each other's experience along with industrial partner's expertise for optimal interaction within the given case study. DCs working on the same approach but on different case studies (e.g., DC-7, -4, -6) will develop joint solutions to cross-cutting challenges and learn to exploit various elements and systems for developing new methods and tools tailored to the scope and the needs of that specific process safety domain. Various process safety insights generated by each DC project from a multi-disciplinary approach will be discussed and exchanged between DC students during workshops (see training by research) regularly to ensure cross-fertilization and synergy among different projects.

3. DCs contributions to the ProSafe research program

DCs projects are expected to contribute to the research program per WPs as follows:
WP2 Model-based foundation for improved risk assessment & process safety (model to improved safety): WP2 aims to significantly advance the tools and methods for effective

and improved risk assessment and process safety using model-based methods. DC-1 will develop an efficient methodology to predict and propagate the model output uncertainty in risk criteria estimation in QRA. By performing a comprehensive uncertainty and sensitivity analysis and including the sources of uncertainties, DC-1 will evaluate their impact on QRA results and propose measures for robustifying the methodology. DC-5 will develop a framework for benchmark analysis and selection of QRA models to ensure consistency in their application to assess major accident effects. DC-8 will use CFD tools together with new accident mathematical models to improve consequence analysis in QRA studies and DC-9 will develop a methodology to perform QRA, which will make use of improved mathematical models to quantify the effects of major accidents on hydrogen facilities. DC-1 and -5 will work in close collaboration to improve the QRA methodologies, as well as DC-5 and -8 to improve consequences assessment. DC-9 will in part make use of the results from the previous DCs to apply them to hydrogen facilities specifically. Results from DC-5 and -8 will also be used by DC-6 to fill the cause and consequences database.

WP3 Artificial intelligence/machine learning for risk monitoring and safe process operation (data to improved safety): WP3 aims to develop neuro-symbolic solutions that integrate data-driven concepts, frameworks, and technologies based on deep learning and symbolic ML, to provide big data science for risk monitoring and safe process operation underpinned by established domain knowledge. For this DC-4 will design numeric AI (deep learning algorithms) to develop novel predictive analytics for online risk monitoring and fault diagnosis. DC-6 will develop a hybrid, regressible, and robust ML methodology that identifies abnormal events, and integrates process phenomenological knowledge and historical data. DC-7 will complement DC-6 with physics-informed machine learning algorithms tailored to control chemical processes. DC-11 will apply advanced symbolic ML methods to learn interpretable models of cause and effects of faults and abnormal behaviors that can be used to predict deviations from normal operation and establish a platform for early detection of abnormal events during plant operation. DC-12 will use inputs from DC-4 (online risk monitoring) and DC-11 (online detection of abnormal events) to develop an efficient online neuro-symbolic ML for predicting the consequences of abnormal events and diagnostics in terms of likely causes and related mitigation. Output from DC-4, -11, and -12 will be used for the definition of major hazard scenarios among others as part of the development of the harmonized QRA methods in WP2.

WP4 Hybrid approaches and tools integration (model & data to improved safety): WP4 focuses on the synergistic and smart integration of model-based and data-driven methods for improved process safety (RO3). For that, DC-2 will develop a novel hybrid modeling framework for risk monitoring that combines model-based algorithms with ML algorithms. DC-2 works in close collaboration with DC-4 to bridge the gap between model-based and data-based approaches for safety. DC-3 contributes through the design of novel algorithms for short-term optimal operation by using robust model predictive control, state estimation, and risk monitoring methods. DC-10 contributes through the integration of knowledge-based models with data-driven online learning to build a long-term prognostic model framework for planned maintenance in plants. DC-10 works in close collaboration with DC-3 to build prognostic degradation models.

WP5 Domain applications to selected high hazards multisector process industries: This WP focuses on comprehensive testing, validation, and evaluation of the ambitious and new process safety concepts and methods developed by the doctoral students on selected case studies from high-risk industries as defined in RO4. Thus, all DC projects contribute to this WP. More specifically, DC-1, -7, and -2 will test and validate the urea case studies together with RISKTEC as the relevant industry partner. DC-4, -5, -9, and -10 will work on the regasification plant and other energy vectors distribution (such as ammonia and methanol) in collaboration with Port de Barcelona as the industry partner. Finally, we will

use hydrogen production as a case study to test and validate methods and tools developed by DC-3, -6, and - 8 in collaboration with Kairos as the relevant industry partner. Overall, this ensures that the methods and tools from WP2, 3, and 4 are tested iteratively and validated across three sectors comprehensively.

4. Conclusions

ProSafe network undertakes innovative and original research and offers unique multi-sectorial and multi-disciplinary research and training opportunities for a total of 12 doctoral candidates (DCs) in the disciplines of machine learning (ML), artificial intelligence (AI), and process systems engineering (PSE) with domain knowledge of process industry and process safety.

Acknowledgments

References

https://prosafe.dtu.dk/
ProSafe: Smart Integraion of Process Systems Engineering & Machine Learning for Improved Process Safety in Process Industry. 101119358-PROSAFE, HORIZON-MSCA-2022-DN

Identification of Critical Inputs in QRA Studies using Monte Carlo-Based Sensitivity Analysis

Mercedes Belda-Ley[*], Gürkan Sin

PROSYS, Department of Chemical and Biochemical Engineering, Technical University of Denmark, Kgs. Lyngby, DK-2800, Denmark

* mbele@kt.dtu.dk

1. Introduction

Quantitative Risk Assessment (QRA) is a well-established methodology used in different fields to identify, quantify and evaluate the risks associated with human and industrial activities. It provides a structured and extensive approach to calculate risk values, providing as a result the ability to identify major risk contributors and to assist with decision-making among others. Owed to its extensiveness and complexity, numerous decisions and assumptions are to be made throughout its execution. With the intention of harmonizing and facilitating the execution of QRAs, multiple guidelines and methodologies have been developed. However, these diverge depending on the country, region, and can further be translated differently by each risk analyst, aggravating the uncertainty in the estimation of QRA results. Consequently, QRA reliability has frequently been questioned, reiterating and analysing its – inherent – uncertainties and related implications (e.g., Rae et al., 2014). This scrutiny has led to proposing and developing diverse strategies for treating its uncertainty (e.g., Abrahamsson, 2002; Xu et al., 2023) as well as discussing the role of sensitivity analysis in QRA (e.g., Flage and Aven, 2009).

In this context, the Monte Carlo (MC) methods provide a suitable framework for performing uncertainty analysis to complex problems (Sin and Espuña, 2020) where the description of the context, e.g., possible inputs, can be highly uncertain, as is the case for QRA (Abrahamsson, 2002; Li et al., 2022). Instinctively, these methods also serve as an effective framework for sensitivity analysis, since it is closely related to uncertainty analysis. MC-based sensitivity analysis has been applied to specific sections composing QRA in Pandya et al. (2012), however, the focus of this work was set on analysing the influence of model parameters in the calculated output.

This study presents an initial framework for applying MC-based Global Sensitivity Analysis (GSA) to QRA with the goal of pinpointing the most critical input parameters driving uncertainty in risk estimates. The aim is to quantify the contribution of individual input uncertainties to the variance of the overall risk outputs, i.e., the impact that the assumptions and decisions made throughout the QRA studies may have in the calculated output.

2. Methods

This study examines the effects modelling of an instantaneous release from an acrylonitrile tank, whose subsequent events include liquid pool formation, liquid evaporation and dispersion. Acrylonitrile is a highly toxic and volatile flammable liquid generally stored in unpressurized tanks at ambient temperature. It is assumed that, after the release, acrylonitrile forms a liquid pool spreading to the available surface of the bund surrounding

the storage area. This area includes three tanks for acrylonitrile storage of 500 m^3 capacity each and the bund was designed following ITC – MIE APQ 7, the Complementary Technical Instruction for the Storage of Toxic Liquids in Fixed Containers (Royal Decree 656/2017). The sensitivity analysis comprises acrylonitrile pool evaporation – of the non-boiling pool – and subsequent dispersion – a neutrally buoyant gaussian dispersion. The input variables sampled consist of the wind speed, ambient temperature, cloud cover and day-time or night-time conditions. Wind speed and ambient temperature input distributions are based on available meteorological data (Danish Meteorological Institute, n.d.) and are respectively approximated to a Weibull distribution with parameters A = 5.6115 and B = 2.0647 (m/s) and to a normal distribution with μ = 10.8671 and σ = 6.7939 (°C). Cloud cover follows discrete distributions from 0 to 10 with equal probabilities.

Appropriate sampling strategies are selected for each input, and subsequently the stability class based on the Pasquill-Gifford classification is determined for each sample according to the cloud cover, wind speed and whether it is day-time or night-time. Following the pertinent dispersion coefficients for the y-axis, σ_y, and the z-axis, σ_z, are calculated. Two main outputs are calculated, first, the evaporation rate in g/s. The results are subsequently fed to the dispersion model as a continuous source of toxic gas in order to calculate the second output: acrylonitrile airborne concentration in g/m^3 at a certain distance of interest downwind from the source, more particularly at 211 m.

Two different sensitivity indices are generated for the latter output. First, the Standardized Regression Coefficients (SRCs) are computed using available MATLAB functions for linear least-squares solver, *lsqlin*, and multiple linear regression, *regress*. Second, the first order effect (S_i) and total order effect (ST_i) indices are computed using the approximations of the variance-based GSA indices given by Sobol, Saltelli and Jansen, which are manually implemented in MATLAB. In order to ensure statistical consistency and reliability of the sensitivity indices, the convergence of the first two moments – mean and variance – of the output distributions, guided by the Law of Large Numbers (LLN), is implemented. In this regard, the graphical method of Maximum-to-Sum plots provides an indication of the required number of MC simulations for a re sensitivity analysis.

3. Results and discussion

MC simulations are executed sampling from the above-mentioned input distributions and the two outputs calculated, whose distributions are characterized by a mean value of 346.33 (g/s) and 0.3644 (g/m^3) and standard deviation values of 107.89 (g/s) and 0.8899 (g/m^3) respectively. These values indicate that the concentration values are highly spread in comparison to the evaporation rate, which exhibits a Coefficient of Variation (CV) of 0.31 against that for the concentration of 2.44. Figure 1 further demonstrates this statement by displaying a slower convergence of the logarithmic Maximum-to-Sum plots for concentration in comparison to the evaporation rate. This can be attributed to the fact that evaporation rate is only affected in this study by the ambient temperature, while concentration is additionally affected by the other input variables considered in the work.

The number of MC simulations performed – 500 000 – ensures the validity of the sensitivity analysis, by allowing the output distributions moments to converge towards zero, as can be seen in the Maximum-to-Sum plots in Figure 1. SRCs are calculated including as inputs the stability class and the dispersion coefficients, providing a goodness of the fit – coefficient of determination, R^2 – of 0.588 for *lsqlin* method and 0.622 for the *regress* method.
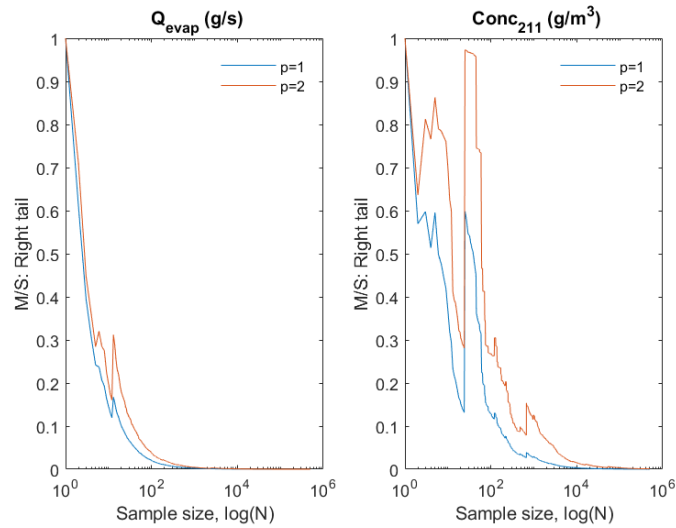
Figure 1. Logarithmic Maximum-to-Sum plots for evaporation rate (left) and concentration (right).

Table 1 shows that there is sufficient agreement between the two linear regression methods for the sampled inputs. On the contrary, the obtained SRC values for the stability class and dispersion coefficients show a significantly lower agreement. However, given that the of R^2 for both methods are below 0.7, the validity of these results is debatable.

Table 1. SRC and SRC^2 values for concentration (g/m^3) at 211 m downwind.

Input variable	SRC - *lsqlin*	SRC^2 - *lsqlin*	SRC - *regress*	SRC^2 - *regress*
Wind speed (m/s)	-0.3214	0.1033	-0.1639	0.0269
Cloud cover	-0.0976	0.0095	-0.0785	0.00617
Day-time/Night-time	-0.1159	0.0134	-0.1514	0.0229
Ambient temperature (°C)	0.1242	0.0154	0.1243	0.0155
Stability class	1.0000	1.0000	1.8726	3.5066
σ_y (m)	-0.3488	0.1216	1.1554	1.3348
σ_z (m)	0.7607	0.5786	0.0905	0.0082

Global sensitivity analysis results, S_i and ST_i, presented in Table 2 show general agreement for all the sensitivity indices calculated – Jansen and Saltelli approximations to ST_i are the same. According to these results, wind speed variations – in other words, assumptions – are likely to have a considerable impact in the variability of the airborne acrylonitrile concentration, whereas the other factors play a less significant role in the uncertainty of the concentration estimates. This can be explained due to the fact that wind speed affects both, the gaussian dispersion calculations as well as the considered stability class for it.

Further analysis on the behaviour of the output led to the understanding that the concentration values differed significantly for each stability class. Figure 2 clearly depicts this difference, which is particularly noticeable for stability class F. From stability classes A to F, the mean and dispersion of the calculated concentration mostly increases. This observation agrees with the definition of the stability classes, which provides from A to F more stable atmospheric conditions, hence, preventing the dispersion of the toxic gas. Following this evidence, the output values were sorted and grouped according to their stability class and the SRC coefficients for each group were newly determined, this time

dropping the stability class related inputs and day-time or night-time for SRC calculations. As a result of the separation the number of samples per stability class is different.

Table 2. First order and total order effects for concentration (g/m³) at 211 m downwind.

Input variable	S_i – Sobol	S_i – Saltelli	S_i – Jansen	ST_i – Sobol	ST_i – Saltelli / Jansen
Wind speed (m/s)	0.4318	0.4444	0.4387	0.8788	0.8868
Cloud cover	0.0107	0.0091	0.0095	0.1031	0.1050
Day-time/Night-time	0.0737	0.0689	0.0738	0.4562	0.4536
Ambient temperature (°C)	0.0163	0.0159	0.0142	0.0982	0.1022

The results included in Table 3 represent the results for the two implemented MATLAB regression functions, *lsqlin* and *regress*, as in this second estimation the computed coefficients align for both methods. The separation of the different stability classes for the sensitivity analysis provides a more suitable methodology for calculating sensitivity indices based on linear regression and MC methods. The R^2 values are mostly above 0.7, hence, indicating that linear regression is a sufficiently adequate method for this sensitivity analysis, except for stability class D. The reason behind stability class D presenting a poor fit for linear regression can be explained by the fact that, following the Pasquill-Gifford classification, overcast conditions, i.e., cloud cover of 10, are always assigned to belong to category D, regardless of the other atmospheric conditions. Consequently, there are wider ranges and more diverse combinations of input values in this stability class group.
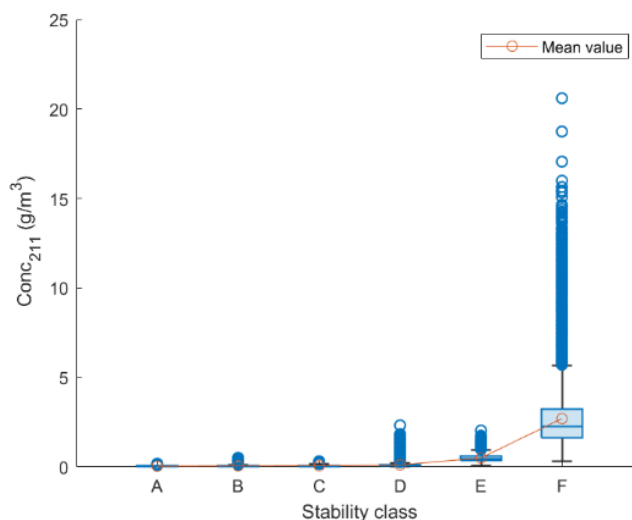

Figure 2. Box chart and mean for the calculated acrylonitrile concentration per stability class.

Furthermore, the CVs after the separation have been reduced in comparison to the one computed above for the combined stability classes. The updated CV values fall below 0.7 for all stability classes, being much lower than the previous value of 2.44. Beyond this, there is general agreement for all stability classes that the influence of the wind speed and ambient temperatures are significant. Naturally, the higher the wind speed, the more effective acrylonitrile dispersion and the lower its concentration at the point of interest. On the contrary, the higher the ambient temperature, the higher the evaporation rate of acrylonitrile from the liquid pool will be, resulting in a higher airborne concentration of the

toxic substance. These logics are adequately evidenced in the SRCs, yielding negative values for wind speed and positive values for ambient temperature.

Table 3. SRC values for concentration (g/m^3) at 211 m downwind per stability class calculated with the method.

Input variable	A	B	C	D	E	F
Wind speed (m/s)	-0.7384	-0.7221	-0.4929	-0.5948	-0.5300	-0.7464
Cloud cover	-0.0271	0.0030	0.2733	0.0956	0.0067	0.0507
Ambient temperature (ºC)	0.5503	0.4657	0.5874	0.4585	0.8174	0.5141
R^2	0.8260	0.7487	0.8506	0.5793	0.9411	0.7911

Based on the SRC results depicted in Table 3 and the coefficient of variation reduction, it can be deduced that, despite the concentration values being determined after sampling from the same ensemble of input values, it would not be completely appropriate to consider that the output values belong to a unique output distribution. This circumstance is additionally related to the reason behind the requirements for high number of MC simulations for the distribution of the acrylonitrile concentration combining all stability classes to converge following the LLN. Instead, the concentrations obtained are better understood as separated distributions for each stability class, suggesting that complete QRA sensitivity analysis including all types of weather conditions is a challenging endeavour. However, the impact of this condition for GSA, in contrast to linear regression, would appear to be overcomed.

4. Conclusions

Overall, the work proposes a starting point for advanced, comprehensive sensitivity analysis based on MC methods for QRA. A sensitivity analysis is performed on two interconnected sub-models belonging to QRA where the LLN determines the necessary number of MC simulations to be conducted. The results provide evidence that the stability classification has a strong impact on the airborne concentration results for neutrally buoyant gases. As a result, the calculated output behaves in a more complicated manner than one solely distribution that can be straightforwardly studied through sensitivity analysis. Different requirements, challenges and suitable sensitivity analysis indicators for effectively applying sensitivity analysis to QRA are outlined in this study. The methodology showcases a framework for conducting GSA to QRA and an initial approach for the treatment of stability classes and its impact in effects modelling for QRA sensitivity analysis. The identification of key contributors to the variability in QRA results will be pivotal for harmonizing the QRA procedure and enhance its reliability.

References

Abrahamsson, M., 2002. Uncertainty in Quantitative Risk Analysis - Characterisation and Methods of Treatment. [Licentiate Thesis, Division of Fire Safety Engineering, Lund University]. Fire Safety Engineering and Systems Safety.

Flage, R. & Aven, T., 2009. Expressing and communicating uncertainty in relation to quantitative risk analysis. Reliability: Theory & Applications, 2(2–1,13), 9–18.

Li, Y., Wang, Y., Lai, Y., Shuai, J., & Zhang, L., 2022. Monte Carlo-based quantitative risk assessment of parking areas for vehicles carrying hazardous chemicals. Reliability Engineering & System Safety, 231, 109010. https://doi.org/10.1016/j.ress.2022.109010

Ministerio de Economía, Industria y Competitividad, 2017, Royal Decree 656/2017, of June 23, which approves the Regulations for the Storage of Chemical Products and their Complementary Technical Instructions MIE APQ 0 to 10, Boletín Oficial del Estado.

Danish Meteorological Institute, n.d. Observationer. DMI. https://www.dmi.dk/friedata/observationer

Pandya, N., Gabas, N., & Marsden, E., 2012. Sensitivity analysis of Phast's atmospheric dispersion model for three toxic materials (nitric oxide, ammonia, chlorine). *Journal of Loss Prevention in the Process Industries*, *25*(1), 20–32. https://doi.org/10.1016/j.jlp.2011.06.015

Rae, A., Alexander, R., & McDermid, J., 2014. Fixing the cracks in the crystal ball: A maturity model for quantitative risk assessment. Reliability Engineering & System Safety, 125, 67–81. https://doi.org/10.1016/j.ress.2013.09.008

Sin, G. and Espuña, A., 2020. Editorial: Applications of Monte Carlo Method in Chemical, Biochemical and Environmental Engineering. Front. Energy Res. 8:68. https://doi.org/10.3389/fenrg.2020.00068

Xu, Y., Reniers, G., Yang, M., Yuan, S., Chen, C., 2023. Uncertainties and their treatment in the quantitative risk assessment of domino effects: Classification and review. Process Safety and Environmental Protection, 172, 971-985. https://doi.org/10.1016/j.psep.2023.02.082

Exploratory Analysis of the HIAD Database: a Machine Learning Approach to Support Hydrogen Risk Assessment

Jairo Andrés Meneses-Gelves[1], Rafael Amaya-Gómez[2], Pascale Vacca[1], Elsa Pastor[1,*]

[1]Centre for Technological Risk Studies (CERTEC), Universitat Politècnica de Catalunya · Barcelona Tech, Barcelona East School of Engineering (EEBE). Avinguda Eduard Maristany, 16, 08019 Barcelona, Spain;
[2]Department of Industrial Engineering, Universidad de los Andes, Cra 1E No. 19A-40, Bogotá, Colombia

*elsa.pastor@upc.edu

1. Introduction

The growing interest in hydrogen technologies due to the global energy transition introduces new safety challenges arising from the unique physicochemical properties of hydrogen. Although previous studies have explored the application of machine learning to extract lessons learned from historical incidents and accident databases from the chemical industry, research specifically focused on hydrogen-related events remains limited. Tamascelli et al. (2022) utilized classification models trained on the Major Hazard Incident Data Service (MHIDAS) to estimate the severity of chemical accidents. Tamascelli et al. (2023) extended this approach using meta-learning and transfer-learning techniques in the context of ammonia. Similarly, Kurian et al. (2020) applied supervised learning and keyword analysis to a database of oil sands incident reports, developing trend analyses, risk matrices, and prevention strategies.

The present study explores the application of machine learning techniques to historical hydrogen-related accidents and incident databases. It presents a structured data pre-processing framework tailored to machine learning applications to gain insight on hydrogen-related events. It includes an exploratory and unsupervised learning assessment to detect hidden relationships between input features and accident outcomes (e.g., fatalities or injuries). This work is aligned with the implementation of Safety 5.0 principles, which aims to incorporate artificial intelligence, digital technologies, and real-time analytics into risk management practices (Pasman & Behie, 2024). Post-accident analysis and safety-informed decision making can benefit from identifying how machine learning approaches can extract meaningful patterns from structured hydrogen-related events.

2. Methods

The overall workflow is outlined in Figure 1. The methodology develops in three steps. First, data extraction from the Hydrogen Incident and Accident Database (HIAD) database, which comprises hydrogen-related events reports. Second, data pre-processing encompasses two sub-steps: (i) feature selection, whereby a set of accident descriptors is chosen based on literature review, and (ii) data cleaning, which standardizes categorical labels and filters out records missing any of the key outcome variables (in this study defined as number of fatalities and number of injuries). Finally, accident-based analysis applies Multiple Correspondence Analysis (MCA) to the resulting dataset, transforming the categorical

feature set into a low-dimensional factor space. Detailed explanations of each stage are given in the following sections.
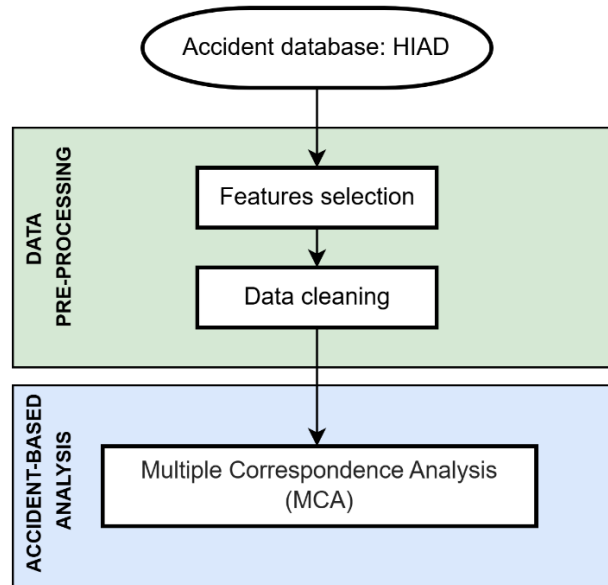

Figure 1. Methodology workflow.

2.1 Accident database: HIAD

The accident data are extracted from the Hydrogen Incident and Accident Database (HIAD) version 2.1, provided as an Excel file (Joint Research Centre, 2025). This dataset comprises 954 unique reports from 1785 to 2025 around the world. related to hydrogen incidents and accidents. Maintained by the European Commission's Joint Research Centre (JRC), the database is specifically dedicated to documenting hydrogen-related events.

Data collection in HIAD 2.1 is based on a systematic approach that harvests information from publicly available primary and secondary sources, including peer-reviewed literature, government investigation reports, and open-access event summaries. To support the standardized information in the database, HIAD 2.1 incorporates three integrated modules: the Data Entry Module (DEM), which uses structured templates and controlled vocabularies to capture event descriptors; the Data Retrieval Module (DRM), which enables multi-criteria filtering and data export; and the Data Analysis Module (DAM), which provides both pre-configured statistical overviews and customizable analytical outputs. This modular architecture enhances the consistency and efficiency of the entire data lifecycle.

HIAD 2.1 employs a five-level labelling system to define the data quality. Unvalidated submissions begin at Quality 1 (not publicly released), while validated records advance through successive levels up to Quality 5, representing full data richness, including original investigation files and detailed quantitative information. JRC analysts review each entry for completeness, consistency, and traceability before a quality label is assigned.

2.2 Data pre-processing: Features selection and data cleaning

The original HIAD dataset was consolidated into a single table by merging columns from multiple worksheets based on their Event ID, thereby unifying core metadata, facility characteristics, consequence metrics, and quality labels into one record per event. Subsequently, a subset of 20 accident features was selected according to the framework proposed by Tamascelli et al. (2022), as shown in Table 1.

To develop the Machine Learning approach, the Country (CO) feature was excluded in favour of broader regional grouping to capture essential spatial variability while avoiding the high-cardinality and sparse encoding issues that can degrade classifier performance. Likewise, the Year (YE) feature was omitted since temporal trends did not enhance the causal–consequence relationships of interest. Finally, only descriptors present in at least 70 % of the 954 reports were retained, ensuring adequate data coverage for a robust machine learning analysis.

Table 1. Accident features.

Code	Description	Data type	Missing values (%)	Selected feature
ID	Event ID	Numerical	0.0%	No
Q	Quality of the data	Categorical	0.0%	Yes
NA	Nature of the consequences	Categorical	0.0%	Yes
RE	Region (continent)	Categorical	0.0%	Yes
YE	Year	Numerical	0.0%	No
CA	Causes	Categorical	0.0%	Yes
EV	Event Initiating system	Categorical	0.9%	Yes
CL	Classification of the physical effects	Categorical	1.0%	Yes
CO	Country	Categorical	1.3%	No
AP	Application type	Categorical	1.9%	Yes
NUI	Number of injures	Numerical	5.9%	Yes*
OP	Operational condition	Categorical	11.7%	Yes
NUF	Number of fatalities	Numerical	12.4%	Yes*
LOD	Location description	Categorical	13.8%	Yes
ST	Storage/process medium	Categorical	15.1%	Yes
RET	Release type	Categorical	17.9%	Yes
LOT	Location type	Categorical	27.5%	Yes
IG	Ignition source	Categorical	77.2%	No
REA	Release amount	Numerical	82.6%	No
FL	Flame type	Categorical	89.9%	No

*Proposed categorical variable

Regarding the data cleaning step, categorical label unification was done by standardizing text entries to a consistent format and correcting typographical variations, thereby reducing noise and ensuring uniform category encoding. Since the subsequent machine learning approach requires at least one observed outcome per record, any accident report lacking fatality and injury information was excluded. However, reports that included at least one of these target variables were retained to preserve partially observed cases and maintain sample diversity. This filtering procedure removed 260 records from the original 954, leaving 694 data events available.

The numerical variables (NUI and NUF) were modified into categorical variables following the CCPS Tier 1 Process Safety Event (PSE1) criteria, whereby any event with one or more fatalities qualifies as a catastrophic event (Center for Chemical Process Safety, 2018). Based on these standards, both NUI and NUF were converted as shown in Table 2.

Table 2. Accident consequences categories. People harmed refers to injuries or fatalities.

Category	Description
0	No people harmed
>1	More than 1 people harmed
Unknown	Not reported

2.3 Accident-based analysis: Multiple Correspondence Analysis (MCA)

The Multiple Correspondence Analysis (MCA) approach was selected because the features are categorical or have been categorized (as shown in Table 2). Unlike Principal Component Analysis (PCA), which optimally represents continuous variables in a low-dimensional Euclidean space, MCA can accommodate any number of categorical variables by transforming them into a complete indicator matrix (Greenacre, 2010). This transformation preserves the χ^2 distances between category profiles following the PCA framework, so they are defined as the difference between categorical observations to quantify the degree of similarity among individuals or categories. This approach enables the simultaneous exploration of associations among variable categories. MCA itself is an extension of classical correspondence analysis to more than two categorical variables.

The MCA begins by constructing an indicator matrix in which each row represents an event and each column represents one category of one feature. From this matrix, a correspondence table of relative frequencies is computed, and a singular value decomposition (SVD) yields principal axes (dimensions) that capture the largest share of the total inertia of the categorical cloud. Both individuals (events) and categories (accident features) are in two clouds that their dimensions come from the number of categories and registers and they are used to evaluate similarities depending on the closeness. Further details on this approach can be found in Amaya-Gómez et al. (2021) and Greenacre (2010). Each event and each category are then projected onto these new axes, producing factor coordinates that reveal the clustering of similar events and co-occurrence patterns among categories. By retaining the first few dimensions, MCA reduces data complexity while maintaining the interpretability of categorical relationships. In this work, the package of "FactoMineR", "FactoExtra" and "Factoshiny" in RStudio 2024.12.1 is implemented to evaluate the MCA results in terms of the inertia (variability) described, and the obtained individuals and categories clouds.

3. Results and discussion

3.1 Exploratory analysis of the HIAD 2.1

The distribution of the fatalities and injuries grouped by decade is shown in Figure 2. Both fatalities and injuries increased steadily from the 1960–1970 decade through 2000–2010. However, both curves turn downward from 2010–2020 to 2025, showing an apparent decline. This post-2010 decrease likely stems from significant advances in hydrogen safety practices. For instance, the first edition of NFPA 2, Hydrogen Technologies Code, was published in 2011.

Regarding the events occurring prior to 1960, the most significant contribution to the high-fatality value corresponds to the LZ-129 Hindenburg disaster in 1937, which resulted in 35 fatalities. In contrast, the main injury value arises from the 1959 explosion at a Japanese chemical plant, which resulted in 11 fatalities and 44 injuries.
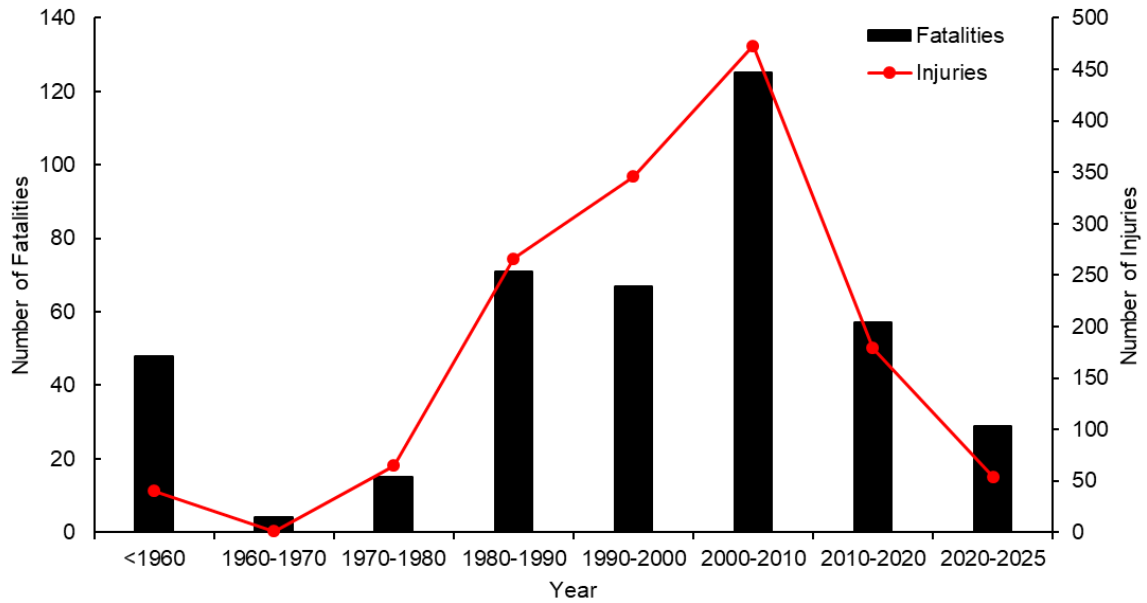
Figure 2. Number of fatalities and injuries per decade.

Figure 3 illustrates the proportional distribution of hydrogen-related accidents by region and the total of events across decade. For the period before 1960, North America, Europe and Asia contributed exactly with one event, yielding equal proportions. From 1960 onwards, Europe's share of proportion of the events increased steadily, whereas North America's share declined. Event proportions in Oceania and South America remain negligible, reflecting the developing adoption of hydrogen technologies in those markets.
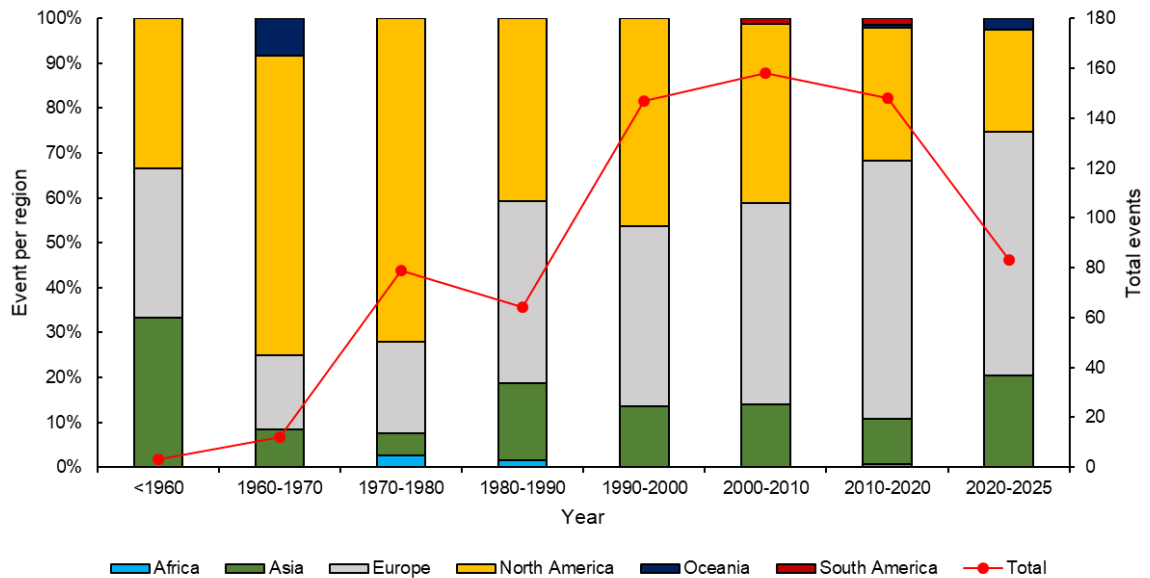

Figure 3. Distribution of hydrogen-related events (bar) and total events (line) per decade.

3.2 Machine Learning approach: Multiple Correspondence Analysis

The scree plot of principal inertia (Figure 4) shows the associative structure of the categorical variables and guides the selection of dimensions for further analysis. The first two dimensions account for 6.85% of the total inertia (3.87% and 2.98%, respectively), indicating that this two-dimensional plane explains a modest share of the event–feature cloud variability. Although this proportion appears small, it exceeds the baseline reference of 2.9% (equivalent to the average inertia per dimension under an independent model), confirming that the first plane captures meaningful structure rather than noise.

The observed inertias were compared against the 0.95-quantile of inertias derived from randomly permuted indicator matrices to determine the number of dimensions carrying substantive information. Fourteen dimensions shown inertias greater than this permutation-based threshold (23.79% cumulative inertia versus 18.19% expected at the 95% quantile), suggesting that only these axes represent genuine associations among accident descriptors. Consequently, subsequent clustering and typology development draw exclusively on the factor coordinates of these significant axes, ensuring that derived event classes reflect true categorical co-occurrence rather than sampling artefacts. However, the analysis presented in this study focuses on the first two dimensions. This choice reflects a deliberate focus on the most interpretable plane of variation, even when it accounts for a modest proportion of the categorical cloud.
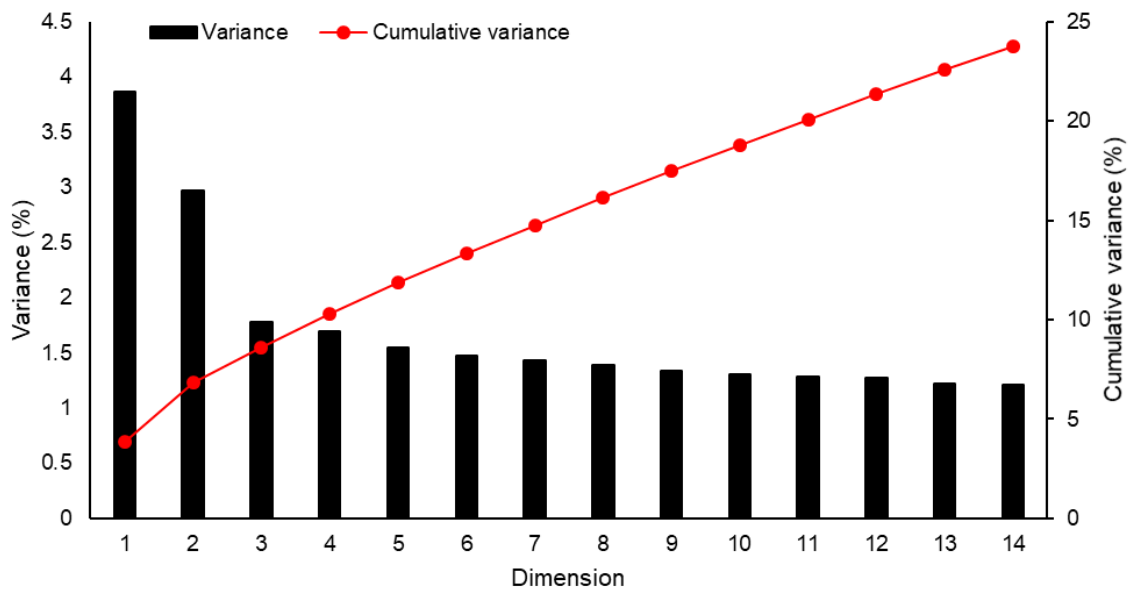

Figure 4. Decomposition of the total inertial.

Figure 5 shows the correlation ratio for the first two MCA dimensions. Each axis quantifies the correlation ratio between a variable and its respective component. If this correlation ratio is close to unity for a given component, individuals in the same category have similar coordinates (Husson et al., 2017). This visualization, therefore, highlights which variables co-vary most tightly in the reduced space. In this study, the supplementary elements (NUI and NUF) lie in close proximity to three variables: Operational Condition (OP), Location Type (LOT), Quality of the data (Q), and Region (RE). The OP variable distinguishes whether the process state at the time of the accident was "normal," "abnormal," or "unknown," and its strong alignment with the first two dimensions suggests that deviations from standard operating regimes are highly predictive of human-impact severity. Similarly,

the LOT variable, which categorizes the event environment as "open," "confined," "semi-confined," or "unknown," exhibits a high correlation ratio, indicating that spatial enclosure characteristics materially influence casualty outcomes. The Quality of the data (Q) correlates with the dimensions in a manner that underscores the importance of data completeness. Finally, the RE variable confirms the information discussed in Figure 3. These correlations affirm that process state, spatial confinement, and regional factors underpin the principal patterns of human harm captured by the MCA.
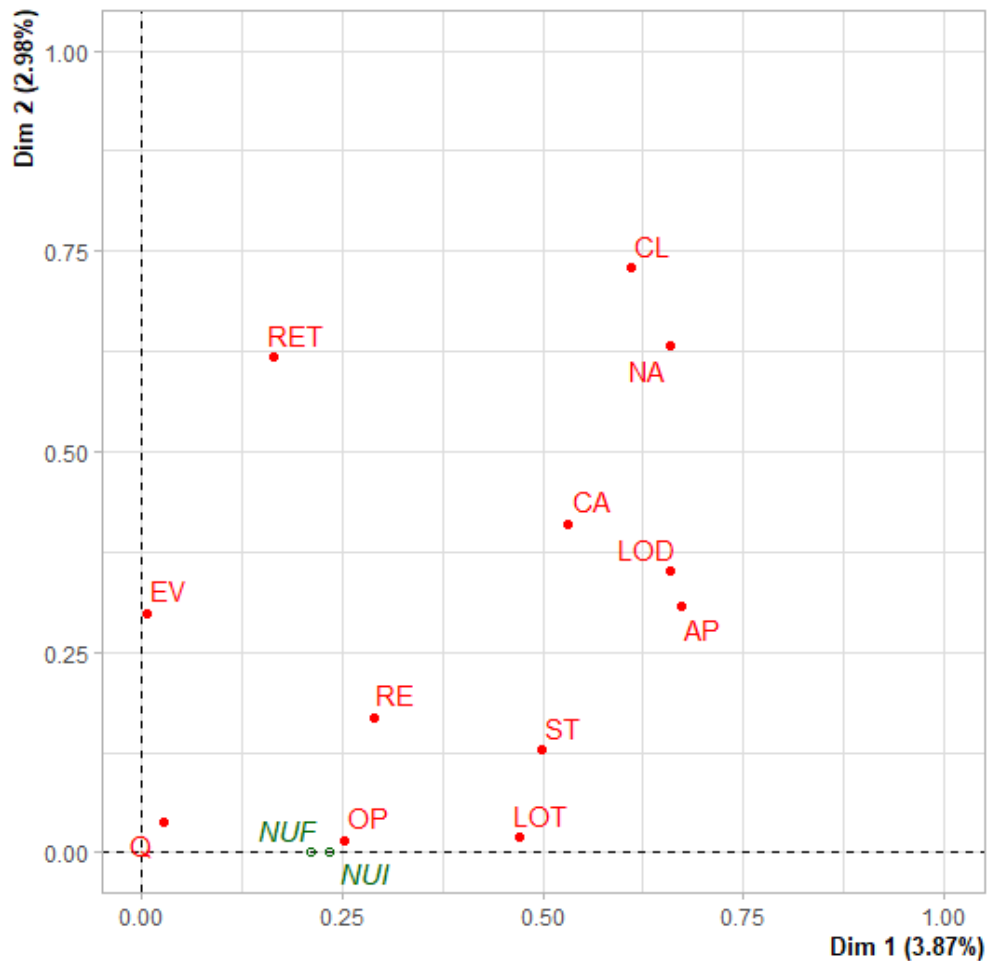

Figure 5. Variable correlation with the two principal MCA components.

Figure 6 presents the individual factor map defined by the first two MCA dimensions. The Wilks test was conducted to identify which categorical variables best discriminate among event points on this plane, with lower p-values indicating stronger separation. Among the two factors (NUI and NUF), the NUI variable yielded the most significant p-value, confirming it as the primary driver of distance between individual accidents on these axes. In the map, each point represents a single hydrogen-event report. For the black points, related with NUI>1, they are predominantly on the positive side of Dim 1, indicating that high-injury events share similar categorical profiles. The sharing labels had high frequency for events that occurred in industrial applications (AP = "Industry"), were driven by explosive failure modes (NA = "Explosion"), took place within industrial facility types (LOD = "Industrial"), and coincided with abnormal operational conditions (OP = "ABNORMAL").
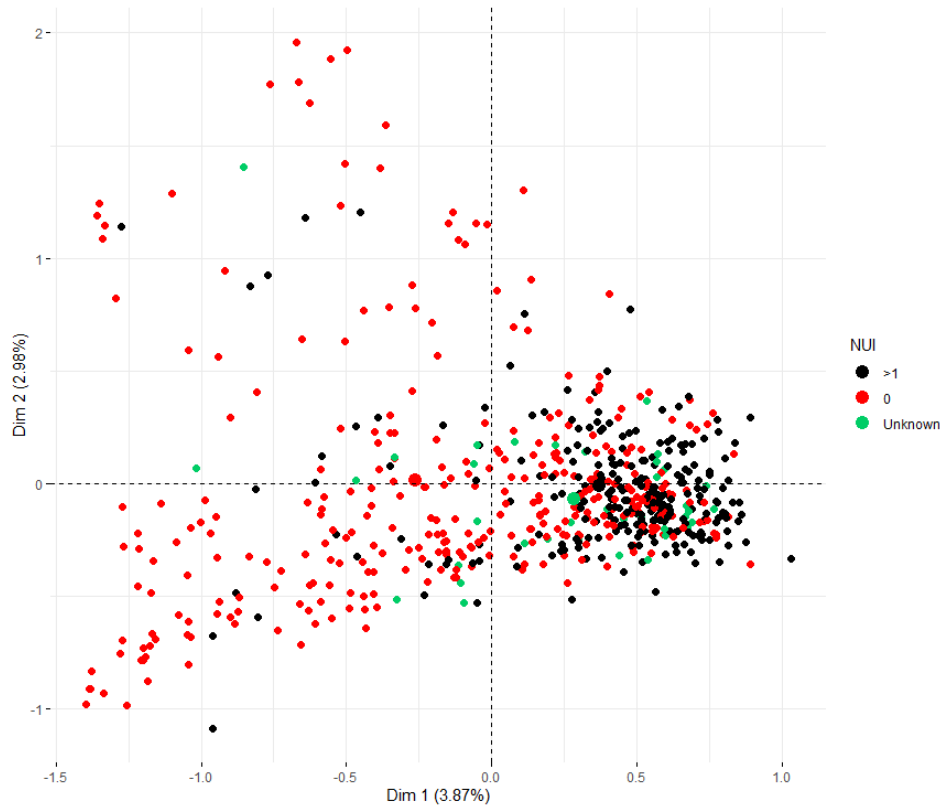
Figure 6. Individual factor map.

Figure 7 illustrates the MCA factor results, highlighting those with an associated squared-cosine (cos²) values greater than 0.2. The events in which both the NUI and NUF fall into the "zero" category tightly around the "normal" operational condition and the "open" location type. This alignment intuitively reflects that events without human casualties tend to occur under routine process states and in unconfined environments. The NUI and NUF in the category ">1" cluster with the following categories: CL= "Hydrogen release and ignition", NA= "Explosion", AP= "Industry", and LOD= "Industrial". This means that events with more than one fatality or injury are most likely to involve hydrogen releases and ignition with an explosion as a consequence in industrial settings. However, these categories associated squared-cosine values, which measure the level of association among categories, remain uniformly low, indicating that neither dimension captures a large proportion of their variance. This outcome demonstrates a substantial level of noise in the dataset. It suggests that the current categorical descriptors and their granularity may insufficiently isolate the principal accident severity drivers.

Several strategies merit consideration to reduce data noise and enhance signal clarity in future analyses. First, refining or consolidating low-frequency categories will prevent sparse levels from disproportionately inflating dimensionality. Second, exploring alternative accident descriptors could yield more discriminative feature sets. Finally, applying supervised feature-selection techniques or regularized embedding methods before MCA can help identify the most informative variables and suppress random variation. Together, these refinements promise to strengthen the robustness of MCA-derived typologies and improve the interpretability of hydrogen-event analyses.
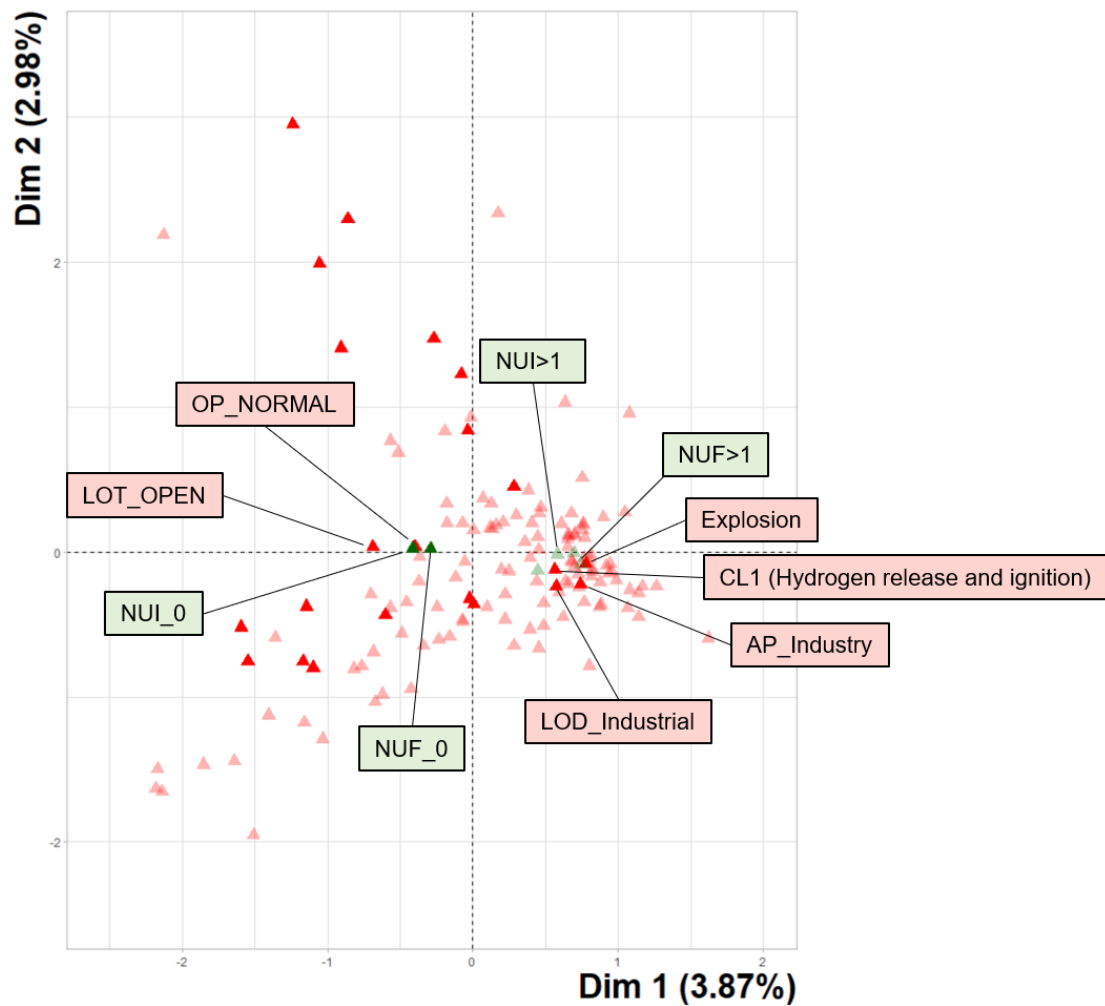
Figure 7. Categories factor results with a Cos^2=0.2.

4. Conclusions

This study examined a Machine Learning exploration of the Hydrogen Incident and Accident Database (HIAD 2.1). Integrating a pre-processing framework with a Multiple Correspondence Analysis, this work demonstrates that low-dimensional representations of 694 hydrogen-related events can be obtained despite the database's high categorical complexity and missing-value patterns.

The analysis identifies operational conditions, spatial confinement, and geographic regions as the categorical triad most strongly associated with the severity of human impact. Events occurring under abnormal process states and confined environments cluster in the same factor space as events with more than one injury, whereas casualty-free events align with normal operations in open settings.

This work establishes a transferable workflow aligned with Safety 5.0 principles, illustrating how unsupervised learning can increase post-event investigations, guide the prioritisation of safeguards and improve the risk assessments for emerging hydrogen infrastructures. Nevertheless, the modest inertia captured by the first MCA plane signals residual noise arising from sparse or low-frequency categories. Future research should therefore refine label taxonomies and incorporate higher-fidelity process descriptors.

Acknowledgments

References

Amaya-Gómez, R., Bastidas-Arteaga, E., Muñoz, F., & Sánchez-Silva, M. (2021). Statistical Soil Characterization of an Underground Corroded Pipeline Using In-Line Inspections. Metals, 11(2), 292. https://doi.org/10.3390/met11020292

Center for Chemical Process Safety. (2018). Process Safety Metrics: Guide for Selecting Leading and Lagging Metrics. AIChE. https://www.aiche.org/sites/default/files/docs/pages/ccps_process_safety_metrics_-_april_2018.pdf

Greenacre, M. J. (2010). Correspondence analysis. WIREs Computational Statistics, 2(5), 613–619. https://doi.org/10.1002/wics.114

Husson, F., Lê, S., & Pagès, J. (2017). Exploratory multivariate analysis by example using R (Second edition). CRC Press Taylor & Francis Group.

Joint Research Centre. (2025). European Hydrogen Incidents and Accidents database HIAD 2.1. European Commission.

Kurian, D., Sattari, F., Lefsrud, L., & Ma, Y. (2020). Using machine learning and keyword analysis to analyze incidents and reduce risk in oil sands operations. Safety Science, 130, 104873. https://doi.org/10.1016/j.ssci.2020.104873

Pasman, H. J., & Behie, S. W. (2024). The evolution to Industry 5.0 / Safety 5.0, the developments in society, and implications for industry management. Journal of Safety and Sustainability, 1(4), 202–211. https://doi.org/10.1016/j.jsasus.2024.11.003

Tamascelli, N., Paltrinieri, N., & Cozzani, V. (2023). Learning From Major Accidents: A Meta-Learning Perspective. Safety Science, 158, 105984. https://doi.org/10.1016/j.ssci.2022.105984

Tamascelli, N., Solini, R., Paltrinieri, N., & Cozzani, V. (2022). Learning from major accidents: A machine learning approach. Computers & Chemical Engineering, 162, 107786. https://doi.org/10.1016/j.compchemeng.2022.107786

Exploring Discrepancies between Consequence Analysis Software: from Validation to Common QRA Initiating Events

Lorenza Saturnino[1] , Alba Àgueda[2] , Miguel Muñoz[1] , Eulàlia Planas[2,*]

[1]*NOVOTEC - Process Safety and Major Accidents Department. Cerdanyola del Vallès, 08193, Spain;*

[2]*Centre for Technological Risk Studies (CERTEC), Universitat Politècnica de Catalunya · Barcelona Tech, Barcelona East School of Engineering (EEBE). Avinguda Eduard Maristany, 16, 08019 Barcelona, Spain*

*eulalia.planas @upc.edu

1. Introduction

Quantitative risk analysis (QRA) consists of a set of methodologies for estimating the risk posed by a given system in terms of human loss or, in some cases, economic loss (Casal, 2008). Throughout QRA, varying degrees of uncertainty influence the reliability of the results.

Consequence analysis, which models different loss-of-containment scenarios, is especially uncertain due to the complexity of physical phenomena like dispersion, fires, and explosions. These processes are highly nonlinear and governed by multiple interacting variables, necessitating the use of mathematical models that approximate these complex systems. The approximations introduced during modelling represent a form of knowledge-based uncertainty (Abrahassom, 2002), which arises from the inherent limitations in our understanding and representation of these hazardous events.

Among the various modelling approaches, integral models are the most widely used in QRA due to their low computational demands. These models are typically based on pseudo-one-dimensional representations, in which the system is analysed along a primary spatial axis. Unlike one-dimensional models, three-dimensional effects are incorporated in a simplified way, often through correction factors or semi-empirical correlations calibrated using field test data.

Several available software tools —such as PHAST, EFFECTS, and ALOHA— implement these integral models, each with its own algorithms, tuning parameters, and assumptions. Numerous studies have compared the predictive capabilities of different modelling tools across a variety of release scenarios (Bernatik et al., 2011; Bubbico & Mazzarotta, 2008; Hanna et al., 1993; Mazzola et al., 2021). In some instances (Hanna et al., 1993; Mazzola et al., 2021), simulation results were benchmarked against experimental data that were independent of those used in model development—providing a basis for model validation and enabling an assessment of predictive accuracy. These validation exercises revealed discrepancies between tools, although such differences generally fell within an acceptable range, supporting their practical use in QRA. However, in other studies (Bernatik et al., 2011; Bubbico & Mazzarotta, 2008), suitable experimental datasets were unavailable, and comparisons were limited to the outputs generated by different software. While this approach offers insight on the range of possible predictions, it does not allow for conclusions about accuracy. Moreover, a critical concern remains: it is unclear whether the acceptable discrepancy between software tools observed during validation persists when models are applied to QRA scenarios that deviate from the controlled conditions under which they were

originally validated. This issue raises the possibility that discrepancies between software predictions may increase in real-world applications, thereby amplifying uncertainty in consequence estimation.

This study investigates whether inter-software discrepancies become more pronounced as scenarios move from controlled validation cases to initiating events commonly used in QRA, potentially leading to an increased divergence in predictions and a loss of accuracy in consequence estimation. By comparing ammonia dispersion predictions from PHAST, EFFECTS, and ALOHA across both validated and common QRA scenarios, this work seeks to evaluate the stability of inter-software variability and its implications for the reliability of QRA outcomes.

2. Methods

This study compares ammonia dispersion predictions from three software tools—PHAST v9.0, EFFECTS v12.3, and ALOHA v5.4.7—across both validation and QRA scenarios.

2.1 Definition of the baseline discrepancy and the QRA scenario-related discrepancy

This study investigates whether inter-software discrepancies become more pronounced when moving from controlled experimental scenario used for validation to the initiating events typically considered in QRA. The core objective is to assess whether the relative agreement observed during validation holds under more generalized conditions, or whether divergence increases—potentially compromising the reliability of consequence estimation.

To quantify this effect, a baseline discrepancy is defined as the relative difference between software outputs when modelling a scenario for which the experimental data are available. This baseline reflects the expected level of variability between tools that is considered sufficiently accurate for that specific case due to prior validation. A comparable metric, referred to as the QRA scenario-related discrepancy, is calculated for typical QRA scenarios for which experimental data are not available.

The discrepancy D_{ij} between two software tools i and j is calculated as represented in equation (1).

$$D_{ij} = \frac{(R_i - R_j)}{(R_i + R_j)} \tag{1}$$

Where R_j and R_i are the results predicted by the software i and j, respectively. This formulation is applied both to the experimental validation case (yielding the baseline discrepancy) and to QRA scenarios (yielding the QRA scenario-related discrepancy).

The discrepancy D_{ij}, as defined in this work, ranges from –1 to 1. A value of 0 indicates perfect agreement between the software compared, while positive or negative values reflect which software produces higher results. Values close to zero suggest high consistency, whereas larger absolute values (e.g., above 0.2) highlight significant divergence.

By comparing the QRA scenario-related discrepancy to the baseline discrepancy, it is possible to assess whether the predictive agreement between software tools deteriorates when simulating QRA initiating events. If the discrepancy observed in QRA scenarios exceeds the baseline one, this suggests that the acceptable variability established during validation is no longer maintained. Such an increase in discrepancy may indicate a loss of predictive reliability when the models are applied outside the controlled conditions under which their accuracy was originally verified.

2.2 Description of the experimental and QRA scenarios simulated

As reference case for the baseline discrepancy, the Desert Tortoise field experiment was selected. This experiment involved the horizontal release of pressurized liquid ammonia, with the release direction nearly aligned with the prevailing wind direction (Goldwire et al., 1985). The experimental campaign consisted of four tests at different spill rates. The test chosen to be the reference case in this study is Desert Tortoise 1 (DT1). The data describing the release conditions, weather parameters, and measured values were obtained from the SMEDIS database (UK Health and Safety Executive et al., 2001). This database was developed during the European project with the same name, which aimed to establish a methodology for evaluating dense gas atmospheric dispersion models. The main parameters defining the DT1 test conditions are presented in Table 1. The measured variable was the concentration of ammonia, recorded at 29 different locations within the test field.

Table 1: Desert Tortoise 1 test parameters (Goldwire et al., 1985; UK Health and Safety Executive et al., 2001).

Parameter	Value
Substance	Ammonia
Pressure [barg]	12.6
Temperature [ºC]	21.5
Spill mass [kg]	10200
Release point (x,y,z) [m]	(0, 0, 0)
Release direction	Horizontal, 45º from N
Release duration [s]	126
Ambient pressure [bara]	0.909
Ambient temperature [ºC]	29.3
Soil temperature [ºC]	31.7
Relative humidity	0.132
Surface roughness [m]	0.003
Average wind speed [m/s]	7.42
Average wind direction	223.7º from N
Reference height for wind [m]	2
Stability class	D
Cloud cover	0.01

The other two simulated scenarios are initiating events defined in the BEVI guideline (Bevi, 2009), the Dutch standard for conducting QRA. For pressurized vessels, the two continuous release scenarios considered as initiating events in risk assessments are:

- A continuous release through a 10 mm diameter orifice, with the release duration defined either by the time required to fully empty the tank or a maximum of 1800 seconds.
- A continuous release of the entire tank contents over a fixed duration of 10 minutes.

The storage parameters used in the simulation software were selected based on the study by Orozco et al. (2019), in which ALOHA was employed to model an actual accidental release from ammonia storage tanks in an industrial setting. Furthermore, each scenario was modelled two times, with varying wind and atmospheric stability class parameters. Table 2 summarizes the storage parameters and meteorological conditions adopted to

simulate the BEVI initiating events. For consistency with the DT1 case, concentration levels at various locations were compared across the three software tools.

Table 2: BEVI scenarios simulation parameters (Orozco et al., 2019).

Parameter	Value
Substance	Ammonia
Pressure [barg]	11.75
Temperature [ºC]	15
Mass in the tank [kg]	120,000
Release point (x,y,z) [m]	(0, 0, 0)
Release direction	Horizontal
Ambient pressure [atm]	1
Ambient temperature [ºC]	15
Soil temperature [ºC]	15
Relative humidity	0.7
Surface roughness [m]	0.25
Average wind speed [m/s] and stability class	1.5F-5D
Reference height for wind [m]	10

2.3 Models adopted in the different software

To model the baseline and QRA scenario-related discrepancies, different software tools were employed, each utilizing its own modelling approach. The selection of discharge and dispersion models in PHAST, EFFECTS, and ALOHA was based on the technical recommendations provided by the software developers. This section outlines the selection and application of these models within each software, emphasizing the key choices and assumptions made for each scenario.

In PHAST, the discharge process is modelled using the DISC module, which simulates the flow from stagnation conditions to the orifice and subsequently from the orifice to atmospheric conditions (DNV, 2023a). Following this, the Unified Dispersion Model (UDM) utilizes the output from DISC to simulate atmospheric dispersion. For the discharge phase, PHAST allows users to choose among several modelling options for the expansion from stagnation to the orifice, from the orifice to the atmosphere, and for droplet formation.

During the validation of PHAST, a specific combination of these models was identified as the most accurate for simulating the DT1 scenario (DNV, 2023b). It is important to note that this combination is not the default configuration used by the software for similar release scenarios. Therefore, DT1 was simulated using the model combination recommended in PHAST validation study, whereas the BEVI scenarios were modelled using the software's default assumptions.

The models used in EFFECTS to simulate the scenarios under investigation were also selected based on the recommendations provided in the user manual (GEXCON, 2024). No specific adjustments or parameter settings were proposed for the DT1 scenario, as validation of the software against this particular experiment —performed using EFFECTS v10.1— showed an underprediction of the concentrations of approximately 50% (Ruiz Pérez, 2017). A more recent validation, introduced in EFFECTS v12.5, is still very recent and has not yet been made publicly available.

In ALOHA, all models employed were the default ones, as the software does not provide the user with the option to select or modify modelling approaches.

3. Results and discussion

This section focuses on the comparison of results using PHAST as the reference software. However, Figure 1 also provides a visualization of both the baseline discrepancy and the QRA scenario-related discrepancies between EFFECTS and ALOHA.

In the DT1 case, ALOHA and EFFECTS showed absolute baseline discrepancies of approximately 0.3 and 0.5, respectively, relative to PHAST, generally underpredicting ammonia concentrations.

In the BEVI scenarios, the discrepancies varied depending on the type of release and meteorological conditions. For the BEVI scenario involving a 10 mm orifice release, the discrepancy between PHAST and ALOHA remained similar to the baseline level. However, in the 10-minute release scenario under 1.5F weather conditions, the discrepancy between PHAST and ALOHA increased significantly, reaching values around 0.7.

The discrepancies between PHAST and EFFECTS across both BEVI scenarios ranged between 0.5 and 0.6, comparable to the baseline discrepancy but slightly higher.

While ALOHA predicted higher concentrations than PHAST in the BEVI scenarios, EFFECTS maintained the trend observed in the DT1 case, continuing to underpredict concentrations relative to PHAST.

The differences suggest a change in predictive agreement when moving from controlled validation conditions to more generalized QRA scenarios. According to the framework outlined in the methodology, discrepancies exceeding the baseline imply that the acceptable variability established during validation is no longer maintained. The observed increases in discrepancy indicate a potential loss of predictive reliability.
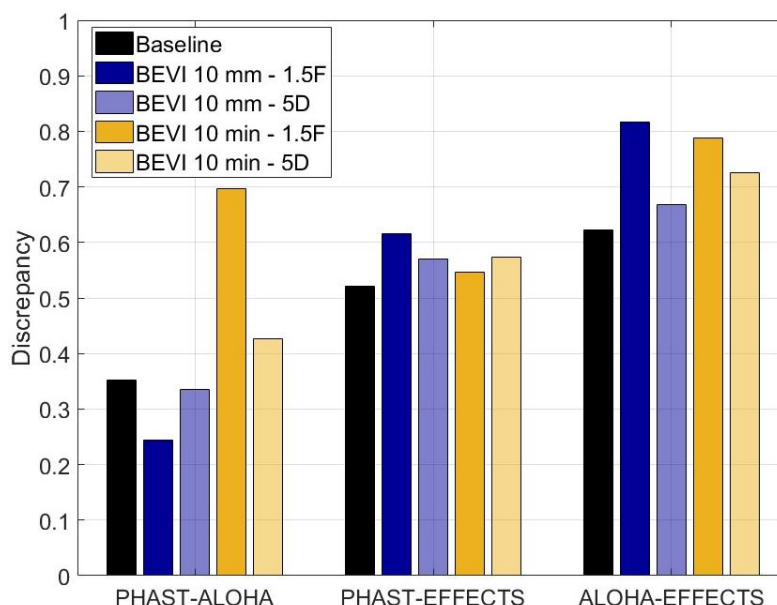

Figure 1: Comparison of baseline discrepancy with QRA scenario-related discrepancy.

4. Conclusions

This study examined the consistency of ammonia dispersion predictions from three widely used tools implementing integral models —PHAST v9.0, EFFECTS v12.3, and ALOHA v5.4.7— across both controlled validation scenarios and initiating events used in QRA. While the tools demonstrated relatively consistent performance under validation conditions, notable differences emerged when applied to typical QRA scenarios.

The results suggest that model agreement observed under validation conditions may not consistently extend to broader QRA applications, particularly where input data are less detailed or more uncertain. The discrepancy observed among tools in QRA contexts may represent a source of uncertainty not fully addressed in typical validation exercises. While these findings point to the potential value of considering inter-model differences within uncertainty assessments, further investigation is needed. This study represents a preliminary step toward a more comprehensive understanding of model behaviour in QRA settings. Future work will explore additional substances, a wider range of scenarios, and a more detailed examination of model structures and assumptions.

Acknowledgments

References

Abrahassom, M. (2002). *Uncertainty in Quantitative Risk Analysis—Characterisation and Methods of Treatment.* Fire Safety Engineering and Systems Safety.

Bernatik, A., Senovsky, P., & Pitt, M. (2011). LNG as a potential alternative fuel – Safety and security of storage facilities. *Journal of Loss Prevention in the Process Industries*, *24*(1), 19–24. https://doi.org/10.1016/j.jlp.2010.08.003

Bevi. (2009). Reference Manual Bevi Risk Assessments, v. 3.2. *National Institute of Public Health and the Environment (RIVM)*, 189.

Bubbico, R., & Mazzarotta, B. (2008). Accidental release of toxic chemicals: Influence of the main input parameters on consequence calculation. *Journal of Hazardous Materials*, *151*(2–3), 394–406. https://doi.org/10.1016/j.jhazmat.2007.06.002

Casal, J. (2008). *Evaluation of the Effects and Consequences of Major Accidents in Industrial Plants. Industrial Safety Series* (Vol. 8). Elsevier.

DNV. (2023a). *DISC Discharge Scenarios Theory—PHAST 9.0 Technical Documentation.*

DNV. (2023b). *UNIFIED DISPERSION MODEL Validation—PHAST 9.0 Technical Documentation.*

GEXCON. (2024). *EFFECTS v12—User and reference manual.*

Goldwire, H. C., McRae, T. G., Johnson, G. W., Hipple, D. L., Koopman, R. P., McClure, J. W., Morris, L. K., & Cederwall, R. T. (1985). *Desert Tortoise Series Data Report 1983 Pressurized Ammonia Spills.* Lawrence Livermore National Laboratory.

Hanna, S. R., Chang, J. C., & Strimaitis, D. G. (1993). Hazardous gas model evaluation with field observations. *Atmospheric Environment. Part A. General Topics*, *27*(15), 2265–2285. https://doi.org/10.1016/0960-1686(93)90397-H

Mazzola, T., Hanna, S., Chang, J., Bradley, S., Meris, R., Simpson, S., Miner, S., Gant, S., Weil, J., Harper, M., Nikmo, J., Kukkonen, J., Lacome, J.-M., Nibart, M., Björnham, O., Khajehnajafi, S., Habib, K., Armand, P., Bauer, T., … Ek, N. (2021). Results of comparisons of the predictions of 17 dense gas dispersion models with observations from the Jack Rabbit II chlorine field experiment. *Atmospheric Environment*, *244*, 117887. https://doi.org/10.1016/j.atmosenv.2020.117887

Orozco, J. L., Van Caneghem, J., Hens, L., González, L., Lugo, R., Díaz, S., & Pedroso, I. (2019). Assessment of an ammonia incident in the industrial area of Matanzas. *Journal of Cleaner Production*, *222*, 934–941. https://doi.org/10.1016/j.jclepro.2019.03.024

Ruiz Pérez, S. (2017). *TNO Dense Gas Model Verification and Validation.*

UK Health and Safety Executive, Cambridge Environmental Research Consultants, & Electricité de France. (2001). *Scientific Model Evaluation of dense gas DISpersion models (SMEDIS) database—Excel spreadsheets version 2.4.*